BMR JOURNAL
OF AUSTRALIAN GEOLOGY & GEOPHYSICS

VOLUME 7 NUMBER 4 DECEMBER 1982

BMR JOURNAL
OF AUSTRALIAN GEOLOGY & GEOPHYSICS

VOLUME 7 NUMBER 4 DECEMBER 1982

CONTENTS

Front cover: Scientific illustrator and artist Peter Shouten's reconstruction of *Wabularoo*, an extinct Middle Tertiary Bulungamayid from Riversleigh in northwestern Queensland, described in a paper in this issue. The name Wabularoo is a combination of 'Wa'bula', a Waanyi Aboriginal word meaning 'long time ago', and the Australian slang for kangaroo.

Issued March 1983

AUSTRALIAN GOVERNMENT PUBLISHING SERVICE CANBERRA 1982

Department of National Development and Energy, Australia

Minister: Senator the Hon. Sir John Carrick, K.C.M.G.

Secretary: A. J. Woods

Bureau of Mineral Resources, Geology and Geophysics

Director: R. W. R. Rutland

Editor, BMR Journal: I. M. Hodgson

The BMR Journal of Australian Geology & Geophysics is a quarterly journal of research and related activities. Contributions are from officers of the BMR, from BMR officers working in collaboration with others, or requested work sponsored by the BMR. In addition to articles the Journal may include shorter notes and discussion of papers published in it. Discussion of papers is invited from anyone.

Annual subscription to the Journal is $25 (Australian). Individual numbers, if available, cost $8.50. Subscriptions, etc., made payable to the Receiver of Public Moneys in Australian dollars should be sent to the Director, Bureau of Mineral Resources, Geology and Geophysics, P.O. Box 378, Canberra, A.C.T. 2601, Australia.

Other matters concerning the Journal should be sent to the Director, marked for the attention of the Editor, BMR Journal.

The text figures in this issue were drafted by P. Jorritsma, P. Griffiths, & B. Pashley.

ISSN 0312-9608

Printed by Graphic Services Pty Ltd, 516-518 Grand Junction Road, Northfield, S.A. 5085

BMR Journal of Australian Geology & Geophysics, 7, 231-254

LATE DIAGENETIC HISTORY OF THE NINMAROO FORMATION (CAMBRO-ORDOVICIAN), GEORGINA BASIN, QUEENSLAND AND NORTHERN TERRITORY

Bruce M. Radke

The Cambro-Ordovician Ninmaroo Formation is an extensive, predominantly carbonate unit in the southeastern Georgina Basin of Queensland and the Northern Territory. Following deposition and syndepositional diagenesis (eogenesis), which included hypersaline and moderate evaporitic overprints, the formation was further overprinted during three additional diagenetic stages: early telogenesis (near surface), mesogenesis (burial), and late telogenesis (uplift and erosion). An inventory of diagenetic products is presented. Extensive dolomitisation, unquantified hydrocarbon migration, and sulphide mineralisation during mesogenetic and mixed mesogenetic–late telogenetic stages were structurally controlled. During late mesogenesis, intercrystalline porosity developed with pervasive dolomitisation, while other types of porosity in limestones were occluded by calcite cement or hydrocarbons. Development of moldic, collapse-breccia and cavern porosity, karstification, and dedolomitisation developed in both stages of telogenesis, but were better developed in the later, prolonged stage. The duration of each stage varied locally with the burial and tectonic history. Consequently, both time and spatial variations of diagenetic paragenesis exist. Regions of differing history are the Toko Syncline, Smoky Anticline and western platform, and the Burke River Structural Belt.

Introduction

The Cambro-Ordovician Ninmaroo Formation in the southeastern Georgina Basin is a predominantly carbonate unit of widespread extent (Fig. 1), with varied lithofacies and diagenetic history. The formation accumulated during the Late Cambrian (Payntonian) and Early Ordovician (early Arenigian) under epeiric marine and saline environments with subsequent overprinting, and now comprises five primary carbonate lithofacies: ooid, peloid, flat-pebble conglomerate, skeletal, and mixed limestone lithofacies (Radke, 1980). The present distribution and thickness of these lithofacies were influenced by syndepositional structural events and later by the structural and erosional history, which has also controlled late-diagenetic modification of the sequence.

This paper presents the diagenetic history of the Ninmaroo Formation and emphasises aspects of economic interest. The objectives of the paper are: to describe the late diagenetic effects in the Ninmaroo Formation and order them in time; to explain them using a model of diagenetic evolution; and to examine and discuss regional variations in this diagenetic evolution.

An inventory of diagenetic products is presented. This provides evidence for a generalised paragenesis of the Ninmaroo carbonates and models of late diagenesis. Variations in this diagenetic history are related to different structural and erosional histories for different areas of the formation.

Early diagenesis (eogenesis), was shortlived. Although it was a complex phase responsible for significant overprinting of the sediments, only a summary is presented. The main focus is on the later telogenetic and mesogenetic stages.

Inventory of diagenesis

Stratiform breccias

Stratiform breccias are minor yet significant rock types within the sequence. They are recognised mainly in limestone because the fabric is generally obliterated during dolomitisation. Small-scale features, they are not directly related to faulting, and are categorised as stratiform bodies, and subdivided on internal texture into two types (Table 1).

Type A stratiform breccia has varied internal texture. The host limestones generally consist of ooid–peloid grainstone, which commonly fills surface irregularities around cryptalgal domes.

The breccias are lens-shaped, and tend to be conformable with the bedding (Fig. 2); on a smaller scale, breccias may be irregular or cross-cutting. Grainstone and wackestone are dominant, but packstone textures occur where finer particles or crystal silt have infiltrated an open grainstone fabric.

Clasts are oligomictic, consisting of fragments of the host rock. In the larger breccia bodies, clasts are mostly angular to subangular, equant to tabular, but in grainstone textures they are more rounded. In places, angular clasts contain cavities shaped like sulphate crystals (Fig. 3A). Most clasts are between 0.1 and 3 cm across, but angular blocks may be up to 20 cm, tabular, and oriented subparallel to the base of the breccia body. Sorting is usually poor, with apparent multiple modes in clast size. In larger bodies with moderately sorted grainstone textures, clasts are coated with thick isopachous cements, now micritised, but with relict regular lamination.

Matrix of either fine detritus, cement fragments, or both, may form 30 to 60 per cent of the breccia. The cement is laminar fibrous stalactitic calcite, with alternations of chalcedonite and quartzine or coarse calcite sparry mosaics. The cavity floors may be covered by cross-laminated silts of yellowish brown to red iron-stained detrital carbonate, quartz, feldspar, and traces of sulphates. Sulphate crystal pseudomorphs or nodules are normally present in the adjoining host rocks (Fig. 2B).

Type B stratiform breccia (Table 1) occurs exclusively in ooid or peloid grainstone and follows the zones of oomoldic or peloid-moldic porosity, which may be conformable with the original stratification, but may also cut across it where joint, fault, or stylolite surfaces control the shape of the body. Single or multiple breccia bands enhance the original lamination with both colour and textural variations. The breccia matrix is usually yellow, salmon pink, or red.

Texturally, the breccia is a wackestone with 'floating' angular and subangular clasts (0.3 to 5 cm across) that have indented to shard-like morphology (Fig. 3B). Some clasts have a regular faceted appearance. This breccia is always oligomictic and always has varied clast orientation. Quartzine may selectively replace clasts or host rock, but never the matrix. Authigenic K-feldspar overgrowths are common on detrital silt material. The matrix varies from 40 per cent to 100 per cent.

Discussion. Both types of stratiform breccia formed by solution and collapse processes. Type A, with varied textures, reflects cavity formation in the host rock during solution. Type B, regardless of the initiating process, developed from solution and structural instability of the host rock, but continuous

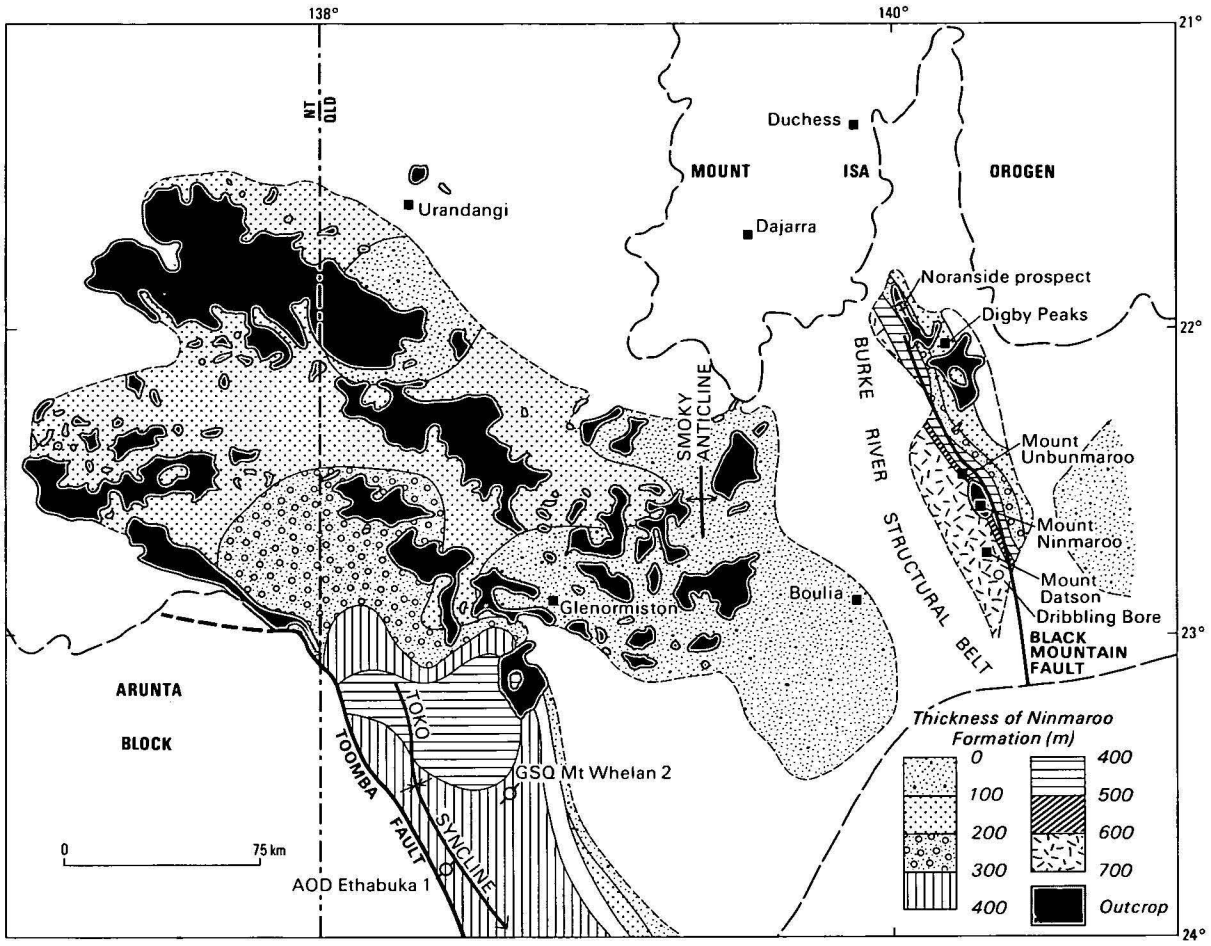

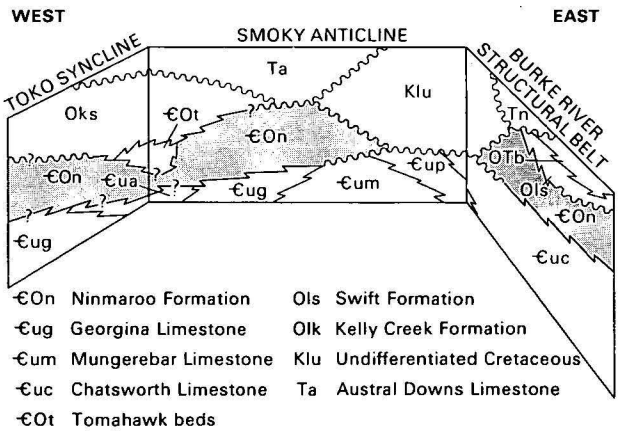

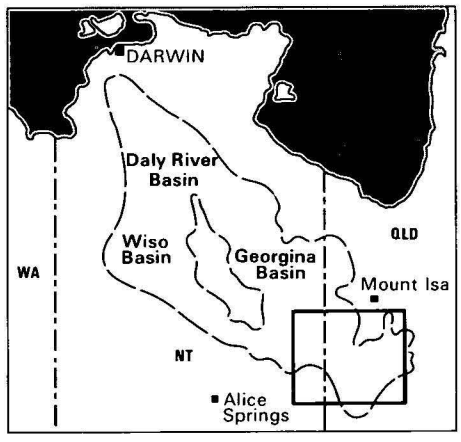

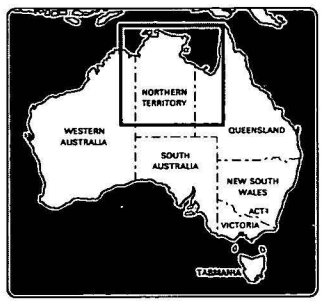

Figure 1. Location, geographic extent, thickness and stratigraphic relationships of the Ninmaroo Formation (after Radke, 1980).

Table 1. Comparison of stratiform breccia types A and B.

	Breccia type A *Sulphate-moldic collapse*	*Breccia type B* *Grain-moldic collapse*
Association	rarely a combined phenomenon	
Stylolitic overprint	40 per cent of occurrence	50 per cent of occurrence limestone;
Host — rock type	limestone dominant; mottled ooid and peloidal grainstone, algal domed stromatolites	exclusively ooid and peloidal grainstone
Breccia body — shape	conformable planar sheets dominant (60 %); pods or irregular (40 %)	planar sheets up to several metres extent
— size	1–10 cm thick, but up to 50 cm	less than 10 cm thick
Boundaries — upper	distinct or gradational	distinct and gradational
— lower	distinct or gradational; may be stylolite accentuated	distinct planar, may be stylolite enhanced
Relationship to host	conformable sheets; comformable or cross-cutting pods	conformable or crosscutting or a combination
Breccia texture	grainstone, 'floating clast' wackestone, packstone	wackestone
Matrix	cement (fibrous and equant calcite fabrics, megaquartz, quartzine, chalcedonite); silt, siliciclastic and relict carbonate particles.	calcite, crushed cement fragments and insoluble residues from solution
	30–40 percent	40–100 percent
Associated features	sulphate pseudomorphs in host rock	moldic porosity of grains; authigenic K feldspar; authigenic euhedral quartz; quartzine.
Mechanism of formation	cavity formation — dissolution of the more soluble sulphates produces cavities which are partly or totally infilled by partly collapsed material.	"continual settling" — developing grain moldic porosity weakens the rock to the point of structural failure and collapse.

adjustment of the host rock by settling precluded cavity formation, retained lithostatic pressure, and hence clast margins developed into stylolites. Subsequent stylolite formation has modified the earlier fabrics and in B type breccias the earlier features may be totally obliterated.

Dolomitisation has been controlled by stylolitic features, and has commonly been selective in its replacement of the breccia matrix. The selectivity has been enhanced by the relative resistance of the dolomite to solution. There is an apparent continuum from collapse to purely stylolitic fabrics in which evidence of the initiating processes has been completely overprinted.

Type A stratiform breccia is similar to those described by Middleton (1961), having distinct lower contacts and gradational upper contacts that enclose oligomictic, rotated clasts in a fine-grained, iron-stained matrix. Middleton (1961) proposed solution of interbedded sulphates at the base of these zones as the cause of cavity formation. Breccia formation by sulphate solution has been implied from evidence of former sulphates in the host (Blount & Moore, 1969; Friedman & Sanders, 1978) and the surface morphology of some clasts that show pseudomorphs of sulphate crystals (Fig. 3A)

Solution of bands of sulphate in a partly or wholly lithified rock resulted in sheet-like cavities, in which fragments of host rock

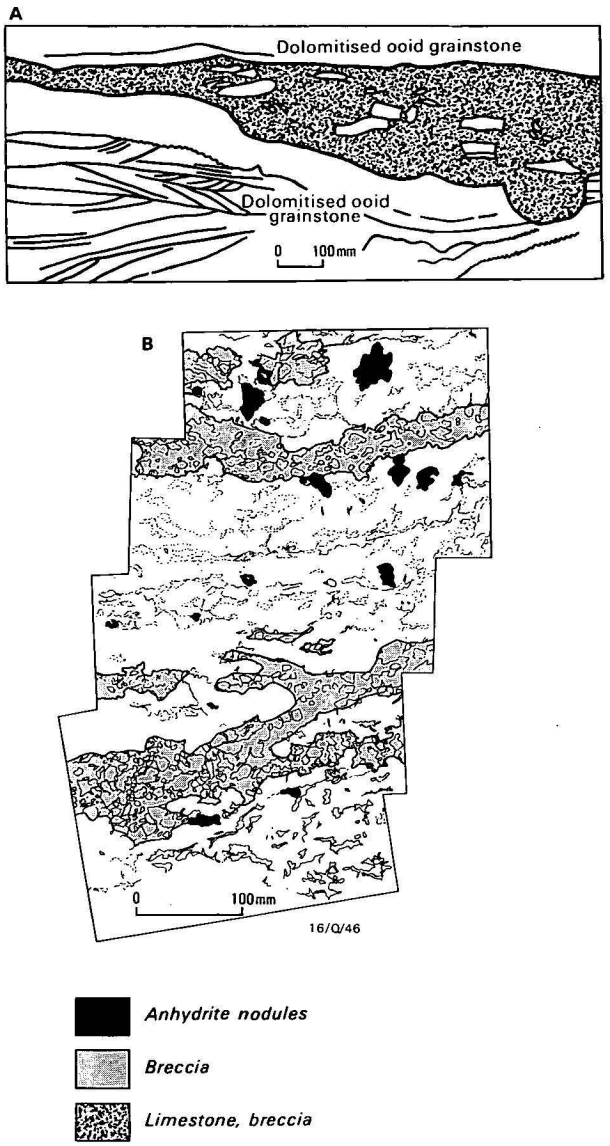

Figure 2. Stratiform breccias.
A — Segment of a stratiform solution cavity (stippled) in a dolomitised, cross-stratified ooid grainstone. The cavity has sharp, planar, and irregular contacts. It is now filled with angular and rounded clasts in a matrix of pisolitic to peloidal carbonate. B — Semi-stratiform breccia in a bioturbated peloidal wackestone–mudstone host. Silicified anhydrite nodules occur in the host rock, but not in the collapse-breccia zone. Figure 3A shows the texture of this breccia. Scale is 10cm.

collapsed and geopetal structures developed by accumulation of insoluble residues. Where the amount of sulphates was insufficient for solution to cause collapse, their moulds were preserved by later calcite growth. In cavities with large pore space, laminar stalactitic cements of calcite were precipitated and, in places, replaced by quartzine. Such features have been reported in modern speleothems by Broughton (1973). Voids may also be filled with alternating layers of chalcedonite and quartzine (Fig. 3C), suggesting fluctuating sulphate content in the precipitating fluids. Traces of the more insoluble sulphates, baryte and celestite, may be present in the residual matrix of

Figure 3.
A — Oligomictic collapse breccia in bioturbated thrombolitic limestone. The breccia exhibits a stylolite-enhanced, close-fitted fabric. The matrix is dolomite and dedolomite. Crystal outlines (co) on some clasts indicate former sulphates. Specimen 79712617. B — Wackestone texture in breccia with clasts of ooid grainstone. Clasts have shard-like surfaces of oomoldic outline. The matrix consists of siliciclastics, dolomite, and crushed calcite cement. Photomicrograph, plane-polarised light; 74712658; 1-mm bar scale. C — Isopachous cement of alternating quartzine (q) and chalcedonite (ch) lining the wall of calcite speleothems. Photomicrograph, crossed polars; 74712318; 1-mm bar scale. D — Open-framework collapse breccia with dedolomite clasts, interbanded geopetal detritus (d) and saddle dolomite crusts (sd). 74712750; 1-cm bar scale. E — Breccia in dolostone, comprising dolostone and galena (g) clasts, saddle dolomite and silcrete cements. Galena clasts have oxidised rims (ox). 74712755; 1-cm bar scale. F — Replacement calcite (c) within the basal core of a saddle dolomite crystal (sd). Replacement by calcite has been controlled by cleavage traces within an apparently unstable zone of the crystal. Photomicrograph of cathodoluminescent image; 74712750; 1-mm bar scale. G — Saddle dolomite cement (sd) encrusted with non-ferroan stalactitic calcite (sc) which has recrystallised (rc) in optical continuity with the saddle dolomite substrate. Photomicrograph, crossed polars; 74712337; 1-mm bar scale.

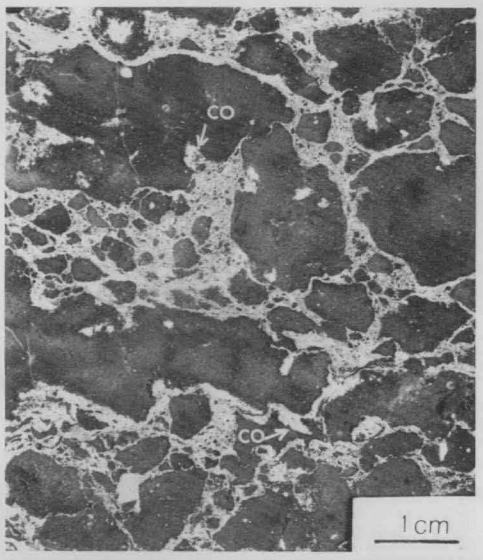

A

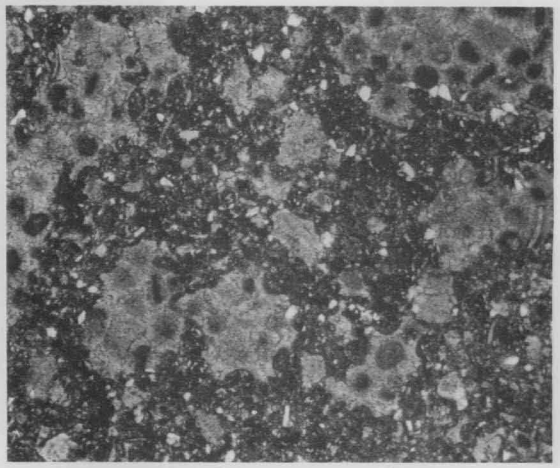

B

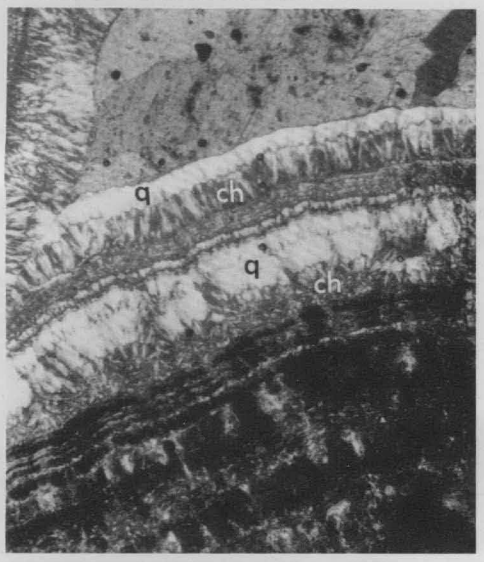

C

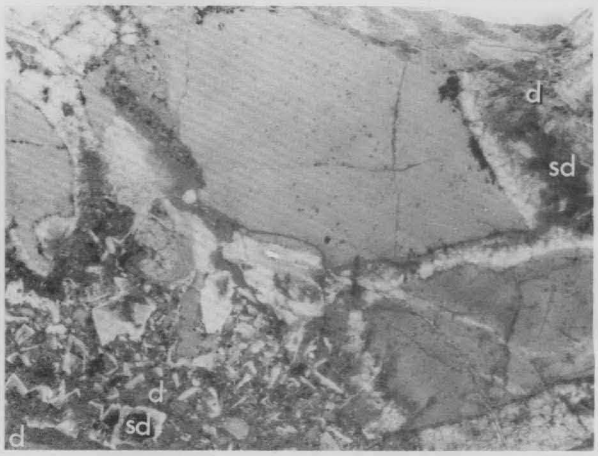

D

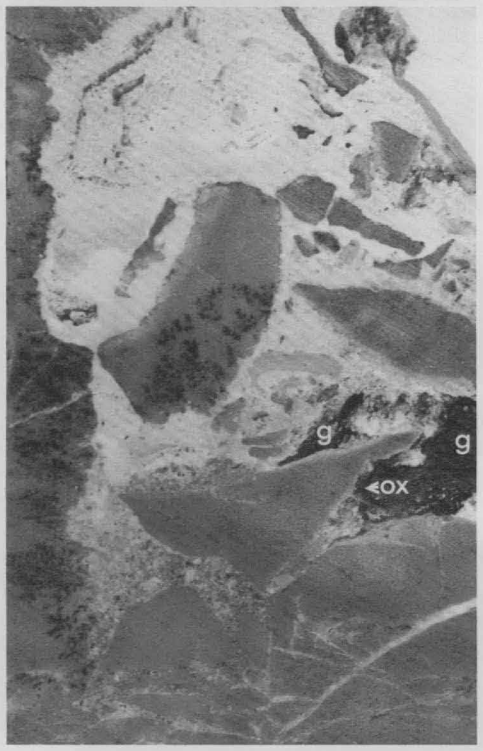

E

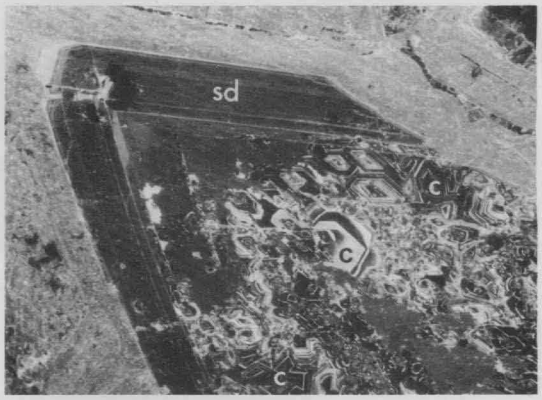

F

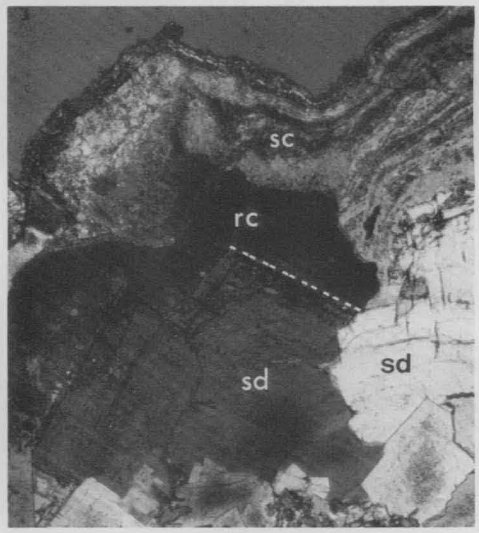

G

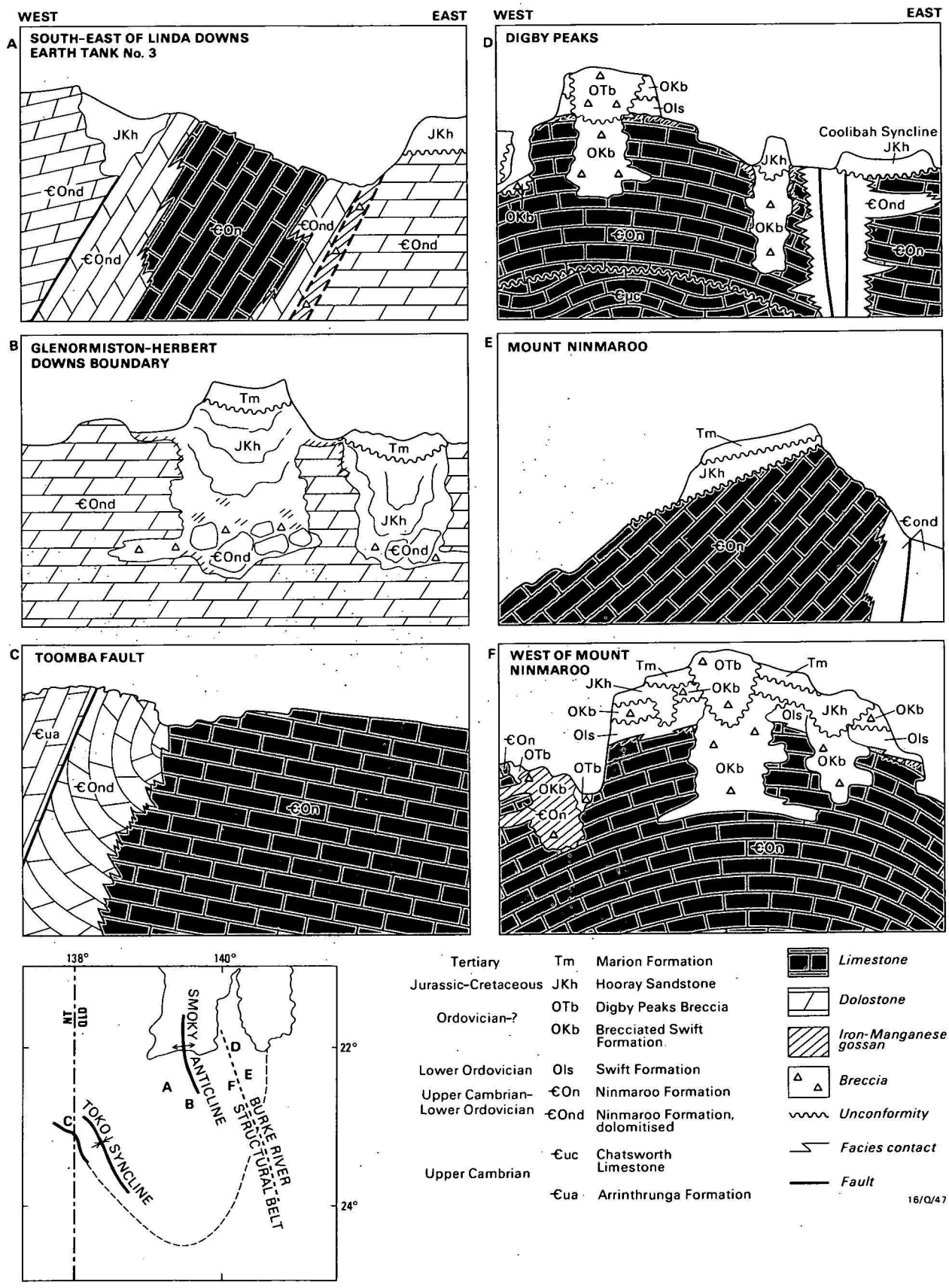

Figure 4. Stylised structural and stratigraphic settings of the Ninmaroo Formation.

the breccia and these also indicate the earlier presence of other sulphates.

With early sabkha precipitates (Radke, 1980), silica replacement of the sulphate commonly preceded sulphate solution. When the host limestone was later preferentially leached, insoluble crystal pseudomorphs accumulated as a condensed residue. Continued solution of sulphates may lead to further brecciation of the host rock (Middleton, 1961).

Type B breccia is the product of extensive moldic porosity. Half-moon ooids may have been precursors of this feature. In zones of significant moldic porosity, the relict cement rims enclosing the porosity collapsed, probably when overburden pressures exceeded structural strength (Rees & others, 1976; Conley, 1977).

The collapse occurred in planes parallel to bedding, or oriented according to the packing and size of the original particles (Conley, 1977, figure 8). Breccia clasts were produced where the planes of collapse had an intersecting fabric, and the clasts had planar faces with predictable angular relationships. These faceted clasts have a superficial appearance to crystals. The fragmented rim cements became a clast-supporting matrix of crushed crystals and shards (Fig. 3B) with other insoluble residues.

Development of moldic porosity, collapse, and production of matrix was a continuing process, which increased matrix abundance and reduced the size of the clasts. In contrast to the cavity-forming processes in the formation of type A breccia, small moldic cavities were destroyed by collapse and crushing. Stylolite formation was common in the matrix, along matrix–clast boundaries, and on the boundaries of the breccia body.

Nodule and crystal pseudomorphs of sulphates are relatively common in ooid grainstones, and quartzine replaces clasts. Collectively, these are evidence that the breccias originated with the solution of sulphates.

Discordant breccias

Discordant breccias occur along fault zones and joints, and in dolines. They are most common in dolostone, but are also present in limestone and chert. They are poorly exposed and, consequently, are not as well understood as stratiform breccias.

The breccia bodies are discordant with bedding, but conformable on a large scale with faults, joints, and dolines. Locally, the contact with the host rock may be irregular, or gradational with type A stratiform breccia (Fig.4A,B,F). In dolines and solution-enhanced joints, several breccias may be superimposed with the youngest commonly placed centrally and cutting across older breccias (Fig. 4F).

This breccia is predominantly monomictic with packstone texture, but texture is variable. Clasts are mostly angular with equant to irregular and elongate shapes, variably sized from centimetre to decimetre scale and possibly larger. Clast composition is that of the host rock: dolostone, limestone, chert, or sandy carbonate. The sorting is poor, but variable. Matrix is also variable, from dolomite crystal silt, dedolomite, siliciclastic silt to chalcedonic insoluble residues. Interclast spaces may be incompletely filled, but interparticle and shelter porosities are generally occluded with coarse saddle dolomite, poikilotopic calcite, goethite masses, and calcitic or chalcedonic stalactitic cements (Fig. 3C). Crystalline precipitates may be interlaminated with the geopetal silts (Fig. 3D). Traces of sulphides or oxidised remnants are ubiquitous as voidfill and replacement of matrix. In rare instances, the sulphide is reworked as discrete clasts, such as at the Noranside Lead prospect (Fig. 3E). Most exposed breccias are oxidised and, commonly, only ferrous and manganiferous sesquioxide cements remain.

Discussion. Discordant breccias are attributed to tectonism and solution-collapse events. Tectonic brecias are recognised by their distribution along faults: they are generally tabular and have one abrupt margin against the fault (Fig. 4E) (rarely exposed) and the other transitional, through a narrow zone of intense fracturing or foldingor both, into the host rock. The breccias formed during movement on the fault, but timing is difficult to ascertain.

Discordant solution-collapse breccias are recognised by their shape, which usually conforms to solution-enlarged joints, caverns, and dolines. Frequently, they have shelter porosity and interlamination of matrix and cements, indicating filling of an open space. Localisation of dolines and caverns may be controlled by structure, such as joint intersections and faults (Fig. 5), or selective solution of rock type. Although sulphates were present in the sequence, it is often difficult to link discordant breccias with sulphate solution.

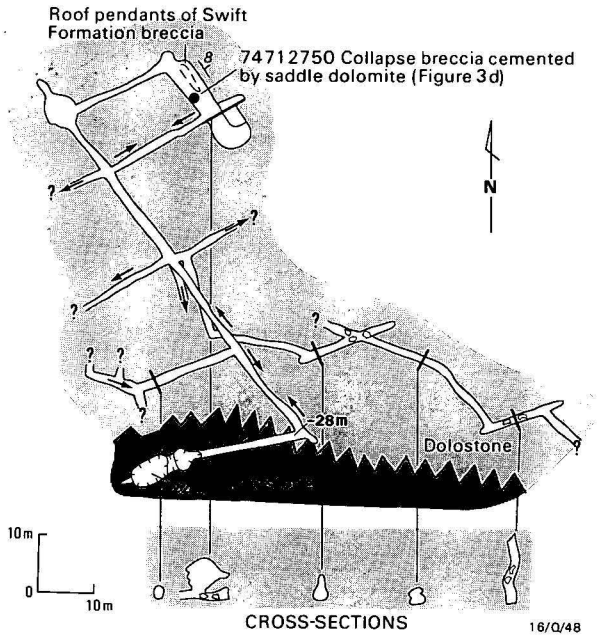

Figure 5. Joint-controlled cavern system with solution-collapse breccias of several generations, including recent breccias that are forming from host rock and indurated breccias. 4.5 km west of Digby Peaks.

Figure 6. Variable late diagenetic paragenesis in a porous limestone.
A — This example is a flat-pebble conglomerate with solution-enhanced shelter porosity. B — Tectonic fracturing of the rock enhanced hydrocarbon migration. Hydrocarbons were trapped in blind processes within the shelter porosity. C — Calcite spar nucleated on water-wet surfaces of the host. D — An advanced stage of cement sealing in hydrocarbons, as seen in some surface exposures of domal structures. E — Saddle dolomite, sulphides, fluorite, and minor calcite nucleated on water-wet surfaces in close proximity to hydrocarbons. F — Total occlusion of water-saturated areas. Fluorite has also partly replaced the host limestone. G — Weathered limestone with lost hydrocarbons and subsequent calcite voidfill, oxidation of pyrite to goethite, and consequent dedolomitisation of saddle dolomite. Iron and manganese have exsolved from the dolomite lattice as sesquioxide inclusions in the replacement calcite. H — In areas of minimal hydrocarbon accumulation, host rock was dolomitised with associated minor pyrite replacement. Sphalerite precipitated as pendant cements and pyrite formed geopetal layers. Calcite and saddle dolomite cementation followed. I — Stylolites follow former porosity zones. Bitumen, sulphides and large carbonate crystals are preferentially preserved. Calcite occlusion of remaining porosity in tensional veins is ubiquitous.

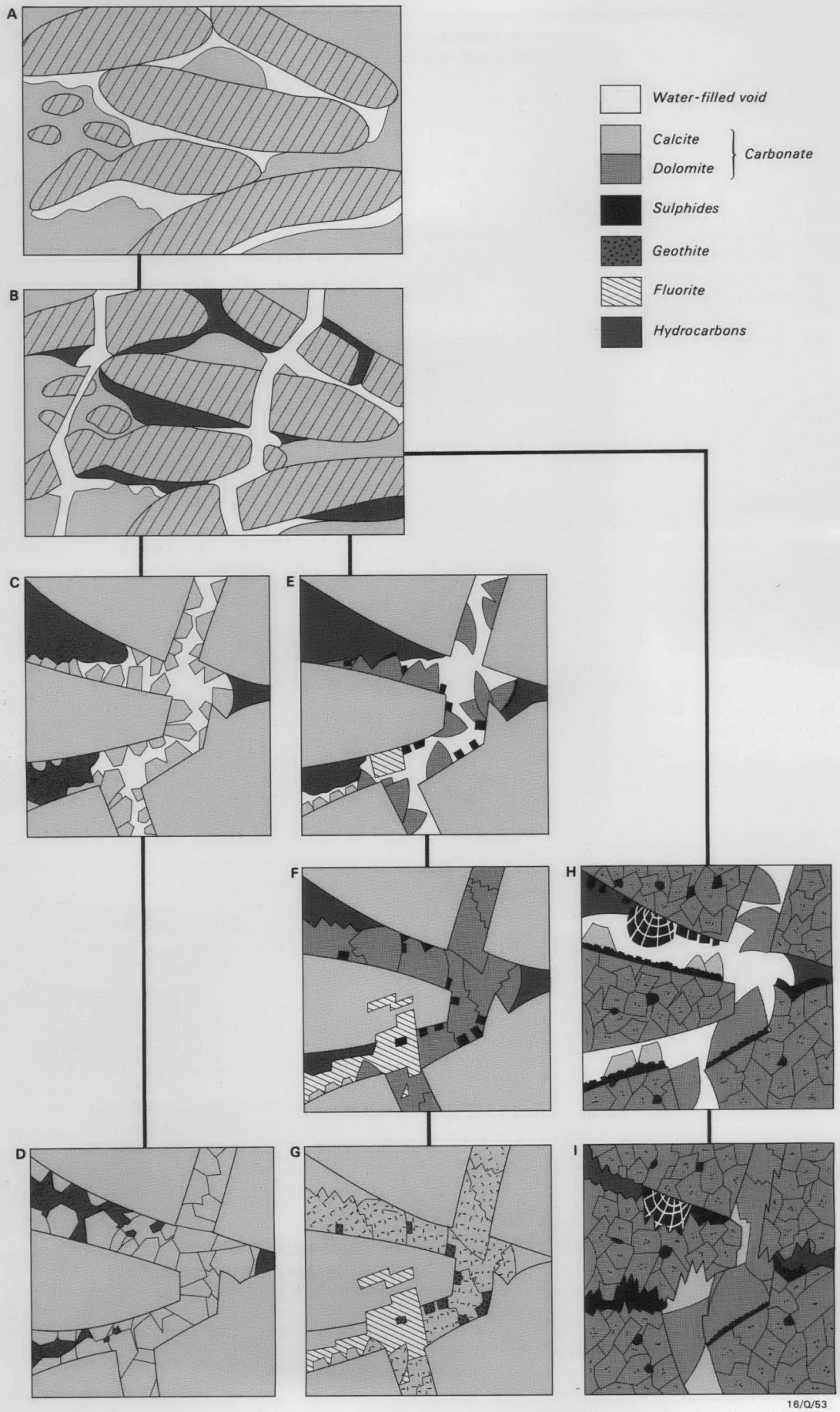
A
B
C
E
F
H
D
G
I
Water-filled void
Calcite
Dolomite
Carbonate
Sulphides
Geothite
Fluorite
Hydrocarbons
16/Q/53

Solution-collapse breccias first developed when solution was lithologically selective. Later carbonate solution apparently continued for a long time, controlled by structure and rock type, and produced several generations of breccia (Fig. 4F). Regional geology indicates that brecciation began in the Palaeozoic and continued through Mesozoic to post-Tertiary times.

Calcite

Authigenic calcite is the most abundant void-filling and replacement mineral (Figs. 6, 7). Several microfabrics predominate as void-fill and are also present as replacement phases: drusy spar, blocky poikilotopic calcite, stalactitic fringes, and microcrystalline cements.

Drusy spar (Bathurst, 1958; Orme & Brown, 1963) is a common non-ferroan calcite with characteristic increasing crystal size away from particle surfaces into void centres. The initial drusy cement usually is non-ferroan, but commonly grades into ferroan calcite. Drusy spar is most common in grainstones, as a continuous or intermittent cement filling porosity.

Blocky poikilotopic calcite (Evamy & Shearman, 1965; Davies, 1971) is a common cement occluding moldic porosity. It is also a replacement phase after sulphate, silica, aragonite, and dolomite (as dedolomite). Coarse calcite pseudospar of generally equant shape and variable size has curved, crenulate, or straight boundaries. The spar is generally clear, but may contain patches of tiny rounded crystals of birefringent minerals (probably dolomite), which impart a clouded appearance to the calcite. The inclusions commonly outline curved crystalline forms suggestive of saddle dolomite or gypsum precursor. This microfabric is apparently synchronous with and also postdates hydrocarbon inclusions.

Stalactitic or fibrous calcite is a common microfabric in macro-cavern porosity, and in the vug porosity of dolostones. It is rare in bituminous limestones, where it fills only the sites of previous hydrocarbon occlusion and commonly forms geopetal cements overlying drusy or poikilotopic calcite. In dolostone, stalactitic fringes are commonly not isopachous, but form pendants. This microfabric is most abundant in cavern porosity, forming a variety of speleothem forms, and is commonly interbanded with chalcedonic and gypsum cements.

Microcrystalline calcite (micrite) (Folk, 1959) has an equigranular texture with crystals less than four micrometres diameter, producing an aphanitic mesoscopic appearance. As a void-filling precipitate in calcretes, its chemical origin is recognisable by its nonconformity to geopetal structures, and may have crude lamination imparted by colour or varying distribution of siliciclastic silt particles. It forms a crust on indurated surfaces, occurs in fractures and breccias, and may be gradational with replacement microfabrics. Replacement micrite is most common in bituminous variegated ('two-tone') limestones.

Pseudomorphs of dolomite. Calcite pseudomorphs of dolomite are either single crystals or calcite mosaics. Single crystals are either spear-shaped with curved faces (Fig. 6G), or rhombs that are turbid with inclusions of iron sesquioxides (Shearman & others, 1961). The curved faces and bands of inclusions indicate a precursor of saddle dolomite. The replacement calcite is non-ferroan, but may retain undulose extinction, also characteristic of saddle dolomite. Replacement of the dolomite begins on the crystal margins especially on the oldest surfaces, and along cleavage planes (Fig. 3F). The replacement front is commonly defined by a rim of opaque iron sesquioxides. Within the replaced zone, small irregular inclusions of the oxides are generally concentrated along the cleavage and may be either randomly scattered throughout the calcite or concentrated in distinct growth bands.

In some dolostones, vugs after sulphates are encrusted with euhedral saddle dolomite crystals that commonly include non-ferroan calcite growth bands in the younger zones of the crystal. These calcite bands or 'frames' are generally uniform in thickness and syntaxial with the enclosing dolomite, a feature described by Zenger (1973). Alternatively, the dolomite–calcite contact is irregular with solution features defined by a thin discontinuous layer of opaque oxides. The calcite may or may not be syntaxial. Where it is syntaxial with the host, the calcite commonly has fine, irregular stalactitic growth laminae, indicating that the originally fibrous calcite recrystallised in crystallographic continuity with the dolomite (Fig. 3G).

Pseudomorphs after dolomite may also be recognised as rhombs containing xenotopic equant calcite. This may be either lucid and subhedral, or anhedral with small inclusions that impart a dusty appearance. Small rhombic forms are commonly concentrated in sedimentary laminae. The bands comprise calcitic rhombs in a dark matrix of iron sequioxides and insoluble residues that have been concentrated by stylolite formation. They emphasise the sedimentary laminae, being yellow, orange, or red, which is distinctively different from the host, and have been described in the field as 'two-tone' limestone (Brown, 1961, Radke, 1980).

Discussion. Calcite has precipitated as both cement and replacement mineral. Drusy spar is predominantly an early cement, indicating phreatic conditions, but also precipitated later, when blocky poikilotopic calcite was both a cement and replacement phase. Fibrous calcite is both an early and late diagenetic fabric. Early acicular aragonite cements were replaced by this fabric. Stalactitic calcite is considered indicative of waterfilm precipitation (Kendall & Broughton, 1978), a common event under vadose coditions. Microcrystalline calcite was of a similar origin, but was not common.

Replacement of dolomite by calcite was originally described and termed dedolomitisation by von Morlot (1847). The textures described above were recognised using the criteria of Shearman & others (1961). Dedolomitisation results from the incongruent solution of dolomite at low P_{CO_2} (Yanat'eva, 1955). This solution is enhanced in the presence of waters with initially high Ca^{2+}/Mg^{2+} ratios and sulphate, which is mostly produced by solution of gypsum (Yanat'eva, 1955), anhydrite (Lucia, 1961), or the oxidation of pyrite (Evamy, 1963). The consensus is that dedolomitisation is a near-surface weathering process and generally indicative of unconformities (Schmidt, 1965; de Groot, 1967; Evamy, 1967; Friedman & Sanders, 1967; Goldberg, 1967; Moore, 1971). Most calcite produced by this process from ferroan dolomite has iron sesquioxide inclusions along growth bands or scattered throughout. During leaching of magnesium, the reduced iron was oxidised and remained as sesquioxide inclusions.

During deposition of the Ninmaroo Formation, when conditions were intermittently evaporitic and emergent, environments existed where replacement of protodolomite could have occurred. The majority of dedolomite replaces coarsely crystalline dolomite. Dedolomite after finely crystalline dolostone is difficult to attribute to either early telogenetic or late telogenetic origins.

Cainozoic dedolomitisation can be inferred from evidence of fluctuations in groundwater sulphate in a Tertiary–Holocene cavern system within massive dolostone and dedolomite. There

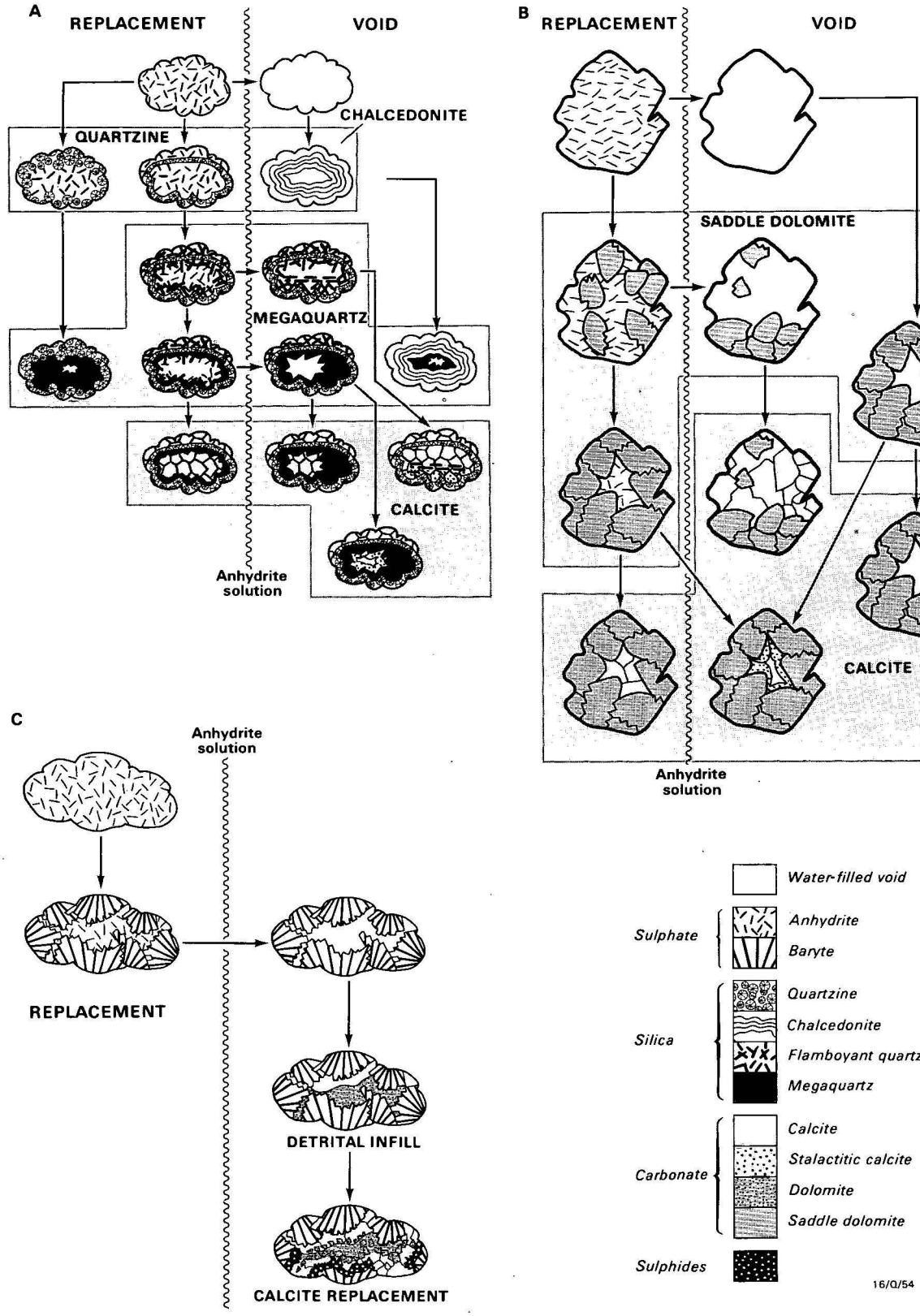

Figure 7. Alteration of sulphate nodules by replacement, solution, and void-filling processes (after Radke, 1978).
A — Anhydrite nodule altered with replacement and void-filling by silica and calcite. The replacement trend was initially by chalcedonic quartz, then megaquartz and, finally, calcite. Of the chalcedonic quartz, quartzine was the dominant replacement phase and void-filling was by either chalcedonite or quartzine. Quartzine void-filling is dependent on sulphate-rich pore waters. B — Anhydrite nodule with replacement or void-filling, or both, initially by saddle dolomite and then calcite or fluorite. Geopetal features were produced where sulphate was dissolved after only partial replacement. C — Anhydrite nodule partly replaced by baryte splays before solution of remaining anhydrite. The cavity was filled by detrital dolomite and clay, with subsequent authigenic dolomite. Late sulphate reduction of baryte produced a pyritic rim against the replacement calcite.

is patchy replacement by spherulitic quartzine of speleothem cements in the caverns. Quartzine replacement of gypsum has been described in modern calcitic speleothems by Broughton (1973). The silica cements consist of alternations of chalcedonite and quartzine (Fig. 3C), which may indicate fluctuations of sulphate content in the precipitating waters (Folk & Pittman, 1971).

Dolomite

Dolostone is a major rock type in the Ninmaroo Formation, and its distribution is structurally controlled. In the central Smoky Anticline region, the sequence is flat-lying and consists mostly of dolostone with only local interbeds of light dolomitic limestone. In the Toko Syncline and the Burke River Structural Belt, where the sequence is folded, bituminous limestone is dominant in the tops of structures. These are exposed within breached domes (Fig. 8A,4). Dolostone is ubiquitous along cross-cutting faults, in less-folded strata, and on the lower flanks of the major anticlines. Steeply dipping fault blocks also contain cores of bituminous limestone, enclosed in dolostone that adjoins the confining faults (Fig. 8B). The dolostone occurs in three ways: as laminar and mottled dolomitic limestone, stratiform dolostone, and massive/void-filling dolostone. These may grade into one another or be superimposed, and may not always be distinguishable.

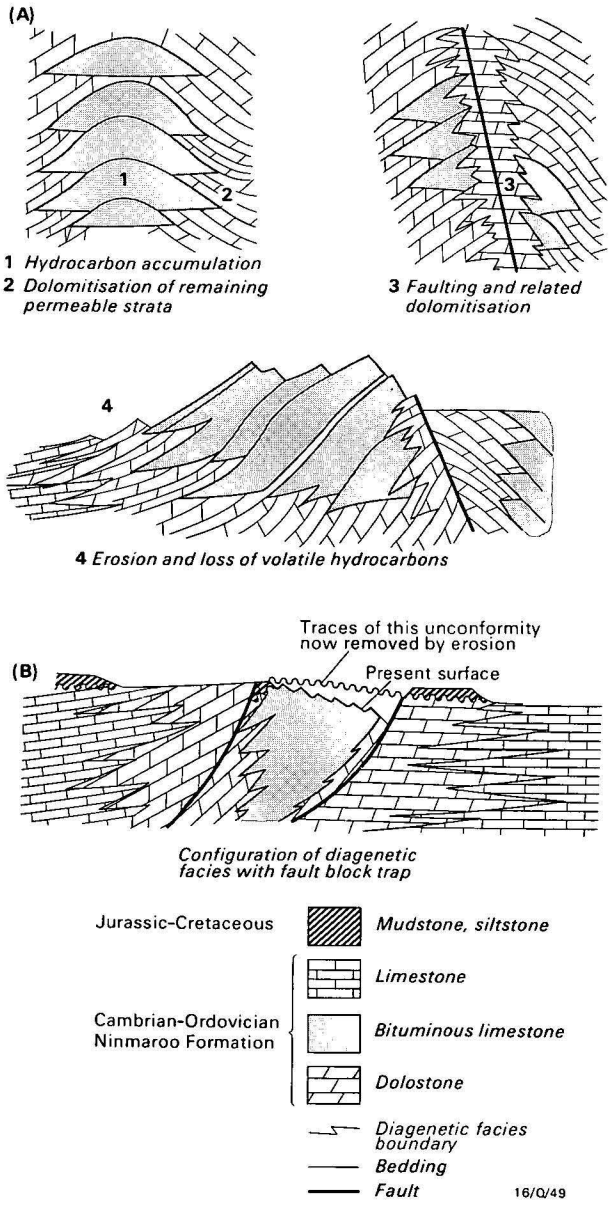

Figure 8. Structural and hydraulic control of late diagenetic facies. A — Development of faulted and dolomitised domes. During brine migration, hydrocarbons accumulated in structural traps (1). Hydrocarbon-saturated areas were excluded from aqueous interaction and, hence, dolomitisation while adjacent strata were subsequently dolomitised by interaction with the brines (2). Later faulting disrupted the structural traps, providing a conduit for hydrocarbon escape and further dolomitisation by brines migrating up the fault (3). With erosion and breaching of these traps, hydrocarbons escaped and much of the remaining porosity was occluded by telogenetic calcite cements (4). B — In fault blocks with steeply dipping strata, the core may contain relict hydrocarbons after erosion. The confining faults have influenced dolomitisation, whereas in flat-lying strata this stratiform replacement has been more varied.

Laminar and mottled dolomitic limestone. Many variegated or 'two-tone' limestones (Brown, 1961) have enhanced structures from partial dolomitisation. Dolostone laminae may be all or partly dolomite, which occurs as euhedral rhombs (0.1-1 mm) with small, clouded subspherical centres and clear outer rims. They have higher concentrations of fine siliciclastic sand than the adjacent host limestone. Stylolites, if present, occur in and adjacent to the dolostone laminae. The dolomite may be dedolomitised and stained yellow, orange, or red. Although dolostone laminae in limestones commonly coincide with sedimentary laminae and structures, they may also be discordant and follow small-scale fractures and stylolites. Mottling enhances many sedimentary features such as bioturbation (Fig. 9A), shrinkage cracks, cryptalgalaminites, and sulphate nodules, as well as later diagenetic inhomogeneities from patchy cementation and pressure-solution.

Stratiform bedded dolostone. Stratiform dolostone is commonly interbedded with limestone in flat-lying strata. It is generally structureless, but relict sedimentary structures are poorly preserved in places. Crystal size of the dolomite is variable, but commonly follows the particle size of the limestone precursor. Dolomite crystals are up to millimetre-sized, subhedral to anhedral, and 'dusty' with numerous small fluid inclusions concentrated in crystal centres. Clear euhedral rims occur on crystals that face into voids. The dolostones commonly have intercrystalline porosity, but this may be occluded by calcite or diagenetic clays. Moldic porosity after sulphate nodules and mesogenetic sulphate crystals (Fig. 9B) is sometimes present.

This dolostone type is dominant throughout the Smoky Anticline region and on eastern and western margins of the Toko Syncline. It is common in the exposed Datson and Corrie Members in the Burke River Structural Belt. Scattered beds occur throughout the sequence, with lesser amounts in the central Toko Syncline. Light-coloured limestone interbedded with such dolostone in less-deformed strata contrasts with the occurrence of bituminous limestone structurally higher in folded and steeply dipping strata.

Massive and void-filling dolostones. These are related in that they consist of mainly saddle dolomite in replacement and void-filling modes, respectively. Saddle dolomite is characterised by its turbid appearance, undulose extinction, and curved crystal faces and cleavage (Radke & Mathis, 1980).

Replacement saddle dolomite forms massive dolostone (Fig. 9C) in irregular bodies adjacent to and along fault zones, and crude stratiform bodies interbedded with limestone. It is porous and has a coarsely crystalline isotropic fabric of millimetre-sized subhedral crystals. The porosity is from solution-enlarged moulds after a soluble mineral, most probably anhydrite. Both bodies have gradational contacts with the host carbonate, where saddle dolomite selectively replaces original particles rather than cements. In the massive saddle dolomite, relict precursor crystals and particles are evident from inclusion

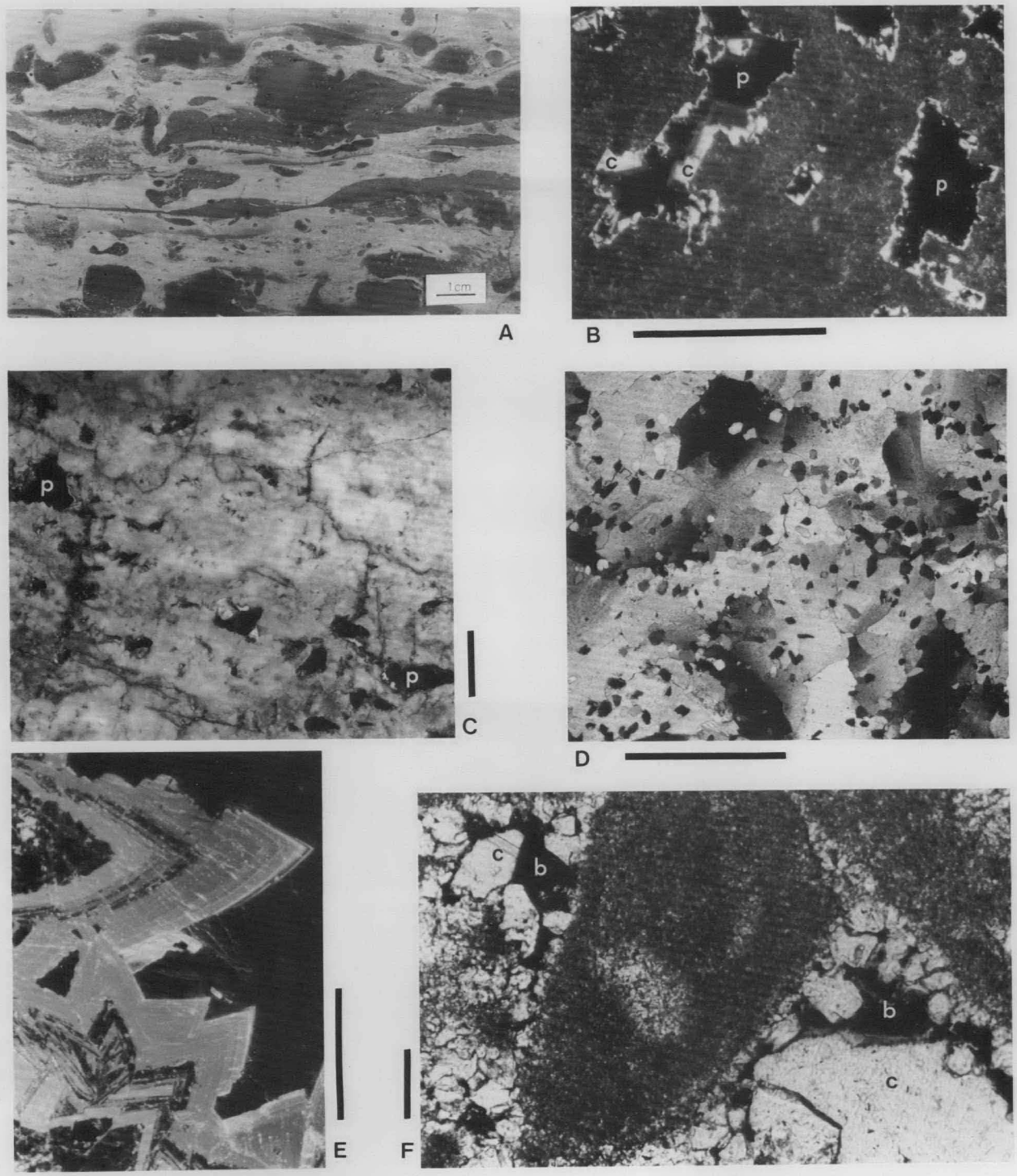

Figure 9.
A — 'Two-tone' bioturbated mudstone showing stylobedding and stylonodular structures emphasised by dedolomitisation of reactate in host limestone. Rock slab; 74712267; bar scale 1 cm. B — Moldic porosity (p) partially occluded by calcite spar (c). Moulds in the dolostone suggest former sulphates. Photomicrograph of cathodoluminescent image; 74712516; 1-mm bar scale. C — Coarsely-crystalline and turbid saddle dolomite with irregular, solution-enhanced moldic porosity (p) that is partly occluded by calcrete. Dolomitised fault zone. 74712591; 1-cm bar scale. D — Poikilotopic fabric of replacement saddle dolomite with scattered siliciclastic particles. Photomicrograph, crossed polars; 74712428; 1-mm bar scale. E — Saddle dolomite cement in a solution vug. Note spear-shaped outline, curved faces, and cleavage. Photomicrograph of cathodoluminescent image; 74712732; 1-mm bar scale. F — Bitumen (b) occluding interparticle porosity in a clast grainstone. Calcite spar (c) is unevenly distributed. Larger crystals on the lower surfaces of the porosity indicate that hydrocarbons were present during much of the cementation phase. Photomicrograph, plane-polarised light; 74712615; 100-cm bar scale.

patterns. Detrital quartz and feldspar with euhedral authigenic rims are commonly enclosed in the large poikilotopic dolomite crystals (Fig. 9D).

The dolomite is a void-filling cement in a variety of pore types: vein (late-forming), fracture, cavern, collapse-breccia, moldic after sulphate nodules (Fig. 7B), and shelter porosity on the undersides of flat pebbles (Fig. 6E, F) and large skeletal particles. It is in millimetre-sized subhedral to euhedral crystals with characteristic curved faces (Fig. 9E). Saddle dolomite is commonly an early cement and total occlusion of porosity is by a combination of contemporaneous ferroan and nonferroan calcite, fluorite, baryte, pyrite, sphalerite, or galena. In outcrop, the mineral is commonly completely or partly dedolomitised and opaque orange to deep red.

Discussion. In the laminar and mottled dolomitic limestone, most primary features, apart from bioturbation, indicate hypersaline to evaporitic conditions (Logan, 1961; Kendall & Skipwith, 1968; Logan & others, 1974; Friedman & Radke, 1979), the probable environment of penecontemporaneous dolomite formation. Such dolomitisation of fine-grained carbonates has been linked with hypersaline conditions in lagoons (Alderman & Skinner, 1957; Deffeyes & others, 1965), general hypersaline conditions (Friedman & Sanders, 1967; Folk & Land, 1975), and, more specifically, to the supratidal zone (Shinn & others, 965)) and the peripheral belt of sabkhas (Butler, 1969; Kinsman, 1969).

'Two-tone' laminae and mottling are characteristic features of the Jiggamore Member, and are also common in the Unbunmaroo and Mort Members of the Ninmaroo Formation (Radke, 1981). The original abundance of this dolomite, although thought to be minor, is unknown because it has been modified by additional dolomite overgrowths, dedolomitisation, and pressure solution.

The distribution of bedded dolostone, light-coloured and bituminous limestone across various structures indicates an inverse relation between relict hydrocarbon content and the proportion of dolostone in the sequence. One interpretation (Fig. 8) is that hydrocarbons were trapped in suitable structures and isolated the host carbonates from migrating connate fluids, which caused subsequent dolomitisation in other porous beds. Ubiquitous large idiotopic crystal moulds that cut across dolomite textures in these dolostones (Fig. 9B) indicate that sulphates were at some stage also precipitated from these brines. This model also explains the dolostone distribution near the Zelten Oilfield in Early Tertiary carbonates of Libya, as documented by Bebout & Pendexter (1975). The oil pool is confined by water to porous limestones within a broad structure. A thick dolostone facies occurs off the structure and pinches out under the oil pool, with its upper boundary paralleling the oil–water contact. Bebout & Pendexter considered the origin of the dolomite questionable, but proposed two models: an early diagenetic facies-controlled process and one of late diagenetic dolomitising fluids, although no reference was made to an existing hydrocarbon body.

In the massive and void-filling dolostone, saddle dolomite is thought to have precipitated from warm (50-150°C), saline, mesogenetic water under mild to strongly reducing conditions (Beales, 1971; Choquette, 1971). Scant fluid inclusion data from Ninmaroo Formation material suggests temperatures above 100°C. The dolomite precipitated contemporaneously with hydrocarbon accumulation (Mathis, 1978) and sulphide precipitation (Beales, 1971; Choquette, 1971; Dunsmore, 1973; Ebers & Kopp, 1979, Radke & Mathis, 1980). Traces of methane and ethane in fluid inclusions of saddle dolomite confirm the contemporaneous events (Shearman, Imperial College, London, personal communication, 1979). Passive replacement of host limestone supports the conclusion of Choquette (1971) that much of the carbonate for saddle dolomite replacement is of local origin.

Fluorite

Fluorite is a trace mineral in bituminous limestone and dolostone. It occurs both as replacement and void-filling phases, in three forms: as small poikilotopic cubes under syndepositional indurated surfaces, and as both voidfill of secondary porosity and replacement.

The small fluorite cubes are colourless, light-yellow, or purple, millimetre-sized, and enclose small euhedral dolomite rhombs. They occur in concentrations of up to 5 per cent in finely crystalline laminar dolostone, which also hosts eogenetic chert nodules. In chert nodules underlying erosion surfaces, replaced fluorite is discernible as relict poikilotopic forms. Small (1 μm spheres or rod shapes up to 3 μm long) and large fluid inclusions are abundant in the fluorite, and concentrated slightly along cleavages. Both types have low relief. Larger inclusions are irregular to elongate angular forms, about 30 μm long, with a slightly higher relief. Rare earth concentrations in the fluorite are low: Y,7 ppm, Ce and La, 5 ppm.

Other fluorite occurrences. Fluorite is commonly an interstitial void-filling mineral, where it forms anhedral crystals, 0.1–30 mm across. As a replacement of host limestone, it forms euhedral crystals, 0.08–2 mm across (Fig.6G).

Both void-filling and replacement fluorite are amber yellow in dolostones and purple in bituminous limestones. Purple coloration is normally inhomogeneous and concentrated in cleavage-controlled patches, which have wispy gradational margins. Yellow fluorite may also have patches of purple, but these are small and occur only near the crystal faces. Fluid inclusions occur similarly to those in the small cubes discussed above.

In bituminous limestone, fluorite occurs in peloid, flat-pebble, and ooid grainstones, and domed cryptalgal boundstones. It is present as a void-filling mineral associated with ferroan calcite, saddle dolomite, baryte, and pyrite. It can predate or postdate these minerals. It is present in secondary dilatational veins and fractures, solution-enlarged joints, and solution vugs resembling sulphate moulds. Such vugs are common in the flat-pebble conglomerates on the undersides of the pebbles or at points of contact between pebbles.

In dolostone, yellow fluorite and saddle dolomite occlude solution vugs after spheroidal sulphate nodules. In this occurrence, rare earths have higher concentrations; Y,56 ppm, Ce,129 ppm, La,4 ppm.

Discussion. Small fluorite cubes are considered eogenetic because of their replacement by early chert (Radke, 1978) and low rare earth content. The host sediment prior to dolomitisation and silicification was most probably highly aragonitic. Fluorine concentration in marine aragonitic sediments is variable, but may be as high as 1600 ppm (Carpenter, 1969). Fluorine rarely exceeds 100 pm in dolomite (C.H. Moore, University of Louisiana, personal communication, 1977) as it is less readily accommodated in the dolomite lattice. Thus, during dolomitisation of an aragonitic sediment, such as in marginal sabkhas (Butler, 1969), fluorine liberated from the aragonite, but not incorporated in the dolomite, is precipitated as fluorite (Moore & others, 1972). This is analogous to the formation of celestite during the dolomitisation of aragonitic sediments in the same setting (Kinsman, 1969).

The evidence for late diagenetic emplacement of fluorite is its filling of fractures that were contemporaneous with the development of large-scale folding, and its coprecipitation with ankeritic saddle dolomite, which is indicative of higher-temperature formation.

Yttrium concentrations of above 90 ppm in fluorite are thought to indicate high temperature and an igneous source, whereas lower concentrations are characteristically, though not unequivocally, from deposits of Mississippi Valley type (Smith, 1974). Its concentration in void-filling fluorite in the Ninmaroo Formation (56 ppm), is, consequently, compatible with a Mississippi Valley type model. Smith (1974) documented fluid inclusion studies that suggested fluorite precipitation in a North Pennine orefield was from brines in a temperature range of

119–210°C. Bailey & Cameron (1951) and Freas (1961) proposed that brines at 75–130°C were associated with the formation of fluorite in upper Mississippi Valley deposits. These temperatures are comparable to those of 50–150°C proposed for the precipitation of saddle dolomite in the St Genevieve Formation in Illinois (Choquette, 1971). The combined occurrence of saddle dolomite and fluorite in the Ninmaroo sequence implies similar temperatures.

Hydrocarbons

Known occurrences of hydrocarbons in the Ninmaroo Formation are sparse but varied: bituminous staining of limestones; bitumen residues in relict mesogenetic porosity (Figs. 6, 9F); bitumen residues along stylolites (Fig. 6I); traces of hydrocarbons leaking from cavern systems; methane and other hydrocarbon inclusions in saddle dolomite and calcite cements; and bituminous calcretes. Bituminous staining in limestones is evident in the breached dome structures along the Burke River Structural Belt (Casey & others, 1960), along the western flanks of the Toko syncline, and in very tight fault blocks in the Smoky Anticline area (Fig. 8). In these structural settings, the staining is strongest in the fine-grained, less permeable lithologies in contrast to lighter-coloured limestone, which was previously more porous, but has since been flushed. Large clasts in some flat-pebble conglomerates shown various concentric patterns of bitumen staining, which indicate former hydrocarbon migration and subsequent flushing.

Scattered blobs of bitumen and bituminous zones occur in dolostones on the eastern limb of the Toko syncline, and in the upper levels of domes in the Burke River Structural Belt. The extracted organic matter of these residues contained 28 per cent saturates, 14 percent aromatics, and 57 percent polar compounds, with the saturates having pristane/phytane ratios of 2.5, similar to other extracts of secondary hydrocarbons from the Toko Sequence (K. Jackson, BMR, personal communication, 1979). Some porous flat-pebble conglomerates contain bitumens as the last phase of porosity occlusion. This prevented total cementation by calcite (Fig. 9F). Most probably, the limited staining on the tops of domes indicates areas of longest preserved porosity, because of a longer period of occlusion by hydrocarbons. In more compacted sequences, as in the Toko Syncline, bitumen is concentrated along stylolites, commonly with traces of pyrite and amber sphalerite.

Cavern systems intersected by drillholes in the Digby Peaks area gave exhalations of air with a bituminous odour. The air had traces of methane (< 30ppm) with minor ethane and butane. Traces of methane and ethane have also been detected during the digestion of saddle dolomite from the Digby Peaks area.

In the Smoky Anticline area, the sequence is mainly barren dolostone, but locally, Holocene calcretes in joints are highly bituminous. Elsewhere, salt-saturated soils around dolines indicate connate brines and possibly minor hydrocarbons still escaping from the formation (Fig. 4B).

Discussion. Evidence indicates that hydrocarbon migration has occurred in the formation and that the slow escape of some hydrocarbons from the sequence is a present day phenomenon. Ratios of extractable organic matter to the total organic content in bituminous Ninmaroo limestones are sufficiently high to confirm that an oil generation phase has been attained (D. McKirdy, BMR, written communication, 1979). A higher thermal maturity of the formation is expected in the Toko Syncline and the Burke River Structural Belt, where there has been deeper burial. In the Toko Syncline thermal maturity is indicated by extrapolation of data from the overlying units in drill holes AOD Ethabuka No. 1 and GSQ Mt Whelan No. 2. Maturity of the sequence in AOD Ethabuka No. 1 is indicated by ultra-violet fluorescent colours of lamellar alginites and acritarchs equivalent to 0.7–0.9% Ro vitrinite (A. Kantsler, University of Wollongong, written communication, 1980) and conodont colour alteration indices (CCAI) of 1.5–2.3 (Nicoll, 1979).

Against the Toomba Fault, CCAIs of 1–2 imply lower maturity. (R.S.Nicoll, BMR, personal communication, 1979). In GSQ Mt Whelan No. 2 on the eastern limb of the syncline, reflectance data of in situ organic matter (K. Jackson, BMR, personal communication, 1979) and extrapolation of vitrinite data from the overlying sequence (R.O. Smith, Geological Survey of Queensland, personal communication, 1979) confirm maturity, but not overmaturity. In the Burke River Structural Belt, in addition to the presence of void-filling bitumens, CCAIs of 1–1.5 (R.S.Nicoll, BMR, personal communication, 1979) indicate the sequence is not overmature.

Although the Ordovician sequence is considered very poor for source rock potential, the Cambrian, especially the Marqua beds and Georgina Limestone, is considered a good source (Jackson, 1982).

Consequently, the staining hydrocarbons are not in situ material, but a relict of an earlier migration and accumulation phase that has since been dissipated with faulting and erosion of caprock. Fluorite and saddle dolomite emplacement was related to the brines responsible for the migration and short-lived accumulation of hydrocarbons. If hydrocarbon migration extended into the Cainozoic in the Burke River Structural Belt, then potential unconformity traps are probable where impermeable Mesozoic cover has not yet been eroded from over domes of the Ninmaroo Formation.

Porosity

Porosity is generally very low in Ninmaroo Formation carbonates (Konecki *in* Casey & others, 1960) but varies significantly between carbonate types.

The limestones have very low porosity (<5%) and are virtually impermeable (<1 md) regardless of their original texture. However, the flat-pebble conglomerates had large interparticle and fracture porosity early in diagenesis. Some has survived to the present, although most has been occluded by precipitation of saddle dolomite, poikilotopic calcite, fluorite, and authigenic clays (Fig. 6F).

Bedded and massive dolostones have higher porosity (4–10.5%) with correspondingly higher horizontal permeability (.1–437 md), but very low (<5 md) vertical permeability. Porosity is predominantly as intercrystalline and vugular mesopores, and is commonly isolated in thin bands or patches by impermeable shaly or carbonaceous laminae and stylolites, which accounts for the very low vertical permeability.

Coarsely crystalline massive saddle dolomite is common as a replacement and void-filling phase along fault zones, and has high porosities, resulting from fracture and crystal moldic pores. This combination gives reticulated small channels and better permeability.

Sandstone interbedded with the carbonates is most common in the terrigenous lithofacies (Radke, 1980) across the Smoky Anticline and Toko Syncline. This has high porosity (15-25%) and good permeability to gas (15-300 md horizontal, 3-144 md vertical). Porosity is mostly interparticular in mesopores, with some moldic mesopores after calcareous skeletal components.

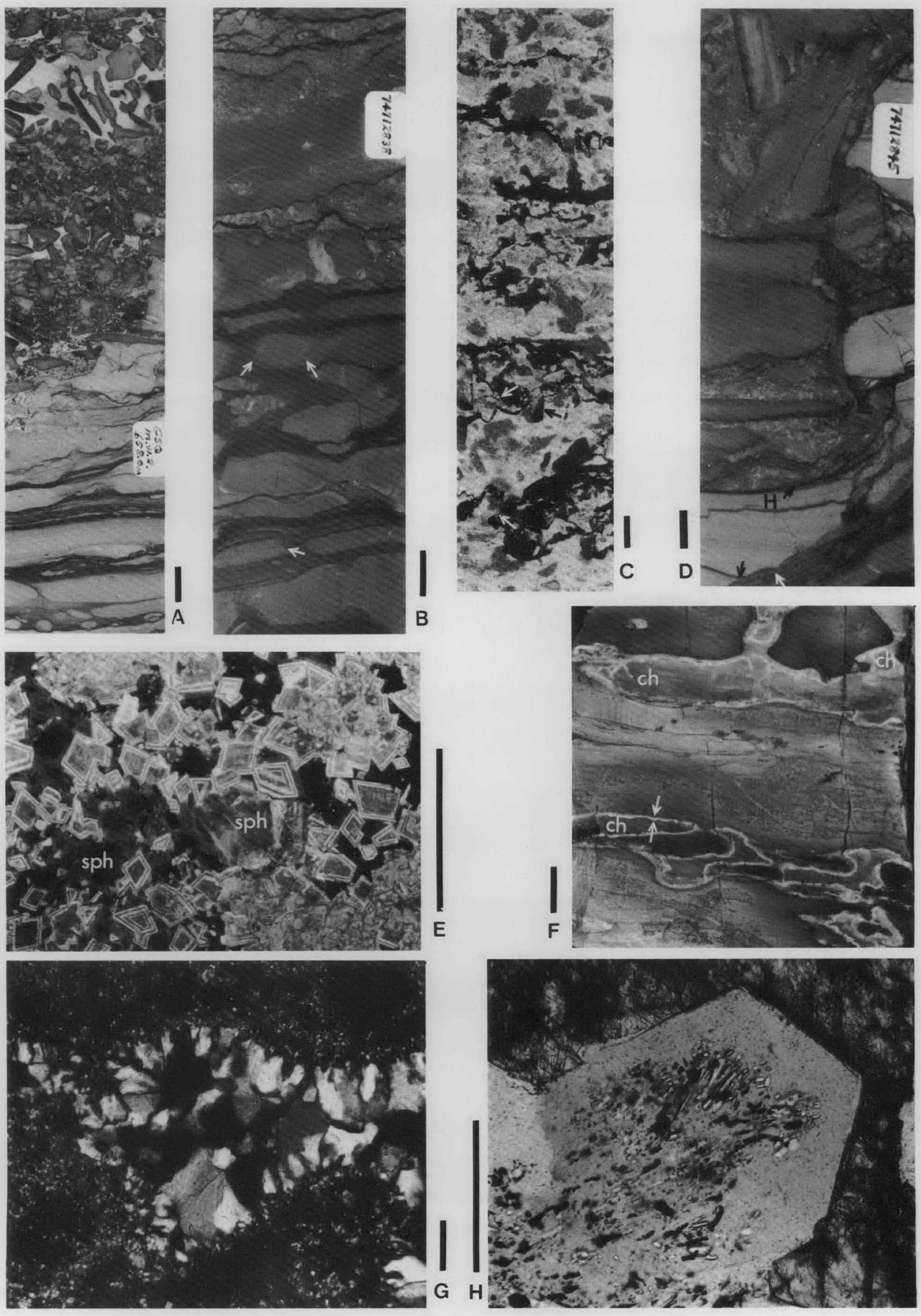
A
B
C
D
H
sph
sph
E
ch
ch
ch
F
G
H

Discussion. Generally, preservation of primary and early diagenetic porosity to the present is rare as much occlusion occurred during and after hydrocarbon migration with the precipitation of saddle dolomite, calcite, and fluorite. Subsequent vadose karstification has developed significant cavern porosity in much of the exposed sequence. Some of this has existed since the middle to late Palaeozoic, as indicated by cave-collapse breccias that have been cemented by mesogenetic minerals and later exhumed within present cave systems (Fig. 5).

Silica

Authigenic silica is present as four microfabrics in cherts. Microquartz is dominant over megaquartz, chalcedonite, and quartzine, and lutecite, all of which may be present in a single chert nodule (Fig. 10F) or stringer.

Microquartz occurs as a replacement of original lime mud and peloid, ooid, and skeletal particles (Fig. 10G).

Megaquartz occurs as both replacement and void-fill. As a replacement feature it occurs randomly in limestones as small euhedral crystals with inclusion-rich irregular centres and outer, inclusion-free rims; within sulphate nodules, in optical continuity with quartzine, either as clear idiotopic quartz with thin bands rich in sulphate inclusions, or as inclusion-rich flamboyant quartz (Figs. 7A, 10H) (Folk & Pittman, 1971). The latter variety of megaquartz is characterised by random undulose to 'pinfire' extinction, irregular subcrystals, and numerous fluid and sulphate inclusions. Flamboyant quartz may be gradational with normal megaquartz. As a void-filling, megaquartz forms drusy quartz mosaics, usually on a microquartz substrate of replaced particles in chert nodules (Fig. 10G), as well as directly on calcite cements.

Chalcedonite has a characteristic void-filling occurrence in interparticle porosity, skeletal moulds, and solution cavities (Fig. 11A), where it is usually encrusted on a microquartz or quartzine substrate (Fig. 3C).

Quartzine (Fig. 11B) and **lutecite** have mainly replacement fabrics with only a minor void-filling occurrence of quartzine, where it alternates with chalcedonite in isopachous rims lining the walls of large solution cavities in massive dolostone (Fig. 11A). These fabrics replace the periphery of anhydrite nodules (Fig. 7A), intraskeletal moulds filled with anhydrite laths, and gypsum crystal cements.

Discussion. Cherts are generally selective in both diagenetic and depositional facies. Chert is locally abundant in and around areas of pervasive dolomitisation. It occurs as discrete nodules, as replacement of skeletal particles (especially chitons, nautiloids and ribeirioids), in interparticle porosity of skeletal grainstones, and as stratiform laminae, which are gradational with one or more of the modes of occurrence.

Chert is most abundant in the Datson Member of the Ninmaroo Formation (peloidskeletal limestone lithofacies IIps of Radke, 1980), where it may form up to 50 per cent of the sequence as thin interbedded laminae. Other occurrences as nodules are in the peloid limestone-dominant lithofacies (IIp), where they are closely associated with sponge spicules in skeletal limestones, cryptalgal limestones — which may originally have had a rich diatom flora — lime mud-supported sediments, and sulphate nodules or crystals.

Silicification has frequently been a local accretionary process, successive younger phases having precipitated on older chert nuclei, thus producing a record of silicification throughout diagenesis. Silicification was most prolific as a replacement of sulphate, and as a phase contemporaneous with early dolomitisation. Subsequent accretion has been during weathering, with chalcedonite and quartzine being the more abundant microfabrics.

Stylolitic features

Stylolitic features (Logan & Semeniuk, 1976) are significant in the formation and are locally accentuated by 'two-tone' or variegated colour weathering effects (Fig. 9A). In approximate order of decreasing abundance, the features are stylolamination, stylobedding, stylomottling, stylonodules and stylobreccioids.

Stylolamination is variably superimposed on primary lamination, such as cryptalgalaminites and siliciclastic–carbonate alternations (Fig. 10A), or on pre-existing laminar diagenetic lithological variations. It is best developed at distinct contacts between contrasting lithologies, such as siliciclastic, dolostone, and limestone laminae.

Stylobedding is a similar exaggeration of pre-existing lithological variation between thicker intervals. The most distinct partings between carbonate beds are siliciclastic-rich and smooth, hummocky, or irregular. At carbonate junctions, stylolite surfaces have greater amplitudes (Fig. 10B), but these tend not to have stylocumulates in such abundance and are consequently less obvious.

Stylomottling, where only isolated patches of the host carbonate are stylolitic, is attributable to bioturbation, desiccation cracks, scattered sulphate nodules, or crystal clusters (Fig. 10C), and also the superimposition of later events such as selective dolomitisation.

Stylonodular structures are transitional between stylobedding and stylolamination or stylobreccioids. These occur randomly (Fig. 10B) or in closely spaced horizons. The nodules are usually discoid to irregular and have either distinct stylobounded outlines or transitional margins of numerous small anastomosing stylolaminae, which become denser away from the nodule into the host carbonate. Features such as indurated patches, non-bioturbated areas or silicified sulphate nodules

Figure 10.
A — Stylolamination and partly developed stylonodules in fine-grained silty carbonate. An overlying synsedimentary hard-ground surface and open-framework conglomerate show little evidence of stylosolution because of earlier and complete cementation. Core slab; 74712853; bar scale 1cm. B — Stylobedding (upper) and stylonodular (lower) structures. Hummocky to irregular stylolites define contacts between distinctive, well-cemented lithotypes. Stylonodules have sharp to gradational margins with a stylolaminated host of predominantly stylocumulate material. Core slab, 74712838, bar scale 1 cm. C — Transition in dolostone from stylomottling to stylobreccioid structure defined by peaked stylolite surfaces (arrows). The cause of mottling in the dolostone is uncertain, but angularity of boundaries and the interconnected fabric could mimic clusters of sulphate crystals. Core slab, 74712828, bar scale 1 cm. D — Pebble conglomerate with fabric-fitted stylobreccioid structure adjacent to a hardground (H). Discordant stylolamination is developed under the hard-ground at the expense of the light grainstone. Laminae (arrow) can be traced from this grainstone into the stylolaminae. Core slab, 74712845, bar scale 1 cm. E — Intergrown iron-poor sphalerite (sph) and euhedral saddle dolomite. Photomicrograph of cathodoluminescent image; 74715782; 1-mm bar scale. F — Stratiform chert (ch) in a dolomitised skeletal grainstone. Upper chert laminae are interconnected by bioturbation structures. The thin concentric accretion rim (arrow) indicates several phases of silica precipitation. Rock slab; 74712317; Bar scale 1 cm. G — Megaquartz drusy cement filling interparticle porosity. Particles are replaced by microquartz in a silicified peloidal grapestone. Photomicrograph, crossed polars; 74712708; 1-mm bar scale. H — Euhedral crystal offlamboyant megaquartz facing into centre of a partially silicified anhydrite nodule. An initial replacement by the quartz is indicated by bladed sulphate inclusions in a felted fabric. The outer lucid rim is probably a void-filling phase following solution of remaining sulphate. Photomicrograph, crossed polars; 74712669; bar scale 0.5 mm.

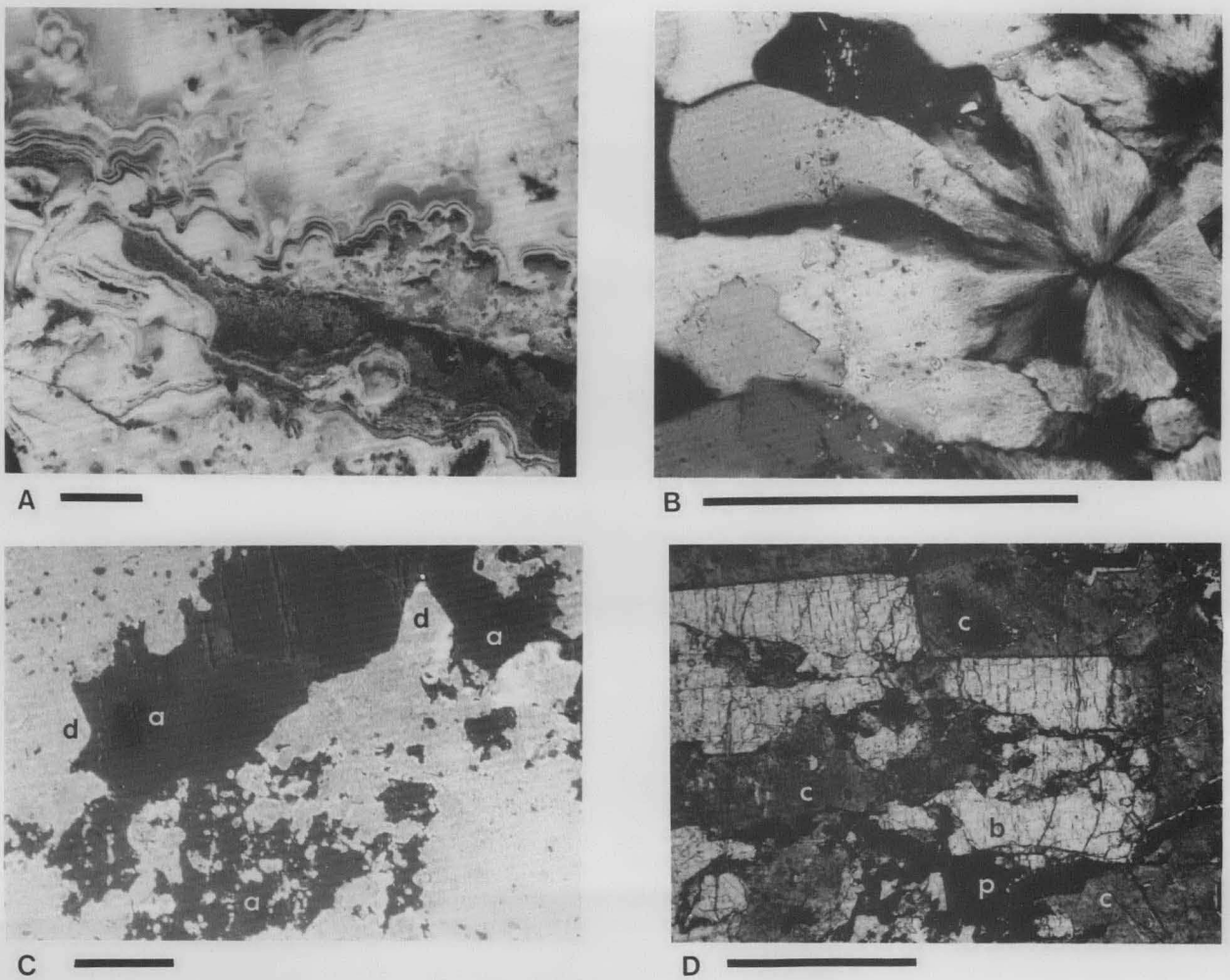

Figure 11.
A — Colloform chalcedonite, fibrous calcite and quartzine cements encrusting collapsed clasts in a macrocavity. There is a repeated alternation of cement types. Rock slab; 74712318; bar scale 1 cm. B — Fibrous quartzine spherulite with overgrowths of megaquartz in optical continuity with bundles of quartzine fibres. Zones of rod-shaped sulphate inclusions in the megaquartz indicate both phases are a replacement of sulphate within this silicified anhydrite nodule. Photomicrograph; 74712665; bar scale 0.5 mm. C — Solution cavity in dolostone, rimmed by an initial dolomite cement (d) and occluded by coarsely crystalline anhydrite (a). Dolomite replacement along cleavage of the anhydrite is apparent below the lower margin of the cavity. Photomicrograph of cathodoluminescent image; 74712833; 1-mm bar scale. D — Bladed baryte crystals (b) replacing a sulphate nodule. Calcite (c) now partially replaces baryte as well as filling moldic porosity after the nodule. A reaction rim of pyrite (p) defines the replacement calcite–baryte contact. Photomicrograph, plane-polarised light; 74712548; 1-mm bar scale.

are emphasised by a surrounding stylocumulate or dolomitic reactate matrix (Logan & Semeniuk, 1976). In outcrop the dolomitic matrix has invariably weathered to ochre-coloured dedolomite, which imparts a striking 'two-tone' appearance. Fracturing of banded limestones during tectonism commonly produces numerous idens in the more competent bands, which subsequently transform into oblate nodules.

Stylobreccioids are most commonly an enhancement of pre-existing inhomogeneity in rudites (Fig. 10D), collapse breccias (Fig. 3A), and tectonic breccias. They were also produced where stylonodular and stylobedded structures progressed to the extreme. A telo–mesogenetic stylobreccioid follows zones of oomoldic porosity and forms type B stratiform breccias with a stylocumulate matrix. (Fig. 3B).

Discussion. This range of structures is thought to be caused by pressure solution, which has exaggerated preexisting variations in the fabric. At the mesoscale, the degree of solution which occurred at iden (Logan & Semeniuck, 1976) boundaries was proportional to the differences in solubility and competence of abutting lithologies. Most occurrences indicate that pressure solution has only exaggerated preexisting structures and not distorted or destroyed them. Commonly, the modified structures are difficult to distinguish from original features except where diagenesis has preserved some of a preexisting feature, as in the case with many chert nodules. It is disconcerting that the least obvious effects are probably the most significant quantitatively. Pressure solution structures indicate reduced carbonate permeability during their development (Buxton & Sibley, 1981). Stages of this can be seen in the sequence, especially in bedded dolostone. In the central Toko Syncline, carbonate and sulphide have precipitated on the porous side of stylolitic contacts — the main concentration sites of minor sulphides (pyrite and amber sphalerite), saddle dolomite, and calcite (Fig. 10E). Where pressure solution was more extensive, the mineralisation has been reduced to scattered idens of sulphide, coarse calcite, and dolomite, stylobounded against thin bituminous seams. Such stylolites are now effective barriers to vertical permeability except where fracture porosity has connected the permeable bands (Radke & Duff, 1980).

Pressure solution structures are ubiquitous in the sequence. However, quantification of the significance of pressure solution is nearly impossible, because of limited subsurface data and the difficulty of assessing outcrops where only the most resistant and homogeneous lithotypes are preserved.

Generally, pressure solution appears greatest in the more tectonised zones in the Burke River Structural Belt and on the

western side of the Toko Syncline. Impure carbonates have the highest density of stylostructures, and the density is greater in limestone than dolostone, in which it is apparent that previous dolomitisation has reduced inhomogeneity and hence susceptibility to pressure solution.

Sulphates

Late diagenetic sulphates are anhydrite, baryte, and celestite, which are distinguished from their primary occurrences by paragenetic associations. They are generally cross-cutting or are void-filling cements that postdate calcite and saddle dolomite cements. Anhydrite is preserved only in the subsurface, owing to its relative high solubility, and hence it is mainly recognised as pseudomorphs and crystal moulds.

Anhydrite occurs as patches of millimetre to centimetre-sized subhedral crystals or as radial splays of bladed euhedral crystals. As a replacement mineral, it is generally clear, coarsely crystalline and poikilotopic, enclosing siliciclastic particles. As a void-filling cement, anhydrite occludes remaining porosity in solution vugs after saddle dolomite (Fig. 11C),calcite or fluorite. This void-filling mode is most commonly leached, but its former presence is evident from calcite pseudomorphs or crystal moulds defined by fine discontinous bands of goethite or pyrite crystals in calcite or dolomite. Anhydrite is most abundant in coarsely crystalline dolostone and with vein-filling saddle dolomite. In limestone, it is predominantly a replacement mineral in intraclast and flat-pebble conglomerate, and in sulphate nodules.

Baryte has a replacement mode as very coarse, millimetre to centimetre-sized tabular crystals in radial splays (Figs. 7C, 11D) in sulphate nodules. Calcite, saddle dolomite, and fluorite may be associated. In some calcitised nodules and bedded crystalline dolostone, baryte is interspersed as subhedral crystals.

Celestite occurs as euhedral to subhedral crystals, 10–100 μm, closely associated with baryte in calcitised sulphate nodules, and as a trace mineral in collapse-breccia zones.

Discussion. Sulphates occur only as traces in both limestone and dolostone, but may be up 7 per cent in some replacement horizons. Anhydrite is the most abundant, with baryte and celestite only present in trace amounts. Sulphate emplacement is late and it is difficult to be more specific. The source of sulphates emplaced during calcitisation of anhydrite nodules is apparently local, from former evaporitic species. However, some sulphates postdate saddle dolomite. Much of the sequence today still contains saline water (Appendix E, Casey & others, 1960), the probable source of these later phases, with little or no meteoric intermixing except close to the water table. The saline fluids are known to be slowly effluxing in several areas: the doline zone along the eastern side of the Georgina River, Glenormiston Sheet, and the Black Mountain Fault zone in the Dribbling Bore area. Table 2 compares water chemistry from a playa at the latter occurrence, and a mixed meteoriconnate zone near the water table in the Digby Peaks area. Effluxing of brine has probably continued since hydrocarbon migration and dolomitisation, although it is unknown how its composition has varied since that time.

Cave deposits in steeply-dipping dolostone of the Ninmaroo Formation next to the Black Mountain Fault at Mount Datson comprise calcite and chalcedonic speleothems, which contain pseudomorphs after gypsum and aragonite. The chalcedonic bands consist of alternating zones of quartzine and chalcedonite (Fig. 3C) which indicate fluctuating salinities during their precipitation (Folk & Pittman, 1971). The slight tilting of the geopetal features in these speleothems implies a post-Cretaceous, probable Tertiary emplacement, and supports the model of continued efflux of brines up dip and up faults since the Palaeozoic.

Table 2. Chemical analyses of surface and groundwaters in contact with the Ninmaroo Formation.

	Dribbling Bore surface playa	*Digby Peaks groundwater*		
		CRAE DP1 21.5 m	*CRAE DP2 46.2 m*	*CRAE DP3 44.6 m*
Na	123 900	1190	47.4	174
K	640	4.8	29.9	10.5
Ca	290	248	39.9	73.6
Mg	8 230	128	36.2	68.5
Fe	1.3	0.03	0.01	0.07
Mn	1.1	ND	0.001	ND
Sr	20.5	3.75	0.5	1.05
Ba	0.3	0.1	0.1	0.05
Pb	0.073	0.006	0.032	0.027
Zn	0.295	0.064	0.061	0.066
Cu	0.054	0.018	0.038	0.070
Cl	186 000	2060	66	333
PO_4	32	ND	0.01	0.055
SO_3	32 300	555	25	161
F	ND	0.4	0.45	2

All analyses in ppm.
Analyses by AMDEL Laboratories

Sulphides

Sulphides are presently known in scattered minor occurrences in the sequence, and consist mainly of pyrite with traces of sphalerite and galena.

Pyrite is ubiquitous, but is scattered in low concentrations. It has several common occurrences. (1) In carbonate cements, pyrite may form thin discontinuous zones of subhedral crystals at the junction of iron-poor and iron-rich calcite bands. (2) Bands of euhedral to subhedral crystals partly fill moldic porosity after sulphate nodules, and this pyrite may predate — or postdate saddle dolomite cement rims in the vugs. (3) Pyrite, with calcite, occludes small tensional fractures (Fig. 6G). (4) In stratiform cavities and collapse breccias (Fig. 4B, D, F) it may occur as a minor geopetal precipitate. (5) Along stylolite bands it forms replacement patches of anhedral crystals associated with bitumen residues.

Sphalerite is rare. It is mostly amber-coloured, but thin purple growth bands are sometimes evident in thin section. Sphalerite occurs as subhedral masses completely replacing bituminous clasts in dolostones, stalactitic pendant cements in cavern porosity with saddle dolomite and geopetal pyrite cements (Fig. 6H), and subhedral centimetre-sized blobs with calcite as remnant concentrations along bitumen-stained stylolites in dolostone (Fig. 6I). It is always found in dolostone, commonly close to a limestone contact or associated with saddle dolomite (Fig. 10C) and poikilotopic calcite cements. This species has no detectable iron or other metals, so it is assumed that the colour banding is due to hydrocarbon inclusions.

Galena is known only from the Digby Peaks (Connor, 1978) and Noranside (Carter & others, 1961) areas. At the Noranside prospect, galena occurs as anhedral centimetre-sized lumps with oxidised rims, reworked in a calcrete-cemented dolostone breccia (Fig. 3C) along one joint set over the top hinge of a tight monoclinal fold. The galena originally precipitated as a vein-fill between two phases of saddle dolomite precipitation prior to readjustment and brecciation on the joint set and subsequent calcrete cementation.

Concentrations of goethitic pseudomorphs of sulphide nodules occur over extensive areas of both the Ninmaroo–Mesozoic Allaru Mudstone unconformity in the Smoky Anticline region (Australian Aquitane Petroleum, 1972), and the Ninmaroo–

Swift contact in the Burke River Structural Belt. The nodules are spheroidal, tabular or irregular, centimetre to decimetre-sized, with surfaces of interpenetrating cubic and octahedral forms. These crystal forms have been attributed to pyrite, galena, or fluorite (Australian Aquitane Petroleum, 1972), and to pyrite alone (D. McColl, BMR, personal communication, 1975).

Discussion. Sites of probable sulphide emplacement, as indicated by geochemistry (Draper, 1976, 1978), are collapse breccias in karst systems at Digby Peaks (Fig. 4D) and along the broad crest of the Smoky Anticline (Fig. 4B), where karstification has occurred repeatedly from the pre-Mesozoic to the Holocene. Subsequent near-surface oxidation of the sulphide in these structures has obscured original host relationships. Manganiferous gossans with anomalous zinc, barium, and phosphorus (Table 3) occur around collapsed dolines in the vicinity of Digby Peaks (Fig. 4D) and in a decalcified sandstone in the Corrie Member along a gentle anticline west of Mount Ninmaroo (Fig. 4F). No boxwork fabrics have been recognised in these gossans, and it is possible that manganese scavenging of these elements occurred subsequently.

Barton (1967) speculated that zinc is a catalyst for abiogenic sulphate reduction reactions and that sphalerite is a byproduct along with carbonates. This model would explain the sphalerite-hydrocarbon-saddle dolomite/calcite association in the Ninmaroo Formation observed by Radke & Mathis (1980).

Table 3. Geochemical summary of the Ninmaroo Formation and selected gossans.

	Ninmaroo Formation average	*Burke River Structural Belt*	*Toko Syncline and Smoky Anticline*	*Doline gossan at Digby Peaks*	*Stratiform gossan west of Mt Ninmaroo*
Ca %	30.2	31.1	30.5	10.0	10.26
Mg %	3.23	2.58	4.2	.15	.15
Insoluble residue %	12.4	12.1	10.5	47.4	—
Sr %	.03	.03	.03	.01	.01
Fe %	.15	.13	.17	.25	22.65
Mn %	.03	.04	.03	.13	.88
F %	.03	.02	.01	.05	.03
P ppm	153	192	107	2390	4258
Cu ppm	8	6	13	135	18
Pb ppm	282	537	20	42	< 5
Zn ppm	24	26	19	5200	256
Ba ppm	274	327	134	4253	448
Number of samples	379	193	114	3	9
Analytical method	A	A	A	A	B
Source	Draper (1978)			Draper (1976)	

A — Ca, Mg, Sr, Fe, Mn, IR of carbonate fraction, P, Cu, Pb, Zn, Ba, F of total rock.
B — total rock

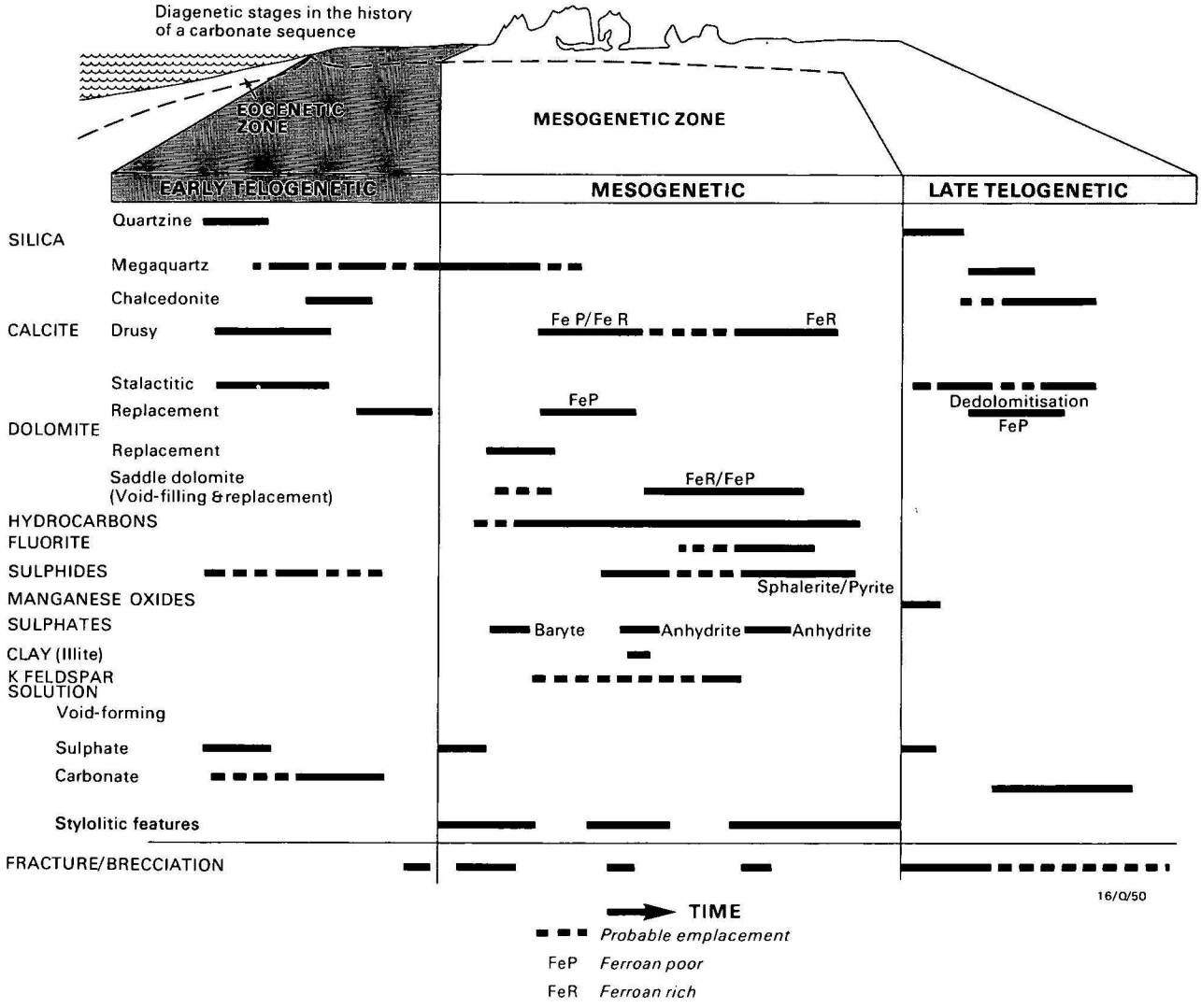

Figure 12. Generalised paragenetic sequence in the Ninmaroo carbonates.
Diagenetic phases after Choquette & Pray (1970).

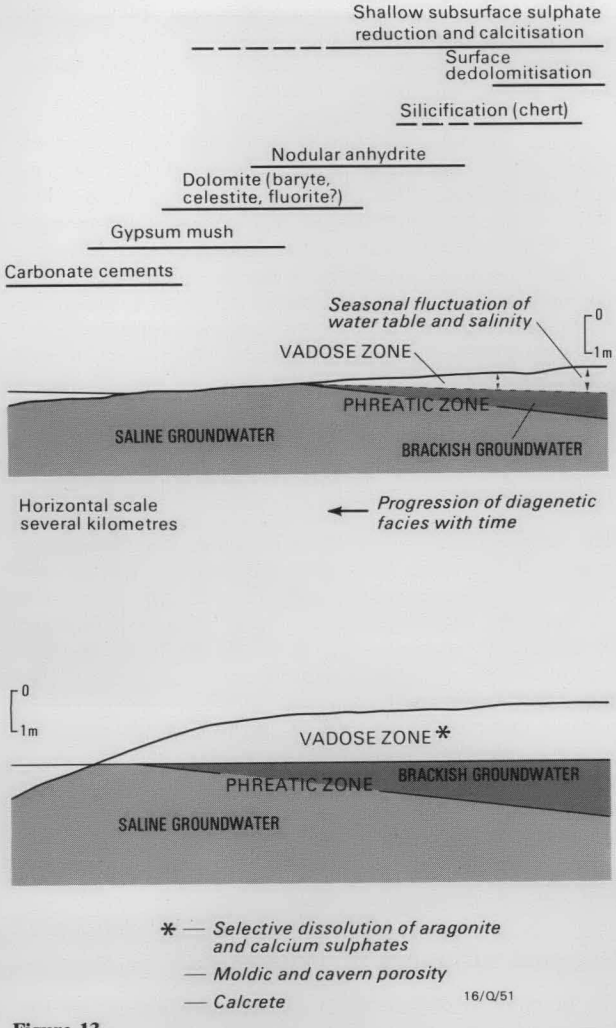

Figure 13.
A — Eogenetic diagenesis on a sabkha. Idealised profile shows a high groundwater table, with a thin landward lens of brackish water. Seasonal fluctuations of the water table range from surface flooding to a lowered phreatic zone and a narrow vadose zone during the dry season. Bars indicate the spatial distribution of diagenetic fields at one point in time. These diagenetic fields migrate laterally with progradation of the shoal. B — Early telogenetic diagenesis. Idealised profile of an emergent shoal surface during a drop in relative sea level shows a lowered water table and enlarged vadose zone. Selective solution of sulphates and aragonite produced moldic porosity, cavities and collapse breccias. Calcrete cements precipitated in the vadose zone.

Diagenetic stages

Diagenesis is the sum of all physical and chemical changes in a sediment after its accumulation, excluding metamorphism (Friedman & Sanders, 1978). The history of these changes can be subdivided genetically into three stages (Choquette & Pray, 1970), which are distinguishable by environment, process, and product. These are: eogenesis–the early burial stage, after sediment accumulation when there is interaction with near-surface fluids, and prior to deep burial; mesogenesis–the relatively long intermediate stage of deeper burial; and telogenesis — the stage of interaction with vadose and shallow phreatic environments during uplift and erosion, following eogenesis or mesogenesis.

These diagenetic stages may produce similar or overlapping mineral assemblages. With the time–genetic classification of diagenesis outlined above, recognition and distinction of different stages in one mineral product is necessary. Distinction has been possible from petrographic relations that indicate relative timing of emplacement, control of their distribution by known tectonic or erosional events, and geochemical differences between stages.

Four stages are recognised in the Ninmaroo Formation: eogenesis, early telogenesis, mesogenesis, and late telogenesis. A generalised paragenesis in the context of these stages is presented in Figure 12 and discussed below. Eogenesis is only briefly described, as it will be the subject of further discussion in a later paper.

Eogenesis

The overprinting of sedimentary features by eogenetic processes is generally widespread, although specific processes tend to be lithologically selective. The general paragenetic sequence in a porous host carbonate is:

1 — partial aragonite or Mg-calcite cementation;
2 — initiation of very slow dolomitisation of muddy carbonate sediments and minor fluorite precipitation;
3 — displacive growth of gypsum crystals and clusters within sediment porespaces;
4 — overgrowth of some gypsum by anhydrite, which develops spheroidal nodules;
5 — partial replacement of anhydrite nodules by chalcedony and flamboyant quartz;
6 — a renewed cycle of displacive and passive sulphate precipitation;
7 — dedolomitisation of earlier formed protodolomite.

This paragenetic sequence is interpreted as the result of lateral migration of diagenetic facies through, firstly, normal marine and then increasingly saline deposits during progadational deposition. The diagenetic facies occurred synchronously in a crude zonation conforming to the accretionary margin of shoals with a central sabkha (Fig. 13).

Early sulphate emplacement was temporally and environmentally selective. Gypsum precipitation was prolific on hypersaline flats in porous peloidal and skeletal grainstones, and algal boundstones. Anhydrite nodules later developed around these precursor gypsum crystals. Early silicification of sediment particles and anhydrite nodules was most prolific in skeletal sediments rich in sponge spicules and siliciclastic silt, and in algal and diatom-enriched evaporitic sediments, although replacement of the nodules was usually incomplete (Radke, 1978).

Early telogenesis

The paragenetic sequence during this transitory period (Fig. 12) represents dominant vadose and lesser meteoric phreatic processes. The transition from eogenesis was gradual during lateral sedimentation and buildup of shoals above mean water level, with the corresponding development of a vadose zone and meteoric phreatic zone (Fig. 13A). Sulphates were dissolved by downward percolating rainwater in the vadose zone, and by the meteoric groundwaters in the phreatic zone. Localised silicification in both void-filling and replacement modes continued in the presence of sulphates, producing quartzine (length-slow chalcedony). As sulphate concentrations or the rate of silica precipitation diminished, this phased into megaquartz replacement and chalcedonite voidfill (Fig. 7A). At this stage, random aragonitic particles and cements were leached, producing moldic porosity. Stalactitic calcite cement fabrics developed in the vadose zone while continuous rim cements (drusy mosaics) developed in the phreatic zone. Minor disseminated pyrite precipitated during solution and replacement of the remaining gypsum and anhydrite.

Small (metre-scale) eustatic fluctuations (Radke, 1980), which affected the depth of the vadose zone (Fig. 13B), superimposed an additional complexity on the lateral migration of diagenetic facies. Consequently, these fluctuations caused oscillation between telogenetic and eogenetic diagenesis for a significant period before sufficient accumulation and burial forced a

transition into mesogenetic conditions. The paragenetic sequence (Fig. 10) is, therefore, a simplification of a more complex superimposition of eogenetic and telogenetic imprints.

The overall result of telogenesis was the dramatic increase in porosity: moldic porosity by the solution of sulphates and aragonitic components; cavern and breccia porosity where collapse breccias (Fig. 2) developed.

Mesogenesis

The regional structural history dictated the depth of burial and its duration. The mesogenetic phase commenced in the Early Ordovician and lasted for the order of 100 million years. This stage features mostly porosity occlusion and dolomitisation.

Megaquartz replacement and void-filling continued from early telogenesis until ferroan-poor calcite became the dominant precipitant occluding pre-existing porosity with drusy and poikilotopic textures. Pervasive dolomitisation was significant as a virtual complete replacement of individual beds and whole stratiform sequences, or localised as a halo along fault zones (Figs. 8, 9C, D). Intercrystalline porosity developed in the dolostones. Hydrocarbon migration began before and continued over this period of dolomitisation with contemporaneous void filling and replacement by ferroan and saddle dolomite, fluorite, minor clays, sulphides, and poikilotopic ferroan calcite (Fig. 6). Pyrite was the most abundant sulphide, although amber low-iron sphalerite and galena (Fig. 3E, 10E) have localised occurrence. Timing of precipitation of these various phases varied locally. In addition, anhydrite, baryte, and traces of celestite were emplaced, mainly as replacement of calcite and former anhydrite, as well as void-filling phases following sulphide precipitation. K-feldspar precipitated as authigenic overgrowths on detrital feldspar particles.

Pressure solution phenomena have produced a significant overprint on the sequence as an enhancement of many structures, as they were selective of preexisting rock fabric. Stylolamination developed in and enhanced primary lamination and lithological contacts, emphasised earlier laminar dedolomitisation, and developed into stylonodular fabrics. Stylobrecciation was most common in flat-pebble conglomerate limestone and as a superimposed feature on solution collapse breccia. In ooid grainstone it developed after brittle structural failure in zones of moldic porosity. Irregular, sutured stylolites are not as common, but occur in rocks with isotropic fabric. Bitumen residues commonly line stylolites, often with traces of pyrite or sphalerite, and indicate that these horizons were formerly zones of higher porosity.

Discussion. The spatial relations between structure and distribution of bituminous limestone and dolostone indicate that hydrocarbon accumulation was in structural domes and sealed fault blocks. The entrapment of hydrocarbons in these structures precluded subsequent alteration of the host carbonate; while, elsewhere, brines pervasively dolomitised the sequence and precipitated minor anhydrite as a late-stage replacement. Most existing fault zones influenced fluid movement and localised precipitation of and replacement by saddle dolomite (Fig. 8). Recurring movement on these faults produced brecciation locally, and repeated emplacement of the mesogenetic phases. Post-Cretaceous movement on these faults, as indicated by the displacement of the Mesozoic sequence, disrupted domal structures and developed tensional veinlets, forming conduits for hydrocarbon escape and further migration of warm brine. Saddle dolomite emplacement was long fault zones and in more permeable strata by both replacement and precipitation. Minor sulphides (pyrite, sphalerite and galena), fluorite, ferroan calcite, authigenic K-feldspar and baryte precipitated on the margins of these alteration zones as void-filling cements in veins and solution vugs after sulphate. Where fluorite and sulphides were absent, ferroan calcite precipitated synchronously with saddle dolomite to occlude all porosity.

Although sulphides have not been found in contact with all these minerals, the surface morphology of pseudomorphs after sulphides indicates that they were the initial phase filling solution vugs after sulphates. Fluorite is most abundant on the edge of local dolomitisation zones associated with faults, or as a final void-filling phase following precipitation of saddle dolomite. It is not clear when or how often sulphide mineralisation occurred along faults. Post-Cretaceous mineralisation is evident from the presence of pseudomorphs after sulphide concretions both in Cretaceous rocks that fill karst dolines in Ninmaroo Formation dolostones, and along the Ninmaroo Formation–Cretaceous unconformity.

Late telogenesis

This stage commenced during uplift and erosion of the sequence, with the return to vadose and meteoric phreatic diagenesis. The paragenetic sequence (Fig. 12) commenced with solution (Fig. 7B) and replacement of late diagenetic sulphates by quartzine. Extensive, carbonate solution produced joint-controlled caves, solution-collapse breccias, and dolines. Filling of this cavern and breccia porosity was predominantly by collapse material, but was initially with manganese and manganese-barium-phosphorus minerals as thin stalactitic crusts and patchy replacement nodules. Subsequent stalactitic calcite (Fig. 3G) and minor chalcedonite were volumetrically more significant. Extensive dedolomitisation of dolostone sequences produced mottled rust-coloured or orange limestones.

Regional variations in diagenesis

The duration of diagenetic stages and individual events has been mainly influenced by local structural, burial, and erosional history. Marked variations in diagenetic history consequently occur across these structural provinces, which have different tectonic and erosional histories. The Toko Syncline and Burke River Structural Belt (Fig. 1) are thicker, folded sequences which have been flexuring with episodic fault movements since Ninmaroo sedimentation. Subsequent erosion and exposure has affected the diagenetic regime only in the upper area of breached folds. This history contrasts with that of the platform area north of the Toko Syncline and to the east where this platform area is arched and faulted over the Smoky Anticline (Fig. 1). These areas have been exposed and karstified for most of the time since Ninmaroo deposition.

Toko Syncline

Structural and erosional history. The Toko Syncline is an asymmetric feature aligned northwest–southeast and plunging gently to the southeast (Fig. 1). The faulted western margin has near vertical to overturned sequences (Fig. 4C) fragmented by interconnected arcuate thrusts along the Toomba Fault Zone (Harrison, 1979, 1980). The eastern flank rises gently northeast to the Smoky Anticline. No localised subsidence occurred until the middle Ordovician, when basement tilted to the south (Harrison, 1979). Probably as a result of the Alice Springs Orogeny in Late Devonian or Early Carboniferous time, thrusting of the Precambrian Arunta Block from the southwest formed the western margin of the structure (Harrison, 1980). Tensional faulting developed perpendicular to this thrust, producing stepped fault blocks. Minor readjustments on these have continued into the Tertiary (C. Simpson, BMR, personal communication, 1981).

Diagenetic history. Eogenetic events were comparable to the generalised paragenesis. Early telogenesis was characterised by solution of sabkha sulphates and the development of vadose stalactitic and phreatic syntaxial calcite cements. Silica (quartzine–megaquartz) replacement of sulphates was virtually non-existent.

Mesogenesis featured hydrocarbon migration, as evident in the staining of flat-pebble conglomerates, which contain clasts with bituminous rims or concentrically zoned bituminous and leached bands. These indicate hydrocarbon migration and subsequent leaching. Bands confined by shales feature bituminous limestone at the base, and grade up to leached and moldic porosity towards the top. Stylolite formation which was significant, is now highlighted by bitumen residues and scattered remnants of void-filling calcite and amber sphalerite. These are remnants of former stratiform cavities that were partly filled by pyrite, sphalerite, saddle dolomite, calcite, and hydrocarbons, prior to subsequent pressure solution. This degree of stylolite formation probably reflects compression and increased overburden pressure during over-thrusting, a component of northerly movement in the Precambrian Arunta Block during the Alice Springs Orogeny (C. Simpson, BMR, personal communication, 1981). Periodic compressional phases have occurred subsequently with localised thrust adjustments.

Along the over-thrust western margin, the near-vertical carbonate sequence was pervasively dolomitised next to the fault zone (Fig.4C) to coarsely crystalline saddle dolostone (Fig.9C). This alteration zone has an abrupt transition across the monoclinal fold axis (Fig.4C) into relatively unaltered gently dipping limestone. The buried sequence in the centre of the syncline is still in the mesogenetic stage, unaffected by a second telogenetic stage that is apparent on the west, north, and east margins (Fig.14). Dedolomitisation of the dolostones is extensive on these exposed margins and especially along the Toomba Fault.

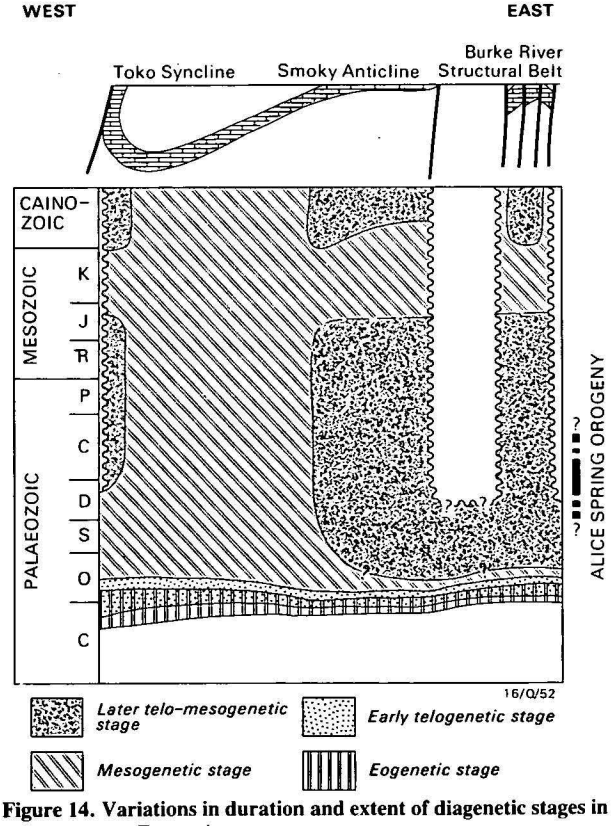

Figure 14. Variations in duration and extent of diagenetic stages in the Ninmaroo Formation.

Burke River Structural Belt

Structural and erosional history. The Burke River Structural Belt (Opik, 1960), is superimposed on a basement of granites and metasediments of the Mount Isa orogen (Tucker & others, 1979). The Palaeozoic sequence has been displaced by a series of major en-echelon northwest and north-northwest-trending faults and associated flexures. Folding has had slow continuous or episodic development from the early Ordovician to the Quaternary, as indicated by gentle folding of the Tertiary sequence and increased magnitude of the deformation down the sequence (Fig.4E). Related faulting, which is most likely the expression of basement movements, had repeated adjustments over this period. The Ninmaroo Formation is exposed in faulted domes such as at Mounts Unbunmaroo, Ninmaroo (Fig.4E), and Datson, and in broad southward plunging anticlines further north at Digby Peaks (Fig.4D). Along the larger faults, more extreme folding has occurred, probably from wrench-thrust fault movements. Much of the Ninmaroo Formation was exposed in the tops of domes from the mid-Palaeozoic to the Jurassic. Uplift prior to the Jurassic on the western side of the belt (west of Beantree No. 1) enabled complete erosion of the Palaeozoic sequence.

Diagenetic history. Generally, eogenetic and early telogenetic stages were moderately short. Early telogenesis entailed primarily meteoric solution of sulphates with some replacement of anhydrite nodules by quartzine and megaquartz. Thin bands of collapse breccias developed where the volume of sulphates was greater (Fig. 2B), usually on the tops of biostromes in A2 sedimentary cycles (Radke, 1980).

The duration of mesogenesis varied locally, because larger domes were partly exhumed and faulting caused erosion of parts of the sequences in the mid-Palaeozoic. Hydrocarbon migration started relatively early, some hydrocarbons being trapped in relict moldic porosity after sulphate nodules and in interparticle porosity of fine-grained carbonates. This hydrocarbon saturation protected much of the folded sequences from brine invasion and pervasive dolomitisation (Fig. 8). Continued tensional fracturing during episodic folding created vein porosity. This was subsequently filled by saddle dolomite and secondary sulphate. Post-Cretaceous faulting caused significant displacements, creating conduits that localised extensive dolomitisation and the escape of hydrocarbons where suitable traps were breached (Figs. 8, 4E).

The second telogenetic stage was considerably earlier where erosion re-exposed the sequence. Silicification was extensive as overgrowths on early telogenetic chert nodules, and generally followed areas of dolomitisation. Dedolomitisation was extensive, resulting from solution of relict sulphates and oxidation of sulphides. Solution of carbonate was mostly controlled by joint and fault porosity (Fig. 5), and continued for a long time in the northern Digby Peaks area, from late Palaeozoic to present (Fig.4D). Mixing of mesogenetic brines and telogenetic meteoric waters caused intermittent formation of saddle dolomite and minor sulphides throughout solution-collapse and detrital fill in these karst systems (Fig.3D). Cavern systems close to fault zones at Mount Datson were partly filled with speleothem cements of stalactitic calcite and alternating chalcedonite and quartzine (Fig.3C), indicating sulphate fluctuations in the groundwater. Traces of sulphate and pseudomorphs after gypsum crystals are present in these speleothems. Managanese oxides are prolific as coatings in cavern and breccia porosity of dolines in the Digby Peaks–Swift Hills region — an area of earlier precipitation of manganoan saddle dolomite. The only known occurrences of manganoan saddle dolomite are Digby Peaks and the Glenormiston River area over the Smoky Anticline.

Smoky Anticline

Structural and erosional history. The Smoky Anticline is a broad arch that plunges gently south, with the Palaeozoic sequence overlying the western margin of the Mount Isa Orogen basement where it abuts the Arunta Inlier (Tucker & others, 1979). The cover of Ninmaroo Formation carbonates is thin. The area was intermittently emergent in the Late Cambrian and Early Ordovician during most of the period of Ninmaroo sedimentation (Radke, 1980). Karst developed. The surface was buried by Jurassic sediments, but subsequently exhumed and further enhanced by karstification (Fig.4B). The thickness of sequence removed by erosion is unknown. The sequence is gently flexured, locally well-jointed, and has faulting oriented north-northwest that predates and postdates Mesozoic burial (Fig. 4A).

West of the Smoky Anticline and to the north and northwest of the Toko Syncline, the Ninmaroo Formation flattens into an extensive area that has had a similar history of prolonged exposure and erosion. Well-developed jointing has been enhanced by karstification, but major faulting is not apparent.

Diagenetic history. During deposition of the Ninmaroo Formation the Smoky Anticline and adjacent platform region to the northwest were only briefly submerged, becoming emergent before sedimentation ceased elsewhere. Consequently, the telogenetic phase was prolonged (Fig.14). Much of the basal sequence was dolomitised and synsedimentary cherts formed under sabkha conditions. Silicification (megaquartz and chalcedonite precipitation) continued during later erosion. The region remains unfolded, although extensively jointed and faulted. Consequently, most of the sequence has remained an open system. Mesogenesis was probably short-lived, and it is unknown what degree of burial, if any, occurred prior to the Mesozoic. This diagenesis was probably a mixed telogenetic–mesogenetic type with connate brines migrating up dip from the Toko Syncline and up faults, mixing with a small and seasonally variable meteoric groundwater zone. The brines caused extensive and pervasive dolomitisation with subsequent saddle dolomite replacement. Moldic porosity after sulphates and vein porosity were occluded by sulphide, saddle dolomite, and fluorite cements. Fluorite is most abundant on dolostone–limestone contacts. Hydrocarbons were trapped only in tight fault blocks sealed by Jurassic mudstones, (Fig. 8B) and it is probable that, since erosion of this capping, hydrocarbons have continued escaping to the present, as indicated by bituminous calcrete filling joints in exposed weathered dolostone. Late-stage replacement in the sequence by mesogenetic sulphates was volumetrically minor, but extensive.

Over the long telogenetic stage, significant solution of carbonate and sulphate produced karst with dolines, prior to the Jurassic. In the Georgina River–Herbert Downs area, this karst topography was thinly covered in the Jurassic–Cretaceous period, and the dolines were probable sites of efflux of fluids from the Ninmaroo Formation into this cover. Evidence for this includes fossilised rootlets of probable Cretaceous age in the cave fill, and centimetre to decimetre-sized pyrite nodules in Mesozoic mudstones in the dolines. Upwelling of saline fluids has continued to the present day and moist salt-expanded soils are localised near these dolines in the surrounding and overlying Holocene regolith. Doline development has continued in the Cainozoic as indicated by collapse and disruption of Mesozoic fill and its Tertiary calcrete–ferricrete profiles. Presently, the dolostone remains a good aquifer, containing mainly saline water, but with localised lenses of fresh meteoric waters.

Economic implications

The relatively close timing of known sulphide mineralisation and hydrocarbon migration is apparent from the paragenetic sequence (Fig. 12). However, constraints on the absolute timing of these events are difficult to establish. Additionally, regional variations in tectonism and consequent burial and erosional history of the sequence have caused local variations in the generalised diagenetic sequence (Fig. 14). Apart from in the Toko Syncline, mesogenetic and late telogenetic stages were repeated during and after Mesozoic deposition (Fig. 14). The presence of sulphide mineralisation along the Ninmaroo Formation–Mesozoic unconformity and within the overlying Mesozoic sequence implies a syn-Mesozoic or post-Mesozoic phase. Hydrocarbon migration, which is closely related, probably continued during the second mesogenetic stage caused by Mesozoic burial. Post-Mesozoic migration is further supported by the venting of trace hydrocarbons from cavern systems and the occurrence of bituminous Quaternary calcretes in joints in exposed dolostones.

Consequently, post-Ordovician and Mesozoic cover has caprock potential and unconformity traps are possible. The regolith in the Swift Formation and mudstones in the Cretaceous Allaru Mudstone have especial potential as caprocks.

Sulphide mineralisation is likely to halo preexisting or present hydrocarbon traps and dolostone bodies, in addition to being localised in extensive cavern conduits that developed during the telogenetic stage preceding Mesozoic deposition. Post-Mesozoic movement on established faults and continued development of adjacent structures have created potential mineralisation sites. These include the Mount Ninmaroo, Datson, and Unbunmaroo domes next to the Black Mountain Fault, and monoclinal structures paralleling faults in the Noranside–Signal Hill area.

Conclusions

After eogenesis the Ninmaroo Formation was overprinted by three later diagenetic stages: early telogenesis, mesogenesis, and late telogenesis. These correspond to post-depositional emergence, burial, and uplift with erosion. Some areas had mixed mesogenesis–telogenesis, where the sequence was near surface, but acted as a site of efflux for deeper mesogenetic fluids.

The duration of each stage was dependent on the local history of burial and tectonism.

Three regions of differing diagenetic history in the four tectonic areas of the formation are the Toko Syncline, Smoky Anticline and the adjacent platform area to the north of the Toko Syncline, and the Burke River Structural Belt.

Early telogenesis featured: solution of carbonate and evaporitic sulphate to produce moldic, cavern, and collapse-breccia porosity; the replacement of sulphate and carbonate by chalcedony and megaquartz; calcite cementation in drusy and stalactitic textures; and minor sulphide precipitation.

Mesogenesis featured extensive calcite cementation; regional dolomite and saddle dolomite emplacement with development of intercrystalline porosity; associated precipitation of minor sulphides (pyrite, minor sphalerite and galena), fluorite, K-feldspar, and clays; and the migration of hydrocarbons. Secondary sulphates, baryte, celesite, and anhydrite, were later emplaced. Stylolite formation took place throughout burial.

Late telogenesis incorporated a continuation of chalcedonic and quartz replacement and cementation, stalactitic calcite cementation, dedolomitisation, and precipitation of manganese oxides. The solution of remaining primary and secondary sulphates developed moldic and breccia porosity, with cavern porosity also resulting from carbonate solution.

Timing of hydrocarbon migration varied regionally, probably starting during the Late Devonian Alice Springs Orogeny, recurring during Mesozoic burial of the sequence, and continuing into the Cainozoic. Sulphide precipitation occurred predominantly where hydrocarbons were present. Karst-related mineralisation is syn-Mesozoic and post-Mesozoic sedimentation.

Acknowledgements

Assistance with field work and discussions were freely given by E.C. Druce, J. Kennard, J.H. Shergold, J. Draper, and C. Pointon throughout the duration of the BMR Georgina Basin project. Technical and logistic support was provided by K. Heighway, and this is much appreciated. The development of diagenetic models has come through stimulating discussions with R.L. Mathis, G.M. Friedman, C.H. Moore Jr, A.C. Kendall, and W. Rogers. K.A.W. Crook, B. Logan, P.J. Davies, C.J. Simpson, and J.H. Shergold are thanked for their constructive criticisms of the manuscript.

References

Alderman, A.R., & Skinner, H.G.W., 1957 — Dolomite sedimentation in the south-east of South Australia. *American Journal of Science*, 255, 561–67.

Australian Aquitane Petroleum Pty Ltd., 1972 — Georgina field survey No. 2, September 1972 field report. *Unpublished company report prepared by P.Artru & R. Niay.*

Bailey, S.W., & Cameron, E.N., 1951 — Temperatures of mineral formation in bottom-run lead-zinc deposits of the upper Mississippi Valley, as indicated by liquid inclusions. *Economic Geology*, 48, 626–51.

Barton, P.B., Jr., 1967 — Possible role of organic matter in the precipitation of the Mississippi Valley ores. *In* Brown, J.S. (editor), Genesis of stratiform lead-zinc-barite-fluorite deposits. *Economic Geology, Monograph* 3, 371–8.

Bathurst, R.G.C., 1958 — Diagenetic fabrics in some British Dinantian limestones. *Liverpool and Manchester Geological Journal*, 2, 11–26.

Beales, F.W., 1971 — Cementation by white sparry dolomite. *In* Bricker, O.P. (editor), Carbonate cements. *The John Hopkins University Press, Baltimore*, 330–8.

Bebount, D.G., & Pendexter, C., 1975 — Secondary carbonate porosity as related to Early Tertiary depositional facies, Zelten Field, Libya. *American Association of Petroleum Geologists, Bulletin*, 59, 665–93.

Blount, D.R., & Moore, C.H. Jr, 1969 — Depositional and non-depositional carbonate breccias, Chiantla Quadrangle, Guatemala. *Geological Society of America, Bulletin*, 80, 429–42.

Broughton, P.L., 1973 — Replacement of gypsum by length-slow chalcedony in the karst subsurface. *Caves and Karst*, 15, 21–3.

Brown, G.A., 1961 — Stratigraphy, structure and sedimentary petrology of some lower Palaeozoic limestones from the Boulia area, Queensland. *M.Sc. Thesis, Melbourne University*, (unpublished).

Butler, G.P., 1969 — Modern evaporite deposition and geochemistry of coexisting brines, the Sabkha, Trucial Coast, Arabian Gulf. *Journal of Sedimentary Petrology*, 39, 70–89.

Buxton, T.M., & Sibley, D.F., 1981 — Pressure solution features in a shallow buried limestone. *Journal of Sedimentary Petrology*, 51, 27–36.

Carpenter, R., 1969 — Factors controlling the marine geochemistry of fluorine. *Geochimica et Cosmochimica Acta*, 33, 1153–67.

Carter, E.K., Brooks, J.H., & Walker, K.R., 1961 — The Precambrian mineral belt of north-western Queensland. *Bureau of Mineral Resources, Australia, Bulletin* 51.

Casey, J.N., Reynolds, M.A., Dow, D.B., Pritchard, P.W., Vine, R.R., & Paten, R.J., 1960 — The geology of the Boulia area, Western Queeensland. *Bureau of Mineral Resources, Australia, Record* 1960/12 (unpublished).

Choquette, P.W., 1971 — Late ferroan dolomite cement, Mississippian carbonates, Illinois Basin, U.S.A. *In* Bricker, O.P. (editor), Carbonate cements. *John Hopkins University Press, Baltimore*, 339–46.

Choquette, P.W., & Pray, L.C., 1970 — Geological nomenclature and classification of porosity in sedimentary carbonates. *American Association of Petroleum Geologists, Bulletin*, 54, 207–50.

Conley, C., 1977 — Origin of distorted ooliths and pisoliths. *Journal of Sedimentary Petrology*, 47, 554–64.

Connor, A.G., 1978 — Annual Report: Digby Peaks A to P 160SM north-west Queensland. *C.R.A. Exploration Report*, 9132 (unpublished).

Davies, P.J., 1971 — Calcite precipitation and recrystallization fabrics — their significance in Jurassic limestones of Europe. *Geological Society of Australia, Journal*, 18, 279–92.

Deffeyes, K.S., Lucia, F.J., & Weyl, P.K., 1965 — Dolomitization of Recent and Plio-Pleistocene sediments by marine evaporite waters on Bonaire, Netherlands, Antilles. *In* Pray, L.C., & Murray, R.C., (editors), Dolomitization and limestone diagenesis — a symposium. *Society of Economic Paleontologists and Mineralogists, Special Publication* 13, 71–88.

de Groot, K., 1967 — Experimental dedolomitization. *Journal of Sedimentary Petrology*, 37, 1216–20.

Draper, J.J., 1976 — Progress report on Georgina Basin geochemistry — results of 1974 field season. *Bureau of Mineral Resources, Australia, Record* 1976/57 (unpublished).

Draper, J.J., 1978 — Progress report on Georgina Basin geochemistry — results from 1975, 1976 field seasons. *Bureau of Mineral Resources, Australia, Record* 1978/23, (unpublished).

Dunsmore, H.E., 1973 — Diagenetic processes of leadzinc emplacement in carbonates. *Transactions of the Institution of Mining & Metallurgy, Section B*, 82, B168–73.

Ebers, M.L., & Kopp, O.C., 1979 — Cathodoluminescent microstratigraphy in gangue dolomite, the Mascot-Jefferson City District, Tennessee. *Economic Geology*, 74, 908–18.

Evamy, B.D., 1963 — The application of a chemical staining technique to a study of dedolomitization. *Sedimentology*, 2, 164–70.

Evamy, B.D., 1967 — Dedolomitization and the development of rhombohedral pores in limestones. *Journal of Sedimentary Petrology*, 37, 1204–15.

Evamy, B.D., & Shearman, D.J., 1965 — The development of overgrowths from echinoderm fragments. *Sedimentology*, 5, 211–34.

Folk, R.L., 1959 — Practical petrographic classification of limestones. *American Association of Petroleum Geologists, Bulletin*, 43, 1–38.

Folk, R.L., & Land, L.S., 1975 — Mg/Ca ratio and salinity: two controls over crystallization of dolomite. *American Association of Petroleum Geologists, Bulletin*, 59, 60–8.

Folk, R.L., & Pittman, J.S., 1971 — Length-slow chalcedony: a new testament for vanished evaporites. *Journal of Sedimentary Petrology*, 41, 1045–58.

Freas, D.H., 1961 — Temperature of mineralization by liquid inclusions, Cave-in-Rock fluorspar district, Illinois. *Economic Geology*, 56, 542–56.

Friedman, G.M., & Radke, B.M., 1979 — Evidence for sabkha overprint and conditions of intermittent emergence in Cambrian–Ordovician carbonates of northeastern North America and Queensland, Australia. *Northeastern Geology*, 1, 18–42.

Friedman, G.M., & Sanders, J.E., 1967 — Origin and occurrence of dolostones. *In* Chilinger, G.V., Bissell, H.J., & Fairbridge, R.W., (editors), Carbonate rocks, origin, occurrence, and classification. *Elsevier, Amsterdam*, 267–348.

Friedman, G.M., & Sanders, J.E., 1978 — Principles of sedimentology. *John Wiley, New York.*

Goldberg, M., 1967 — Supratidal dolomitization and dedolomitization in Jurassic rocks of Hamakhtesh Haqatan, Israel. *Journal of Sedimentary Petrology*, 37, 760–73.

Harrison, P.L., 1979 — Recent seismic studies upgrade the prospects of the Toko Syncline, Georgina Basin. *APEA Journal*, 19, 30–42.

Harrison, P.L., 1980 — The Toomba Fault and the western margin of the Toko Syncline, Georgina Basin, Queensland and Northern Territory. *BMR Journal of Australian Geology & Geophysics*, 5, 201–14.

JACKSON, K.S., 1982 — Geochemical evaluation of the petroleum potential of the Toko Syncline, Georgina Basin, Queensland, Australia. *BMR Journal of Australian Geology & Geophysics*, 7, 1–10.

KENDALL, A.C., & BROUGHTON, P.L., 1978 — Origin of fabrics in speleothems composed of columnar calcite crystals. *Journal of Sedimentary Petrology*, 48, 519–38.

KENDALL, C.A. St. C., & SKIPWITH, Sir P.A. d'E., 1968 — Recent algal mats of a Persian Gulf lagoon. *Journal of Sedimentary Petrology*, 38, 1040–58.

KINSMAN, D.J., 1969 — Modes of formation, sedimentary associations and diagnostic features of shallow-water and supratidal evaporites. *American Association of Petroleum Geologists, Bulletin*, 53, 830–40.

LOGAN, B.W., 1961 — *Cryptozoon* and associated stromatolites from the Recent, Shark Bay, Western Australia. *Journal of Geology*, 69, 517–33.

LOGAN, B.W., HOFFMAN, P., & GEBELEIN, C.D., 1974 — Algal mats, cryptalgal fabrics, and structures, Hamelin Pool, Western Australia. *In* LOGAN, B.W., READ, J.F., HAGAN, G.M., HOFFMAN, P., BROWN, R.G., WOODS, P.J., & GEBELEIN, C.D., Evolution and diagenesis of Quaternary carbonate sequences, Shark Bay, Western Australia. *American Association of Petroleum Geologists, Memoir* 22, 140–94.

LOGAN, B.W., & SEMENIUK, V., 1976 — Dynamic metamorphism; processes and products in Devonian carbonate rocks, Canning Basin, Western Australia. *Geological Society of Australia, Special Publication* 6.

LUCIA, F.J. 1961 — Dedolomitization in the Tansill (Permian) Formation. *Geological Society of America, Bulletin*, 72, 1107–10.

MATHIS, R.L., 1978 — Carbonate sedimentation and diagenesis of reef and associated shoal-water facies, Sligo Formation (Aptian), Black Lake Field, Natchitoches Parish, Louisiana. *M.S. thesis, Rensselaer Polytechnic Institute, Troy, New York.*

MIDDLETON, G.V., 1961 — Evaporite solution breccias from the Mississippian of southwest Montana. *Journal of Sedimentary Petrology*, 31, 189–95.

MOORE, C.H.Jr., 1971 — Pseudospar dedolomite "cements" of evaporite solution collapse breccias. *In* BRICKER, O.P., (editor), Carbonate cements. *John Hopkins University Press, Baltimore*, 347–51.

MOORE, C.H., Jr., SMITHERMAN, J.M., & ALLEN, S.H., 1972 — Pore system evolution in a Cretaceous carbonate beach sequence. *Proceedings of the 24th International Geological Congress*, Section 6, 124–36.

NICOLL, R.S., 1979 — Conodont color alteration in petroleum exploration well Ethabuka 1, Queensland. *BMR Professional Opinion* GEOL 79.018 (unpublished).

OPIK, A.A., 1960 — Cambrian and Ordovician geology. *In* HILL, D., & DENMEAD, A.K., The geology of Queensland. *Journal of the Geological Society of Australia*, 7, 89–109.

ORME, G.R., & BROWN, W.W.M., 1963 — Diagenetic fabrics in the Avonian Limestones of Derbyshire and North Wales. *Proceedings of the Yorkshire Geological Society*, 34, 51–66.

RADKE, B.M., 1978 — Carbonate sedimentation in tidal and epeiric environments and diagenetic overprints: the Ninmaroo Formation (Upper Cambrian–Lower Ordovician), Central Australia. *Ph.D thesis, Rensselaer Polytechnic Institute, Troy, New York.*

RADKE, B.M., 1980 — Epeiric carbonate sedimentation of the Ninmaroo Formation (Upper Cambrian–Lower Ordovician), Georgina Basin. *BMR Journal of Australian Geology & Geophysics*, 5, 183–200.

RADKE, B.M., 1981 — Lithostratigraphy of the Ninmaroo Formation (Upper Cambrian Lower Ordovician), Georgina Basin. *Bureau of Mineral Resources, Australia, Report* 181; *BMR Microform* MF153.

RADKE, B.M., & DUFF, P., 1980 — A potential dolostone reservoir in the Georgina Basin: the Lower Ordovician Kelly Creek Formation. *BMR Journal of Australian Geology & Geophysics*, 5, 160–3.

RADKE, B.M., & MATHIS, R.L., 1980 — On the formation and occurrence of saddle dolomite. *Journal of Sedimentary Petrology*, 50, 1149–68.

REES, M.N., BRADY, M.J., & ROWELL, A.J., 1976 — Depositional environments of the Upper Cambrian Johns Wash Limestone (House Range, Utah). *Journal of Sedimentary Petrology*, 46, 38–47.

SCHMIDT, V., 1965 — Facies, diagenesis, and related reservoir properties in the Gigas Beds (Upper Jurassic), northwestern Germany. *In* PRAY, L.C., & MURRAY, R.C., (editors), Dolomitization and limestone diagenesis. *Society of Economic Paleontologists and Mineralogists, Special Publication* 13, 124–68.

SHEARMAN, D.J., KHOURI, J., & TAHA, S., 1961 — On the replacement of dolomite by calcite in some Mesozoic limestones from the French Jura. *Proceedings of the Geologists Association, London*, 72, 1–12.

SHINN, E.A., GINSBURG, R.N., & LLOYD, R.M., 1965 — Recent supratidal dolomite from Andros Island, Bahamas. *In* PRAY, L.C., & MURRAY, R.C., (editors), Dolomitization and limestone diagenesis, a symposium. *Society of Economic Paleontologists and Mineralogists, Special Publication*, 13, 112–23.

SMITH, F.W., 1974 — Factors governing the development of fluorspar orebodies in the north Pennine orefield. *Transactions of the Institution of Mining & Metallurgy, Section B*, 84, B71 (abstract).

TUCKER, D.H., WYATT, B.W., DRUCE, E.C., MATHUR, S.P., & HARRISON, P.L., 1979 — The upper crustal geology of the Georgina Basin region. *BMR Journal of Australian Geology & Geophysics*, 4, 209–26.

VON MORLOT, A., 1847 — Sur l'origine de la dolomite. *Compte rendu de l'Academie des Sciences, Paris*, 26, 311–15.

YANAT'EVA, O.K., 1955 — Effect of aqueous solutions of gypsum on dolomite in the presence of carbon dioxide. *Akademiya Nauk SSSR, Doklady*, 101, 911–12.

ZENGER, D.H., 1973 — Syntaxial calcite borders on dolomite crystals, Little Falls Formation (Upper Cambrian), New York. *Journal of Sedimentary Petrology*, 43, 118–24.

BMR Journal of Australian Geology & Geophysics, 7, 255-268

PALYNOLOGY OF TERTIARY LAKE BUNYAN, COOMA, NEW SOUTH WALES

J.R. Tulip[1], G. Taylor[2], & E.M. Truswell[3]

Pollen and spore assemblages have been recovered from coaly lenses and marginal facies of Tertiary lacustrine sediments at Lake Bunyan, north of Cooma, southern New South Wales. Remains of lake sediments in the area are extensive, and a variety of facies has been recognised. Clays are dominant, but volcanogenic conglomerates, sands, silts, coals, diatomites, and a marginal quartzose facies also occur. Palynological assemblages have been recovered from coaly lenses and from the marginal facies. The pollen and spore suite is poorly diversified. Pollen of *Nothofagus* dominates, and that of podocarpaceous conifers is well represented. Myrtaceous pollen is common in a few samples only, proteaceous pollen is very rare, and there is occasional local dominance by aquatic taxa. Dating is made difficult by a lack of known stratigraphic marker species. In general, the assemblage resembles microfloras of the *Proteacidites tuberculatus* Zone, which spans the early Oligocene through early Miocene interval in the Gippsland Basin. The presence of *Haloragacidites haloragoides*, however, is more in accord with the *Triporopollenites bellus* Zone, of late early to late Miocene age. Detailed comparison with other palynological suites from highland sites dated by association with basalts suggests an age for the Lake Bunyan deposit of 12–21 m.y., i.e. late early to middle Miocene. In comparison with other Miocene pollen floras from southeastern Australia, the Bunyan assemblage lacks forms indicative of subtropical rainforest, and forms indicative of cool temperate rainforest are poorly diversified. These features, combined with the relative abundance of conifer pollen in the assemblage, may reflect conditions somewhat cooler than other areas of southeastern Australia during the Miocene. An interpretation of pollen spectra from the deposit suggests that a variety of lake edge and bog communities successively surrounded the sites examined.

Introduction

Lake Bunyan is the name used by Taylor & others (1980) to describe the depositional site of a suite of Tertiary lake deposits between Cooma and Bredbo, in southeastern New South Wales. The deposits occur along the present course of the Murrumbidgee and Numeralla Rivers and their tributaries (Fig. 1). Remnants of lake sediments have been identified at Billillingra near Bredbo (Pillans, 1977; Taylor & others, 1980), on the Big Badja River, the Numeralla River near Numeralla, and at Rose Valley (Fig. 1). The most extensive and best documented deposits occur along Middle Flat Creek near Bunyan. Diatomite deposits at Middle Flat have been mined since 1896 (Herbert, 1968), but the associated lake sediments were not recognised until recently (Taylor & others, 1980).

The origin of the lake is uncertain, but, as no deposits have been found north of Bredbo, it is likely that damming of the ancestral Murrumbidgee was caused by intermittent movement on the Murrumbidgee Fault in this area. The exact extent of the lake in the past is unknown, although most lake deposits occur below the 780 m contour, and this may represent the possible extent of the lake. Figure 1 shows several deposits above the 780 m contour, extending up to 830 m. The present position of these may be due to post-depositional tectonism.

A multidisciplinary investigation of the Lake Bunyan sediments is currently being undertaken jointly by the CSIRO Divisions of Soils and Mineral Physics, the School of Applied Science of the Canberra College of Advanced Education, the Bureau of Mineral Resources, and the Research School of Earth Sciences, Australian National University. To date, this has included detailed studies of the petrology, clay mineralogy, and sedimentology of the sediments, a palaeomagnetic study of weathered profiles within the sequence (Schmidt & others, 1982), and a palynological study. This paper reports the results of the palynological study together with a brief summary of facies recognised in the lake sediments.

The palynological study was undertaken to determine as precise an age as possible for the deposits, age estimates by other means having proved inconclusive. The relation of the sediments to adjacent Eocene basalts of the Monaro Province (Wellman & McDougall, 1974) is obscure, as nowhere have they been seen in contact. However, it is likely that the clays that make up a high proportion of the sediments were derived from the weathering of Eocene basalts.

Other fossils recovered from the sequence have provided only broad ages, although all accord with a post-Eocene date. Diatomites from Middle Flat, in the upper part of the sequence, were examined by Thomas & Gould (1981a,b), who expressed reservations about the biostratigraphic use of freshwater diatomites, but commented that the Middle Flat deposits were probably no older than diatomites from Black Duck Creek in southwest Queensland. The latter have been dated by associated basalts as late Oligocene.

Plant macrofossils have been recovered from clays below a lignitic horizon near the drill hole Bega 1, but have been examined only in a preliminary fashion. Dr. D. Christophel (personal communication to G. Taylor, 1980) indicated that fern and angiosperm leaf remains from this locality are most similar to a mid-Miocene flora from the Morwell coal seam in the Latrobe Valley, but expressed reservations about the stratigraphic significance of this similarity. Fragmentary fish remains from an unspecified diatomite locality near Cooma were identified by Hills (1946) as closely comparable with those of the extant Murray Cod (*Maccullochella macquariensis* — (Cuvier & Valenciennes)), but again this is of limited biostratigraphic significance.

Results of recent palaeomagnetic studies (Schmidt, P.W., Taylor, G., & Walker, P.H., unpublished data, 1982; Taylor & others, 1980), using palaeo-pole positions obtained from weathered profiles within the sequence, suggest a Late Tertiary age, but margins of error are wide. This determination contrasts with the Palaeocene–Eocene determination made on the same weathered sequence by Pillans (1977), using similar techniques.

Establishing a precise age for the lake deposits is useful in understanding the tectonic evolution of the southern highlands. Setting an age limit to the deposit would date movement on the Murrumbidgee Fault and set an upper limit to the age of topography associated with the lake upstream along the Murrumbidgee. The palynology of the deposit is also of interest for the information it provides on the evolution of highland Tertiary vegetation and climate.

[1] 6 Mara Place, Waramanga, ACT 2611
[2] Dept. of Applied Science, Canberra College of Advanced Education, P.O. Box 1, Belconnen, ACT 2616
[3] Bureau of Mineral Resources, PO Box 378, Canberra, ACT 2601

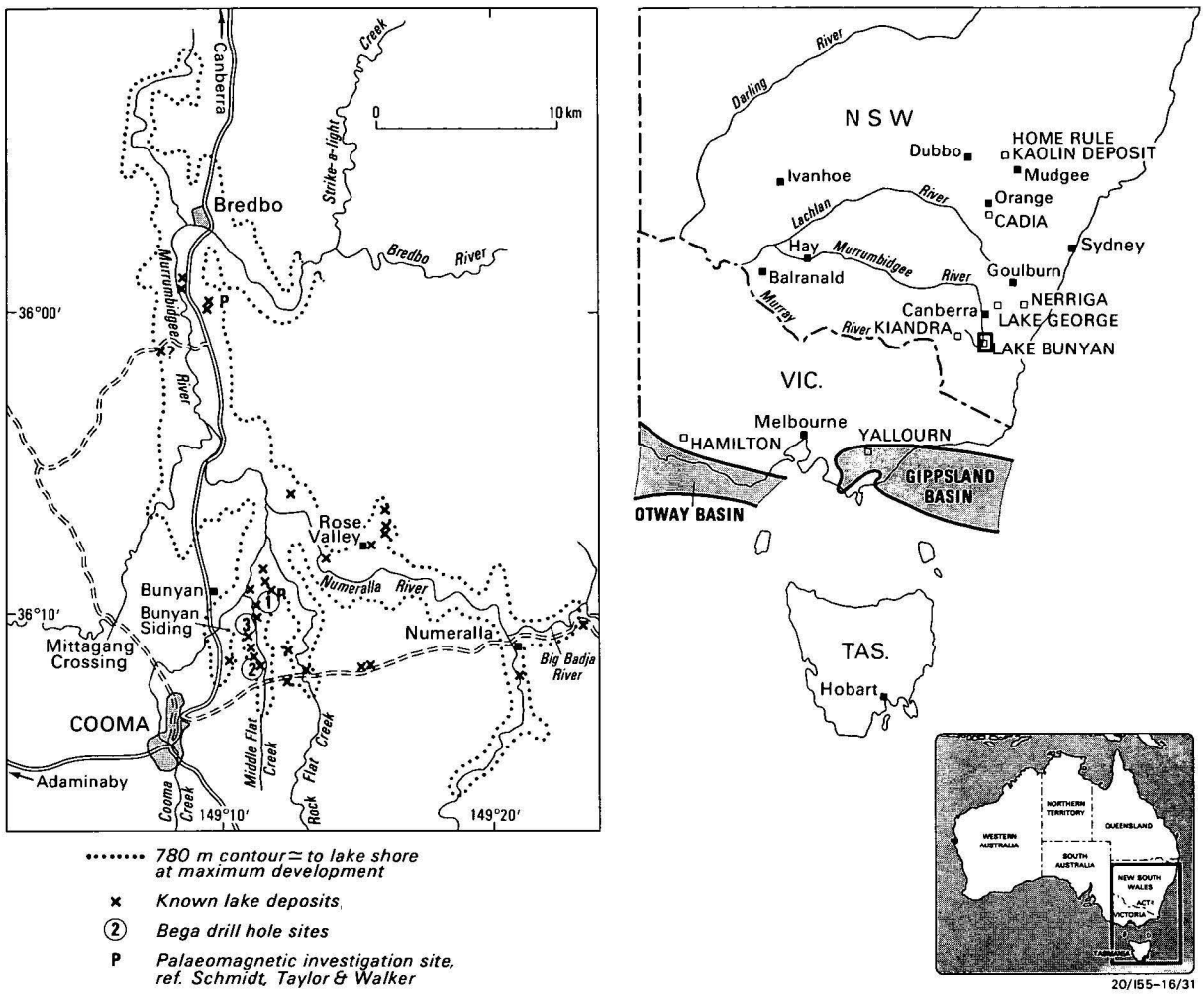

Figure 1. Locality map showing known Tertiary lake deposits, the possible extent of former Lake Bunyan and BMR Bega drillhole sites. Inset shows southeastern Australia with the localities of other Tertiary palynological sites discussed in the text.

Material and lithology

Material examined in this study is from three coreholes, Bega Nos. 1, 2 and 3 (Grid refs. Cooma 1:100 000 Sheet; 974966, 959927, 958950), drilled by the Bureau of Mineral Resources in the Middle Flat area (Figs. 1 & 2).

Five broad facies groups have been recognised based on field, subsurface and petrographic studies:

Clay facies. This is the dominant facies and occurs in various amounts at most sites. The clays are dominated by 0.2–0.1 μm sized, well crystallised kaolinite, with minor smectite and haloysite. Quartz sand occurs scattered through the clays and in the sandy laminae. The clays are massive to well laminated, grey to red, and commonly disturbed. Primary gypsum occurs as lenticular clusters of crystals at a few sites. Thin lenticular diatomite lenses occur throughout the shallower parts of this facies. Secondary sesquioxide nodules and mottles, siderite rosettes and nodules, jarosite, and barite occur as secondary minerals.

Volcanogenic facies. This consists of interbedded sand, silt, clay, and conglomerate made up of pebbles and granules of basalt, basic glass, and metamorphic and acid volcanic rock-fragments. Basic volcanogenic material dominates. The sands and silts are dominantly olivine and feldspar euhedra and subhedra, glass, with minor quartz and metamorphic rock fragments. Most of the components have been altered in places to goethite, clay, chalcedony and other products, and the facies has a high proportion of clay matrix. The facies is generally well bedded and graded beds up to 1 cm thick are common. Wet sediment deformation and bioturbation structures are common. Siderite, as nodules and rosettes, is a common secondary mineral. This facies is typified also by numerous soils developed through the sequence (Fig. 2).

Marginal quartzose facies. This occurs at the base of the cores, as thin bands in the body of the deposit, and at or near the lake margins. It is composed entirely of quartz granules, sand and silt with minor clay and durable rock fragments; it is well bedded, frequently crossbedded and often shows lenticular lamination. Thin wispy lignitic stringers and laminae occur at some sites, with secondary sesquioxides as mottles and siderite rosettes and nodules. Diatom and sponge spicule concentrations are locally high in the finer beds of this facies.

Coaly facies. Coal seams, up to 0.75 m thick, are interbedded with clays over a 13 m section in Bega 1, the only locality yet discovered containing a substantial thickness of this facies. The coals in general contain abundant macrofloral remains and are highly pyritic.

Diatomite facies. This consists of a thick sequence (15 m) of massive to very well laminated diatomite. It also contains clay-rich beds and partings, zones of brecciation and opalisation, and palaeosols consisting primarily of organic residues. Thomas & Gould (1981) have described the diatom flora from this facies.

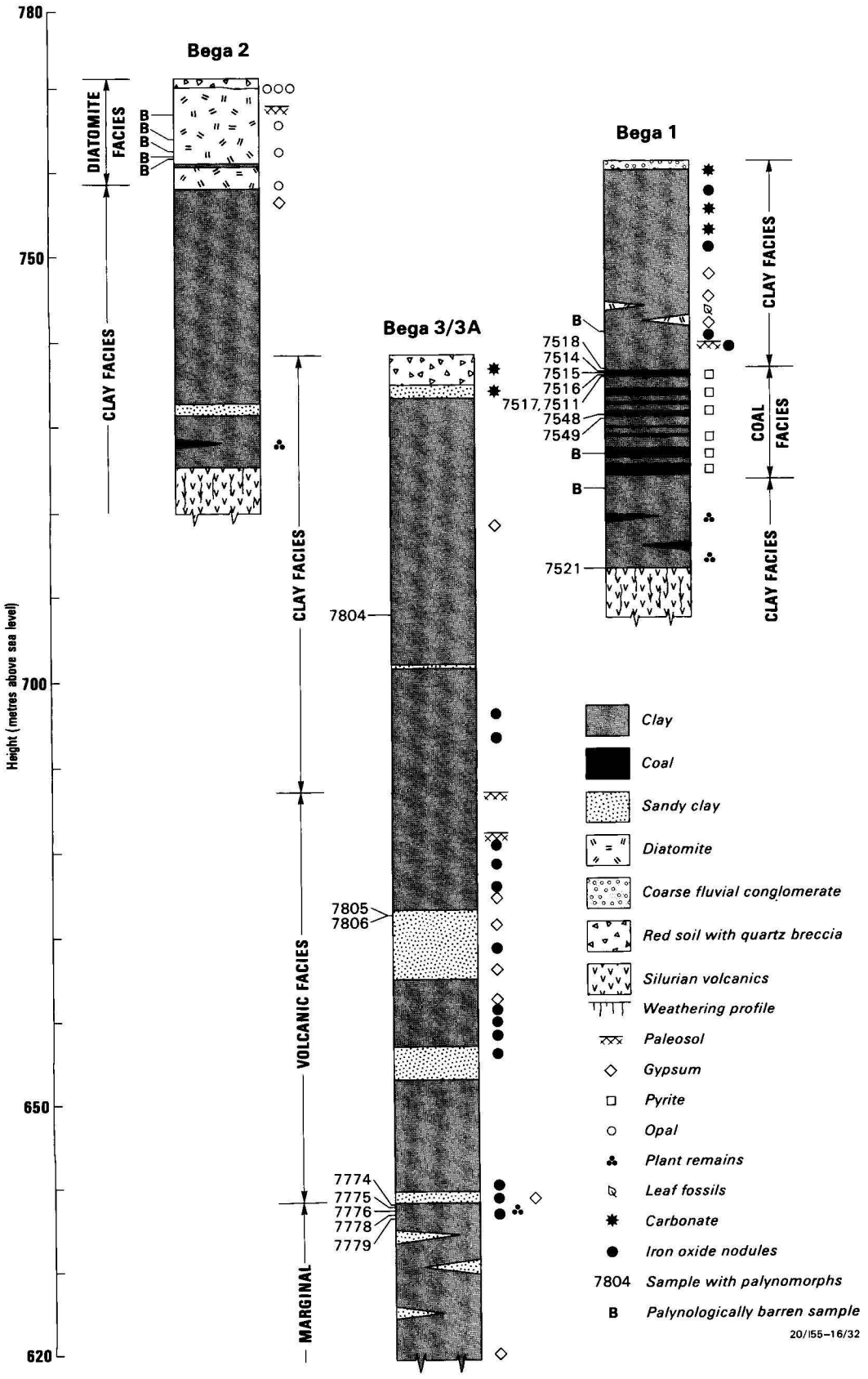

Figure 2. Stratigraphic sections through BMR coreholes Bega 1, 2 and 3/3A.
Facies to which sequences are assigned are shown beside the columns. Palynological sample horizons are indicated by numbers to the left of each column. Numbers are those of the MFP palynological collection of the Bureau of Mineral Resources. Barren samples are indicated by B.

Palynologically productive samples are concentrated in two short sequences in Bega 1 and Bega 3 (Fig. 2). Productive samples from Bega 3 come from the top of marginal quartzose facies sediment, just beneath volcanogenic sediments. Those from Bega 1 come from a coaly lens within the coaly facies. Two other productive samples come from below the main sequences in both Bega 1 (7548) and Bega 3 (7779). One sample from Bega 3 (7804) occurs in the clay facies. Bega 3 is situated near the centre of Middle Flat, while Bega 1 was drilled within 40 m of marginal facies sediments and Palaeozoic basement outcrop (Fig. 1).

Composition of the assemblages

The Lake Bunyan palynological assemblage is of low diversity when compared to other Tertiary assemblages from southeastern Australia (e.g. Owen, 1975; Luly & others, 1980).

Table 1. List of palynological species in BMR Bega cores, with their relative abundances.
These are expressed as a percentage of the total number of palynomorphs observed, excluding *Sparganiaceaepollenites* species, *Inaperturopollenites* species, and *Schizosporis*. All percentages are based on counts of 200 grains from terrestrial taxa.

	BEGA 3							BEGA 1					
	7779	7778	7777	7776	7775	7774	7804	7548	7517	7511	7515	7514	7518
Gleicheniidites circinidites (Cookson) Dettman 1963	+												
Lycopodiumsporites sp. cf. sp.1 of Owen 1975			+		+		+						
Lycopodiumsporites sp. cf. sp.3 of Owen 1975			+										
Ceratosporites sp.		+	+	+	+	+							
Trilete spores	8	1.4	1.4	.4	.7	5.6	8.2			.7		1.0	1.6
Reticuloidosporites sp.	+		+		+		33.0						
Laevigatosporites spp.	18.1	3.5	2.4	+	1.2	2.4	18.2	2.5	3.2	4.2	24.4	31.7	14.9
Podocarpidites spp. (undiff.)	4.9	12.8	16.0	4.3	12.6	9.4	11.5	+	.6	8.1	5.0	1.0	4.8
Podocarpidites ellipticus Cookson 1947	+	+	+	+	+	+				+	+	+	
P. marwickii Couper 1953	+	+											
P. cf. *multesimus* (Bolkovitina) Pocock 1963	+	+	+	+									
P. sp.1 cf. P.sp. Owen 1975		+	+	+		+				+	+	+	.5
P. sp.2	+	4.4	.8	+	+	.7							
P. sp.3 cf. sp. Partridge 1971	.8	1.8	.4	+		.7				4.9	1.3	.5	
Parvisaccites catastus Partridge 1973			+										
Lygistepollenites florinii (Cookson & Pike) Stover & Evans 1973		+	+							+	+		
Alisporites grandis (Cookson) Dettmann 1963		+		+	+	+				+			
'Phyllocladus' paleogenicus Cookson & Pike 1954	1.9	5.8	5.2	+	1.9	.3	4.9			.3	2.1		1.1
Dacrycarpites australiensis Cookson & Pike 1953	+	.5	2.8	+		.3		+		2.3		.5	.5
Podosporites microsaccatus (Couper) Dettmann 1963	22.3		+	55.2	2.4	.3		.4	+		18	+	35.6
Micocachryidites antarcticus Cookson 1947		+								+			
Araucariacites australis Cookson 1947	2.7	4.9	1.9	2.1	+	.3		1.2	2.0	10.1	+		1.6
Dilwynites granulatus Harris 1965	6.2	+	+						.7	+	+		
D. sp. cf. *D. tuberculatus* Harris 1965													
Liliacidites spp.								.4	.5	.3	.8	.5	
L. lanceolatus Stover 1973					+	+							
Tricolpites psilatus Martin 1973		+						+				.5	
T. retiformis Martin 1973											+	5.5	2.3
T. sp.1								1.6	1.6	2.0	3.0	7.2	.5
T. sp.2							+		.2	1.6	.8	.9	1.1
Undifferentiated tricolpates	+	+			+			+	+	+	+	+	
Ilexpollenites anguloclavatus McIntyre 1968													
Tricolporites sphaerica Cookson 1947	+	+		+									
T. microreticulatus Harris 1963												.5	
Undifferentiated tricolporates	+	+		+	+	+			1.0	.7			
Myrtaceidites mesonesus Cookson & Pike 1954									.5	+	+	+	+
M. parvus Cookson & Pike 1954	9.1	3.5	21.2	15.0		.3							1.6
Nothofagidites emarcidus (Cookson) Harris 1965	8.4	12.4	9.9	7.3	27.7	35.2	9.9	6.2	29.3	23.8	21.0	24.0	6.4
N. heterus (Cookson) Stover & Evans 1973	8.4	19.5	15.3	4.3	37.2	30.0	23.2	16.3	18.7	3.6	16.4	16.7	3.2
N. falcatus (Cookson) Stover & Evans 1975		+		+				3.9	3.5	6.2		.9	
N. incrassatus (Cookson) Owen 1975								14.4					
N. deminutus/vansteenisii (Cookson) Stover & Evans 1973	+	2.6	5.7	1.3	2.5	1.7			1.5	1.3		.5	
N. brachyspinulosus (Cookson) Harris 1965	17.1	10.3	9.4	6.4	4.2	4.9		3.1	9.1	7.8	7.6	8.1	.5
N. sp. cf. *N. flemingii* (Couper) Potonie 1960	+	+	+			+							
N. asperus (Cookson) Stover & Evans 1973	+	2.6	3.3	+	5.9	2.8		11.7	15.2	11.4	8.4	1.8	+
N. goniatus (Cookson) Stover & Evans 1973		+			+								
Sparganiaceaepollenites sp.													
S. sp. cf. *S. barungensis* Harris 1972	6.0	3.1	2.8	6.4	4.2	.7	287.5	.4	188	139.7	5.9	1.8	
Milfordia homeopunctata (McIntyre)									+				
Graminidites media Cookson 1947									3.0				
Cyperaceae sp.								+	+				
Proteacidites annularis Cookson 1950										+		1.1	
P. minimus Couper 1954	.6	+				.7							
P. ivanhoensis Martin 1973	.6	+	+		+	+							
P. sp. cf. *P. symphonemoides*	+												
P. sp. cf. *P. parvus* Cookson 1950									.7				
Haloragicidites harrisii (Couper) Harris 1971	.8	.9	+	.4		.3			3.5	2.3	+	.2	.6
H. trioratus Couper 1953													
H. haloragoides Cookson & Pike 1954	+												
H. sp. cf. *trioratus*								35.0					
Onagraceae sp.									3.0				
Periporopollenites demarcatus Stover 1973		+											
P. sp. cf. sp.1 of Owen 1975		+	+										
P. sp. cf. sp.2 of Owen 1975				+									
Ericipites sp. cf. *E. scabratus* Harris 1965	+	+						+		+		.4	23.4
Inaperturate pollen grains sp. 1	1.9	5.8	6.6	1.3	6.6	+		+	41.9	6.8	11.8	2.1	2.1
Inaperturate pollen spp.	3.0	3.5	6.6	3.9	+								
Schizosporis sp.									2.5	9.6			1.1

Assemblages from the Bega coreholes consist dominantly of angiospermous pollen of the *Nothofagidites* type. *Nothofagus fusca* types (*N. brachyspinulosus, N. flemingii*) and *Nothofagus menziesii* types (*N. asperus*) are particularly abundant in some samples. Three samples are dominated by species of *Sparganiaceaepollenites*, one by the ericalean form *Erecipites* sp.cf. *E. scabratus*, and one by the casuarinaceous *Haloragacidites* sp.cf. *H. trioratus*. Myrtaceous pollen is well represented in a few samples, but is absent from most. Proteaceous pollen is very rare, as are other types of angiosperm grains.

Conifer pollen is common in most samples, and includes diverse podocarpaceous forms. *Podosporites microsaccatus* is abundant in some spectra. Pollen of Araucariaceae (referred here to *Araucaria*) is common only at two horizons. The diversity of spores is low, and trilete species are rare.

Most forms observed could be identified with published Tertiary form genera and species. However, some forms are not identical to figured type specimens; these have only been compared to published species. New species have not been erected here, as detailed taxonomy is outside the scope of this work; in any case, new species were represented by rare grains only.

Representative palynomorphs from the Bega coreholes are illustrated in Figures 5 and 6. Form species identified are listed in Table 1, together with relative abundances. The relative abundances were calculated to exclude *Sparganiaceaepollenites* species, as these were overwhelmingly abundant in three samples and their inclusion in the pollen sum would have made comparisons of pollen spectra difficult. Forms of uncertain affinity, probably algal in origin, were also excluded from the pollen sum. Pollen spectra for each of the samples analysed are illustrated in Figure 4; the botanical affinities of species identified are given in Table 2.

Dating the deposit

Tertiary palynological dating in southeastern Australia is based for the most part on correlations with spore and pollen zones established in the Gippsland Basin of eastern Victoria (Stover & Evans 1973; Stover & Partridge 1973). The Gippsland zonal sequences are illustrated in Figure 3. That basin contains the most complete sedimentary record for the Tertiary period in eastern Australia; it is also the most intensively studied from a palynological viewpoint, and has come to serve as a reference or standard sequence for the Tertiary. Marine sequences in the basin have been correlated with planktic foraminiferal zones, thus establishing their relationship to the global Tertiary timescale. Details of the correlation of the Gippsland Basin palynological zones with pan-tropical planktic foraminiferal zones are given in Abele & others (1976), and shown in Figure 3.

The palynological zones erected within the Gippsland Basin are in essence, concurrent range zones, depending for their definition on overlapping stratigraphic ranges of a number of taxa. In practice, the base of a zone is recognised by the first appearance in time of as few as two or three taxa. In all cases

Table 2. Botanical affinities and pollen production and dispersal abilities of modern taxa identified in Lake Bunyan.
Data on production and dispersal taken from Luly & others (1980). UK = Unknown.

		Production			*Dispersal*		
		low	*moderate*	*high*	*local*	*extra local*	*regional*
Fossil genus	*Botanical affinity*						
Ceratosporites	Unknown						
Gleicheniidites	Gleicheniaceae			X	X		
Lycopodiumsporites	Lycopodiaceae						
Reticuloidosporites	Pteridophyte		X	X	X	X	
Laevigatosporites							
Podocarpidites	Podocarpaceae		X	X		X	X
Parvisaccites							
Alisporites							
Podosporites							
'Phyllocladus'	*Phyllocladus*		X			X	
Dacrycarpites	*Dacrycarpus*	X	X		X		
Microcachryidites	*Microcachrys*		X		X		
Lygistepollenites	*Dacrydium*		X	X	X	X	X
Araucariacites	Araucariaceae						
Dilwynites	Coniferae?	—	UK	—	—	UK	—
Liliacidites	Liliaceae						
Ilexpollenites	*Ilex*						
Myrtaceidites parvus/mesonesus	Non-eucalypt Myrtaceae	X	X		X	X	X
Nothofagidites emarcidus							
Nothofagidites heterus							
Nothofagidites deminuta/vansteenisii	*N. brassii* group			X		X	X
Nothofagidites falcata							
Nothofagidites incrassatus							
Nothofagidites sp. cf. *flemingii*							
Nothofagidites brachyspinulosa	*N. fusca* group			X		X	X
Nothofagidites asperus							
Nothofagidites goniatus	*N. menziesii* group		X			X	
Sparganiaceaepollenites	Sparganiaceae/Typhaceae	X	X		X	X	
Milfordia	Restionaceae		X	X	X		
Graminidites	Graminidae		X			X	X
Cyperaceae	Cyperaceae	X	X		X	X	
Proteacidites	Proteaceae	X	X		X	X	
Haloragacidites harrisii							
Haloragacidites trioratus	Casuarinaceae			X		X	X
H. sp. cf. *trioratus*							
H. haloragoides	Haloragaceae	X			X		
Onagraceae	Onagraceae	X			X		
Periporopollenites	Unknown	UK			UK		
Ericipites	Epacridaceae	X	X	X	X	X	

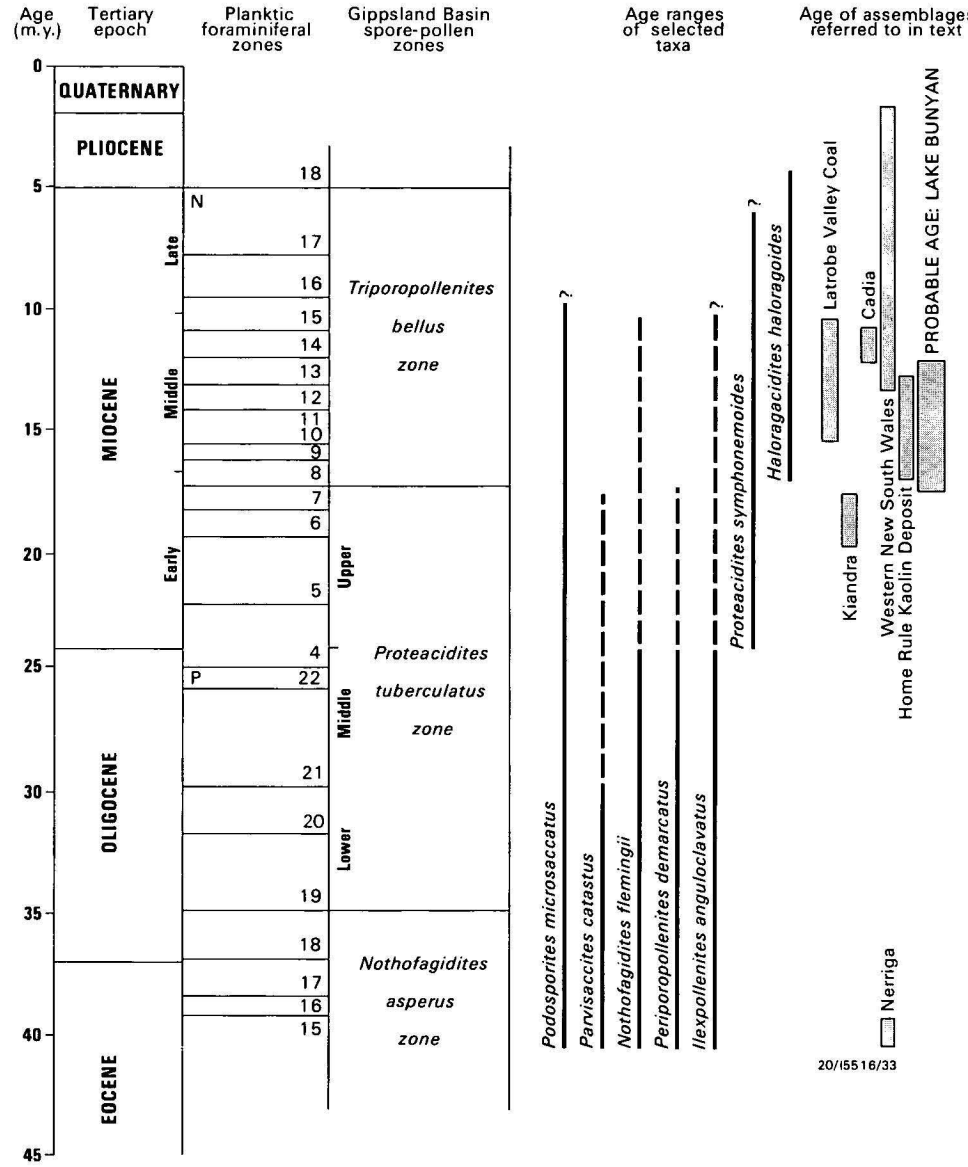

Figure 3. Stratigraphic correlation chart, showing spore and pollen zones of the Gippsland Basin, age ranges of selected taxa and the age ranges of other palynofloras mentioned in the text.

Correlation with the standard timescale and planktic foraminiferal zones is from Abele (1976). (Age ranges of selected taxa : solid line = range in Gippsland Basin, broken lines = extended range in highlands, noted by Owen 1975).

recognition of the zones is reinforced by quantitative considerations, by changes in the relative abundance of the pollen of individual species or of major plant groups. Difficulties in identifying the Gippsland Basin zones away from their type area arise both from the problems of locating diagnostic index fossils, which are frequently rare, and from problems in interpreting the significance of fluctuations in the relative abundance of major plant groups. Indeed, the practice of using such variations in relative frequency as stratigraphic markers is hazardous, as it may obscure geographic variations within the regional vegetation at any given interval within the Tertiary.

Correlation of the highland Lake Bunyan deposit with the standard sequence is difficult, because of the remoteness of that deposit from the Gippsland Basin. Lake Bunyan represents an inland highland rather than a coastal lowland depositional site. Pollen spectra may thus reflect floral differences related to these differing environments, which may hinder stratigraphic correlation.

Pollen assemblages from three highland sites, viz. Nerriga, Kiandra, and Cadia, which have been dated by potassium-argon age determinations on associated basalt flows, were examined by Owen (1975), and provide intermediate, well-dated tie points between the Lake Bunyan deposit and the Gippsland Basin standard. At Nerriga, some 150 km northeast of Lake Bunyan, sediments referable to the *Nothofagidites asperus* Zone underlie late Eocene basalts. At Kiandra, 75 km northwest of Lake Bunyan, a palynological assemblage referable to the middle or upper *Proteacidites tuberculatus* Zone was described from 'deep lead' lacustrine and fluvial sediments beneath a basalt flow dated as 21 m.y. (Wellman & McDougall, 1974). The assemblage from Cadia, 300 km north on the Central Tablelands near Orange, is the most remote from Lake Bunyan. The microflora there is derived from fluvial sediments interbedded with basalts dated as 12 m.y. or middle Miocene, and is comparable to assemblages of the *Triporopollenites bellus* Zone of the Gippsland Basin.

Because these highland sites are probably more similar environmentally to the Lake Bunyan site than is the Gippsland Basin, a comparison with them is more useful stratigraphically than direct correlation with the Gippsland Basin. Owen (1975) noted that some forms that are stratigraphically restricted in the

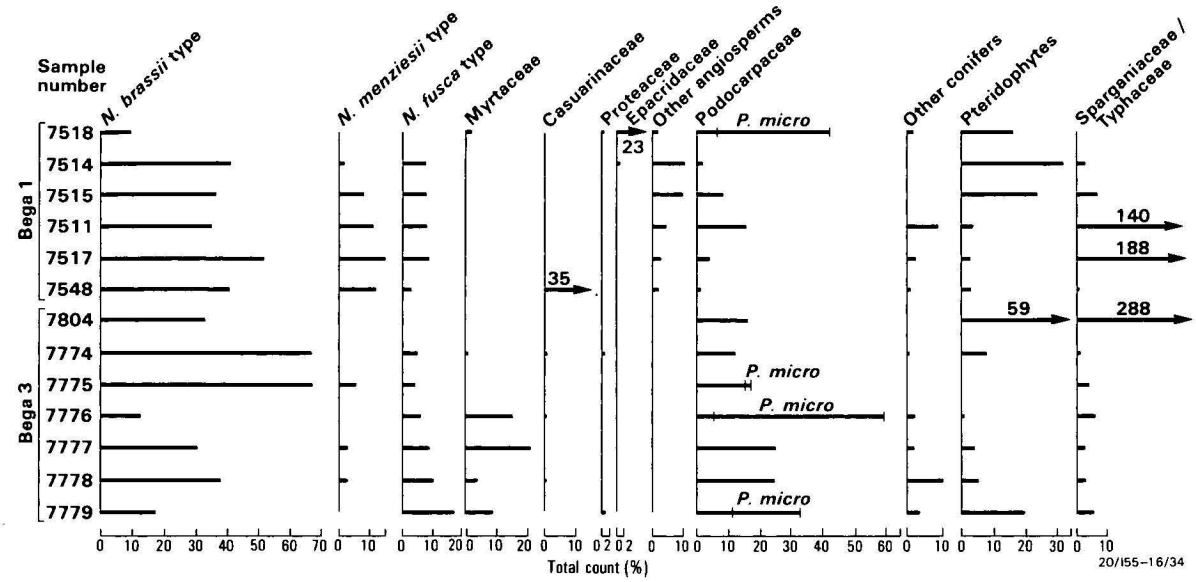

Figure 4. Pollen spectra from Lake Bunyan, expressed as a percentage of the pollen sum.
Pollen sum consists of all land-plant pollen, and excludes Sparganiaceae/ Typhaceae. Relative proportions of these aquatics are expressed as percentages of total dry land pollen. Sample numbers are shown in left-hand column. Pollen categories include the folling fossil taxa: *N. brassii* type, including *Nothofagidites emarcidus, N. heterus, N. falcatus, N. incrassatus, N. deminutus/ vansteenis; N. menziesii type — N. asperus, N. goniatus; N. fusca type — N. flemingii, N. brachyspinulosus;* Myrtaceae, including *Myrtaceidites parvus, M. mesonesus, M. eugenioides; Casuarina*, including *Haloragacidites harrisii, H. trioratus, H.* sp. cf. *trioratus;* Proteaceae, including all *Proteacidites* species; Epacridaceae, including all *Ericipites;* Sparganiaceae/Typhaceae, including all *Sparganiaceaepollenites* species. Other angiosperms, including *Liliacidites* spp., *Graminidites media*, all tricolpate, tricolporate, monocolpate, periporate and triporate forms not in other categories; Podocarpaceae, including all saccate pollen; other conifers, including *Araucariacites* spp. and *Dilwynites* spp.; ferns, including all monolete and trilete spores except *Lycopodiumsporites* spp.

Gippsland Basin have extended ranges in the highlands. *Triporopollenites bellus*, for example, occurs in sediments at Kiandra that are older than those in which it first occurs in the Gippsland Basin; and, at the same site, the occurrence of *Parvisaccites catastus* and *Nothofagidites flemingii* is younger than the range reported from the Gippsland Basin.

Several palynomorphs in the Lake Bunyan flora have been identified with stratigraphically useful forms in the and sland Basin. The ranges of these forms, which comprise *Parvisaccites catastus, Nothofagidites flemingii, Periporopollenites demarcatus, Ilexpollenites anguloclavatus, Proteacidites* sp.cf. *P. symphonemoides* and *Haloragacidites haloragoides* are shown in Figure 3, with the extensions known from the highland areas incorporated.

The Lake Bunyan flora is similar in many respects to Oligocene assemblages from the lower and middle *Proteacidites tuberculatus* Zone of Gippsland Basin. According to Stover & Partridge (1973), *Nothofagidites flemingii, N. goniatus, Periporopollenites demarcatus* and *Ilexpollenites anguloclavatus* end their ranges in that basin at the upper limit of the *P. tuberculatus* Zone, and *Parvisaccites catastus* disappears at the beginning of that Zone. The high abundance and diversity of conifer pollen, particularly *Podosporites microsaccatus*, and the low diversity of angiosperm types are other features of the Lake Bunyan deposits that are similar to late Oligocene to early Miocene assemblages from the Gippsland Basin. These factors all suggest that the Lake Bunyan deposits could be correlated with the middle *Proteacidites tuberculatus* Zone.

However, the ranges of these species in the Gippsland Basin do not overlap with the range of *Haloragacidites haloragoides*, which has been identified in the Lake Bunyan flora. This first appears in the overlying *Triporopollenites bellus* Zone, of late early Miocene to late Miocene age. Moreover, Stover & Partridge (1973) suggested that *H. haloragoides* first appears above the base of the *T. bellus* Zone. Its use as a marker fossil for middle to late Miocene sediments has been widespread (Owen, 1975; Martin, 1977; W.K. Harris, pers. comm., 1982). This aspect of the Lake Bunyan assemblage suggests its correlation with the *Triporopollenites bellus* Zone, which begins in the late early Miocene.

In view of this apparent conflict, some clarification of the possible age of the assemblage may be sought by comparison with the other highland palynological suites. Comparison with the independently dated sites described by Owen (1975) shows great similarities with the floras of both Kiandra and Cadia. The Lake Bunyan flora shares *Parvisaccites catastus, Periporopollenites demarcatus, Microcachryidites antarcticus, Liliaceidites lanceolatus* and *Dilwynites tuberculatus* with Kiandra only, while it shares *Haloragacidites haloragoides* and *Graminidites media* with Cadia only. In addition, the Lake Bunyan deposit contains a form closely comparable to *Proteacidites symphonemoides*, and an unusual variety of four-pored Casuarinaceae pollen (referred to here as *Haloragacidites* sp.cf. *H. trioratus*). Both *P. symphonemoides* and a four-pored Casuarinaceae type of pollen have been recorded from Cadia.

The occurrence of *Parvisaccites catastus, Periporopollenites demarcatus, Nothofagidites flemingii, Nothofagidites goniatus,* and *Ilexpollenites anguloclavatus* in the Lake Bunyan but not the Cadia floras may be stratigraphically significant, indicating that the Lake Bunyan assemblage is older than that of Cadia. Similarly, the occurrence of *H. haloragoides* in the Lake Bunyan and Cadia floras, but not at Kiandra, may mean that the Lake Bunyan sediments are younger than those at Kiandra. This suggests that the Lake Bunyan sediments are intermediate in age between the Kiandra and Cadia deposits, which would bracket them in the interval 12–21 m.y., or late early to middle Miocene, in the *T. bellus* Zone.

Quantitative aspects of the Lake Bunyan microflora do not conflict with this age determination. Although Martin (1977) used a decrease in abundance of *Nothofagidites* species to indicate the *T. bellus* Zone in some boreholes in the eastern Murray Basin, the exact boundary between the *P. tuberculatus* and *T. bellus* Zones is difficult to discern in this area. Stover &

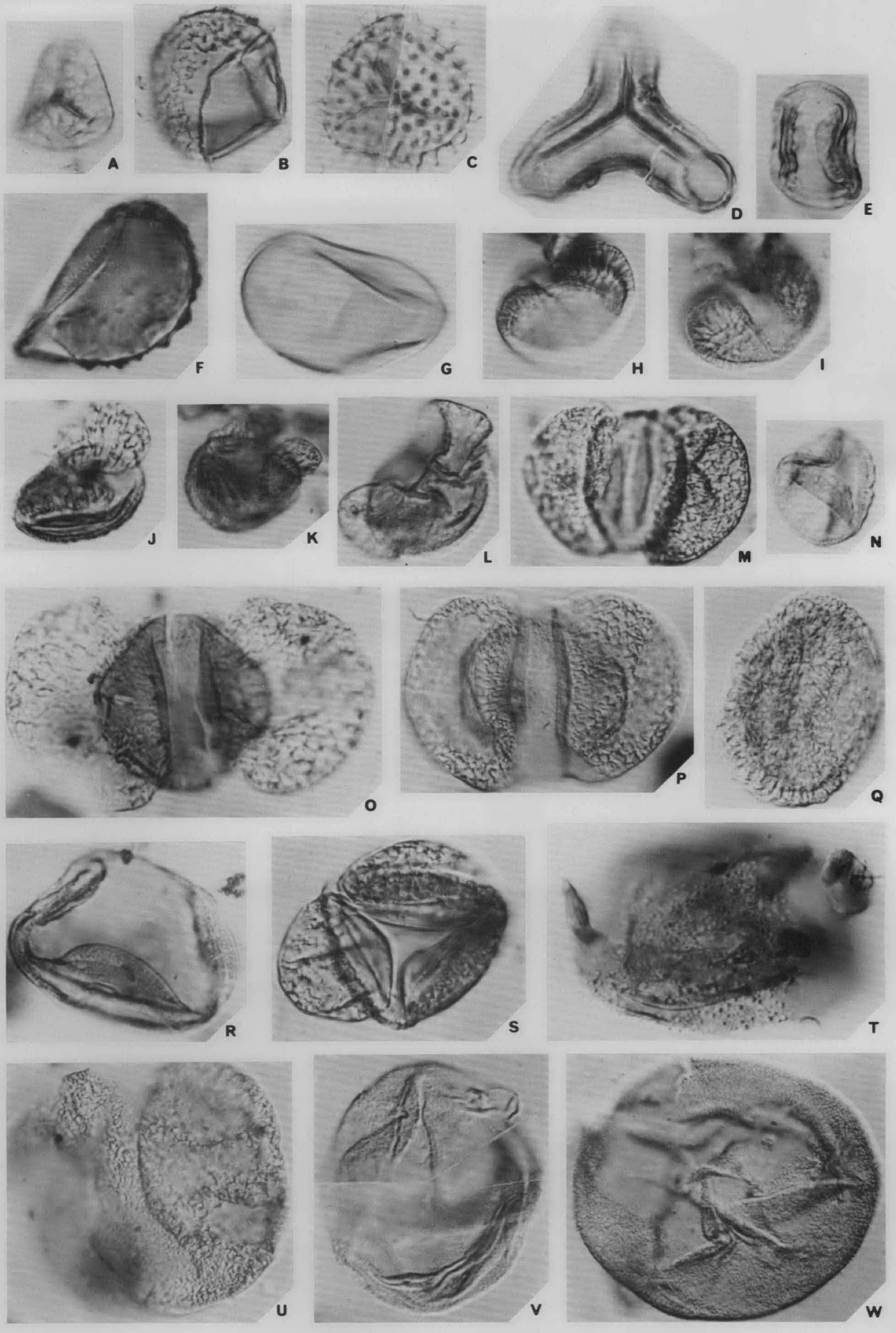
A
B
C
D
E
F
G
H
I
J
K
L
M
N
O
P
Q
R
S
T
U
V
W

Partridge (1973) remarked that *Nothofagidites* species are still abundant in the lower *T. bellus* Zone in the Gippsland Basin, and abundances cited by Luly & others (1980) from Yallourn support the persistence of this taxon into that zone. Hence, the abundance and diversity of *Nothofagidites* species in the Lake Bunyan suite do not preclude correlation with the early part of the *T. bellus* Zone.

The significance of the occurrence of Oligocene (middle *Proteacidites tuberculatus* Zone) palynomorphs at Lake Bunyan is uncertain, because of the extended ranges of these forms in highland sites examined by Owen (1975). There are too few independently dated highland sites to ascertain the full extent of the differences in ranges from the Gippsland Basin. Because of this, the age range suggested for the Lake Bunyan assemblage on the basis of comparison with highland sites, viz. 12–21 m.y. range, should be regarded only as the most probable estimate. Quantitative aspects of the microflora, however, do suggest that the sediments are not younger than middle Miocene.

The presence in the Lake Bunyan sequence of volcanogenic sediment containing olivine and plagioclase pseudomorphs, combined with our suggested age for the sequence, implies that early to mid-Miocene basalts occur near to the depositional site. Basalts of this age have not been recorded. However, a basalt from Mittagong Crossing, just upstream from the lake deposits, is presently being dated, and will provide an independent check on the palynological age determination.

Comparison with other Miocene palynofloras

A comparison of the Lake Bunyan palynoflora with other Miocene assemblages allows that flora to be placed in a regional perspective and some climatic and environmental inferences to be drawn. There are several relevant Miocene deposits in southeastern Australia, which include the highland assemblages of Kiandra and Cadia, and the lowland floras from the Latrobe Valley coal seam in the Gippsland Basin. In addition, McMinn (1981) has documented a mid-Miocene flora from the Home Rule kaolin deposit near Dubbo, New South Wales, and Martin (1973, 1977) described Miocene pollen spectra from the eastern Murray Basin in western New South Wales.

Kiandra

As noted above, the Lake Bunyan flora (Fig. 4) is similar to the Kiandra assemblage. Both floras contain high percentages of diverse *Nothofagidites* species and conifer pollen. Triporate Casuarinaceae pollen is poorly represented in both, as is *Myrtaceidites* pollen. The principal differences in the floras are the higher abundance of trilete fern spores, proteaceous species, and a variety of angiospermous pollen types at Kiandra. The Kiandra flora also differs in its uniformly low content of *Nothofagus menziesii* and *N. fusca* pollen types.

Angiosperm pollen found at Kiandra but not at Lake Bunyan includes *Gothanipollis* spp., *Beaupreadites* spp., *Polycolpites* spp., *Dodonaea sphaerica*, *Cupanieidites orthoteichus* and *Sapotaceoidaepollenites* sp. The botanical affinity of these forms lies with taxa now found in subtropical and warm temperate rainforests. The conifer palynomorph *Phyllocladites mawsonii*, is relateable to *Dacrydium franklinii*, of cool temperate rainforest, and is found at Kiandra, but not at Lake Bunyan.

Cadia

The Cadia assemblage also is more diverse than the Lake Bunyan flora, particularly in trilete fern spores and *Proteacidites* species. Several forms, such as *Sapotaceoidaepollenites* and *Polycolpites* species, with affinities to modern subtropical rainforest taxa appear in the Cadia assemblage, but are absent from Lake Bunyan. The Cadia flora resembles the Lake Bunyan spectra in the relatively high representation of *Nothofagus menziesii* pollen types in some samples and in the variable, occasionally high frequencies of *Myrtaceidites parvus*. *Graminidites media* occurs consistently in low frequencies in the Cadia deposit, and Chenopodiaceae and *Acacia* pollen types also occur sporadically; these last two taxa are absent from Lake Bunyan. Representation of Casuarinaceae pollen at Cadia is variable, and is similar to that in the Lake Bunyan flora.

Latrobe Valley Coal Seams

The palynology of the Yallourn Seam of the Latrobe Valley has been studied in detail and interpreted palaeoecologically by Luly & others, (1980). The seam probably correlates with the lower part of the *Triporopollenites bellus* Zone. It yields high percentages of restionaceous pollen and abundant, diverse *Nothofagus brassii* pollen. It is perhaps slightly younger than the Lake Bunyan deposit.

Luly and his co-workers identified pollen variation in the sequence, which could be related to coal lithotypes representing different stages of hydroseral succession. The light coloured lithotypes reflect open water conditions, and contain high proportions of *Nothofagus brassii* types and Casuarinaceae pollen; darker lithotypes contain greater quantities of Epacridaceae and Proteaceae pollen, while the darkest are rich in Myrtaceae, conifer, *Banksia*, restioneaceous pollen and *Gleichenia* spores. This reflects changing depositional environments from open water conditions, where the regional pollen rain dominates, through epacrid-dominated swamp margin habitats, to raised bog environments, where local sclerophyllous trees, shrubs, and understorey ferns and rushes dominate the pollen spectra.

A remarkable feature of the Yallourn flora is the low but persistent representation of a diverse range of taxa that are today associated with rainforest formations ranging from subtropical to cool temperate (Luly & others, 1980; Table 3). Pollen identifiable with the Sapotaceae, Cunoniaceae, *Quinti-*

Figure 5. Selected spore and pollen types from Bega Nos. 1 and 3 coreholes.
CPC numbers are those of the Commonwealth Palaeontological Collection, Bureau of Mineral Resources, Canberra, where the collection is housed. All magnifications are × 1000. A, *Lycopodiumsporites* sp., CPC 22210; B, *Lycopodiumsporites* sp. cf. sp. 3 of Owen 1975, CPC 22211; C, *Ceratosporites* sp., CPC 22212; D, *Gleicheniidites circinidites* (Cookson), CPC 22213; E, *'Phyllocladus' paleogenicus* Cookson, CPC 22214; F, *Reticuloidosporites* sp., CPC 22215; G, *Laevigatosporites* sp., CPC 22216; H, I, *Parvisaccites catastus* Partridge, CPC 22217; J, *Podocarpidites* sp. 3 cf. sp. A of Partridge 1971, CPC 22217; K, *Microcachryidites antarcticus* Cookson, CPC 22218; L, *Podocarpidites* sp. 2, CPC 22219; M, *Podocarpidites ellipticus* Cookson, CPC 22220; N, *Podosporites microsaccatus* (Couper), CPC 22221; O, *Podocarpidites* sp. cf. *P. multesimus* (Bolkhovitina), CPC 22222; P, *Podocarpidites* sp. 1, cf. sp. 1 of Owen 1975, CPC 22223; Q, *Lygistepollenites florinii* (Cookson & Pike), CPC 22224; R, *Podosporites* sp. cf. *P. microsaccatus* (Couper), CPC 22225; S, *Dacrycarpites australiensis* Cookson & Pike, CPC 22226; T, *Dilwynites* sp. cf. D. *tuberculatus* Harris, CPC 22227; U, *Alisporites grandis* (Cookson), CPC 22228; V, W, *Araucariacites australis* Cookson, CPC 22229.

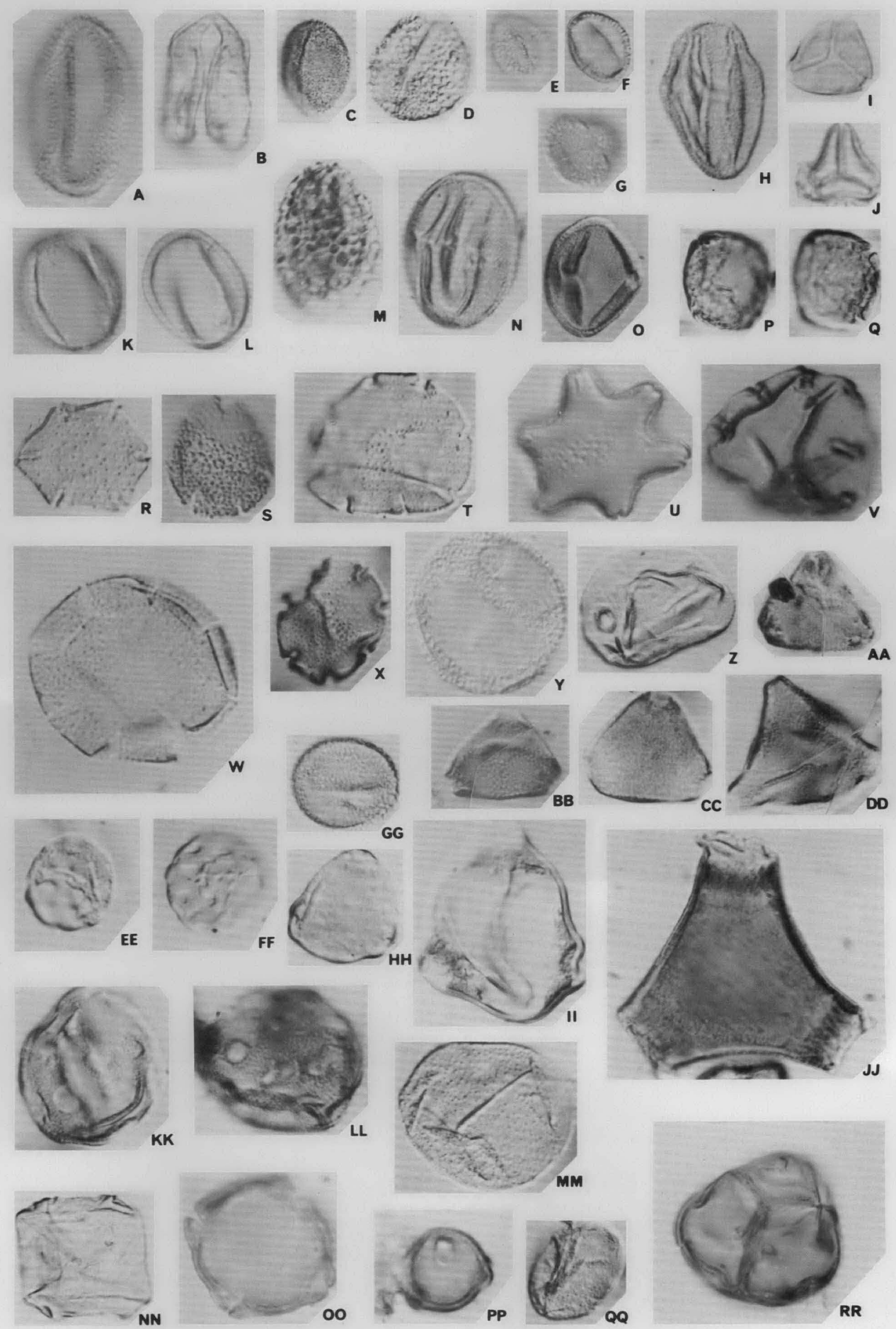
A
B
C
D
E
F
G
H
I
J
K
L
M
N
O
P
Q
R
S
T
U
V
W
X
Y
Z
AA
BB
CC
DD
EE
FF
GG
HH
II
JJ
KK
LL
MM
NN
OO
PP
QQ
RR

nia, and rainforest Myrtaceae, such as *Syzygium* and *Acmena*, are consistently present. This aspect of the flora contrasts with the Lake Bunyan assemblage, which also lacks abundant Restionaceae, *Gleichenia*, and *Banksia*, suggesting that bog habitats near Lake Bunyan differed from those in the Gippsland Basin.

Western New South Wales

Pollen spectra from boreholes at Narrandera and the Hay–Balranald–Wakool areas of central to western New South Wales were described by Martin (1973, 1977). These coreholes span the boundary between the *P. tuberculatus* and *T. bellus* Zones and record a decrease in abundance of *Nothofagidites* species. Assemblages with abundant *Nothofagidites* resemble the Lake Bunyan material in the high representation of *Nothofagus brassii* pollen, but differ in other respects. Casuarinaceae and Myrtaceae pollen are better represented in western New South Wales, and the ratio of araucarian to podocarpaceous conifer pollen is generally higher than in the Bunyan material. Also, angiosperm pollen is more diverse in western New South Wales. In samples correlated with the *P. tuberculatus* Zone, forms such as *Beaupreadites*, *Cupanieidites*, *Drimys*, and *Quintinia* are present. These forms, probably of rainforest affinity, also occur in the Kiandra and Cadia deposits, but not in the Lake Bunyan sediments.

Some indicators of developing aridity, such as Chenopodiaceae pollen, begin to appear in the Hay area before the dramatic decrease in *Nothofagidites* abundance.

Home Rule kaolin deposit

Two mid-Miocene assemblages, dated 12.7–17.5 m.y., were recently detailed by McMinn (1981) from the Home Rule kaolin deposit, near Dubbo in New South Wales. The assemblages again differ from the Lake Bunyan flora. No *Nothofagus menziesii* or *N. fusca* pollen types were recognised at Home Rule, and the diversity of *Nothofagidites* is low. Only two *N. brassii* species, *Nothofagidites emarcidus* and *N.falcatus* occur. Myrtaceous pollen is represented only by *Myrtaceidites mesonesus*, which achieves a relatively high abundance, in contrast to its rare occurrence in Lake Bunyan. *Proteacidites ivanhoensis* is common to both localities.

Comparisons with the late Oligocene and Miocene floras listed above suggest that the Lake Bunyan flora is distinctive. It is characterised by a low diversity, particularly in fern taxa, although the conifer element is reasonably varied. It lacks the diversity of both subtropical and cool temperate rainforest taxa, which are present in microfloral assemblages from the Latrobe Valley and western New South Wales, as well as the other highland sites of Kiandra and Cadia. However, indicators of aridity, such as pollen from chenopods or *Acacia*, are absent, although they occur in nearly contemporaneous sediments in western New South Wales.

Palaeoecology

It is useful, in understanding the organisation and evolution of environments, to interpret pollen spectra in terms of vegetation. However, several factors make interpretation of ancient spectra hazardous. Most serious is the lack of living vegetation modelling those communities represented in ancient spectra.

Modern pollen analysis is based on a knowledge of the relations of modern spectra to extant vegetation. This allows the pollen productivity and dispersal ability of source taxa to be related to their representation in a pollen spectrum, and an estimate to be made of the abundance and distribution of source taxa about the depositional site.

It is possible to divide a pollen spectrum into local and regional elements. The local component consists of poorly distributed pollen, or pollen produced in small quantities; these grains are present in the pollen spectrum only in the immediate vicinity of the source plant. Representation of taxa in the local component varies markedly with distance of the source plant from the sample site. The regional component consists of pollen that is widely distributed, being contributed mainly from taxa such as grasses or canopy trees. The relative abundance of pollen in this category depends less on distance from source taxa than on the relative abundance and pollen productivity of source taxa in the region. The representation of each component depends strongly on the productivity of taxa in each class.

Depositional environment may also strongly affect pollen representation. Davis & Brubaker (1973) demonstrated differential sedimentation of pollen grains in stratified lakes in Wisconsin, U.S.A. Buoyant grains are preferentially accumulated in littoral sediments, owing to wind-induced turbulence in the upper layers of these lakes. Because many herbs produce light, locally distributed pollen, stratification of the lake tends to concentrate these types in littoral sediments and enhance representation of regional, dominantly arboreal pollen in deeper water sediments. Conifer pollen is also buoyant and hence concentrated with local elements in marginal, lake shore sediments. This type of complication may affect pollen spectra from Lake Bunyan.

Because of the many factors that may influence relative abundances in a pollen spectrum, interpretation of spectra is always a speculative exercise. This is particularly so for ancient deposits, where spectra may contain extinct taxa and cannot thus be compared directly to spectra of living vegetation. The the following interpretation, therefore, must be regarded as only one possibility, and its largely conjectural nature is emphasised.

The botanical affinities of pollen taxa identified in the Lake Bunyan deposit and the pollen production and dispersal abilities (after Luly & others, 1980) of modern analogues are given in Table 2. Figure 4 is a pollen diagram showing relative

Figure 6. Selected spore and pollen types from Bega Nos. 1 and 3 coreholes.
CPC numbers are those of the Commonwealth Palaeontological Collection, Bureau of Mineral Resources, Canberra. All magnifications are × 1000. A, *Liliacidites* sp., CPC 22230; B, *Arecipites waitakiensis* McIntyre CPC 22231; C, *Monosulcites* sp., CPC 22232; D, *Liliacidites lanceolatus* Stover, CPC 22233; E, F, G, *Tricolpites retiformis* Martin, E, F, CPC 22234; G, CPC 22235; H, *Tricolpites* sp. 1, CPC 22236; I, *Myrtaceidites parvus* Cookson & Pike, CPC 22237; J, *Myrtaceidites eugenioides* Cookson & Pike, CPC 22238; K, L, *Tricolpites* sp. 2, median and deep foci, CPC 22239; M, *Ilexpollenites anguloclavatus* McIntyre, CPC 22240; N, *Tricolporites microreticulatus* Harris, CPC 22241; O, *Tricolporites* sp. cf. *T. sphaerica* Cookson, CPC 22242; P, Q, *Haloragacidites haloragoides* Cookson & Pike, different foci on same grain, CPC 22243; R, *Nothofagidites emarcidus* (Cookson), CPC 22244; S, *Nothofagidites vansteenisii* (Cookson), CPC 22245; T, *Nothofagidites heterus* (Cookson), CPC 22246; U, *Nothofagidites falcatus* (Cookson), CPC 22247; V, *Nothofagidites* sp. cf. *N. flemingii* (Couper), CPC 22248; W, *Nothofagidites asperus* (Cookson), CPC 22249; X, *Nothofagidites brachyspinulosus* (Cookson), CPC 22250; Y, *Sparganiaceaepollenites* sp. cf. S. *barungensis* Harris, CPC 22251; Z, *Graminidites media* Cookson, CPC 22252; AA, *Proteacidites ivanhoensis* Martin, CPC 22253; BB, *Proteacidites* sp. cf. *P. symphonemoides* Cookson, CPC 22254; CC, *Proteacidites minimus* Couper, 22255; DD, *Proteacidites* sp., CPC 22256; EE, FF, *Periporopollenites* sp. cf. sp. 2 of Owen 1975, CPC 22257; GG, *Sparganiaceaepollenites* sp., CPC 22258; HH, *Haloragacidites harrisii* (Couper), CPC 22259; II, *Onagraceae* type, CPC 22260; JJ, *Proteacidites annularis* Cookson, CPC 22261; KK, *Periporopollenites demarcatus* Stover, CPC 22262; LL, *Periporopollenites* sp. cf. sp. 1 of Owen 1975, CPC 22263; MM, *Inaperturopollenites* sp., CPC 22264; NN, *Mougeotia* sp., CPC 22265; OO, PP, *Haloragacidites trioratus* (Couper) four pored variety, CPC 22266; QQ, *Inaperturopollenites* sp., CPC 22268; RR, *Ericipites scabratus* Harris CPC 22267.

abundances of the major taxa. Local components in this study have been recognised by large fluctuations in the abundance of single pollen taxa. These fluctuations must represent either climatically significant large regional changes in vegetation or variation in the local vegetation. It has been assumed that the latter case is more likely to be correct. Pollen spectra from the sampled sequences in Bega 1 and Bega 3 are considered separately below.

Bega 1

Samples 7511 to 7518 come from a coal lens sampled between depths of 25.6 m and 24.6 m in Bega 1. Spectra from these samples can be divided into three groups; samples 7517 and 7511 have a high abundance of Sparganiaceae pollen; samples 7515 and 7514 have high fern spore counts and a high representation of angiosperms other than *Nothofagus;* sample 7518 is dominated by pollen of the Epacridaceae and *Podosporites microsaccatus;* myrtaceous pollen is also more abundant in this sample than in others from Bega 1.

Pollen from the reed families Sparganiaceae and Typhaceae is distributed irregularly in modern lakes (Dodson, 1977). However, the high abundances in samples 7511 and 7517 suggest its local presence. Reeds are marginal lake-edge dwellers, and the high abundance of *Sparganium* and the presence of the freshwater alga *Mougetia* suggest that these samples were deposited in a nearshore environment. The difference in abundance of conifer pollen between 7511 and 7517 is difficult to explain, but sorting factors mentioned above may be implicated. In addition, conifer pollen, although widely distributed, tends to be extremely abundant close to source vegetation. Thus deposition, production, and dispersal considerations suggest that sample 7511 may reflect an environment either closer to forest vegetation or more marginal than sample 7517.

The decrease in abundance of aquatics and *Sparganium* pollen in samples 7515 and 7514 may reflect a return to more open water deposition or a change in local vegetation to one dominated by ferns and angiosperms. Because these samples lack the alga characteristic of samples 7517 and 7511 and show a high representation of small angiosperm grains other than *Nothofagus,* the latter alternative is the thought more likely.

Sample 7518 reflects a very different local vegetation. The distribution of Epacridaceae pollen is very limited (Macphail, 1979), and podocarps only achieve the over-representation shown by *Podosporites microsaccatus* in this sample when they are locally present, so that this sample reflects mainly local vegetation. These pollen types stem from woody plants, and the sample may reflect a bog forest or heath community that possibly accumulated at or above the water table.

The short spaced sequence in Bega 1 can be interpreted as a hydroseral succession reflecting changes in the local vegetation from a reed community, to a fern and angiosperm (possibly herbaceous) lake-margin community, and finally to an epacrid and podocarp-dominated raised bog forest. This interpretation is consistent with the presence of fossil roots in the coal facies.

The other productive sample in Bega 1, sample 7548, from 30.7 m, is noteworthy for its high proportion of four-pored *Casuarina* pollen. This pollen type is unknown from other Miocene sites except Cadia and therefore is probably a local rather than a regional element. The dominance of a local terrestrial community in sample 7548 contrasts with the dominance of aquatics in samples 7517 and 7511, and may provide evidence of oscillatory lake levels during the accumulation of the coaly facies.

A remarkable feature of the Bega 1 samples is the high ratio of *Nothofagus menziesii* to *N. brassii* pollen types in the lower samples. *N. menziesii* pollen has a restricted distribution (Luly & others, 1980) so that the high levels of *N. menziesii* in Lake Bunyan probably reflect the nearby presence of forest containing *N. menziesii* producers. The decrease in the ratio of *N. asperus* to *N. brassii* types in 7514 and 7518 may reflect the retreat of this forest type from the area, and indicates some climatic variation or change in the local environment.

The Bega 1 samples seem to reflect changing local, non-forest, lake-shore communities against a background of an arboreal pollen rain, which also shows some variability. In contrast to other Tertiary sites, forest including producers of *Nothofagus menziesii* type pollen appears to be prominent in the area at some horizons.

Bega 3

Samples from this corehole also come from a short sequence, but it is more difficult here to discern a unifying process affecting these spectra than it is in Bega 1. The most obvious difference from Bega 1 spectra is in the higher representation of Myrtaceae. These grains are all of one type, in contrast to the variety of forms found in the Latrobe Valley coals (Luly & others, 1980). Modern pollen rain data (Kershaw & Sluiter, 1982; Hope, 1973) suggest that Myrtaceae (except *Eucalyptus*) are generally not well represented in the regional pollen rain. Rainforest Myrtaceae include a variety of forms and are most prominent in subtropical rainforest (Kershaw & Sluiter, 1982). The high representation of Myrtaceae in samples 7777 and 7776 is monotypic, suggesting the local presence of a single myrtaceous taxon rather than the regional occurrence of rainforest with a high myrtaceous component.

In sample 7776, a high Myrtaceae count is associated with an abundance of *Podosporites microsaccatus.* In Bega 1 it was suggested that the source plant for this form grew in a bog forest community; that particular spectrum in Bega 1 also had a higher representation of Myrtaceae than other samples. It may be that the Myrtaceae so common in the Bega 3 samples formed part of a similar bog forest or heath community to that of sample 7518.

The pollen spectrum obtained from sample 7779 in Bega 3 is unusual in the high representation of *Nothofagidites brachyspinulosus.* This is a fossil pollen of the *fusca* type, which is today produced in Australia by *Nothofagus gunnii,* a shrubby treeline species in Tasmania. Representation of closed forest elements such as *N. brassii* types is low in this sample; the other common pollen types are *Podosporites microsaccatus* and *Myrtaceidites parvus.* These forms have been suggested above to reflect, possibly, heath-like vegetation growing in bogs or swamps. Thus, there is here little evidence for any local closed forest vegetation.

The abundance and diversity of conifers are high in most Bega 3 spectra. Today, conifers in the Australasian region occur mainly in montane forests in Tasmania and upper montane forests in New Guinea. Abundant conifers are not characteristic of complex rainforest (Kershaw & Sluiter, 1982) and are generally restricted to disturbed or marginal conditions such as near the tree line, on poor soils or ridge crests. The abundance and diversity of conifers reinforces the idea that local conditions may have been unsuitable for complex, angiosperm-dominated rainforest.

In Bega 3, the high *N. menziesii* type values found in Bega 1 do not occur; the flora contained in samples 7775 and 7774 comprises very little except *N. brassii* types and a few

podocarpaceous grains. These grains may be considered as part of the regional component and, together with the low representation of other forms, suggest deposition some distance from swamp or dry land vegetation. Sample 7804 differs from other Bega 3 samples in the abundance of Sparganiaceae pollen and in the high percentage of the fern spore *Reticuloidosporites* sp. The high Sparganiaceae values are similar to samples 7517 and 7511 in Bega 1, and might suggest a similar littoral depositional environment close to a reed and fern-dominated lake-edge community.

The Bega 3 samples are difficult to interpret in terms of a sequence of events. In the lower samples, the low diversity and high variable representation of only a few forms suggest local communities less complex than subtropical or cool temperate rainforest. Several of those elements suggested to represent swamp forest or bog vegetation in Bega 1 also occur together in these samples. This supports recognition of a bog flora in Bega 1 and suggests that local vegetation surrounding Bega 3 may reflect poor drainage conditions. The occurrence of cool temperate rainforest taxa, such as *Nothofagus* and Podocarpaceae, indicates that such forests did exist in the area, possibly in better drained sites.

Palaeoclimates

It is far more difficult to interpret pollen spectra in climatic terms than it is to suggest types of local and regional vegetation. This is because it is possible to identify few fossil forms with modern species, and the climatic tolerances of families or genera may be very wide. For example, although the example, although the conifer *Phyllocladus* is restricted to montane forests in New Guinea and Tasmania, it occurs also in lowland rainforest in New Zealand (Allan, 1961). Similarly, although producers of the *Nothofagus fusca* pollen type are restricted to sub-alpine environments in Australia, they occur with *Nothofagus menziesii* producers in wet lowland to sub-alpine areas in New Zealand, and extend into cold semi-arid environments in Patagonia (McQueen, 1976). In addition, the habitat range of extinct taxa may differ from those of modern analogues.

Interpretations of Miocene climates in southeastern Australia, on a regional scale, have in the past been based on direct extrapolation, backwards into the Tertiary, of climatic parameters under which modern representatives of Tertiary taxa now grow. Thus, Martin (1973) suggested that precipitation levels in mid-western New South Wales were of the order of 150–180 cm per annum in the late Miocene, based on the modern growth areas of *Nothofagus brassii* producers; and Duigan (1966) invoked similar rainfall figures for the Latrobe Valley, using a tentative analogy with extant gymnosperm and *Nothofagus* forests as a basis for extrapolation. However, Luly & others, (1980) have cautioned against using the distribution of modern taxa to infer palaeoclimates, attributing the present distribution of modern rainforest taxa in eastern Australia to a complex of factors, including low population size, competition within refugia, and recurrent climatic stress during Quaternary glaciations. They suggested that *Nothofagus* forests in the Latrobe Valley of Victoria could have existed, in the Miocene, under rainfall and temperature conditions not substantially different from those of today.

The Bunyan deposit differs from those of the Latrobe Valley in that it does not occur in an area of present high rainfall. The Monaro region around Cooma is an area of orographic aridity. In such areas, the climate may be classified as a sub-humid mesothermal type, with rainfall of 250–400 mm annually, a mean coldest month temperature of 2–18°C, and a mean warmest month temperature of over 25°C (Costin, 1954). It is a region presently subject to frosts and to cold air drainage in the valleys, factors important in the formation of the treeless, grassy valley vegetation of the tableland. The area around Cooma and Bredbo currently supports low open forest and grasslands. Higher, wetter areas to the west, support vegetation types ranging from tall open forest, through sub-alpine woodland, to alpine herbfields. Epacrid-dominated bog communities also occur in this area. To the east, in areas nearer to the coastal escarpment, there are open forests, grasslands, bogs, and small areas of *Casuarina*-dominated heath. Forest may be restricted to the hillsides, and the valley floors covered by grassland.

In comparison with other Miocene assemblages the Lake Bunyan deposits clearly lack taxa that are today associated with subtropical or warm temperate rainforests. Contemporaneous deposits in the Murray Basin and at Kiandra and Cadia do contain such taxa. The absence of these forms from Lake Bunyan suggests that warmer rainforests were not locally present and, hence, that conditions about the site were unsuitable for such forests. Cool temperate rainforest indicator taxa, such as *Drimys* or *Quintinia* are also absent from the assemblage, although more prolific elements of this forest type, such as *Nothofagus* and podocarps do appear.

The poor representation in the Lake Bunyan spectra of rainforest taxa present in other Miocene assemblages may be due to a variety of factors. There is some evidence in the sediments and the flora that conditions about the lake were both cooler and drier than in surrounding regions. Independent evidence for a periodic water deficit is provided most clearly by the development of gypsum in the sequence. This implies concentration of salts and, hence, closed basin conditions, when evaporation from the basin exceeded input from the catchment. However, no clear evidence of aridity is present in the pollen spectrum: there are no chenopods, no *Acacias* or composites, all of which had developed in drier regions of Australia by the mid-Miocene (Martin, 1978). Additionally, *Casuarina*, thought to reflect drier environments in the Latrobe Valley sequence (Luly & others, 1980), is only sporadically represented in Lake Bunyan.

Temperature also influences the distribution of rainforest taxa. Many rainforest species are frost-sensitive, and in New Guinea, forests dominated by *Nothofagus brassii* producers do not extend above altitudes where frosts are common (Hope, 1973). Montane forests above *Nothofagus* forests are depauperate, although rich in conifers (Paijmans, 1978). In Tasmania, conifers are also characteristic of sub-alpine or montane forests; most conifers are not characteristic of complex rainforests, but appear instead to be more tolerant of poor conditions and lower temperatures than other rainforest taxa. It may be then, that the rather impoverished assemblages from Lake Bunyan, which are nevertheless rich in podocarpaceous grains, reflect a response to cold, perhaps frost affected conditions. High relative abundance of *Nothofagus fusca* type pollen may support this inference, as the treeline species in Tasmania, *Nothofagus gunnii*, produces pollen of this type; however, the high abundance of *N. fusca* type pollen must be interpreted with caution.

Much of the Bunyan flora consists of locally produced pollen, which has been interpreted as reflecting swampy conditions. Such conditions may be the product of local topography or microclimate. The dominance of the local element in the Bunyan spectra makes it difficult to infer regional climates.

Today, rainshadow areas of the Monaro are marginal for forest growth, and much of the region supports grassland as climax vegetation (Costin, 1954). The abundance of woody taxa and low abundance of grass pollen or that of other herbaceous taxa

such as composites or chenopods suggests that, in the early or middle Miocene, the region was wetter, if not warmer than at present.

In summary, although the Lake Bunyan flora does not appear to reflect locally growing rainforest, it is not possible to pin down the cause of its absence. Aridity may have been a factor, but the pollen spectrum offers no positive support for this. Alternatively, cold, or poor drainage may have limited rainforest growth about the lake. The depauperate nature of the pollen assemblages and the abundance of conifers may offer some support for lower temperatures and perhaps frosts in the area. While it is apparent that the region experienced different climatic conditions from those of the Gippsland Basin or mid-western New South Wales, it is not possible to give such differences any quantitative expression. Nor, in view of the uncertainties of dating, is it possible to be certain whether such differences relate to spatial or temporal factors.

Conclusions

The microflora recovered from the coreholes Bega 1 and Bega 3 at Lake Bunyan is, by Australian Tertiary standards, a poorly diversified one. Pollen of *Nothofagus*, the southern beech, dominates, and is represented by all three pollen types produced by the genus. The only other major plant taxa represented in any abundance are members of the Podocarpaceae. The assemblage lacks subtropical rainforest elements, which are consistently present in contemporaneous palynofloras from other sites in southeastern Australia, and indicators of cool temperate rainforest are poorly diversified.

This general lack of diversity has proved an impediment to precise age determination for the Lake Bunyan sediments, because pollen species considered to be stratigraphically useful elsewhere are either rare or absent. In its overall impoverishment, the palynoflora bears some resemblance to floras of the *Proteacidites tuberculatus* Zone, which spans the early Oligocene to early Miocene interval in the Gippsland Basin. The presence of the species *Haloragacidites haloragoides* in Lake Bunyan, however, is more suggestive of the younger *Triporopollenites bellus* Zone, of late early Miocene to Pliocene age. Some clarification of the age of the deposit is afforded by comparison with palynofloras from other highland sites, which are dated by associated basalts. This comparison has suggested that the Lake Bunyan deposit may be of an age intermediate between that of deposits at Cadia and at Kiandra; an age bracket of 12–21 m.y. is indicated on this basis. It should be stressed, however, that this late early Miocene to middle Miocene age remains tentative in the light of the limited data available.

Application of Quaternary palynological principles to the pollen and spore assemblages from Lake Bunyan has enabled the sketching in of a picture of the local ecology. In Bega 1, a hydroseral succession may be represented within the coal seam sampled. The abundance of reeds and of algal remains in the basal samples may reflect a lake-edge community that was replaced successively by fern/angiosperm community, and an epacrid/podocarp heath or swamp forest. In Bega 3, the local ecology is less clear, but the same swamp forest or bog communities appear to be represented.

No ready explanation can be advanced for the absence of subtropical rainforest taxa in the Lake Bunyan deposit. Conditions both cooler and drier than surrounding regions are suggested, but cannot be proved unequivocally. Periodic dryness is suggested by the presence of gypsum in the sedimentary sequence, but there are no corresponding indicators of dryness in the pollen spectrum; there are no chenopods or composites that elsewhere indicate that open vegetation conditions had developed. Relative coolness of the area may be reflected in the abundance of conifer pollen and by higher than average frequencies of the *fusca* type of *Nothofagus* pollen. In combination, these microfloral elements are reminiscent of modern treeline vegetation in Tasmania. Today, the area around the Lake Bunyan site is relatively arid, reflecting the rainshadow created by the surrounding high country. The abundance in the pollen spectrum of woody taxa, in contrast to the modern grassy and herbaceous vegetation, suggests that rainfall in the region was considerably higher in the Miocene than it is now.

References

Allan, H.H., 1961 — Flora of New Zealand. *Government Printer, Wellington, New Zealand.*

Costin, A.B., 1954 — A study of the ecosystems of the Monaro region of New South Wales. *NSW Government Printer, Sydney.*

Davis, M.B., & Brubaker, L.B., 1973 — Differential sedimentation of pollen grains in lakes. *Limnology and Oceanography*, 18, 635–46.

Dodson, J.R., 1977 — Pollen deposition in a small closed drainage basin lake. *Review of Paleobotany and Palynology*, 24, 179–93.

Herbert, C., 1968 — Diatomite. *Geological Survey of New South Wales, The Mineral Industry of New South Wales*, 14.

Hills, E.S., 1946 — Fossil Murray Cod (*Maccullochella macquariensis*) from diatomaceous earths in New South Wales. *Australian Museum Record*, 21, 380–2.

Hope, G.S., 1973 — The vegetation history of Mt Wilhelm. *Ph.D. Thesis, Australian National University.*

Kershaw, A.P., & Sluiter, I.R., 1982 — Late Cenozoic pollen spectra from the Atherton Tableland, north eastern Australia. *Australian Journal of Botany*, 30, 279–95.

Luly, J., Sluiter, I.R., & Kershaw, A.P., 1980 — Pollen studies of Tertiary brown coals: preliminary analyses of lithotypes within the Latrobe Valley, Victoria. *Monash University Publications in Geography*, 23.

Martin, H.A., 1973 — Upper Tertiary palynology in Southern New South Wales. *Geological Society of Australia, Special Publication*, 4, 35–54.

Martin, H.A. 1977 — The Tertiary stratigraphic palynology of the Murray Basin in New South Wales. 1. The Hay-Balranald-Wakool Districts. *Journal and Proceedings, Royal Society of New South Wales*, 110, 41–7.

Macphail, M.K., 1979 — Vegetation and climates in Southern Tasmania since the last glaciation. *Quaternary Research* 11, 306–41.

McMinn, A., 1981 — A Miocene microflora from the Home Rule kaolin deposit. *Geological Survey of New South Wales, Quarterly Notes*, 43, 1–4.

McQueen, D.R., 1976 — The ecology of *Nothofagus* and associated vegetation in South America. *Tuatara*, 22(1), 38–68.

Owen J.A., 1975 — Palynology of some Tertiary Deposits from New South Wales. *Ph.D. Thesis, Australian National University.*

Paijmans, K., 1976 — Vegetation. *In* Paijmans, K. (editor), *New Guinea Vegetation. ANU Press, Canberra.*

Pillans, B., 1977 — An early Tertiary age for deep weathering at Bredbo, southern N.S.W. *Search* 8, 81–83.

Singh, G., Opdyke, N.D., & Bowler, J.M., 1981 — Late Cainozoic stratigraphy, palaeomagnetic chronology and vegetational history from Lake George, N.S.W. *Journal of the Geological Society of Australia*, 28, 435–52.

Stover, L.E., & Evans, P.R., 1973 — Upper Cretaceous–Eocene spore-pollen zonation, offshore Gippsland Basin, Australia. *Geological Society of Australia, Special Publication*, 4, 55–72.

Stover, L.E., & Partridge, A.D., 1973 — Tertiary and Late Cretaceous spores and pollen from the Gippsland Basin, southeastern Australia. *Proceedings, Royal Society of Victoria*, 85(2), 237–86.

Taylor, G., Walker, P.H., Jones, N.O., & Hutka, J., 1980 — The nature and significance of lacustrine deposits near Bunyan, N.S.W. *Bureau of Mineral Resources, Australia, Record* 1980/67, (unpublished abstract).

Thomas, D.P., & Gould, R.E., 1981 — Tertiary non-marine diatoms from eastern Australia: Descriptions of taxa. *Proceedings, Linnean Society of New South Wales*, 105(1), 23–52.

Thomas, D.P., & Gould, R.E., 1981 — Tertiary non-marine diatoms from eastern Australia: palaeoecological interpretations and biostratigraphy. *Proceedings, Linnean Society of New South Wales*, 105(1), 53–63.

Wellman, P., & McDougall, I., 1974 — Potassium-argon ages on the Cainozoic volcanic rocks of New South Wales. *Journal of the Geological Society of Australia*, 21(3), 247–72.

BMR Journal of Australian Geology & Geophysics, 7, 269-273

METASOMATIC ZONING IN SAPPHIRINE-BEARING GRANULITES FROM ANTARCTICA

J.W. Sheraton[1], R.N. England[2], & D.J. Ellis[3],

Highly magnesian (mg about 98) granulites, containing sapphirine, enstatite, spinel, phlogopite, and cordierite, occur as xenoliths in Precambrian orthopyroxene-bearing granitic rocks at Mawson and Gage Ridge, East Antarctica. At Mawson, a marginal reaction zone is considerably enriched in Fe, K, and volatiles (H_2O and F), largely at the expense of Mg, with the development of sapphirine + phlogopite-rich assemblages. At Gage Ridge, marginal gain of Fe and to some extent Ca and Na, and loss of Mg are indicated, but there was no significant gain of K or H_2O, possibly because very low P_{H_2O} did not allow crystallisation of phlogopite.

Introduction

Sapphirine-bearing granulites have been recorded from a number of places in high-grade metamorphic rocks of the East Antarctic Precambrian Shield. The rare association sapphirine + quartz, which indicates unusually high temperatures of metamorphism, is restricted to part of the Archaean (>3000 m.y.) Napier Complex of Enderby Land (Dallwitz, 1968; Ellis & others, 1980; Sheraton & others, 1980), but sapphirine occurs in SiO_2-deficient assemblages over a much wider area (Fig. 1). Coexisting minerals include orthopyroxene, spinel, cordierite, phlogopite, and, less commonly, garnet, sillimanite, osumilite, K-feldspar, and plagioclase. Most such occurrences contain dark blue, relatively Fe-rich sapphirine, but in some places, such as Mawson in MacRobertson Land and Gage Ridge in Enderby Land, the sapphirine is colourless to pale pink or purple, reflecting the highly magnesian composition of the host rocks (Sheraton, 1980).

Segnit (1957) first described sapphirine-bearing granulite from the Australian National Antarctic Research Expenditions (ANARE) base at Mawson, where it forms a xenolith, which crops out over an area of about 4 × 6 m, within the late Proterozoic (1084±37 m.y.: Tingey, 1982) Mawson Charnockite (porphyroblastic hypersthene granite). A detailed map of the exposure was made by the authors and three distinct varieties were distinguished (Fig. 2):

Type A — pale cream enstatite (50–70%), pale pink to purple sapphirine (15–20%), pale pink to purple spinel (up to 20%), and colourless to pale brown phlogopite (up to 15%); Type B — phlogopite (40–50%), enstatite (15–25%), sapphirine (10–25%), and cordierite (up to 25%) or minor spinel; Type C — golden brown to dark brown phlogopite (40–85%), pale to dark blue sapphirine (10–35%), cream to brown enstatite/bronzite (mostly 20%), and spinel (up to 5%).

Type C forms a relatively thin (typically 20–50 cm), but continuous zone around the margin of the xenolith, suggesting strongly that it formed by reaction between the enstatite-rich core rock and the granitic country rock. The blue colour of the sapphirine becomes more intense towards the outer margin of this zone. There is a hint of interlayering of types A and B, which may, to some extent, reflect original (?pre-metamorphic) compositional variations, particularly as both A and B appear to be truncated by type C (but see below).

At Gage Ridge, similar pale cream sapphirine-enstatite granulite, with variable amounts of spinel and phlogopite and minor cordierite, occurs as pods in massive orthopyroxene-quartz-feldspar gneiss of Archaean age. Narrow (a few cms) marginal zones contain dark blue sapphirine, brown bronzite, and minor feldspar (plagioclase and perthite), but are not significantly richer in phlogopite.

[1] Bureau of Mineral Resources, PO Box 378, Canberra, ACT 2601
[2] 6 Griffith Street, Holt, ACT 2615
[3] Department of Geology, University of Tasmania, P.O. Box 252C, Hobart, Tasmania 7001.

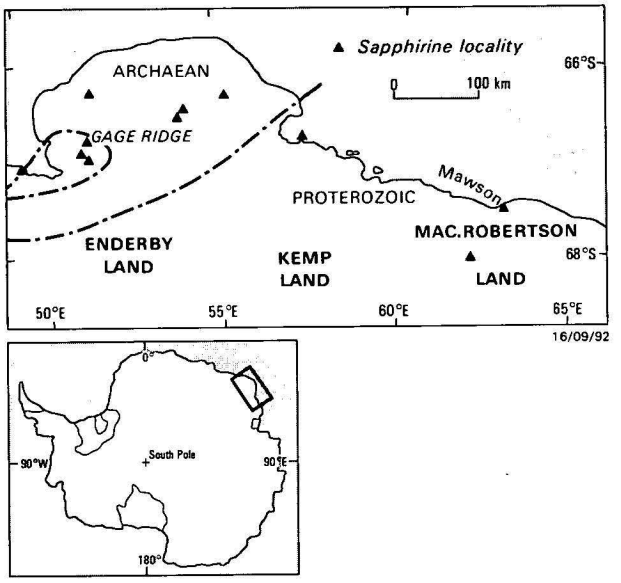

Figure 1. Map showing occurrences of sapphirine in SiO_2-deficient assemblages.
Dashed line indicates area in which the association sapphirine+quartz occurs; dot-dashed line is approximate boundary between granulite-facies metamorphics of the Archaean Napier Complex and the late Proterozoic Rayner Complex.

Representative samples from each locality were chemically analysed to investigate compositional changes associated with the formation of the marginal reaction zones.

Chemical composition

Chemical analyses confirm the exceptionally magnesian character of these granulites, which consist almost entirely of SiO_2, Al_2O_3, and MgO (Table1). Hence, their bulk compositions (excluding K_2O) can be well represented by an SiO_2—(MgO+FeO)—Al_2O_3 plot (Fig. 3). Phlogopite-rich parts contain significant K_2O, but only the marginal zones contain much FeO. Most trace elements (notably V, Cr, Ni, and Cu) tend to be low, whereas Zr, Nb, Th, and U are relatively high, but variable; Rb contents reflect those of K_2O. The Gage Ridge granulites have much higher Li, Be, La, and Ce than those from Mawson, but tend to be less magnesian; as could be predicted from Figure 3, none of the analysed Gage Ridge samples contains spinel. The only analysed cordierite-rich type B granulite from Mawson is significantly higher in SiO_2 than any of the other samples (Fig. 3). Combined water (H_2O^+) contents of the phlogopite-rich granulites are unusually low, so two representative samples were analysed for F. The high values obtained largely account for the low totals of Table 1, and imply very high F contents for the phlogopite (an estimated 4.0% in 73282053, and 5.0% in 77284340).

The highly magnesian compositions of types A and B granulites from Mawson are reflected in those of the constituent minerals (Tables 2–6), with mg (atomic 100 Mg/(Mg + total Fe)) phlogopite (99.2–99.8)>sapphirine (98.6–

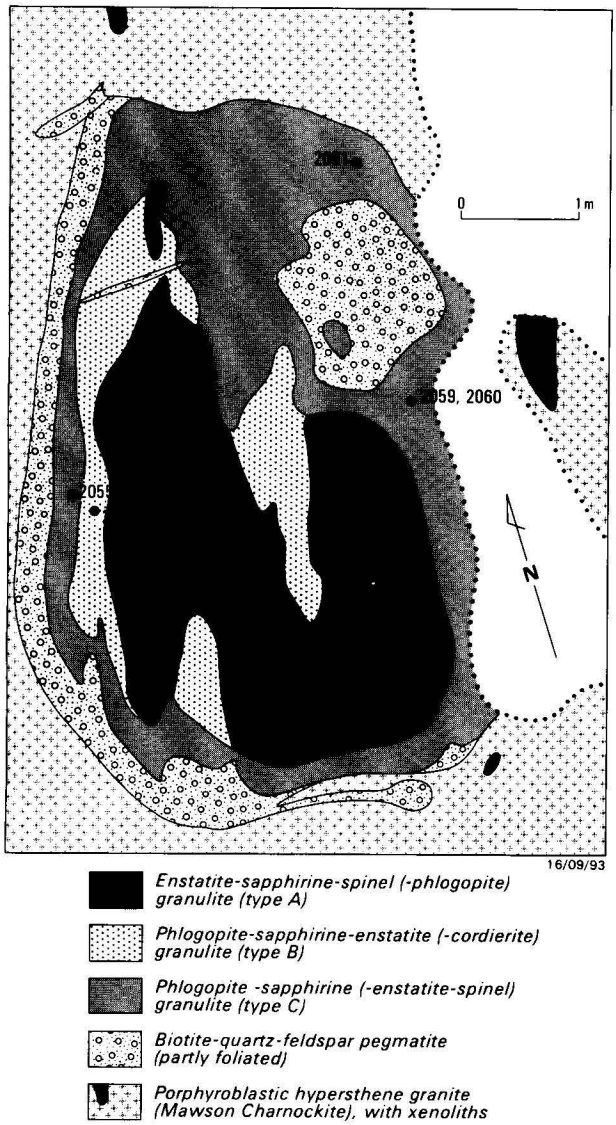

Figure 2. Map of sapphirine-bearing granulite xenolith at Mawson.
Locations of analysed samples (prefixed 7328) are indicated.

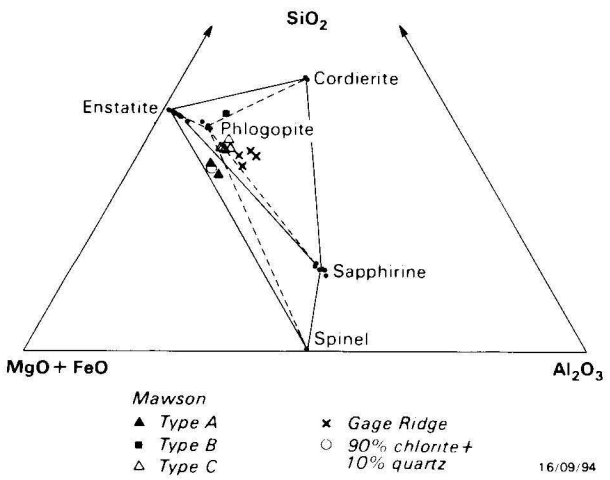

Figure 3. Molecular SiO_2—(MgO + total Fe as FeO)–Al_2O_3 diagram for sapphirine-bearing granulites.
The chlorite composition used in calculating the quartz + chlorite mixture is that of the sheridanite given by Deer & others (1962, p. 140, anal. 13).

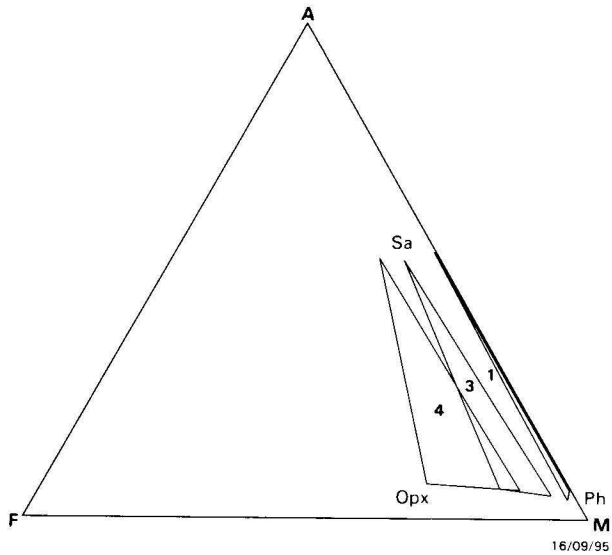

Figure 4. Molecular A(Al_2O_3-K_2O)–F(total Fe as FeO)—M(MgO) diagram showing movement of the three-phase triangle, coexisting sapphirine–orthopyroxene–phlogopite to more Fe-rich compositions.
1, 3, and 4 as in Tables2, 3, and 5.

99.1)>enstatite (96.9–98.3)>spinel (95.5–96.5). Analysed minerals from Gage Ridge are only slightly less magnesian. All these phases become considerably more Fe-rich towards the margins of the bodies (Fig. 4). Slight excesses in total cations for sapphirine (over 7 per 10 oxygens) and orthopyroxene (over 4 per 6 oxygens) may reflect the presence of small amounts of ferric iron. Orthopyroxenes have notably high Al_2O_3 contents (up to 8.9%), but very little eastonite substitution is observed in the Mawson phlogopites. F analyses of two host rocks indicate that the phlogopites from both localities contain about 2 F per formula unit.

The origin of these unusual sapphirine-bearing granulites is obscure, in the absence of diagnostic field relationships, although very similar rocks at Young Nunataks in Enderby Land form part of a layered sequence of probably sedimentary origin. Evaporitic mudstones or other magnesian pelites, or hydrothermally altered mafic igneous rocks are possible protoliths (Warren, 1979; Sheraton, 1980); whereas, the very high MgO and low Cr contents are perhaps more consistent with metamorphism of evaporites (Moine & others, 1981), no metasediments of clearly evaporitic origin have been found in Enderby Land (Sheraton & others, 1980). There is quite a close match (neglecting water) between type A granulite and a mixture of 90% magnesian chlorite (sheridanite) and 10% quartz (Fig. 3). The Gage Ridge granulites are slightly more aluminous, possibly as a result of a higher proportion of clay minerals in the source material (Warren, 1979).

Development of reaction zones

Recalculation of the analyses of the Mawson granulites in terms of cations per 100 oxygens (Table 7) shows that the main chemical changes associated with the formation of the marginal reaction zone are outward migration (loss) of Mg and inward migration (gain) of Fe, K, and H_2O, and (by implication) F. Comparison of the average type A (Table 7, column 1) with average type C (Table 7, columns 2–4) indicates an almost 1:1 replacement of Mg (5.74 Mg per 100 oxygens 'out') by K + Fe (5.96 'in'). However, there are also smaller net gains of Si, Mn, and Na, and loss of Al. Of the trace elements, Ni, Zn, Rb, Sr, Pb, and, possibly V, Cr, and Th show variable, but significant, increases in the marginal type C rocks. Some of

Table 1. Composition of sapphirine-bearing granulites from Mawson (1–7) and Gage Ridge (8–11). 1 and 2 are type A granulites, 3 is type B, and 4–7 are type C.

	1	2	3	4	5	6	7	8	9	10	11
Sample	7328	7328	7328	7328	7328	7328	7328	7728	7728	7728	7728
number	2051	2052	2053	2055B	2059	2061	2060	4338	4340	4343A	4343B
SiO_2	40.4	37.3	46.8	37.7	38.4	37.2	38.7	37.0	36.2	39.4	36.4
TiO_2	0.12	0.14	0.97	0.33	0.16	0.15	0.29	0.73	0.12	0.27	0.46
Al_2O_3	24.4	27.6	18.15	23.5	22.5	21.0	21.8	32.2	26.7	31.2	31.7
Fe_2O_3	0.54	0.90	0.10	0.71	1.41	1.71	2.41	0.21	1.04	0.19	2.06
FeO	0.65	0.55	0.70	1.00	1.90	2.00	4.90	0.36	0.79	0.47	4.70
MnO	0.04	0.05	0.03	0.03	0.06	0.07	0.14	0.01	0.03	0.02	0.12
MgO	33.5	32.0	25.5	25.1	25.7	24.6	21.5	27.9	24.6	25.5	20.2
CaO	0.04	0.12	0.12	0.04	0.07	0.02	0.90	0.13	0.06	0.07	0.78
Na_2O	0.10	0.11	0.59	0.69	0.55	0.55	0.62	0.09	0.27	0.15	0.92
K_2O	0.58	0.68	4.70	7.45	6.57	8.26	5.73	0.68	6.80	0.64	0.16
P_2O_5	<0.01	<0.01	0.01	0.04	0.02	0.03	0.02	0.04	0.03	0.02	0.03
H_2O^+	0.42	0.44	1.10	1.06	1.03	1.07	1.13	0.54	1.18	0.68	0.50
H_2O^-	0.07	0.08	—	0.12	0.09	0.07	0.08	0.02	0.09	0.07	0.09
F	—	—	2.12	—	—	—	—	—	3.77	—	—
Total	100.86	99.97	100.89	97.77	98.46	96.73	98.22	99.91	101.68	98.68	98.12
Total−(O≡F)	—	—	100.00	—	—	—	—	—	100.10	—	—
Trace elements in parts per million											
Li	4	3	10	—	—	—	—	17	34	16	—
Be	<1	<1	1	—	—	—	—	10	1	23	—
V	13	20	22	19	19	11	29	50	32	32	61
Cr	5	4	8	5	6	6	8	7	4	6	14
Ni	6	6	5	7	16	11	18	22	45	21	31
Cu	<2	<2	<2	<2	<2	<2	<2	7	4	41	12
Zn	36	62	8	40	50	92	199	3	13	5	49
Ga	5	8	2	9	7	4	11	9	11	8	19
Rb	61	64	375	530	373	350	297	35	530	49	5
Sr	1	3	7	6	11	6	20	5	13	2	29
Y	7	21	21	13	11	13	14	10	38	5	14
Zr	132	129	765	297	127	136	119	732	103	250	281
Nb	13	13	147	31	27	23	24	44	10	11	26
Ba	16	15	43	36	34	7	35	27	507	10	133
La	<2	2	<2	<2	<2	<2	4	38	22	47	73
Ce	4	11	9	<3	<3	<3	10	73	37	82	127
Pb	1	1	7	6	7	10	8	26	7	9	15
Th	6	17	5	2	14	51	30	240	23	84	101
U	1.5	1.5	3.5	1.5	0.5	3.0	1.0	7.5	1.0	2.5	3.0
mg	98.1	97.7	98.3	96.5	93.5	92.5	84.4	98.9	96.2	98.6	84.6
Estimated modes											
Enstatite/bronzite	55	50	20	—	20	—	30	45	—	50	45
Sapphirine	20	20	10	25	25	10	20	55	25	35	40
Spinel	20	20	—	—	tr	5	tr	—	—	—	—
Phlogopite	5	10	45	75	55	85	50	tr	70	5	tr
Cordierite	—	—	25	tr	—	—	—	—	5	5	5
Plagioclase/perthite	—	—	—	—	—	—	—	—	—	5	10

H_2O^+, H_2O^-, and FeO determined by the Australian Mineral Development Laboratories, Adelaide, and F at University of Tasmania; remaining elements by XRF and AA in BMR laboratory (see Sheraton & Labonne, 1978, for details of methods). tr = trace.

Table 2. Chemical analyses of orthopyroxene.

	1	2	3	4	5	6
SiO_2	56.26	58.21	53.50	51.24	55.91	50.32
Al_2O_3	4.12	1.93	5.87	6.67	5.75	8.91
FeO	1.21	2.15	8.68	16.43	1.74	13.29
MgO	37.72	37.45	31.64	25.22	37.23	27.38
Cations per 6 oxygens						
Si	1.907	1.965	1.868	1.852	1.875	1.793
Al	0.164	0.077	0.242	0.284	0.227	0.374
Fe	0.034	0.061	0.254	0.497	0.048	0.396
Mg	1.906	1.884	1.647	1.359	1.860	1.454
Σ	4.011	3.987	4.011	3.992	4.010	4.017
mg	98.3	96.9	86.6	73.2	97.5	78.6

1. Type A granulite from Mawson xenolith (73282062).
2. Type B granulite from Mawson xenolith (73282053).
3. Type C granulite from Mawson xenolith (76283103A).
4. Iron-rich type C granulite from Mawson xenolith (73282060)
5. Pod from Gage Ridge (77284342).
6. Iron-rich margin of pod from Gage Ridge (77284341).

these variations are illustrated in Figure 5, which shows that different elements have migrated into the xenolith to markedly different extents (in terms of distance from the margin). K, Na, and Rb have migrated furthest, followed by Pb, then Fe, Mn, Ni, Zn, and Sr, and, finally, Ca, which has only travelled a few centimetres in from the contact with the country rock.

Calculations for the Gage Ridge granulites show a similar net gain of Fe, and to some extent Ca and Na, at the expense of Mg. V, Cr, Ni, Zn, and Sr also migrated into the bodies, but there was no gain of K, Rb, or Pb. The reason for this is not clear, as the country rock has a similar composition to that at Mawson, but it may well reflect very low P_{H_2O} preventing crystallisation of phlogopite (Luth, 1967). At Mawson, a possible source of water would have been the late-stage granitic magma that crystallised as pegmatite veins next to the xenolith. The degree of marginal deformation may also have been a significant factor.

Table 3. Chemical analyses of sapphirine.

	1	3	4	5	6
SiO_2	14.03	13.72	14.08	14.40	13.90
Al_2O_3	64.17	62.07	60.91	62.88	61.27
FeO	0.44	5.48	8.38	1.23	7.19
MgO	21.76	18.74	16.54	21.46	18.23
Cations per 10 oxygens					
Si	0.805	0.808	0.840	0.833	0.821
Al	4.338	4.308	4.284	4.283	4.265
Fe	0.021	0.270	0.419	0.060	0.355
Mg	1.861	1.645	1.471	1.850	1.605
Σ	7.025	7.031	7.014	7.026	7.046
mg	98.9	85.9	77.8	96.9	81.9

1, 3–6 as in Table 2.

Table 4. Chemical analyses of spinel.

	1	3	5
Al_2O_3	71.18	67.15	70.17
FeO	1.80	13.41	4.37
MgO	27.02	19.44	25.46
Cations per 4 oxygens			
Al	2.000	1.985	1.995
Fe	0.036	0.282	0.088
Mg	0.960	0.727	0.916
Σ	2.996	2.994	2.999
mg	96.4	72.1	91.2

1, 3, and 5 as in Table 2.

Table 5. Chemical analyses of phlogopite.

	1	2	3	4	5
SiO_2	41.41	42.10	41.94	40.45	41.13
TiO_2	1.10	1.62	0.18	0.22	0.78
Al_2O_3	14.15	12.83	14.37	13.91	17.78
FeO	0.08	0.40	2.21	4.50	0.17
MgO	27.32	26.77	26.73	23.94	25.58
Na_2O	0.93	0.57	0.51	0.38	0.19
K_2O	8.98	8.91	9.99	9.09	9.01
Total	93.97	93.20	95.93	92.49	94.65
Cations per 22 oxygens					
Si	5.807	5.946	5.837	5.876	5.689
Ti	0.116	0.172	0.019	0.024	0.081
Al	2.339	2.135	2.356	2.381	2.898
Fe	0.009	0.047	0.257	0.546	0.020
Mg	5.710	5.636	5.544	5.184	5.272
Na	0.254	0.156	0.136	0.107	0.050
K	1.606	1.605	1.772	1.685	1.590
Σ	15.841	15.697	15.921	15.803	15.600
mg	99.8	99.2	95.6	90.5	99.6

1–5 as in Table 2.

Table 6. Chemical analysis of cordierite.

	2
SiO_2	50.45
Al_2O_3	33.78
FeO	0.18
MgO	13.20
Cations per 18 oxygens	
Si	5.033
Al	3.972
Fe	0.015
Mg	1.963
Σ	10.983
mg	99.2

2 as in Table 2.

Table 7. Cations per 100 oxygens for sapphirine-bearing granulites and granitic country rocks from Mawson.

	1	2	3	4	5
Si	22.07	22.76	23.13	23.54	35.73
Ti	0.06	0.15	0.07	0.13	0.72
Al	17.41	16.73	15.68	15.63	9.92
Fe^3	0.31	0.32	0.72	1.10	0.40
Fe^2	0.29	0.51	1.00	2.49	3.15
Mn	0.02	0.02	0.03	0.07	0.08
Mg	27.73	22.59	22.94	19.50	2.08
Ca	0.05	0.03	0.03	0.59	2.86
Na	0.12	0.81	0.65	0.73	2.29
K	0.46	5.74	5.01	4.45	2.49
P	0.00	0.02	0.01	0.01	0.20
H	1.63	4.27	4.28	4.58	1.14
Total	70.12	73.94	73.55	72.83	61.05

1. Average of 2 type A granulites (Table 1, nos. 1 and 2).
2. Iron-poor type C granulite (Table 1, no. 4).
3. Average of 2 type C granulites (Table 1, nos. 5 and 6).
4. Iron-rich type C granulite (Table 1, no. 7).
5. Average of 5 hypersthene granites (Mawson Charnockite; from Sheraton, 1982).

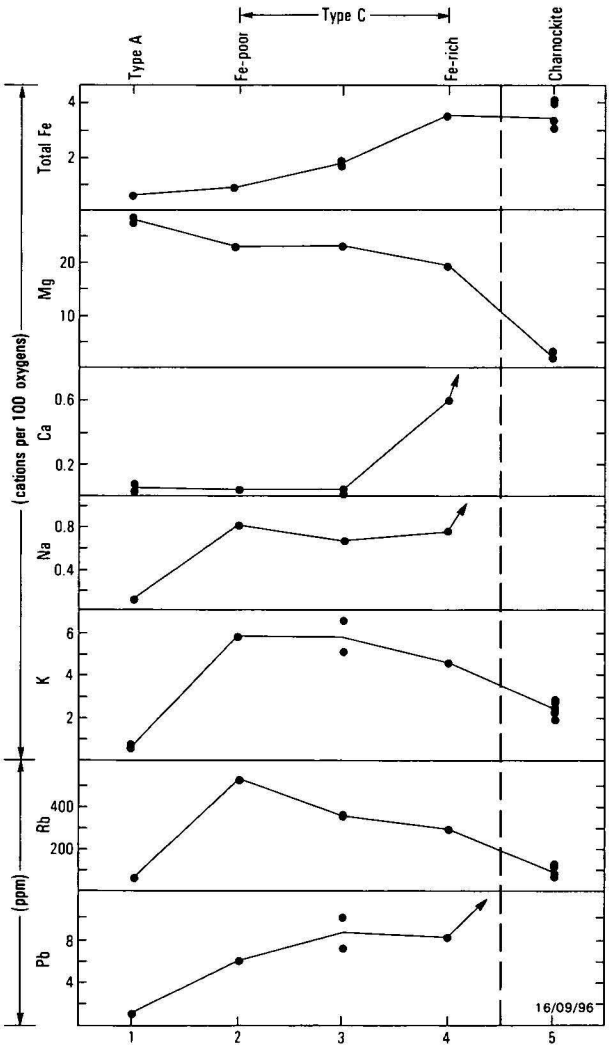

Figure 5. Chemical variations (in terms of cations per 100 oxygens) across margin of the Mawson xenolith.
1 to 5 as in Table 7.

A notable feature of the Mawson type C rocks is their tendency to plot near the join phlogopite–sapphirine in Figure 3. Their simple mineralogy is typical of assemblages formed by metasomatic processes (Thompson, 1959). Visualised in terms of the tetrahedron $MgO(+FeO)$—Al_2O_3—SiO_2—K_2O, of which Figure 3 forms the base, the observed compositional changes involve movement from type A and type B compositions: (i) upwards, with increase in K_2O, to the planes phlogopite–sapphirine–spinel (from type A, e.g., 73282061) and phlogopite–sapphirine–cordierite (from type B, e.g., 73282055B); (ii) towards the steeply dipping plane phlogopite–sapphirine–enstatite. Combination of these two effects leads ultimately to a composition on the join phlogopite–sapphirine.

Type C, which forms a continuous shell around the xenolith, is interpreted as having evolved by reaction of the highly magnesian core rocks with the surrounding granite. It is notable that an outermost cordierite-bearing zone did not form, and that the phlogopite-sapphirine assemblage in contact with the granite is undersaturated in silica (P–T conditions on the Mawson coast were not extreme enough for sapphirine + quartz to be stable). The most likely explanation is that the silica activity of the granitic magma was less than one (i.e. quartz had not begun to crystallise) when type C formed.

The evolution of type B granulite does not fit into this simple model. Its orthopyroxene is much less aluminous than that of type A (Table 2), despite the fact that the topology of Figure 3 implies a more aluminous orthopyroxene than type A at the same P–T conditions. It is thus likely that type B formed, possibly by K + Si metasomatism of type A, in a retrograde process at significantly lower temperature than that prevailing during formation of the type A assemblage.

Acknowledgements

We thank B.I. Cruikshank, K.H. Ellingsen, G.R. Ewers, J.L. Fitzsimmons, C.R. Madden, J.G. Pyke, P. Robinson, and T.I. Slezak for chemical analyses, N.J. Davis for some of the microprobe analyses, and R.J. Tingey and R.G. Warren for critically reading the manuscript. Logistic support in the field was provided by the Antarctic Division, Department of Science and Technology.

References

Dallwitz, W.B., 1968 — Co-existing sapphirine and quartz in granulite from Enderby Land, Antarctica. *Nature*, 219, 476–7.

Deer, W.A., Howie, R.A., & Zussman, J., 1962 — Rock-forming minerals, Volume 3. *Wiley, New York.*

Ellis, D.J., Sheraton, J.W., England, R.N., & Dallwitz, W.B., 1980 — litmilite-sapphirine-quartz granulites from Enderby Land, Antarctica — mineral assemblages and reactions. *Contributions to Mineralogy and Petrology*, 72, 123–43.

Luth, W.C., 1967 — Studies in the system $KAlSiO_4$-Mg_2SiO_4-SiO_2-H_2O: 1, Inferred phase relations and petrologic applications. *Journal of Petrology*, 8, 372–416.

Moine, B., Sauvan, P., & Jarousse, J., 1981 — Geochemistry of evaporite-bearing series: a tentative guide for the identification of metaevaporites. *Contributions to Mineralogy and Petrology*, 76, 401–12.

Segnit, E.R., 1957 — Sapphirine-bearing rocks from MacRobertson Land, Antarctica. *Mineralogical Magazine*, 31, 690–7.

Sheraton, J.W., 1980 — Geochemistry of Precambrian metapelites from East Antarctica: secular and metamorphic variations. *BMR Journal of Australian Geology & Geophysics*, 5, 279–88.

Sheraton, J.W., 1982 — Origin of charnockitic rocks of MacRobertson Land. *In* Craddock, C. (editor), Antarctic geoscience. *University of Wisconsin Press*, 489–97.

Sheraton, J.W., & Labonne, B., 1978 — Petrology and geochemistry of acid igneous rocks of northeast Queensland. *Bureau of Mineral Resources, Australia, Bulletin* 169.

Sheraton, J.W., Offe, L.A., Tingey, R.J., & Ellis, D.J., 1980 — Enderby Land, Antarctica — an usual Precambrian high-grade metamorphic terrain. *Journal of the Geological Society of Australia*, 27, 1–18.

Thompson, J.B., Jr., 1959 — Local equilibrium in metasomatic processes. *In* Abelson, P.H. (editor), Researches in geochemistry. *Wiley, New York*, 427–57.

Tingey, R.J., 1982 — The geological evolution of the Prince Charles Mountains — an Antarctic Archaean cratonic block. *In* Craddock, C. (editor), Antarctic geoscience. *University of Wisconsin Press*, 455–64.

Warren, R.G., 1979 — Sapphirine-bearing rocks with sedimentary and volcanogenic protoliths from the Arunta Block. *Nature*, 278, 159–61.

BMR Journal of Australian Geology & Geophysics, 7, 275-286

MAGNETOTELLURIC PROFILES IN THE McARTHUR BASIN OF NORTHERN AUSTRALIA

J.P. Cull

Magnetotelluric techniques have been used to investigate structural trends in the McArthur Basin. Observations were made at 34 sites, extending 450 km across the Wearyan Shelf, the Batten Fault Zone, and the Bauhinia Shelf. For sites on the Wearyan Shelf, the orthogonal components of resistivity are generally similar, suggesting continuous horizontal strata and uniform basement depths. However, lateral changes in resistivity, evident on the Bauhinia Shelf, become extreme in the Batten Trough. For sites near the Emu Fault, the two components diverge at long periods, indicating a major change in structure with a pronounced vertical contact. Resistivities associated with the Tawallah Group appear distinct enough to show that no appreciable thickness of McArthur Group can be present east of the Emu Fault. The data are consistent with geological models based on the assumption that the Batten Trough formed as a syndepositional graben with rapid changes in depositional thickness at the boundary faults.

Introduction

The McArthur Basin occupies an area of about 170 000 km^2, mainly in the Northern Territory, but extending into Queensland near the Gulf of Carpentaria (Fig. 1). The Carpentarian sediments preserved in the region are relatively undeformed and up to 12 km thick. Extensively exposed sequences of unmetamorphosed rocks provide the type section for the Carpentarian (Dunn & others, 1966) and are typical of the North Australian Platform Cover (Plumb & others, 1980).

The Carpentarian in northern Australia was a period of widespread, stratabound, sulphide mineralisation. The unmetamorphosed McArthur River lead-zinc deposits, and several small stratabound copper deposits, appear to be stratigraphically controlled in this region. Consequently, the thick sequence, widespread exposure, and unmetamorphosed sediments should allow a detailed study of causative evolution. The major structural elements associated with regional tectonism may be defined using geophysical data with geological constraints provided by surface mapping.

Previous attemps to interpret the evolution of the McArthur Basin have been based on a model of the Batten Trough forming as a syndepositional graben, with sudden changes in the depositional thickness across the bounding faults (Plumb & Derrick, 1975). This concept was derived from the observation that the sequences on the stable shelves are much thinner than in the trough (Fig. 2). However, Plumb (1977) noted that it is not possible to demonstrate conclusively from the surface geology alone whether the changes in thickness occur suddenly at the faults or gradually over tens of kilometres (Fig. 2). A magnetotelluric (MT) survey was, therefore, conducted in the McArthur Basin region in an attempt to resolve the principal structural features by their electrical response.

Seventeen MT sites were occupied during each field season in 1978 and 1979, defining an essentially linear traverse over a total of 450 km (Fig. 3). Data were obtained across the major structural zones of the southern McArthur Basin with particular emphasis on the region of the Emu Fault. Significant contrasts in resistivity were anticipated, sufficient to resolve the major features of the Batten Fault Zone and the thickness of basin sediments on the bounding shelves (Cull & others, 1981a, 1981b).

Geological constraints

Geological controls in the McArthur Basin have been described by Plumb & others (1980). In summary, the basin is the relatively undeformed epicratonic basin within which the Carpentarian Tawallah, McArthur, and Roper Groups and their stratigraphic equivalents (Fig. 2) were deposited in the period 1700–1400 m.y. (approx). The basin is bounded by, and unconformably overlies, Lower Proterozoic rocks of the Pine Creek Inlier in the northwest. To the north, south, and east, it extends beneath the unconformably overlying cover of the Early Palaeozoic Arafura Basin, the Early Palaeozoic Georgina and Daly River Basins, and the Mesozoic Carpentaria Basin, respectively; there is no subsurface information available yet to indicate the full extent of the basin in these directions.

In its present form, the McArthur Basin is essentially a structural basin, but palaeogeographic reconstructions suggest that the depositional limits did not extend very far beyond the present northwestern and northeastern limits. The Murphy Inlier to the southeast is, by definition, the boundary between the McArthur Basin and the Northwest Queensland Province.

Stratigraphy

The McArthur Basin succession has a maximum composite thickness of about 12 000 m in the central meridional Batten Trough, but 10 500–11 000 m is more typical. In contrast, about 5 km is typical on the adjacent Arnhem, Caledon, Bauhinia, and Wearyan Shelves (Fig. 2). The succession comprises three major subdivisions: the Tawallah Group and equivalents consist of quartz-rich arenites and subordinate basic volcanics, carbonates, and lutites, and are up to 6 km thick; these are overlain by a dominantly carbonate sequence, the McArthur Group and equivalents, which are up to 5500 m thick; these, in turn, are covered with regional unconformity by the Roper and Malay Road Groups of alternating quartz arenites and micaceous lutites up to 5000 m thick. Shallow-water sediments predominate in the total section, and a remarkable lateral uniformity is a feature of many of the units over wide areas.

The major outcrops of each group are widely separated, but the general features of the successions are consistent; consequently, the resistivities determined for surface outcrops of any sequence have been applied for related units at any depth.

Structure and tectonics

The McArthur Basin contains only shallow-dipping strata in the east and west. Bedding dips rarely exceed 5° on the stable blocks, and even in the meridional deformed belt (Batten Fault Zone) rarely exceed 20°, except adjacent to faults. Surface outcrops are consistent with regional younging on the stable shelves towards a meridional zone of intense and complex block faulting (Fig. 2), where older units have been uplifted. Stratigraphic displacements up to 7500 m occur across these meridional faults, causing exposures of basement in small inliers. A prominent zone of westerly trending faults and thinner sequence, the Urapunga Fault Zone, separates the stable western block. However, the principal fault trends (northwest and north to north-northeast) reflect the major regional patterns of northern Australia.

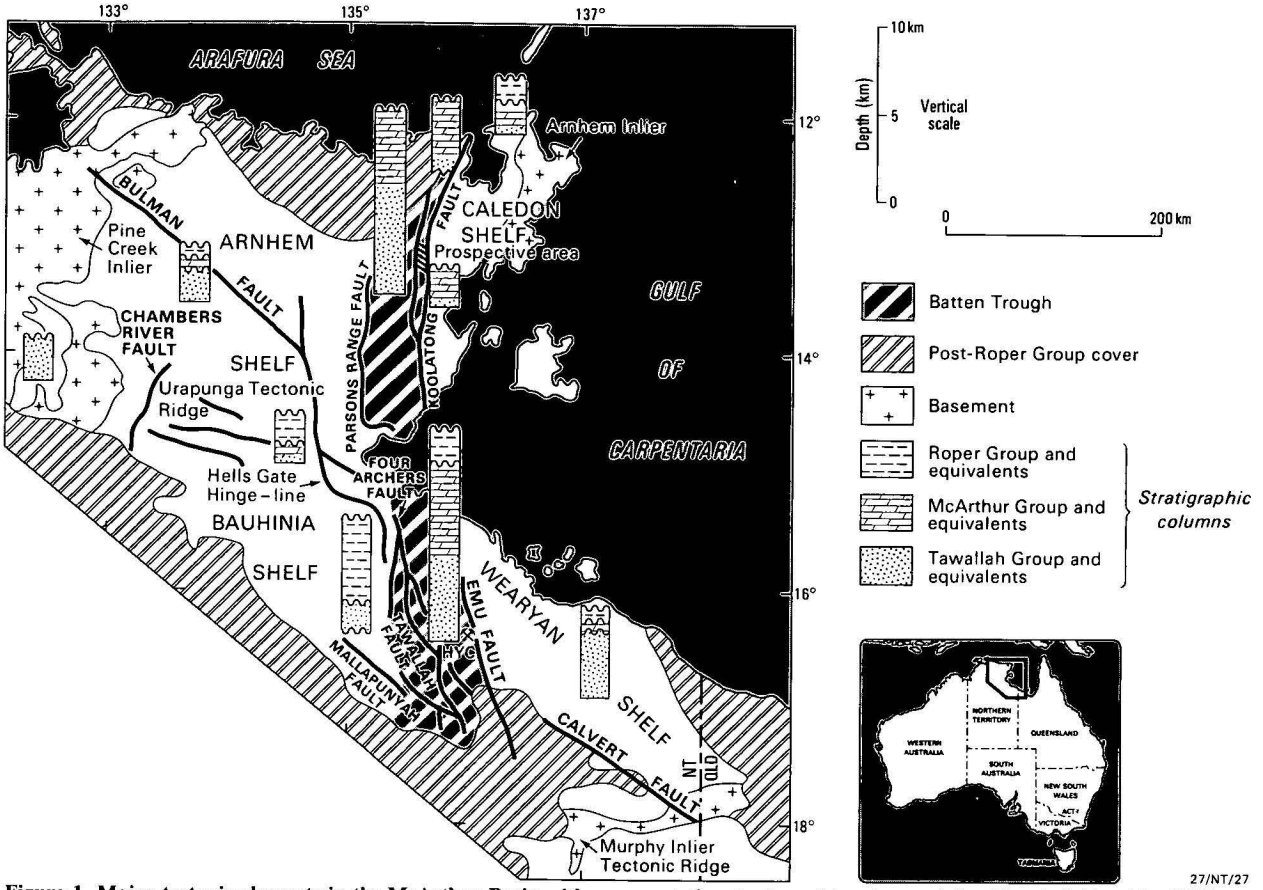

Figure 1. Major tectonic elements in the McArthur Basin with representative stratigraphic columns (after Plumb & Derrick, 1975).

The major faults are easily mapped on aerial photographs and their two-dimensional geometry is well known. However, actual fault planes are rarely observed on the ground, and the attitude of the faults at depth is generally unknown. Although the stratigraphic displacement of individual faults can be readily estimated, the true directions of movement can not always be demonstrated from surface geology.

It has been postulated by Plumb & others (1980) that the major faults of the McArthur Basin were long-lived structures that existed before the basin developed, were active during sedimentation in the basin, and deformed it again after deposition ceased. Differential movements produced the major syndepositional structures, such as the Batten Trough and Urapunga Tectonic Ridge.

Geophysical surveys

Survey criteria

The objectives of the McArthur Basin Project were established by Plumb (1977). The primary aim was to establish the nature of the Emu Fault, now identified as part of a major structural control in the southern McArthur Basin (Figs. 1, 3). It marks the eastern limit of known thick sequences and intense faulting in the Batten Fault zone, and is known to have been active during deposition of at least part of the McArthur Group. It is, therefore, defined as the eastern boundary of the Batten Trough (Plumb & Derrick, 1975). The major McArthur (H.Y.C.) lead-zinc deposit lies immediately next to the fault (Fig. 3), and sydepositional fault movements apparently exerted a major control on the siting and formation of the deposit (Walker & others 1978).

Surface geology indicates that the Tawallah Group maintains a roughly uniform thickness throughout the Batten Fault Zone and Wearyan and Bauhinia Shelves. In contrast, the McArthur Group is very thin (<100 m) on the Wearyan Shelf, is up to 5500 m thick in the Batten Fault Zone, and wedges out gradually onto the Bauhinia Shelf; the southern Batten trough can, therefore, be considered as a half-graben during McArthur Group times. Furthermore, about 300 m of Roper Group is preserved at the western end of the Wearyan Shelf, about 2000 m was deposited across the Batten Trough (now largely eroded), and the group thickens gradually westwards to more than 5000 m on the Bauhinia Shelf.

However, in the critical area, immediately east of the Emu Fault and for some 70 km eastwards, the McArthur Group is not exposed. Subsurface geophysical control is needed to differentiate between the critical half-graben model (Fig.2A) and the possible alternative of a gradually thinning McArthur Group (Fig.2B). To solve this problem several types of geophysical survey were proposed in a traverse across the Emu Fault a few kilometres north of H.Y.C. (Plumb, 1977). Controls were to be established by extending the surveys across the adjacent shelves to allow critical physical parameters to be assessed from areas of known simple structure (Fig. 3).

Existing data

Before 1978, the only full geophysical coverage of the McArthur Basin was that of gravity at 11-km spacing. At this spacing there is little variation in gravity across the McArthur Basin; there is no obvious relation to structure in the sedimentary cover, and most anomalies are tentatively ascribed to variations in the basement.

The gravity data suggest a very low density contrast between the sediments and the underlying basement, which could be expected if the basement comprises low-grade metamorphics and granites of low density. However, a major density contrast

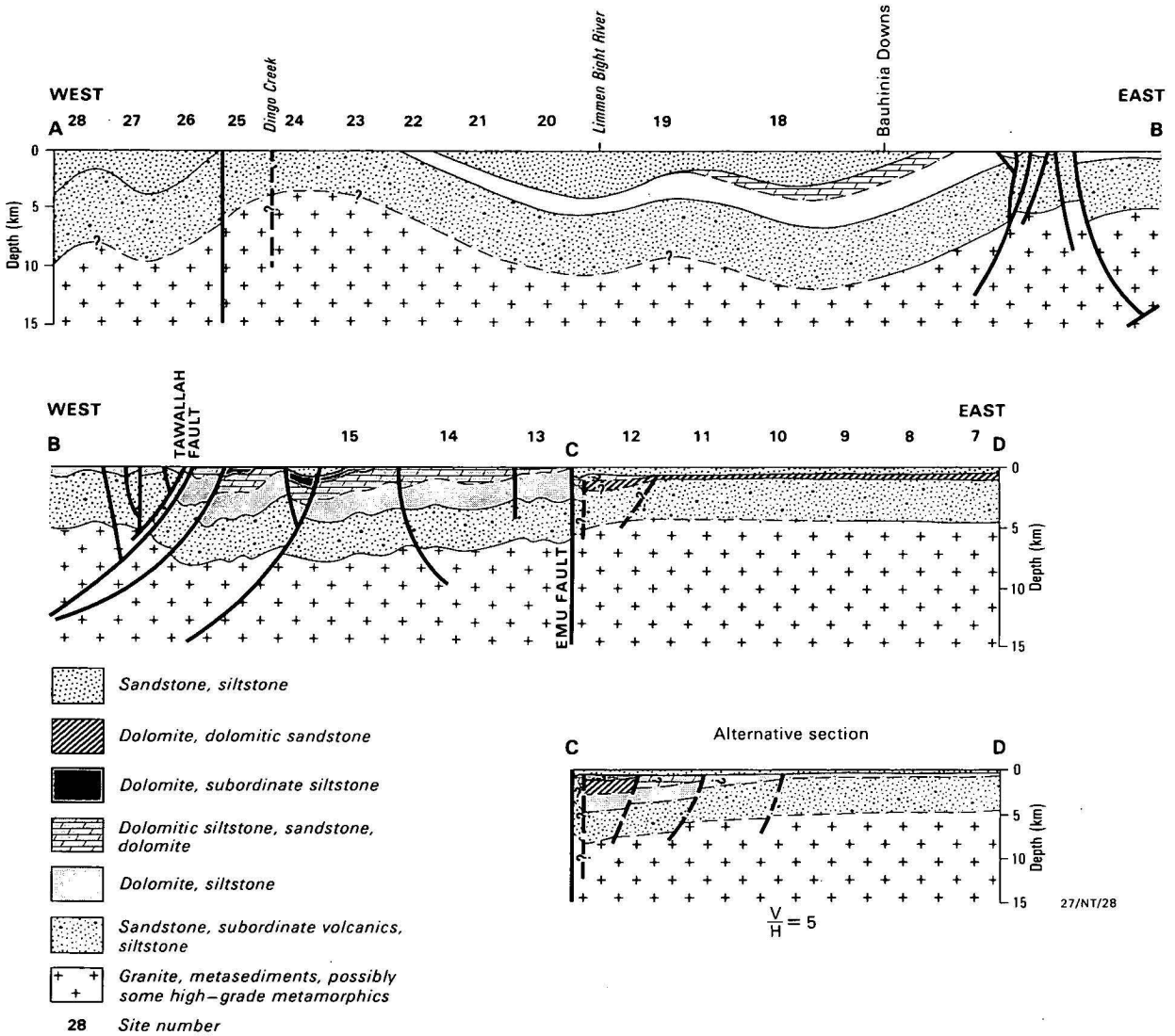

Figure 2. Alternative geological sections across the McArthur Basin constructed from surface geological controls (Plumb, personal communication, 1978) prior to MT soundings at the sites indicated.

may be expected to originate from lateral boundaries associated with the dolomites of the McArthur Group. Marked anomalies were detected in an early traverse from Normanton to Daly Waters (Neumann, 1964), but there are no related trends on the regional grid. More data have now been obtained at closer spacing across the Emu Fault. Detailed interpretations have been made, but major fault anomalies are yet to be detected across known surface contacts (Anfiloff, 1981).

An aeromagnetic survey was conducted over about 7500 km^2, to the north and west of McArthur River, in 1963–64 (Young, 1965). Many of the major geological structures can be recognised, but basic volcanics within the Tawallah Group complicate calculations of depth to true basement. A more complete coverage of the whole basin has been obtained recently, as part of a systematic coverage of Australia, and interpretation is in progress.

Seismic reflection techniques can be used in most circumstances to define structural features with great precision. However, the data must be obtained in profiles extending over distances of tens of kilometres, and sufficient energy must be liberated to penetrate to depths of 10 km. In the McArthur Basin all seismic signals are reduced by the thick carbonates of the McArthur Group, and consequently very large shots would be required as a matter of routine. The cost effectiveness of such a survey is debatable.

Long-range seismic refraction profiles can be obtained as a compromise, giving less detail, but allowing greater mobility with fewer shots. A major survey of this type was conducted by BMR in 1979 to investigate velocity structures in the crust and upper mantle (Collins, 1981). However, the fine detail of basin structure is only partly resolved.

The magnetotelluric survey described in this report was designed to complement the more common geophysical reconnaissance techniques described above. It is the only method currently available that can be used for routine mapping of electrical resistivities at depths of 1–20 km. In addition, the range of frequencies recorded provides a more definitive solution than gravity and magnetics alone. However, the application of MT in any location depends on the existence of an adequate contrast in electrical resistivity. It cannot be assumed that all changes in structure will be accompanied by a unique electrical response, but presurvey modelling (Cull & others, 1981a) did indicate that MT should be able to discriminate between the alternative models, assuming reasonable characteristic resistivities. Consequently, the aims of the survey were firstly to establish the electrical characteristics of the major units encountered, and subsequently to determine the variation in thickness of major units across the Emu Fault.

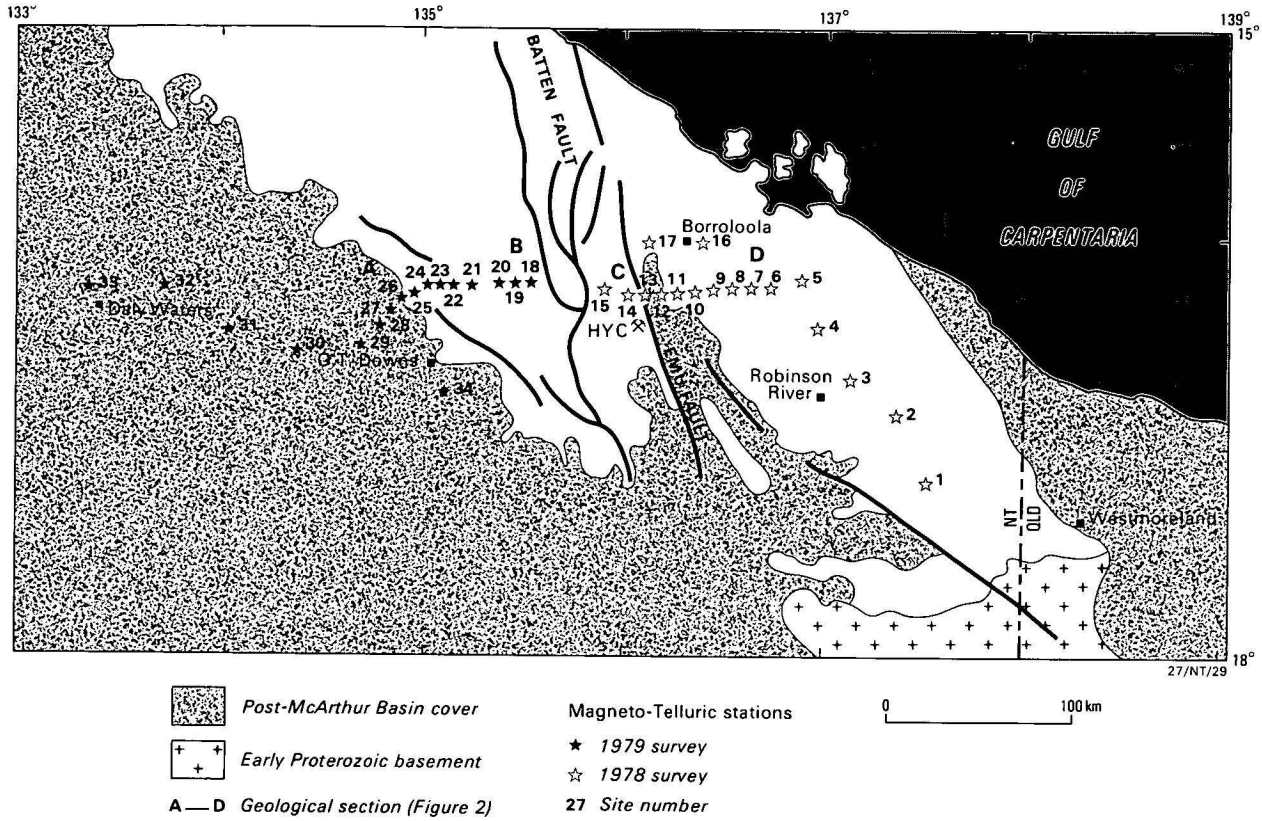

Figure 3. MT site locations defining traverse crossing the Batten Trough with control points established on the Bauhinia and Wearyan Shelves.

Magnetotelluric data

The magnetotelluric method is a geophysical technique for mapping subsurface electrical resistivity. Observations of the natural transient magnetic field (H) are related to associated perturbations in the electric field (E). A detailed description is given by Vozoff (1972) and the basic principles of the BMR system have been described by Cull & others (1981a).

The MT technique depends on electromagnetic energy reaching the Earth's surface from two major sources. Signals with a period greater than about one second are usually due to ionospheric currents at distances of 75 km or greater. Frequences of about 1 Hz are usually produced by electrical or thunderstorm activity in the atmosphere. It is assumed in the magnetotelluric method that these sources are remote, and calculations are based on the assumption of a plane wave source.

A plane electromagnetic wave may strike the Earth's surface at any angle; it is then partly reflected at an angle equal to the angle of incidence and partly refracted at the air/Earth interface. The angle of refraction will depend on the angle of incidence of the wave and the relative velocity of the wave in the air and Earth; typically, this velocity ratio will be many orders of magnitude, so the refracted part of the wave will always propagate downwards in the Earth in a nearly vertical direction.

Penetration of MT signals beneath the surface of the Earth will vary according to the frequency of oscillation (f = 1/T Hz, where T = period in seconds) and the electrical resistivity (P ohm m) of the layers encountered. A measure of penetration is given by the 'skin depth', the depth (d) in an Earth of uniform resistivity at which field amplitude has dropped to 1/e of its surface amplitude at a particular frequency; it is defined by the expression $d = \frac{1}{2}\sqrt{\rho T}$ km. Information on deep layers can be obtained by observing signals at progressively longer periods.

In most MT surveys the magnetic field is measured in three mutually perpendicular directions on the Earth's surface. A vertical component is included so that 2D and 3D structure can be more readily detected. However in a uniform or horizontally layered Earth, all currents, electric fields, and magnetic fields are practically horizontal. Furthermore, the currents and electric fields are orthogonal to the associated magnetic fields, and relative magnitudes are constant in all directions. Any variation in magnitude at constant period is assumed to indicate a 2D structure; these distort the electric fields so that orthogonal components become mixed. Tensor equations are then required to relate the relative magnitudes of E and H.

The ratio of the electric and magnetic fields at each frequency is used to calculate an 'apparent' resistivity (i.e. the resistivity of a uniform Earth that would give the measured E/H ratio) as a function of frequency. Apparent resistivity curves may then be used for the production of multi-layered 1-dimensional resistivity models, using two orthogonal components. The tensor equations relating E and H can be modified at this stage by rotation to ensure that models are generated for structure along strike and across strike. Where necessary, a 2-dimensional model can be generated, using the combined tensor equation.

MT data obtained in the McArthur Basin were compiled using standard digital techniques. Data were recorded in seven overlapping frequency bands, giving a large dynamic range, while preserving maximum economy in the number of data points. Sampling rates were varied from 0.2 to 250 samples/second, corresponding to the range 0.001–40 Hz. Sites were occupied for up to 2 days, during which time up to 150 bands were recorded on disc and transferred to tape.

Full use of the digital equipment permits a very large amount of data to be acquired and processed on site. Most of the necessary Fourier analysis and apparent resistivity calculations were carried out simultaneously with further data acquisition to

provide information on quality control. For this purpose plots were generated indicating apparent resistivities as a function of frequency. Noise levels were assessed by visual inspection, and additional data were recorded in deficient bands.

The principal axes were determined by tensor rotation and the corresponding apparent resistivity and phase curves were generated for each orthogonal component. These data were averaged to 10 points per decade in non-overlapping bands. The final data sets were subject to statistical screening (Moore, 1977) and the averaged values were adopted for all subsequent interpretations. Data sets for 1978 and 1979 have been reported by Cull & others (1981a, 1981b).

Before any interpretation of these data, it is necessary to identify those structural units able to provide a characteristic response unique to the geological problem. Mathematical modelling can then be used to calculate MT profiles across the anticipated basin structure, indicating sensitivity of the model parameters and providing limits to resolution. However, no laboratory data were available to indicate appropriate values for the resistivity of the major rock types in the survey area. Consequently, the preliminary estimates used in the following data reductions have been based on the known stratigraphy related to standard values of resistivity for typical rock types.

In simple geological situations the actual resistivity and thickness of horizontal layers can be calculated from MT signals, using analytical functions (Vozoff, 1972). In other circumstances, a more complex 2D transmission-surface analogy, based on numerical techniques, may be required to solve the relevant Maxwell equations (Swift, 1971; Jupp & Vozoff, 1977). In each case it is necessary to make reasonable estimates of resistivity for each of the major units encountered.

Resistivity estimates

A preliminary examination of the apparent resistivity data at each site indicated that the structure in the Batten Fault Zone is predominantly two-dimensional. The orthogonal components of apparent resistivity appear to diverge, notably at long periods. However, for sites outside the Batten Fault Zone, there is general agreement, particularly at periods less than 1 s. This range corresponds to skin depths commonly less than 5 km. One-dimensional models can, therefore, be formulated to calculate actual resistivities and detect the extent of major units within the basin sequence. Interpretations based on 1D inversions are considered in more detail in the following section. Data from sites located on representative units are shown in Figures 4, 5, and 6. The values of apparent resistivity in each group appear to be internally consistent at short periods, reflecting the near-surface similarity in geology. Values of actual resistivity can, therefore, be extracted for each major group.

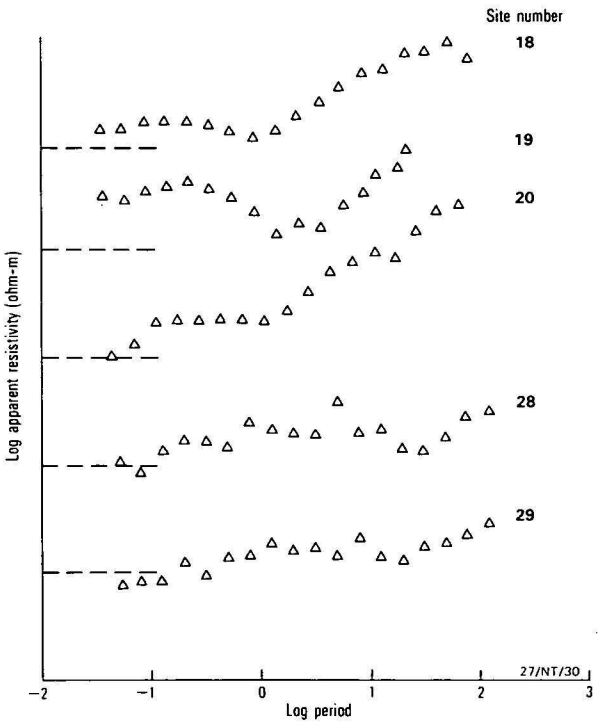

Figure 4. Apparent resistivities for sites located on major sections of Roper Group.
Dashed line represents apparent resistivity of 10 ohm m at each site. Each site offset by 1 decade.

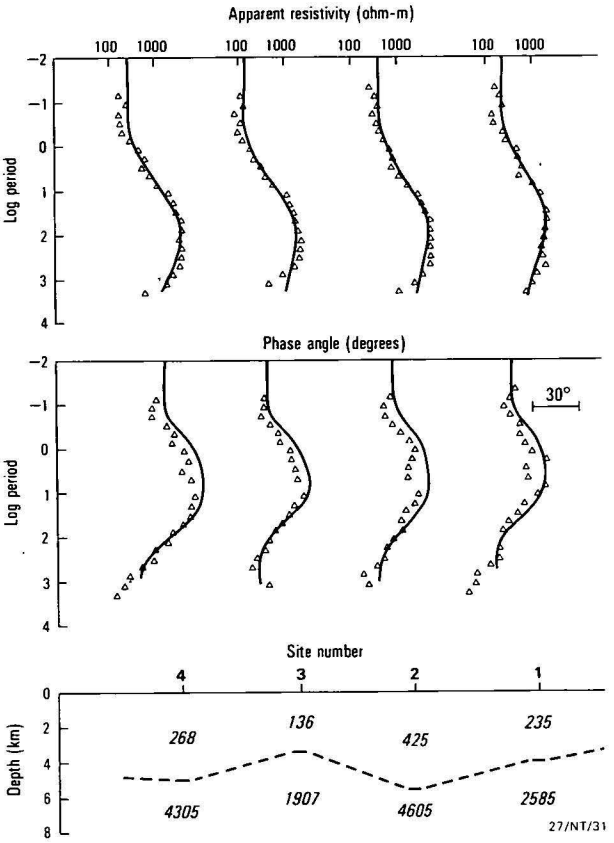

Figure 5. Apparent resistivities, phase data, and 1D inversions for Wearyan Shelf control points located on known section of Tawallah Group.
Results of 1D curve fitting shown as solid line with corresponding cross section below. Resistivities shown relative to base level of 100 ohm m offset by 2 decades for each site. Phase data relative to 45°.

Roper Group

The western part of the Wearyan Shelf is covered by Roper Group sediments having a thickness of about 300 m (Fig. 2). The electrical properties of this unit may attenuate MT signals of much greater skin depth. Consequently, a characteristic response must be established before more detailed analysis of deeper structure near the Emu Fault. Thicker sequences are available on the Bauhinia Shelf, and estimates of resistivity may be more reliable in that area.

Data obtained at sites 18, 19, 20, 28, and 29 during 1979 are considered to be representative of the Roper Group. The sites are remote from the Batten Fault Zone, and orthogonal components of resistivity are nearly coincident at periods less than 1 s. However, the nature of deeper units and the structure of the basement are less well known.

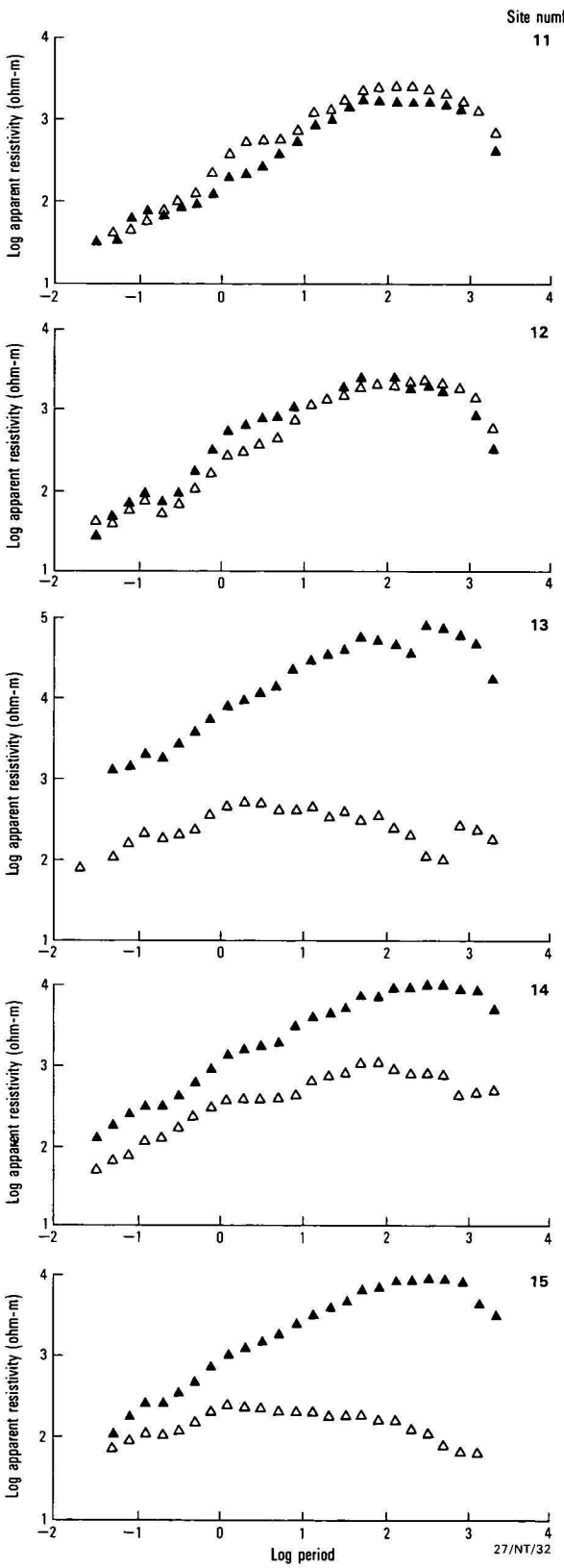

Figure 6. Apparent resistivities for sites located on McArthur Group outcrop in Batten Trough.
Component with E perpendicular to strike shown as solid symbol. Data shown relative to base level of 10 ohm m offset by 4 decades at each site.

Actual resistivities for the Roper Group can be estimated from the average trend in apparent resistivities extrapolated to minimum period (Fig. 4). Values in the range 1020 ohm m are considered to be representative. Such values are typical for fluid-filled shales and sandstones of moderate porosity (Keller, 1971).

Tawallah Group/basement

The Wearyan Shelf has been identified as an area of simple structure. There are extensive exposures of shallow-dipping Tawallah Group rocks (sites 1–4) and the McArthur and Roper Groups, identified elsewhere, appear to be largely absent. Apparent resistivities in the east can, therefore, be attributed to a single horizontal layer, representing the Tawallah Group, overlying Early Proterozoic basement.

Characteristic data were obtained at sites 1–4, established in 1978. Estimates of actual resistivity based on inversion are indicated in Figure 5. Initial models used in the inversion were identical in each case; a standard basement of resistivity 200 ohm m at 5 km depth was adopted from plots of apparent resistivity.

Calculated values of actual resistivity vary by a factor of 2 for both the Tawallah Group and the basement. However, basement depths are for the most part constant, supporting geological observations (Plumb, 1977) that suggest that the Tawallah Group is fully preserved. These depths are also in agreement with seismic refraction results (Collins, in press). They demonstrate the resolving power of MT in the McArthur Basin and justify an extended survey in more complex regions. The representative values of resistivity and thickness indicated in Figure 5 were adopted for models intended to resolve compound layers detected on the Bauhinia Shelf and in the Batten Fault Zone.

McArthur Group

Extensive outcrops of McArthur Group are found only in areas of complex geology associated with the Batten Fault Zone. A thin sequence extends onto the Wearyan Shelf and a thick wedge penetrates the Bauhinia Shelf at depth. Consequently, the only data that can be directly assessed are from sites 13, 14 and 15, established in 1978.

Major structural complexity is indicated by these data. In particular, the orthogonal components of apparent resistivity are highly divergent in the region of the Emu Fault (Fig. 6). A 2D structure is implied, and estimates of actual resistivities based on only one component of field data are unreliable. Values of apparent resistivity, extrapolated to minimum period, range from 100 to 1000 ohm m, depending on both the site and the component considered. Values for site 15, which is farthest from the fault, are further complicated by a local outcrop of the Roper Group.

Estimates of resistivity for carbonates obtained in other surveys also show significant variation (Keller, 1971). Values range from 100 to 2000ohmm, reflecting changes in texture and composition, ranging from limestone to dolomite. Mid-range values of 500 and 1000 ohm m were adopted in the following analysis in an attempt to distinguish boundaries between the McArthur and Tawallah Groups. However, it must be emphasised that the Tawallah Group also contains widespread volcanic and carbonate units associated with high resistivities, similar in magnitude to the McArthur Group carbonates. Lack of precision on the relative values for each unit remains the major limit to resolution in the following interpretation.

Standard response

Three type-sections are shown in Figure 7. The first profile (A) is based on the inversion results obtained above for the Wearyan Shelf. The model consists of a single layer with

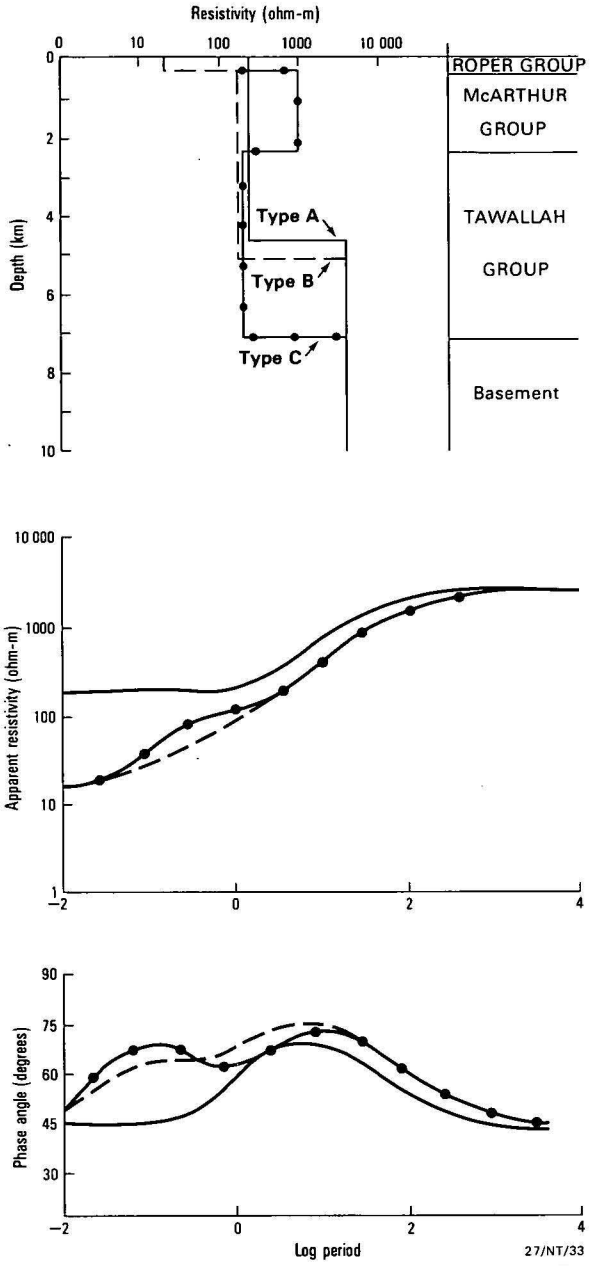

Figure 7. Resistivity type-sections with corresponding MT response for typical basin sequences.

Curve A represents a single unit of Tawallah Group on basement. Curve B includes a surface cover of Roper Group, and Curve C reflects the introduction of McArthur Group between the Roper and Tawallah Groups.

thickness of 5000 m; it represents the Tawallah Group resting on Proterozoic basement. The response is typical of sites 1–4, considered in Figure 5.

The first modification consists of the addition of a 300 m surface layer, representing the Roper Group. The response of this model (B) differs considerably from (A): apparent resistivities are lower at periods less than 1 s, and phase angles significantly different from 45° are no longer characteristic of a single layer. Lateral variations in the structure of the surface layer may, therefore, mask any response from the Tawallah Group. However, some continuity should be preserved on the stable Wearyan Shelf, where structural trends have been accurately predicted.

The third model (C) incorporates a layer of high resistivity, representing the McArthur Group between the Roper and Tawallah Groups. It results in a minor perturbation to the previous response. A low-amplitude inflection appears in the values of apparent resistivity at periods of 0.1–1.0 s. However, a more diagnostic response is generated in the phase data. In particular, the rates of change are more extreme at short periods, and mid-range values are partly suppressed.

The three models described above provide a framework for subjective analysis of the major structural features in the McArthur Basin. In addition, they enable the selection of adequate starting models for comprehensive data inversion.

Interpretations

Interpretations of MT data normally proceed by semi-random inversion techniques, generating ideal numerical solutions, which are then related to any available geological controls. Such an approach is valid for reconnaissance data in simple sedimentary structures. However, specific geological alternatives can be distinguished more directly by including critical parameters in the inversion process.

The alternative geological models and the MT recording sites are shown in Figure 2. The first model shows an abrupt thinning of the McArthur Group west of the Emu Fault, whereas the second profile shows the McArthur Group thinning gradually eastwards over a distance of tens of kilometres. Resistivity data may be used to establish a qualitative MT response for each model. Basement depths may be calculated directly from field data where there are abrupt changes in electrical character at the contact; alternatively, structural trends within the Tawallah Group may be indicated from volcanic marker beds (Cull & others, 1981a).

Wearyan Shelf

The structural simplicity of the Wearyan Shelf has been discussed above. The apparent resistivities for sites 14 conform to the pattern of a single layer resting on an infinite half space (Fig. 5). Type section A (Fig. 7) appears appropriate at each site. However, the character of the data is modified for sites 5–10, which constitute a traverse towards the Emu Fault. There are no obvious lateral boundaries in the traverse associated with diverging components of apparent resistivity (Fig. 8). However, base levels at periods less than 1 s are progressively reduced: short-period values range from 100 ohm m in the east to 10 ohm m in the west. This trend reflects an increasing thickness of Roper Group sediments towards the west (cf. Model B, Fig. 7). Consequently, the phase data show a departure from 45° at short periods and become modified to resemble the diagnostic curve type B (Fig. 7). More complex structure can be justified only in the extreme west (site 10). The base level or apparent resistivity begins to increase and the phase data appear flatter, resembling the diagnostic curve type C.

Depth estimates for sites 5–10 have been based on both the alternative structures generating the response types B and C (Fig.9). Values of resistivity and phase were included in 1D data inversion routines of Jupp & Vozoff (1975). The results are indicated in Figure 9. Depth to basement and Tawallah Group thickness appear consistent with the values calculated at sites 1–4 only for the type B sections (Fig. 9A). A significant thickness of the McArthur Group can be included only at the expense of a major thinning of the Tawallah Group and calculated depths to basement must be simultaneously reduced. These observations support geological models resembling the first alternative in Figure 2, and are consistent with the concept of a graben control at the Emu Fault.

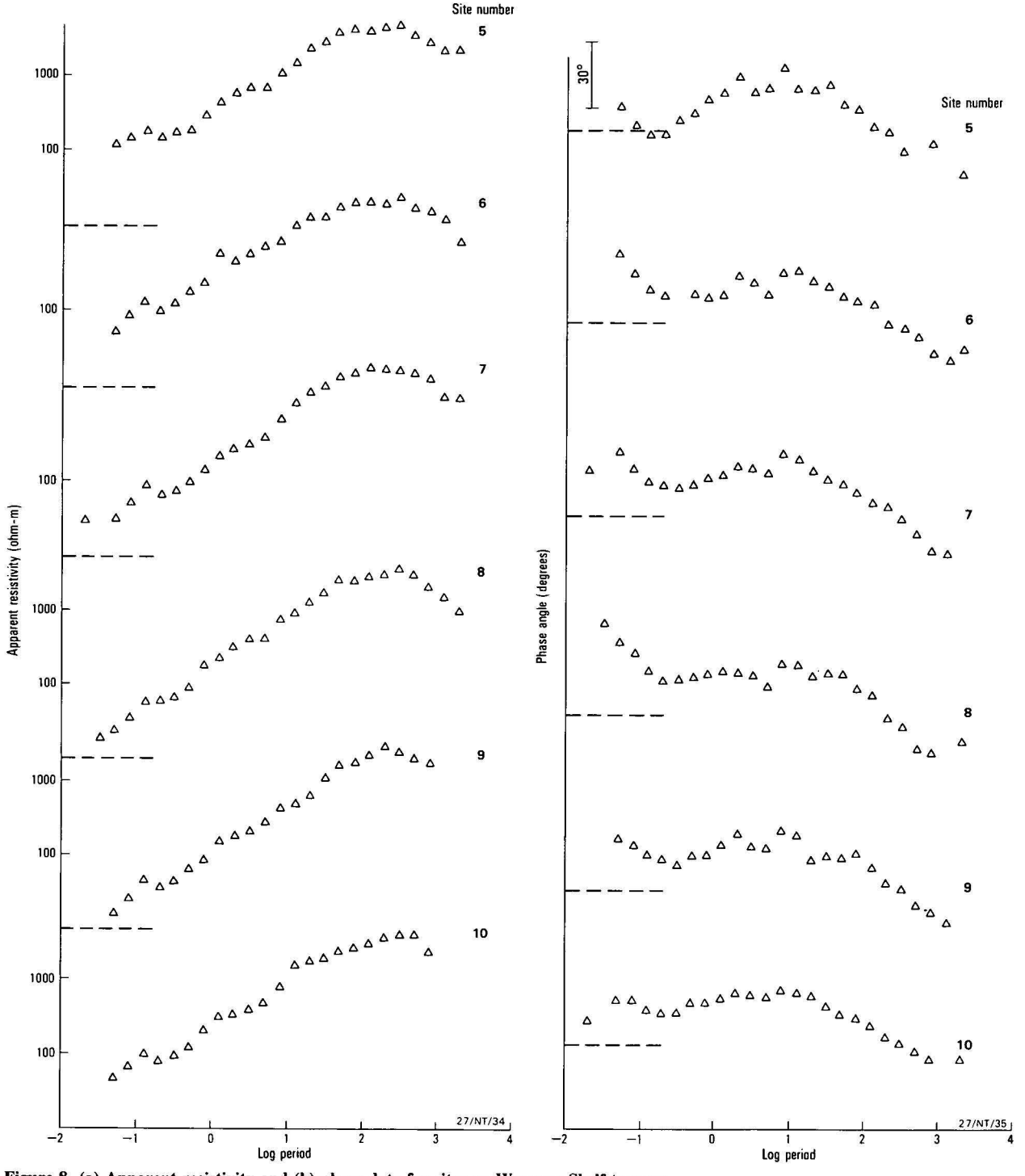

Figure 8. (a) Apparent resistivity and (b) phase data for sites on Wearyan Shelf traverse.
Resistivities shown relative to base level of 10 ohm m offset by 3 decades for each site. Phase data relative to 45°.

Emu Fault

The characteristic response of the alternative structures at the Emu Fault can be further demonstrated using 2D forward models. Values of resistivity for each model were chosen according to the results of 1D inversion. Digital approximations (Swift, 1971) were used to generate synthetic data for each mode. Results are shown in Figure 10 for periods of 2–500 s.

The significance of the Roper Group next to the Emu Fault is immediately apparent. At short periods (<1.0 s) the Emu Fault represents a vertical contact between media with a 10:1 contrast in resistivity. Contacts of this type have been considered by d'Erceville & Kunetz (1962) and Weaver (1963), who have presented analytical solutions demonstrating a characteristic discontinuity in one component (E across strike). A similar discontinuity is evident in the survey data (Fig. 11), indicating an abrupt truncation of the Roper Group.

At long periods, the effect of deeper structure can be resolved in terms of the rate of change of apparent resistivity related to site location. For models in which the McArthur Group resembles a wedge to the east of the Emu Fault (Fig. 10, 2nd insert), there are two diagnostic features. The response curves west of the Emu fault are flatter than the corresponding curves of the vertical contact, and the gradients in the east are more

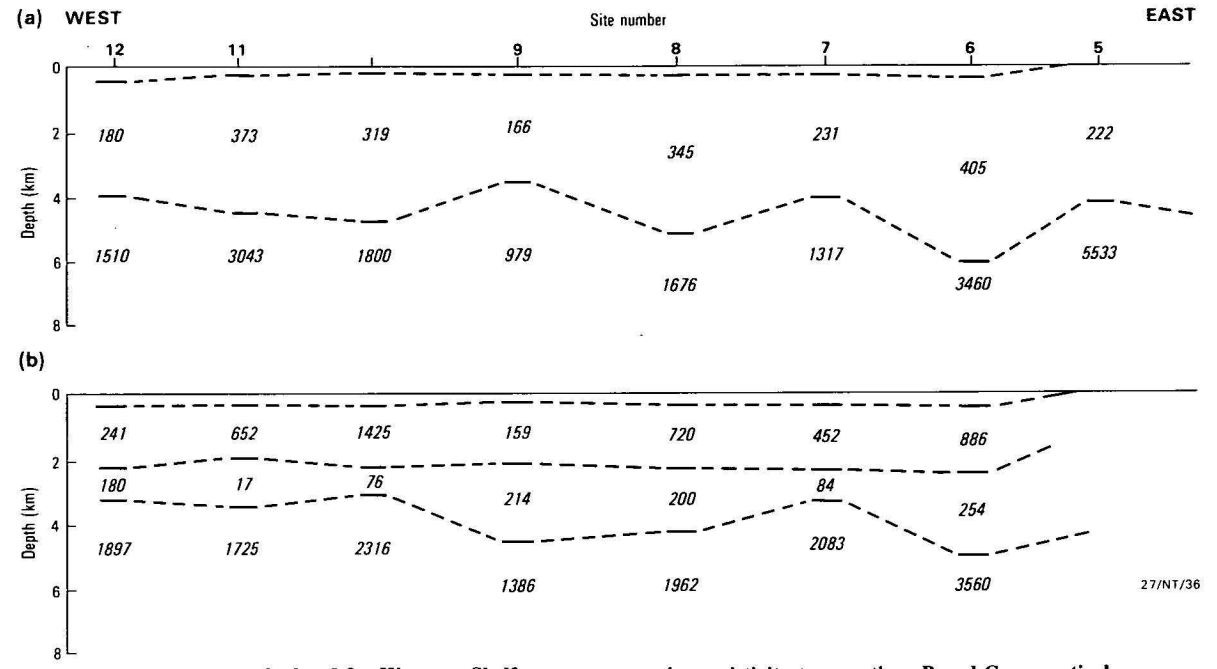

Figure 9. Basement depths calculated for Wearyan Shelf traverse, assuming resistivity type-sections B and C, respectively.

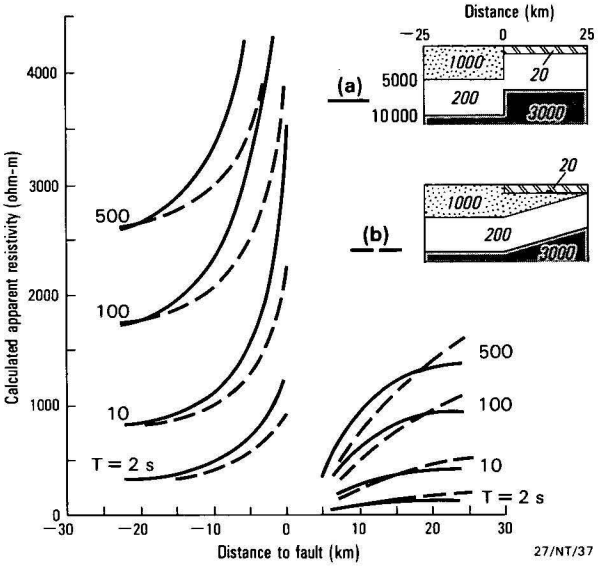

Figure 10. Theoretical MT response for 2D structure at the Emu Fault for (a) abrupt and (b) gradual thinning of McArthur Group.

persistent. The field data (Fig. 11) appear to resemble the first option in Figure 10, suggesting an abrupt truncation of the McArthur Group with a vertical step in the basement depth. However, it must be emphasised that any structure in this region is probably highly complex as a result of multiple movements generated elsewhere in the Batten Fault Zone.

Resistivity values originally assumed to be typical of basement on the Wearyan Shelf (Fig. 7) cannot be used to explain the long-period data at the Emu Fault (Fig. 11): measured values of apparent resistivity near the Emu Fault are consistently higher than synthetic data generated by the simple 2D models of Figure10. Skin depths exceed 15 km at periods of 2 s, and the anomaly must be attributed to increasing resistivities at the base of the crust. Values approaching 5000 ohm m are suggested by the trends in Figure 11.

Bauhinia Shelf

Most sites on the 1979 traverse were located on the Bauhinia Shelf, immediately west of the Batten Fault Zone (Fig. 3). Consequently, any trends in MT response may be obscured by structural changes in the basement. Type sections A,B, and C (Fig. 7) are rarely applicable, and variations in the Roper Group appear to dominate (Fig. 4). Separate starting models were, therefore, required for 1D inversion at each site.

Structural correlations were based on inversions of the more resistive components (E across strike) at each site. These results are generally considered more reliable than those generated by the low-resistivity components, except in the case of regions containing features resembling a conductive dyke (Vozoff & others, 1975; Vozoff, 1972). It must be emphasised, however, that the parameters in each model are not equally well resolved. Initial values assigned to the starting model were allowed to vary only at rates related to the magnitude of their effect on the total response. For example, highly resistive

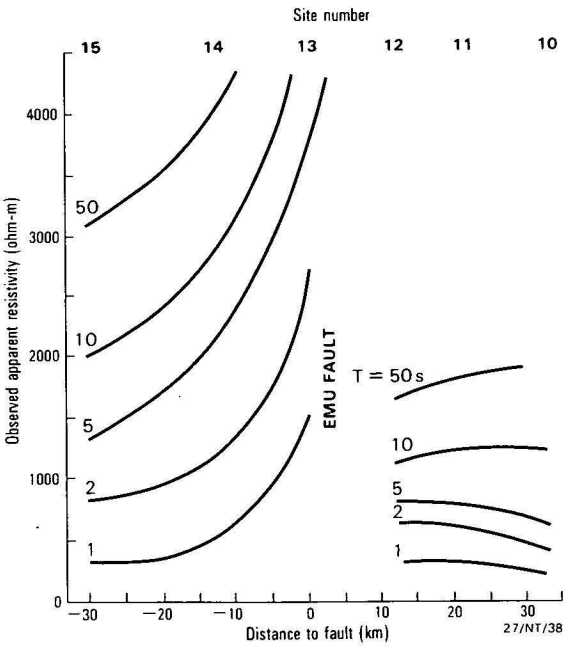

Figure 11. Curves derived from measured apparent resistivities for sites located near Emu Fault, showing discontinuity in E across-strike component.

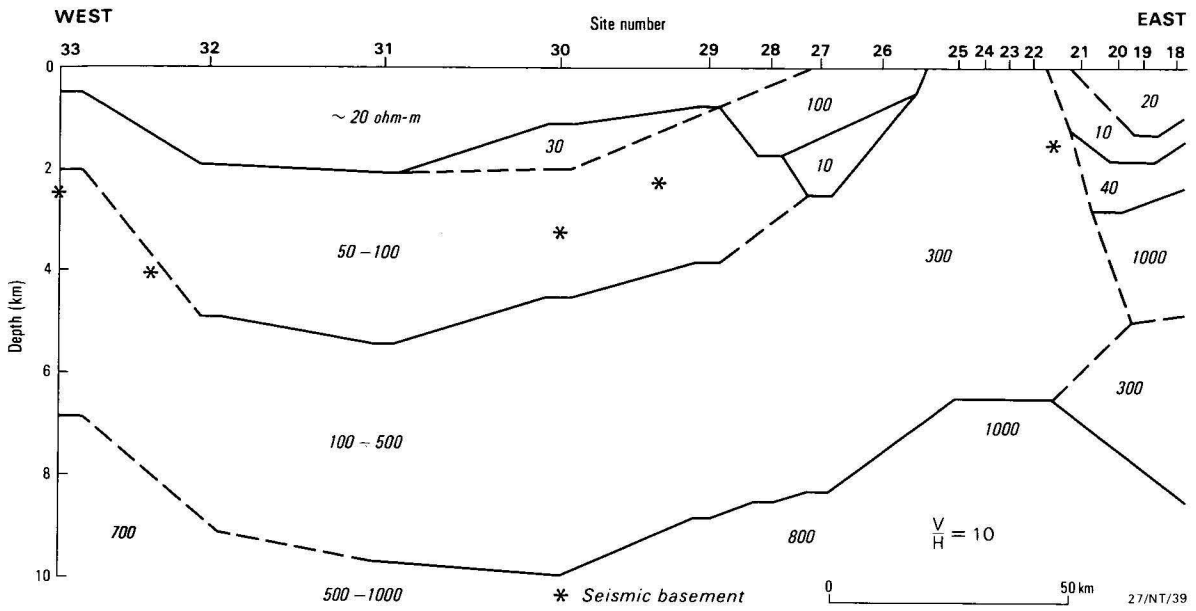

Figure 12. Composite profile based on 1D inversion of MT data on the Bauhinia Shelf.

layers should not significantly attenuate the MT signals and, consequently, there may be no criteria to suggest a modification of the original value. In general, thin resistive layers are usually unmodified by inversion, but when some response is detected, the sensitivity depends on thickness rather than actual values of resistivity (Oldenburg, 1979; Vozoff & Jupp, 1975). Correlations between sites must, therefore, contain a subjective element so that 'resistive' blocks can be related even when actual values of resistivity appear to vary.

Significant lateral changes in resistivity are required to accommodate data from neighbouring sites, and large uniform layers appear to be rare (Fig. 12). Some continuity across a simple syncline is evident beneath sites 18, 19, and 20, with a highly conductive zone forming a marker at depths near 1500 m. This layer is interpreted as an aquifer correlating with known porous sandstones in the Roper Group, trending to the surface near site 21; surface springs can be seen, and the previous continuity in resistivity becomes obscure. High conductivities at shallow depth have been noted also west of site 27, but there is no comparable diagnostic progression in the individual profiles. This return to high conductivities near the surface suggests further intervals of Roper Group section to the west, but the change in character of the conductivity profile must then be attributed to variations in porosity or salinity of associated aquifers, in an area of known complex faulting.

Underlying rocks of high resistivity appear to be confined to the syncline east of site 23. Values of resistivity exceed 1000 ohm m at depths near 3 km for sites 18, 19, and 20, with values of 300 ohm m at 5 km. However, there is no evidence for high values at intermediate depths near site 21, and some thinning is suggested at site 19. These observations are consistent with the geologically postulated boundaries of the highly resistive McArthur Group rocks, lying between the Roper and Tawallah Groups of lower resistivity. But, any estimates of depth are complicated by the presence of the shallower conductive zones associated with the Roper Group. Basement parameters become highly damped during 1D inversion and many diagnostic features can no longer be resolved. Most of the data at site 21 are affected in this way and the apparent lack of any resistive layer may not be conclusive.

Lateral continuity in resistivity structures can be detected again west of site 26. There is, however, a significant change in the character of the resistivity profile from east to west. In particular there is no indication west of site 26 for a layer at shallow depth (<5 km) with values exceeding 1000 ohm m. This supports the geological prediction that there is no carbonate sequence equivalent to the McArthur Group in this region. Basement to the Tawallah Group west of site 26 appears to be characterised by resistivity values in the range 500–1000 ohm m. Such values are at the lower limit of the range for igneous and metamorphic rocks (Keller, 1971) and are well below common values for carbonates.

A maximum value of 10 km has been calculated for depth to basement near site 30. An abrupt change is evident near site 33, with depths of 6 km indicated for Daly Waters. A similar trend can be noted in depths calculated for conductive layers that appear to correlate with the Tawallah Group. The Roper Group–Tawallah Group boundary is indicated by a general increase in resistivities from values near 50 ohm m to values near 150 ohm m, at depths ranging from 5.5 km (site 31) to 2.0 km (site 33, Daly Waters). It appears, therefore, that most of the thinning indicated above can be attributed to loss in the Roper Group.

The resistivity groupings and depths obtained by 1D inversions of MT data are supported by the preliminary seismic refraction results (Collins, in press). A major refractor detected in the region west of site 27 appears to correlate with a resistivity boundary between the Roper and Tawallah Groups. The primary features in each model are identical. There is an abrupt change in depth at Daly Waters, and surface layers become thinner towards the east. However, the MT data suggest a maximum thickness for the Roper Group near site 31 rather than site 32, as suggested by seismic data.

2D inversions

The complexity of the structure in the eastern Bauhinia Shelf is indicated by diverging components of apparent resistivity for sites 18–26. Results of 1D inversion indicate that lateral continuity is minimal and only the gross features can be resolved. However, more detailed models can be formulated using 2D analysis of the combined data sets.

The computer program for 2D inversion involves a least squares error algorithm similar to the one used for 1D analysis (Swift, 1971; Jupp & Vozoff, 1977); approximately 3000 seconds of CPU time are required on a 1.5 μs computer. Core

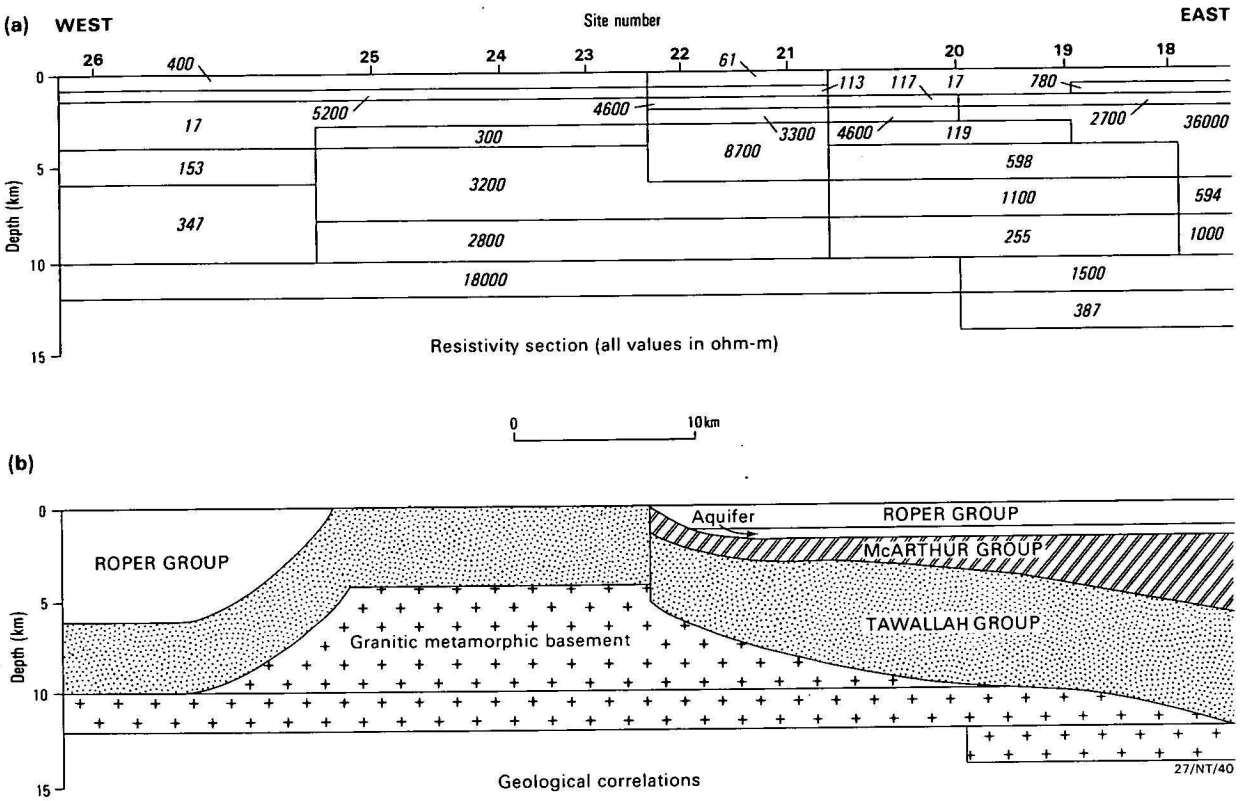

Figure 13. Resistivity cross section and geological interpretation based on 2D inversion of MT data on the eastern Bauhinia Shelf.

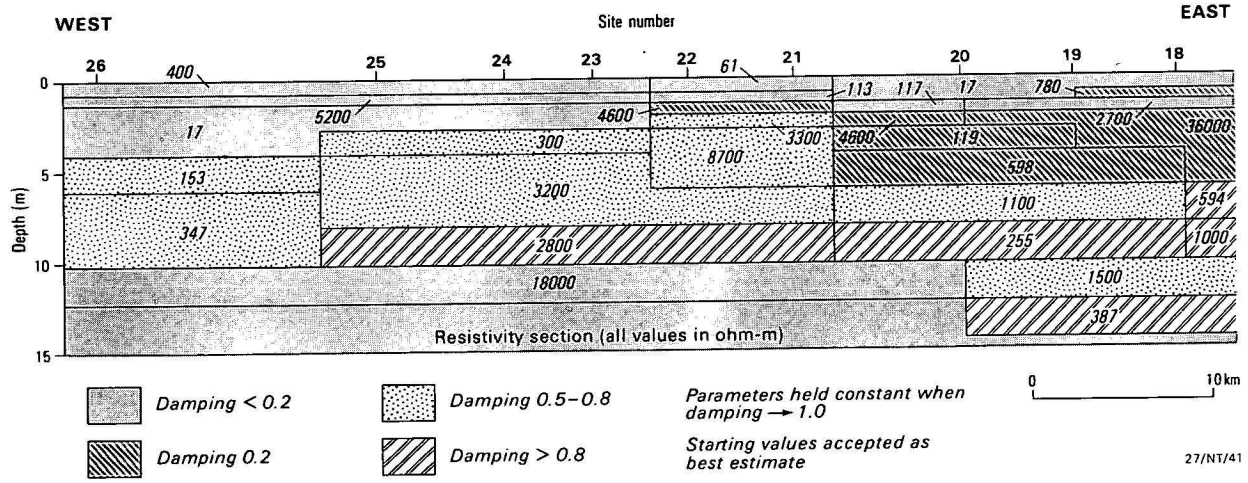

Figure 14. Sensitivity analysis of resistivity blocks identified in 2D inversion.

storage space and central processor time currently limit some of the interpretation capabilities. In particular the only parameter allowed to vary is resistivity; it is necessary that the spatial dimensions of the model remain fixed. However, the 2D model is built of resistivity 'blocks' with two spatial dimensions plus the parameter of resistivity. If inversion shows that the resistivity of one block is the same as that of an adjacent block, the boundary between the blocks can be removed so that the two become one. Consequently, by judicious manipulation of the starting model and a number of re-inversions, an adequate 2D section can be obtained.

Resistivity data for both components at each site on the eastern Bauhinia Shelf were provided as input for a 2D section. Approximate models were formulated from the results of 1D inversion with some qualitative correlations provided by inspection of the relevant pseudosections. The resistivities assigned to each block comprising the model were then varied during inversion, until the model response resembled the field data. The primary features of the composite 1D profile are preserved (Fig. 13), but more detail is available concerning parameter sensitivity (Fig. 14). In particular, there are no well-defined blocks of high resistivity west of site 21.

The highly resistive wedge at depths of 2–6 km in the eastern part of the section appears to be well defined with only minor damping. This wedge may indicate the western extent of McArthur Group rocks, which are known to wedge out westwards to site 22 (Fig. 3), but resolution is diminished by highly conductive surface layers. The central part of the section (sites 23-25), corresponding to an outcropping highly faulted horst of Tawallah Group rocks, is extremely disturbed, and interpretation remains contentious. However, blocks of high resistivity appear at depths near 4 km, consistent with the anticipated depth of basement of crystalline or low-grade metamorphic rocks beneath the Tawallah Group horst, deepen-

ing to 10 km near Daly Waters. The essential features of the 2D inversion are, therefore, that, within the limitations of the computer capacity and program, the inversion has produced a model (Fig. 13b) in reasonable agreement with that predicted from geology (Fig. 3). Although the structure is highly complex, MT can be used to identify any significant body of McArthur Group carbonates at depth. This result supports the selection of the Model 1 alternative across the critical Emu Fault section.

Conclusions

A lack of precision in estimates of resistivity for each unit in the McArthur Basin remains the principal complication in the interpretation of MT data. The alternative geological models can be distinguished in terms of gross electrical response, but detailed transitions in resistivity between the McArthur and Tawallah Groups are obscured by noise. In the McArthur Basin there are three sources of noise to be considered in estimates of resistivity. Random noise results from the nature of the MT signal and the techniques used in the recording; resulting errors can be reduced by routine statistical methods. However, there are two sources of systematic error in resistivity, relating to abrupt changes in (1) geological and (2) physical conditions in the McArthur Basin.

Electrical resistivities measured in the McArthur Basin are not uniquely associated with the major geological units. Perturbations in MT response are introduced by the physical environment both on a microscopic and macroscopic scale. In particular, there are many types of rock contained in each geological unit, and a single representative value of resistivity may not be always appropriate. The Roper Group is most readily identified; it is characterised by low resistivities (<20 ohm m) associated with high porosities. But, resistivities for the Tawallah and McArthur Groups are more difficult to resolve. Typical values are near 300 and 1000 ohm m, respectively, but for most sites the MT response of each is obscured by the Roper Group at the surface.

Perturbations in apparent resistivity are most pronounced where lateral boundaries are detected in surface outcrop. Such contacts are common in the Batten Fault Zone. Apparent resistivities cannot be readily correlated along the major traverse, and 1D inversions are not always appropriate. However, several trends can be identified, and major geological structures can be readily resolved on the Wearyan Shelf.

Data at the eastern end of the traverse are consistent with a single layer representing the Tawallah Group over an infinite half space of granitic/metamorphic basement. The calculated thickness of the Tawallah Group can be preserved, in agreement with surface geology, only if a significant thickness of McArthur Group does not extend east of the Emu Fault.

Vertical movements at the Emu Fault are also suggested by 2D analysis of associated discontinuities in apparent resistivity. Short-period values can be correlated with Roper Group outcrop, but basement structure can be assessed using data at periods greater than 2 s. It is concluded that models based on a graben structure at the Emu Fault accommodate the magnetotelluric data better than any alternative.

Acknowledgements

The data presented in this paper were obtained over two field reasons by the efforts of several people. In particular, the initial system was installed by D.W. Kerr, J.A. Major, R.F. Moore, and A.G. Spence. Routine operations in both seasons were the responsibility of A.G. Spence. Much of the rationale and survey objectives were provided by K.A. Plumb who also assisted greatly in previewing the final manuscript.

References

Anfiloff, W., 1981 — *In* Plumb, K.A. (Co-ordinator), McArthur Basin research, July-December, 1980. *Bureau of Mineral Resources, Australia, Record* 1981/20 (unpublished).

Collins, C.D.N., in press — Crustal structure in the southern McArthur Basin from deep seismic sounding. *BMR Journal of Australian Geology & Geophysics*, 8(1).

Cull, J.P., Spence, A.G., Major, J.A., Kerr, D.W., & Plumb, K.A., 1981a — The 1978 McArthur Basin magnetotelluric survey. *Bureau of Mineral Resources, Australia, Record* 1981/1 (unpublished).

Cull, J.P., Spence, A.G., & Plumb, K.A., 1981b — The 1979 McArthur Basin magnetotelluric survey. *Bureau of Mineral Resources, Australia, Record* 1981/64 (unpublished).

D'erceville, I., & Kunetz, G., 1962 — The effect of a fault on the Earth's natural electromagnetic field. *Geophysics*, 27, 651–65.

Dunn, P.R., Plumb, K.A., & Roberts, H.G., 1966 — A proposal for time stratigraphic subdivision of the Australian Precambrian. *Journal of the Geological Society of Australia*, 13, 593–608.

Jupp, D.L.B., & Vozoff, K., 1975 — Stable iterative methods for the inversion of geophysical data. *Geophysical Journal of the Royal Astronomical Society*, 42, 957–76.

Jupp, D.L.B., & Vozoff, K., 1977 — Two dimensional magnetotelluric inversion. *Geophysical Journal of the Royal Astronomical Society*, 50, 333–52.

Keller, G.V., 1971 — Electrical characteristics of the Earth's crust. *In* Wait, J.R. (editor), Electromagnetic probing in geophysics. *Golem Press, Boulder*, 13–76.

Moore, R.F., 1977 — Screening and averaging magnetotelluric data prior to one-dimensional inversion. *Bureau of Mineral Resources, Australia, Record* 1977/78 (unpublished).

Neumann, F.J.G., 1964 — Normanton to Daly Waters reconnaissance gravity survey, QLD and NT 1954–60. *Bureau of Mineral Resources, Australia, Record* 1964/131. (unpublished).

Oldenburg, D.Q., 1979 — One dimensional inversion of natural source agnetotelluric observations. *Geophysics*, 44, 1218–44.

Plumb, K.A., & Derrick, G.M., 1975 — Geology of the Proterozoic rocks of northern Australia. *In* Knight, C.L. (editor), Economic geology of Australia and Papua New Guinea. Volume 1 — Metals. *Australasian Institute of Mining and Metallurgy, Monograph* 5, 217–52.

Plumb, K.A., 1977 — McArthur Basin Project. *Bureau of Mineral Resources, Australia, Record* 1977/33. (unpublished).

Plumb, K.A., Derrick, G.M., & Wilson, I.H., 1980 — Precambrian geology of the McArthur River — Mount Isa region, northern Australia. *In* Henderson, R.A., & Stephenson, P.J. (editors), The geology and geophysics of northeastern Australia. *Geological Society of Australia, Queensland Division*, 71–88.

Swift, C.M., 1971 — Theoretical magnetotelluric and TURAM response from two dimensional inhomogeneities. *Geophysics*, 36, 38–52.

Vozoff, K., 1972 — The magnetotelluric method in the exploration of sedimentary basins. *Geophysics*, 37, 98–141.

Vozoff, K., & Jupp, D.L.B., 1975 — Joint inversion of geophysical data. *Geophysical Journal of the Royal Astronomical Society*, 42, 977–91.

Walker, R.N., Logan, R.G., & Binnekamp, J.G., 1978 — Recent geological advances concerning the H.Y.C. and associated deposits, McArthur River, N.T. *Journal of the Geological Society of Australia*, 24, 365–80.

Weaver, J.T., 1963 — The electromagnetic field within a discontinuous conductor with reference to geomagnetic micropulsations near a coastline. *Canadian Journal of Physics*, 41, 484–95.

Young, G.A., 1965 — McArthur River area, aeromagnetic survey-1963–64. *Bureau of Mineral Resources, Australia, Record* 1965/173 (unpublished).

BMR Journal of Australian Geology & Geophysics, 7, 287-302

MIDDLE MIOCENE KANGAROOS (MACROPODOIDEA: MARSUPIALIA) FROM THREE LOCALITIES IN NORTHERN AUSTRALIA, WITH A DESCRIPTION OF TWO NEW SUBFAMILIES

T.F. Flannery[1], M. Archer[1] & M. Plane[2].

The middle Miocene macropodoids of the Riversleigh, Bullock Creek, and Kangaroo Well local faunas are the oldest recorded assemblages of kangaroos. Five new species are described here. One, *Bulungamaya delicata* n. gen. and sp., is placed with *Wabularoo naughtoni* Archer, 1979 in the new potoroid subfamily Bulungamayinae. *Gumardee pascuali* n. gen. and sp. is placed within the Potoroinae. *Balbaroo camfieldensis* n. gen. and sp. and *Balbaroo gregoriensis* n. sp. are placed in a new macropodid subfamily, the Balbarinae. *Galanarla tessellata* n. gen. and sp. is placed in the Macropodidae, but cannot as yet be assigned to a particular subfamily. All the new species are from the Riversleigh local fauna, except *B. camfieldensis* from the Bullock Creek local fauna. The previously known Kangaroo Well macropodid appears to be referable to the genus *Balbaroo*. The Bulungamayinae is represented by forms which, although related to potoroines, have bulbous premolars and lophodont molars. The Balbarinae includes generally plesiomorphic forms that may have been ancestral to other macropodids. None of the macropodoid genera described here are known from more recent deposits. This suggests that a radical transition in the dominant kinds of macropodoids took place between middle and late Miocene times.

Introduction

Stirton & others (1968) noted the occurrence of Miocene macropodoids in the Ngapakaldi, Kangaroo Well, Riversleigh, Kutjumarpu, and Alcoota local faunas. Archer (1979) also noted macropodoids recovered from the middle Miocene Namba Formation. To date, only macropodoids from the Riversleigh and Alcoota local faunas have been named and described. Woodburne (1967), in his study of the late Miocene Alcoota local fauna, named two species of macropodoids, *Hadronomas puckridgi* and *Dorcopsoides fossilis*, and noted some 'protemnodont' upper first incisors. Archer (1979) described *Wabularoo naughtoni* from the middle Miocene Riversleigh local fauna of the Carl Creek Limestone, northwestern Queensland. A dentary noted by Tedford (1967) as belonging to a macropodid from this same fauna may be referable to some other marsupial family. The specimen cannot be conclusively shown to have possessed a masseteric canal (this area being broken away), and the M_5, although apparently lophodont in form, has such a low crown as to be dissimilar to any known macropodoid. This paper deals with new and previously described macropodoids from the Riversleigh local fauna, northwestern Queensland (Fig. 1), newly discovered macropodoids from the Bullock Creek local fauna of the Camfield beds, Northern Territory, and the macropodid from the Kangaroo Well local fauna, Northern Territory.

The fossils of the Riversleigh and Bullock Creek local faunas are preserved in freshwater limestone. Deposition of the Tertiary limestone probably resulted from remobilisation and redeposition of underlying Cambrian limestones present at both localities. Fossils of the Kangaroo Well local fauna are also preserved in a limestone. From comparisons with the species of other Miocene fossil localities, Archer & Bartholomai (1978) and Archer (1981) estimated the Riversleigh and Kangaroo Well local faunas to be about 14 million years old and the Bullock Creek local fauna to be about 10 million years old.

In addition to macropodoids described here, the Riversleigh local fauna contains a dromornithid (Aves), *Barawertornis tedfordi* Rich, 1979, a palorchestine, a zygomaturine and a nototherine, *Bematherium angulum* Tedford 1967. Archer (1982b) has noted a thylacinid from the Riversleigh local fauna. Hand (1982) noted the presence of fish, crocodiles,

[1] School of Zoology, University of New South Wales, PO Box 1, Kensington, NSW 2033.
[2] Bureau of Mineral Resources, PO Box 378, Canberra, ACT 2601.

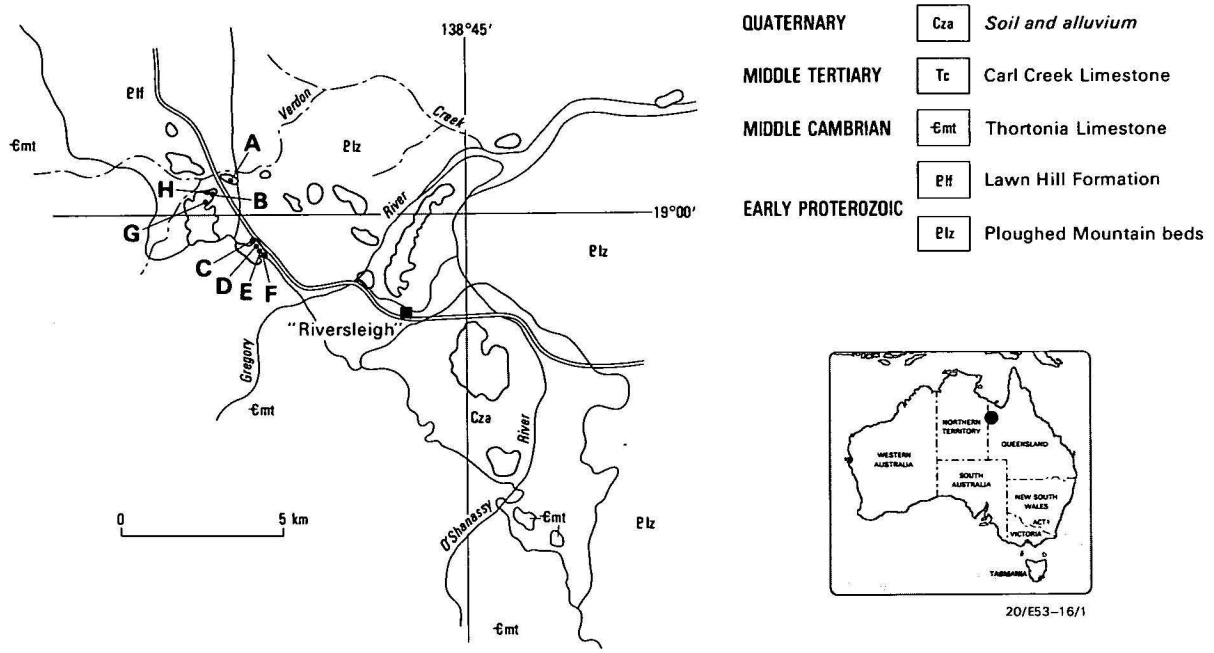

Figure 1. Locality map for Riversleigh sites.

birds, a bandicoot, dasyurids, potoroids, possums, a megadermatid bat and a bat referable to the subgenus *Hipposideros (Brachipposideros)* from the Miocene Nooraleeba local fauna at Riversleigh. Archer (1982a) has described a dasyurid from the Nooraleeba local fauna.

The geology and fauna of the Bullock Creek locality are discussed in Plane & Gatehouse (1968). They noted the presence of a species of *Neohelos* and a thylacoleonid. The thylacoleonid is named *Wakaleo vanderleuri* in Clemens & Plane (1974). Lungfish, turtles, crocodiles, and the dromornithids *Bullockornis planei* and *?Bullockornis* (Rich 1979) are also present at Bullock Creek.

Stirton & others (1968) noted the presence of crocodiles, turtles, and birds at the Kangaroo Well locality, but the single macropodid specimen and a very small and greatly worn tooth of an indeterminate therian are the only mammal specimens recovered from the site thus far.

Because a cladistic approach to the interpretation of phylogenetic relationships has been taken here, the basis for the choice of outgroup needs to be explained. Phalangerids (the species of *Phalanger, Wyulda,* and *Trichosurus*) appear to be the most immediate sister group of the macropodoids on the basis of 1 — the immunological study of Kirsch (1977), which strongly suggests such a molecular relationship, and 2 — a study of macropodoid fossils from the Namba Formation at present being undertaken by T. Flannery and T.H. Rich. Although phalangerids are clearly derived in some character states (e.g. P^2 reduction and some aspects of basicranial morphology), they are accepted here as representing the primitive condition for macropodoids.

Preparation of the material was carried out mechanically and with acetic acid, by R.W. Brown of the Bureau of Mineral Resources, on some specimens, and with acetic acid, by G. Clayton of the University of New South Wales, on others. Figure 2 summarises the taxonomy of new macropodid names proposed here. Dental terminology and homology follows Archer (1976, 1978). QM is a prefix for Queensland Museum fossil specimens, e.g. QM F10646, CPC is a prefix for Commonwealth Palaeontological Collection fossil specimens, e.g. CPC22187, and NMV is a prefix for National Museum of Victoria fossil specimens, e.g. NMVP165000.

Acknowledgements

The cost of preparation of some of this material has been supported by an A.R.G.C. grant to one of us (M.A.). Support for previous field work at Riversleigh, besides that coming from the Bureau of Mineral Resources and the Queensland Museum, has come from Dr. Ray E. Lemley. We would like to thank Dr A. Ritchie, Curator of Fossils at the Australian Museum, and Dr T. Rich, Curator of Vertebrate Fossils at the National Museum of Victoria, for their loans of specimens, and Mr R.W. Brown and Ms G. Clayton for their care in the preparation of this material. Considerable assistance with field work has come from Prof. R. Pascual, Ms G. Clayton, Ms S. Hand, Ms C. Hann, Mr. R.W. Brown, Ms B. Thompson, and Mr H. Van Vlodrop. R.W. Brown photographed the specimens and prepared the plates. We would like to thank Mr and Mrs J. Nelson and Mr and Mrs. F. Naughton of Riversleigh station for their help and for allowing us access to the Riversleigh localities.

Systematics

Superfamily Macropodoidea

Family Potoroidae

Subfamily Bulungamayinae n. subfam.

Subfamilial diagnosis. Bulungamayines differ from macropodids by having a buccally expanded masseteric canal, a sharply ventrally convex dentary margin below M_{2-4}, an I_1 that has greatly thickened dentine and lacks a dorsal enamel flange, and an elongate P_3 that has many fine distinct ridgelets. They differ from hypsiprymnodontines by lacking an I_2, and having lophodont molars and a P_3 with a less convex occlusal margin. Bulungamayines differ from potoroines by having lophodont molars and much more bulbous premolars.

Wabularoo naughtoni Archer, 1979.

Additional material of *Wabularoo naughtoni* is recognised here. A complete left P_3 (CPC22185) from the upper unit at locality G of the Carl Creek Limestone (Fig. 3) is of almost identical morphology with that of the holotype of *W. naughtoni* (Table 1, Figs. 3–4). It has the same number of ridgelets (seven) as does the P_3 of the holotype.

Bulungamaya n. gen.

Type species. *Bulungamaya delicata* n. gen. and sp.

Generic diagnosis. Species of *Bulungamaya* differ from those of *Wabularoo* by being smaller, having less strongly developed molar lophids, and by having a posthypocristid, at least on M_4. They differ from species of *Potorous* and *Caloprymnus* by having a P_3 with six distinct ridgelets. They differ from the species of *Bettongia* by having narrower lower molars and in having M_3 not so greatly reduced in size relative to other molars. They differ from species of *Aepyprymnus* in having much weaker pre-and postprotocristae and pre-and posthypocristae, and in being smaller (Table 1).

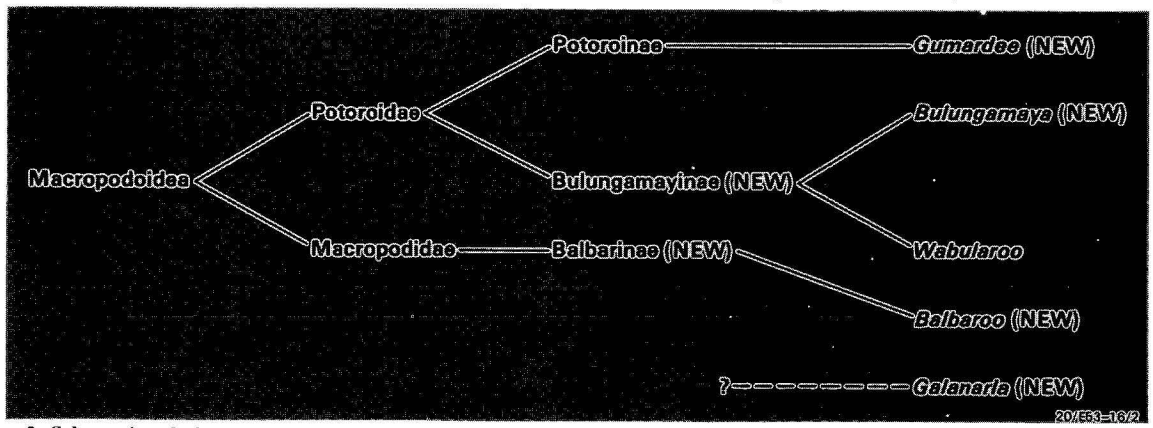

Figure 2. Schematic relations of new taxa.

Table 1. Dental measurements (in mm) for macropodoids of the Riversleigh, Bullock Creek and Kangaroo Well local faunas.
L = length, AW = anterior width, PW = posterior width, MW = maximum width, JD = jaw diastema

Wabularoo naughtoni	CPC22185	P_3	L = 11.2	MW = 5.3	PW = 4.4
Bulungamaya delicata	CPC22187	P_3	6.8	AW 3.3	3.2
		M_2	4.1	2.5	2.8
		M_3	4.1	3.1	2.8
		M_4	4.0	3.1	2.8
		M_5	4.0	2.9	2.3
Gumardee pascuali	QM F10646	P^3	10.6	4.2	4.6
		M^2	5.6	5.7	5.5
		M^3	6.1	6.1	5.4
		M^4	6.1	5.8	4.6
		M^5	4.9	4.7	3.4
Balbaroo camfieldensis	CPC22179	M_2	7.1	3.6	5.0
		M_3	7.7	4.9	5.4
		M_4	8.9	5.4	5.4
		M_5	8.4	5.5	
	NMV P165000	M_3	8.2		
		M_4	8.6	5.6	
		M_5		5.8	.5.5
Balbaroo gregoriensis	CPC22186	M_2	7.3	4.2	4.3
Balbaroo sp.	CPC7349	M_3	7.9	6.9	4.7
Galanarla tessellata	QM F10644	JD	18.7	4.2	4.3
		M_4	6.0	4.9	4.2
		M_5	6.9		4.3
	QM F10645	M^5	6.1	4.7	4.1
Macropodidae Indet.	QM F10649	I^1	3.4		
		I^2	3.9		
		I^3	3.6		
	QM F10648	I^2	3.8		
Macropodoidea Indet.	CPC22182	M^1	5.7	4.5	4.6
	CPC22181	M^2	6.5	6.0	6.2
		M^3	6.9	6.2	6.1
		M^4	6.1	6.3	5.4

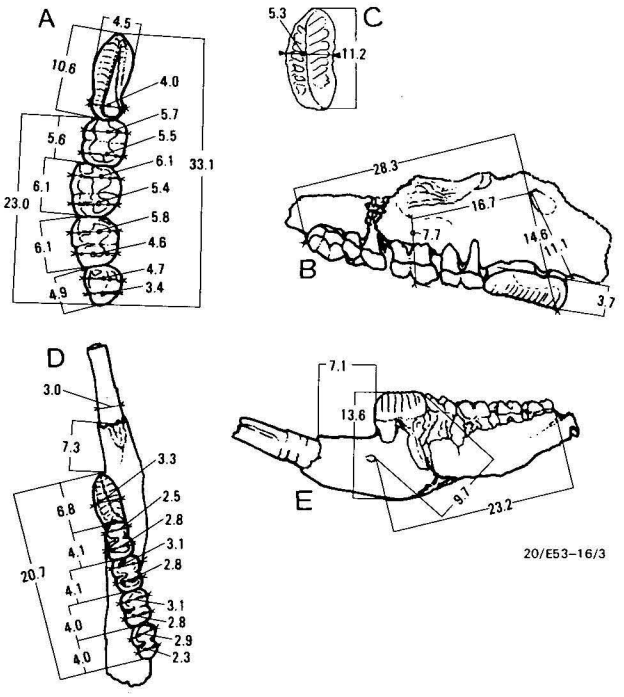

Figure 3. Drawings showing measurements (in mm) of A, occlusal view of teeth, and B, buccal view of holotype of *Gumardee pascuali* (QM F10646). C, occlusal view of P_3 of *Wabularoo naughtoni* (CPC22185). D, occlusal view, and E, buccal view of holotype of *Bulungamaya delicata*, × 2.

Etymology. *Bulungulla* means moon and *mayee* means tooth in the Waanyi language as spoken by Mrs Ivy Stinken of Riversleigh station, a reference to the crescent-moon-shaped P_3 of this species.

***Bulungamaya delicata* n. sp.** (Figs 3–4, Table 1).

Holotype. Fragmentary left dentary (CPC22187) containing I_1, P_3, M_{2-5}. The I_1 lacks the anterior part of the crown. The ventral margin and ascending ramus of the dentary are missing.

Referred specimen. A fragmentary right dentary (QM F10650) containing the root of an I_1.

Type locality and age. The holotype is from the upper unit, at site G, and the referred specimen is from the same unit at site D (Fig. 1) in the Carl Creek Limestone, northwestern Queensland (grid reference, TD557979, Lawn Hill 1:100 000 map). The age of the Carl Creek Limestone is generally interpreted as middle Miocene (e.g. Archer & Bartholomai, 1978).

Diagnosis. The generic diagnosis will serve as that of the species until further species are described.

Etymology. The species name *delicata* refers to the delicate form and small size of this kangaroo.

Description. The dentary. The masseteric canal can be seen to run to below M_3, but a smooth bone surface suggests that it may have extended further anteriorly. The mandibular

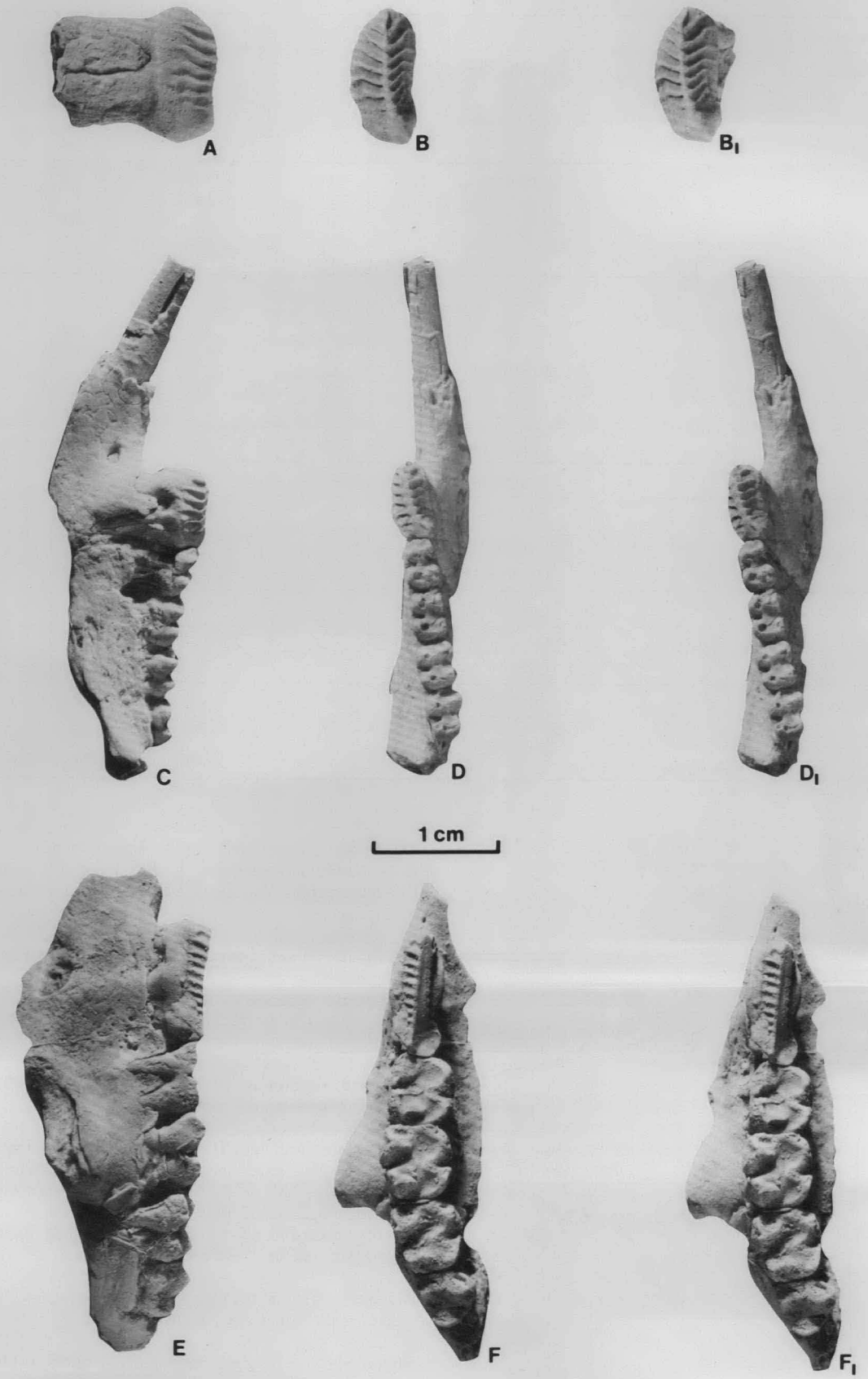

Figure 4. A, buccal view, and B, stereopair of occlusal view of CPC22185, P_3, referred specimen of *Wabularoo naughtoni*. C, buccal view, and D, stereopair of occlusal view of CPC22187, left dentary fragment containing P_3, M_{2-5}, holotype of *Bulungamaya delicata*. E, buccal view, and F, stereopair of occlusal view of QM F10646, right maxilla fragment containing P^3, M^{2-5}, holotype of *Gumardee pascuali*.

symphysis extends anteriorly from below the posterior of P_3. Little else of phylogenetic value can be distinguished on the dentary. The ventral edge and ascending ramus are broken away.

I_1. The distal tip of I_1 is missing, no wear facet being visible on the remaining portion. The enamelled section of the crown extends to within 2 mm of the alveolus of I_1. The I_1 is slightly oval in cross section, with the long axis oriented dorsoventrally. Enamel is restricted to the ventrolingual portion of the tooth, from roughly 30 to 200 degrees of arc. This type of I_1 morphology is seen only in species of *Propleopus*, *Aepyprymnus*, *Caloprymnus*, and *Bettongia* among the macropodoids. However, in these forms the I_1 is usually more laterally compressed.

P_3. P_3 is more bulbous than in potoroines, and consists of an elongate blade ornamented by six distinct ridgelets. The ridgelets curve slightly posteriorly as they ascend the crown. A distinct sharp ridgelet defines the anterior portion of the tooth. Posteriorly, the tooth develops a prominent posterolingual inflection, which is slightly bulbous and without ridgelets. A series of four very slight annular-like rings or ridgelets extends around the base of the crown on the buccal side. The P_3 is broadest about 2mm from its posterior edge.

M_2. M_2 is approximately the same size as M_3, but the protolophid is narrower than the hypolophid. The enamel of both lophids is breached by wear. The enamel is broken away from the posterior face of the metaconid. The paracristid runs at an oblique angle from the region of the protoconid to slightly buccal of the centre of the anterior cingulum. The anterior cingulum is extremely low, broad, and short anteroposteriorly. A premetacristid runs around the margin of the tooth to join the metaconid to the lingual end of the anterior cingulum. The anterior cingulum runs towards the base of the crown buccally until it weakens and becomes indistinguishable near the crown base. A weak cristid obliqua appears to run from a region near the hypoconid to a position just lingual of the protoconid. However, this structure is too abraded to determine much detail or to be sure of its origin. The interlophid valley is broad both lingually and bucally. No ornamentation can be seen on the posterior face of the hypolophid.

M_3. The enamel of virtually all the anterior and lingual surface of M_3 is broken away. The lophids are subequal in width. An enamel fragment indicates that the anterior cingulum was broad, short anteroposteriorly, and low. Both the protolophid and hypolophid are breached by wear. However, the protolophid retains a portion of its crest, indicating that a well-developed loph was present. What appears to have been the beginning of the paracristid can be seen arising from near the protoconid, and it continues in an anterolingual direction to where it is broken off. A very weak cristid obliqua appears to have run longitudinally from a point one-third of the way lingual from the buccal end of the anterior surface of the hypolophid to the same position on the anterior face of the protolophid. The interlophid valley is broad. No ornamentation is visible on the rear face of the hypolophid.

M_4. M_4 is slightly broader than M_3, and the lophids are subequal in width. Enamel is broken away from the buccal portion of the anterior cingulum and the median portion of the rear face of the protolophid. The enamel of both lophids is breached by wear. A premetacristid runs along the tooth margin to join the low, broad, and anteroposteriorly short anterior cingulum. The protolophid shows strong loph development. A very weak cristid obliqua crosses the broad interlophid valley as in M_3. The paracristid is missing. A very slight depression near the apex, on the rear face of the hypolophid may represent a small basin that would have been enclosed by a posthypocristid.

M_5. M_5 is the best-preserved of the molars, having a virtually intact enamel crown. Both lophids are breached by wear. M_5 is approximately the same length as M_4, with the hypolophid being noticeably narrower than the protolophid. The anterior cingulum is broad, anteroposteriorly short, and low. A slight premetacristid runs along the tooth margin to join the anterior cingulum. The paracristid runs from the protoconid to the anterior cingulum closer to the buccal edge of the tooth than in M_2. Only a very small portion of the anterior cingulum is present buccal to the paracristid. A complete loph extends the width of the protolophid. The cristid obliqua and interlophid valley are as in M_4. The posterior surface of the hypolophid is devoid of any ornamentation, lacking the depression indicating the presence of a posthypocristid on M_4.

A fragment of a right dentary (QM F10650) from the upper unit at site D in the Carl Creek Limestone appears to be conspecific with *Bulungamaya delicata*. It contains the cylindrical root of an I_1. The lingual wall of a crypt of a large P_3 is present. A small portion of the symphysis indicates that it was very weakly ankylosed. The root of the I_1 is somewhat thicker than that of the I_1 of the holotype of *B. delicata*.

Discussion. The two species of bulungamayines, *Bulungamaya delicata* and *Wabularoo naughtoni*, are restricted to the middle Miocene Riversleigh local fauna. They are contemporaneous with potoroines, to which they are most closely related, and which are represented at Riversleigh by *Gumardee pascuali* n. sp and an unnamed form.

Bulungamayines share at least four synapomorphic features with potoroines or other potoroids, which are not seen in phalangerids or macropodids, and which indicate the monophyly of bulungamayines and other potoroids. These states are as follows. 1 — the presence of a great thickening of the dentine of I_1, which obscures the dorsal enamel crest of the crown and gives the tooth an oval cross section. This state is only seen in bulungamayines, the species of *Bettongia*, *Aepyprymnus*, *Caloprymnus* and *Propleopus* amongst phalangerids and macropodoids, although some thickening of the dentine is evident in *Hypsiprymnodon moschatus* and the species of *Potorous*. 2 — the possession of an elongate P_3 that possesses many fine ridgelets and a straight occlusal edge. The P_3 of phalangerids and hypsiprymnodontines is finely grooved, but is not elongate and has a convex occlusal edge. In macropodids the P_3 may be elongate with a straight occlusal edge, but it is never as finely ridged as in bulungamayines. The elongate P_3 of macropodids appears to have been derived independently in macropodids. 3 — the possession of a buccally expanded opening of the masseteric canal. Phalangerids lack a masseteric canal, and in macropodids the masseteric canal is not as large as in potoroids; thus, extreme development of the masseteric canal is taken as the derived state. 4 — the dentary is strongly convex below the cheek-tooth row. This condition is not seen in phalangerids or macropodids, but is characteristic of all potoroids, including bulungamayines, with the exception of the species of *Potorous* and the occasional weak development on *H. moschatus*.

A single possible synapomorphic state exists that may indicate a relationship between bulungamayines and macropodids: the presence of lophodont molars. However, in the light of the four synapomorphic states linking other potoroids and bulungamayines, it is most parsimonious to regard the development of lophodonty as being due to convergence between the bulungamayine and macropodid lineages.

The possibility that macropodids have been derived from bulungamayines or any other potoroids seems to be precluded by the four derived states shared by bulungamayines and other potoroids and absent in all macropodids. Also the new subfamily of kangaroos, the balbarines, indicates that the macropodids have had a long history separate from the potoroids.

The molars of *Bulungamaya delicata*, compared to those of *Wabularoo naughtoni*, are lower crowned, have less well-developed lophs, have the paracristid and cristid obliqua placed more buccally and, at least on M_4, appear to have a posthypocristid, not seen in *W. naughtoni*. These characteristics are all reminiscent of the bunodont molar condition, and in these respects *B. delicata* must be considered more primitive than *W. naughtoni*. The P_3s of both these forms, however, are remarkably similar. Apart from size, they differ principally in that that of *W. naughtoni* has one more ridgelet than that of *B. delicata*.

The brachydont molars with well-developed lophs and the elongate, finely ridged premolars of bulungamayines find their closest parallel amongst living kangaroos in the species of *Dorcopsulus* and *Dorcopsis*. It is clear that these forms are not closely related, however, as bulungamayines share synapomorphic states with potoroids (I_1 and dentary morphology) and the species of *Dorcopsis* and *Dorcopsulus* share such states with macropodines (work in preparation). The closest convergence with bulungamayines is seen in the rare *Dorcopsulus macleayi*, which is intermediate in size between *Wabularoo naughtoni* and *Bulungamaya delicata*. The premolars of *D. macleayi* are bulbous, as in bulungamayines, and the premolar ridgelets are finer and more well-developed than in the species of *Dorcopsis*.

The diet and habits of this animal are, however, almost wholly unknown. It inhabits mountain rainforest, probably between 1500 and 1800 metres. Whilst by analogy with other species of forest wallaby it can be inferred to be primarily a browser, its bulbous premolars may be used to pierce hard nuts, fruits, or even insect integument, in much the same way that the bulbous premolars of *Hypsiprymnodon moschatus* are used. On the basis of similar morphology, it seems reasonable to postulate a similar habit for bulungamayines.

The only macropodids known thus far from mid-Miocene sediments are the primitive balbarines. Macropodines (*Dorcopsoides fossilis*) are known from the late Miocene, and bulungamayines had by then presumably become extinct. It thus seems possible that these specialised potoroids, which may have been relatively poorly adapted to the 'lophodont kangaroo niche' became extinct when more advanced macropodids evolved. Early macropodines would have resembled the species of *Dorcopsis* and *Dorcopsulus*, the very species which today seem to be exploiting the same niche occupied by bulungamayines in the mid-Miocene.

Subfamily Potoroinae

Gumardee n. gen.

Type species. *Gumardee pascuali* n. gen. and sp.

Generic diagnosis. *Gumardee pascuali* differs from all known macropodids by having a greatly reduced M^5 and bunodont molars. It differs from hypsiprymnodontines by having a less occlusally convex P^3 with a buccal and a lingual cingulum on its medial portion, and from all known potoroids by having the aforementioned cingulae, and 11 sharp distinct ridgelets on P^3. It differs from the bulungamayines, *Wabularoo naughtoni*, *Bulungamaya delicata*, and from the macropodids *Galanarla enigmatica*, *Balbaroo gregoriensis*, and *Balbaroo camfieldensis* by having bunodont molars and a reduced M^5.

Etymology. *Gumardee* means rat-kangaroo in the Waanyi language as spoken by Mrs Ivy Stinken of Riversleigh station.

Gumardee pascuali n. sp. (Figs 3–4, Table 1)

Holotype. QM F10646. Fragmentary maxilla containing P^3, M^{2-5}.

Type locality and age. The holotype was recovered from the upper unit of the Carl Creek Limestone at site D (Fig. 1), on Riversleigh station, northwestern Queensland. The Carl Creek Limestone is interpreted as being middle Miocene (e.g. Archer & Bartholomai, 1978).

Diagnosis. The generic diagnosis will serve as that for the species until further species are discovered.

Etymology. The species name is in honour of Professor Rossendo Pascual, the noted Argentinian palaeontologist, who accompanied us on our 1981 expedition to Riversleigh and Bullock Creek and left us with the immortal conclusion about the phylogenetic hypotheses presented here — 'for sure maybe'.

Description. The maxilla. The masseteric process is short and rounded, not reaching to the roots of the molars. This condition is seen in all potoroids except *Caloprymnus campestris*, and is also seen in species of *Dorcopsis* and *Dorcopsulus*. The dental foramen is situated above the centre of the P^3.

P^3. P^3 of *Gumardee pascuali* is nearly as long as M^{2-3}. It is heavily worn, but 11 sharp ridgelets are still distinguishable on its buccal side. Only the anterior-most eight ridgelets are visible on the lingual side, owing to the removal of the others by wear. Broad low buccal and lingual cingulae run from near the anterior edge of the tooth to within 3–4 mm of the posterior edge. The tooth is constricted one-third of the way from its posterior end. A slight bulge at the posterolingual corner of the tooth may represent the base of a posterolingual cusp. However, if such a cusp was present, it has since been obliterated by wear.

M^2. M^2 is heavily worn, the anterior cingulum, protoloph, midlink and hypoloph being almost obliterated by wear. There appears to have been a stronger preparacrista than on the more posterior molars. The interloph valley is very narrow both lingually and buccally. Buccally, a small enamel ridge partially closes the interloph valley. The remains of a strong postmetacrista can be seen, but most of it (especially the lingual end) has been obliterated by wear.

M^3. M^3 is larger than M^2. The buccal portion of the anterior cingulum is preserved, showing that a preparacrista connected the protoloph to the anterior cingulum. Low lophs run from the paracone and metacone towards the protocone and hypocone, respectively. The interloph valley is very narrow and not partially closed buccally as in the M^2. The postmetacrista is much weaker than that crest in M^2.

M^4. M^4 is slightly smaller than the M^3, with the hypoloph being narrower than the protoloph. The tooth is heavily worn in much the same fashion as M^3. The anterior cingulum, however, can be seen to extend across the whole width of the tooth. Otherwise, M^4 is similar in morphology to M^3.

M^5. The almost unworn M^5 is much smaller than M^4. The hypoloph is reduced to a small tubercle, which is much lower than the protoloph. The protocone is bulbous and gives rise to a bulbous, ill-defined pre-and postprotocrista. The preprotocrista

joins the centre of the broad anterior cingulid, while the postprotocrista approaches, but does not contact, the hypoloph. The paracone forms the end of a narrow loph that connects to the protocone.

Discussion. Because the type specimen of *Gumardee pascuali* is a maxilla and of approximately the right size to occlude with the type of *Wabularoo naughtoni*, it is necessary to consider why these specimens have been placed in separate taxa. Firstly, it appears that the molars of *G. pascuali* are bunodont in form, as indicated primarily by the morphology of M^5. This conclusion is also supported by the extremely narrow interloph valleys of the other molars, features more characteristic of bunodont potoroids rather than lophodont forms. The molars of *W. naughtoni* are clearly lophodont and have broad interlophid valleys. Secondly, the P^3 of *G. pascuali* has 11 ridgelets on the main crest. Both known examples of the P^3 of *W. naughtoni* have seven. Archer & others (1979) examined ridgelet number in the P3 of *Hypsiprymnodon moschatus* (10 individuals) and *Aepyprymnus rufescens* (23 individuals). They found that the extreme variation in ridgelet number in *H. moschatus* was 2 (i.e. all premolars had either 6 or 7 ridgelets) and 3 in *A. rufescens* (all premolars had 7, 8, or 9 ridgelets). This limited variation in potoroid species with large numbers of ridgelets on P3 seems to indicate that a variation in ridgelet number of 5 would be unlikely within one species. Thirdly, the P_3s of both specimens of *W. naughtoni* are slightly longer than the P^3 of *G. pascuali*, but are considerably broader. In all known macropodoids, P^3 is as long as, or longer, and broader than P_3.

Gumardee pascuali represents the oldest named potoroine. It displays a synapomorphic characteristic for bulungamayines and potoroines, the elongate premolar with many fine ridgelets. It appears to be too specialised in P^3 morphology (possessing buccal and lingual cingulae) to have given rise to any of the living potoroines.

Genus indeterminate

An anterior P_3 fragment (QM F10647) from the upper unit at site D in the Carl Creek Limestone (Fig. 1), probably represents a further species of potoroine in the Riversleigh local fauna. It consists of the anterior one-third to one-half of a tooth, which has a distinct sharp ridge in its anterior edge, and four ridgelets and associated cuspules on the straight main blade. Although the fragment comes from a P_3 of approximately the size of that of *Bulungamaya delicata*, it is far less bulbous and the ridgelets are much coarser.

Family Macropodidae

Subfamily Balbarinae n. subfam.

Subfamilial diagnosis. Balbarines differ from all potoroids except bulungamayines by having lophodont molars. They differ from bulungamayines by lacking a strongly convex ventral margin of the dentary, and by having a smaller opening to the masseteric canal, the M_2 trigonid markedly lower than the talonid, and the M_2 protolophid markedly compressed. They can be distinguished from all known macropodids by the M_2 characteristics mentioned above, and by a small cuspid, possibly a rudimentary paraconid, on the lingual side of the anterior cingulum of the lower molars.

***Balbaroo* n. gen.**

Type species. *Balbaroo camfieldensis* n. gen. and sp.

Generic diagnosis. The subfamilial diagnosis will serve for the genus until further genera of balbarines are recognised.

Etymology. *Balba* means strange in the language of the aborigines of the MacDonnell Ranges, South Australia (Kempe, 1890). Roo is a non-specific term for a macropodid.

***Balbaroo camfieldensis* n. sp.** (Figs 5–6, Table 1)

Holotype. The posterior portion of a left dentary, CPC22179, containing M_{2-5}, but lacking most of the dentary anterior to M_2, and a portion of the coronoid process.

Referred specimen. Left dentary fragment, NMV P165000, containing the posterior root of M_2 and M_{3-5}. The M_5 has been removed from its crypt.

Type locality and age. The holotype was recovered from the 'small hills locality' of the Camfield beds, the site initially discovered at Bullock Creek. The referred specimen comes from the 'Horseshoe West locality' of the Camfield beds at Bullock Creek. The Camfield beds are interpreted as middle to late Miocene in age (e.g. Archer & Bartholomai, 1978).

Diagnosis. *Balbaroo camfieldensis* differs from *B. gregoriensis* n. sp. (see below) in the following features of the M_2. The paracristid is relatively much weaker in *B. camfieldensis*. The small cuspule that may represent the paraconid is much closer to the paracristid in *B. gregoriensis*. The protolophid of *B. camfieldensis* is relatively narrower and less concave anteriorly. The protoconid is higher than the metaconid in *B. gregoriensis*, but the protoconid and metaconid of *B. camfieldensis* are subequal in height. The hypolophid of *B. camfieldensis* is broader than that of *B. gregoriensis*, and the pre-entocristid, which is a poorly defined, rounded structure, appears to be slightly better developed in *B. gregoriensis*.

Etymology. The species name reflects the type locality, the Camfield beds on Camfield station, Northern Territory.

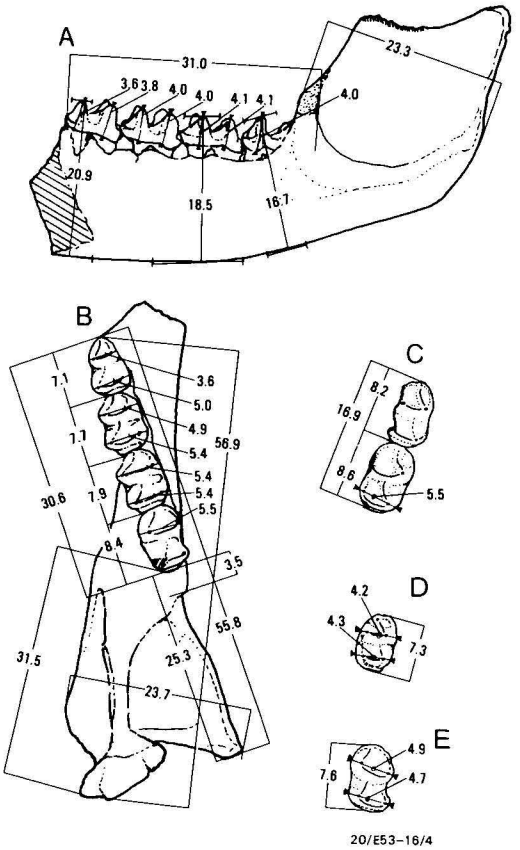

Figure 5. Drawings showing measurements (in mm) of A, buccal view, and B, occlusal view of *Balbaroo camfieldensis* (CPC22179). C, occlusal view of teeth of *B. camfieldensis* (NMV P165000). D, occlusal view of holotype of *Balbaroo gregoriensis* (CPC22186). E, occlusal view of *Balbaroo* sp. (CPC7934) × 2.


A
B
C
D
D1
B1
1cm
E
F
G
G1
H
F1
I
J
J1

Description. The dentary. Because the dentary of the holotype is better preserved than that of the referred specimen, this description is based largely on the holotype. The ventral margin of the dentary forms an almost straight edge until it ascends at the rear of the jaw. The dentary is deepest below the anterior end of M_2, and shallowest below the posterior end of M_5. The horizontal ramus is twisted in an unusual fashion such that, below M_5, the long axis of a cross section of the jaw points ventrobuccally, while below M_2 the long axis of a cross section points ventrolingually. This aspect of dentary morphology is seen to some extent in *Hypsiprymnodon moschatus*, ektopodontids and diprotodontoids. The angle of the dentary is broad and strongly developed. Its lingual margin extends posteriorly in line with the molar row. The buccal face of the horizontal ramus has a very slight groove, starting below the anterior end of M_3, and extending anteriorly to the broken edge of the dentary. Although most of the coronoid process is missing on the holotype, enough is preserved on the referred fragment to demonstrate that it rose at a steep angle (about 90°) to the molar row. The condyle is transversely elongate. In macropodines, this condyle is much narrower, but in some potoroids and all sthenurines, it resembles that seen in *B. camfieldensis*. The opening of the masseteric foramen is relatively small, as it is in macropodines. The tooth row is straight. The posterior-most portion of the mandibular symphysis is preserved, showing that it extended to below the anterior end of M_2.

The M_2. The protolophid of M_2 is markedly narrower than the hypolophid. The paracristid and cristid obliqua are poorly developed. Compression of the trigonid is achieved by moving the protoconid lingually. The anterior cingulum is very low and weakly developed. The paracristid joins the anterior cingulum approximately one-third of the way from its lingual margin. A very small cuspid, hereafter called the paraconid, probably represents the paraconid, but may represent a portion of the premetacristid. It is present on the lingual margin of the anterior cingulum. The interlophid valley is broad and shallow. The weak cristid obliqua originates from near the apex of the hypoconid and ends on the posterior wall of the protolophid below the protoconid. A slight, rounded pre-entocristid runs from the apex of the entoconid, ending in the interlophid valley. A very prominent and broad posterior cingulum is present at the base of the rear face of the hypolophid. It extends across the whole width of the tooth.

M_3. M_3 differs from M_2 in the following ways. It is larger. The protolophid is only very slightly narrower than the hypolophid. The paracristid is buccally more concave. The paraconid is reduced in size, but is present as a small enamel bump at the lingual end of the anterior cingulum. The cristid obliqua is shifted further lingually. The entoconid and hypoconid do not form such prominent apices on the hypolophid. The hypolophid and protolophid are of equal height. The posterior cingulum does not extend as far lingually.

M_4. M_4 differs from M_3 in the following ways. The protolophid and hypolophid are of equal width. The paraconid is more prominent. The cristid obliqua is shifted further lingually. On the referred specimen, it can be seen that the cristid obliqua does not originate at the hypoconid, but rather slightly ventrobuccal to it. The slight wear on the holotype obscures this feature. The posterior cingulum does not extend as far lingually, and a slight vertical depression ascends the rear face of the hypolophid above the lingual- most extension of the posterior cingulum. This area is obscured on the holotype by the anterior cingulum of M_5.

M_5. M_5 differs from M_4 in the following ways. On M_5 of the holotype, the metaconid and the hypoconid are broken away. These cuspids are preserved, however, on the referred specimen. The paraconid is very tiny on the holotype and absent on the referred specimen. The cristid obliqua is more lingually positioned, and originates just ventrobuccal of the hypoconid. The depression on the rear face of the hypolophid is smaller than that on M_4 in the holotype, and is not present on M_5 of the referred specimen.

Discussion. The balbarines are probably the most fascinating and phylogenetically significant kangaroos of the Bullock Creek and Riversleigh local faunas. They appear to represent the most primitive macropodids known, and retain primitive characteristics seen amongst macropodoids only in *Hypsiprymnodon moschatus*. States that appear to be primitive within the Macropodoidea include an M_2 with a greatly compressed trigonid, straight molar rows, and a strongly twisted dentary. These characteristics are seen in some phalangeroids, *Hypsiprymnodon moschatus*, and (straight molar rows) primitive macropodines. The retention of these primitive states in balbarines precludes all potoroids, except possibly *H. moschatus*, from representing structural ancestors for the macropodids. The trigonid of M_2 differs from that seen in *Hypsiprymnodon moschatus* and phalangeroids in that it is lower than the talonid. In the latter forms, the trigonid of M_2 is high and abuts the P_3 to form an extension of its shearing edge. This difference suggests that the anterior tooth row of balbarines was functioning in quite a different manner from that of *H. moschatus* or possums. Features of *B. camfieldensis* that appear to be synapomorphic for macropodids include lophodont molars and a coronoid process that ascends at a steep angle from the plane of the molar row. The transversely elongate condyle of the dentary may represent a primitive condition within the macropodids, because it is also seen in sthenurines, a group of kangaroos that retain many other primitive features, and it is not seen in macropodines. Alternatively, it may represent a primitive macropodoid condition. The relative great depth of the dentary below M_2 is probably an autapomorphic condition. It is otherwise seen only in advanced macropodines, such as the species of *Osphranter*. If the small cuspid on the lingual side of the anterior cingulum is in fact the paraconid, its retention would be an extremely primitive characteristic in balbarines, the species of *Balbaroo* being the only macropodoids to retain such a structure. However, the alternative possibility, that this cuspid represents a remnant of the premetacristid, cannot be dismissed.

***Balbaroo gregoriensis* n. sp.** (Figs 5–6, Table 1)

Holotype. An unworn right M_2, CPC22186. The enamel crown only lacks a portion of the base of the protoconid and hypoconid.

Type locality and age. This specimen was recovered from the upper unit of the Carl Creek Limestone at site G Fig. 1) on Riversleigh station, northwestern Queensland. The Carl Creek Limestone is believed to be middle Miocene in age (e.g. Archer & Bartholomai, 1978).

Figure 6. A, buccal view, and B, stereopair of occlusal view of CPC22179, left dentary fragment containing M_{2-5}, holotype of *Balbaroo camfieldensis*. C, buccal view, and D, stereopair of CPC22186, right M_2, holotype of *Balbaroo gregoriensis*. E, buccal view, and F, stereopair of occlusal view of NMV P165000, right dentary fragment containing M_{3-4}, referred specimen of *Balbaroo camfieldensis*, and G, stereopair of occlusal view, and H, lingual view of M_5 of same specimen (removed from crypt). I, buccal view, and J, stereopair of occlusal view of CPC7349, left dentary fragment containing M_5 of *Balbaroo* sp. from Kangaroo Well.

Diagnosis. *Balbaroo gregoriensis* can be distinguished from *B. camfieldensis* in the following ways. The paracristid of the M_2 of *B. gregoriensis* is better developed than that of *B. camfieldensis*. The paraconid is placed nearer the paracristid, and the protolophid is relatively broader in the former than in the latter. The protoconid is higher than the metaconid in *B. gregoriensis*, these cuspids being of equal height in *B. camfieldensis*. The hypolophid is narrower and the pre-entocristid slightly better developed in *B. gregoriensis* than in *B. camfieldensis*.

Etymology. The specific name is in reference to the Gregory River, northwestern Queensland, which flows past the fossil localities of the Carl Creek Limestone.

Description. The hypolophid of M_2 is markedly wider than the protolophid. The anterior cingulum is low and blunt. A very strong paracristid runs directly from the protoconid to a position just lingual of the centre of the anterior cingulum. The paraconid is situated just lingual to the anterior end of the paracristid. The occlusal edge of the protolophid is concave, the protoconid and, to a lesser extent, the metaconid forming distinct apices on the crest. The broad interlophid valley is only interrupted by a weak cristid obliqua, which runs from the anterior face of the hypoconid to the posterior face of the protoconid. The occlusal edge of the hypolophid is also concave, with the entoconid and, to a lesser extent, the hypoconid forming prominent apices. The height of the hypoconid may have been slightly reduced by wear. The posterior surface of the hypolophid is ornamented by a distinct posterior cingulum. Its buccal extremity is missing, but lingually it ascends to the apex of the entoconid.

Discussion. *Balbaroo gregoriensis* most closely resembles *B. camfieldensis*. The two species are close in size and differ only in morphological details. The genus is too poorly understood at present to allow hypothesising about ancestor–descendant relationships between these forms. However, in having a more prominent paraconid, *B. gregoriensis* may be more primitive than *B. camfieldensis*. It is equally likely, however, that the greater disparity between the width of the protolophid and hypolophid in *B. camfieldensis* is a more primitive characteristic. The two species of *Balbaroo* are clearly congeneric, and to this extent show an affinity between the Riversleigh and Bullock Creek local faunas. They are equally clearly allospecific, which may indicate that the faunas are not of the same precise age. Unfortunately, they offer no clue as to the relative ages of the faunas.

***Balbaroo* sp.**

The single macropodid specimen from the Kangaroo Well local fauna (CPC7349), which has been discussed previously (Stirton & others, 1968) appears to be referable to the genus *Balbaroo*.

Description. The specimen consists of a left dentary fragment containing an unworn M_5 (Figs. 5–6). It differs from *B. camfieldensis*, the only species of *Balbaroo* with which it can be compared, in that the enamel of the M_5 is finely crenulate and the paraconid is more prominent, compared with that on M_5 of *B. camfieldensis*. The angle of the dentary is not as large as in *B. camfieldensis*. The M_5 is smaller than that of *B. camfieldensis*, and probably, on the basis of the size of M_2, also smaller than that of *B. gregoriensis*. Apart from these differences, the Kangaroo Well specimen resembles *B. camfieldensis* more closely than any other kangaroo.

Discussion. Whilst this specimen probably represents a third, smaller species of *Balbaroo*, it will not be named here, as the material is fragmentary and the specimen cannot be compared with *B. gregoriensis*. Finely crenulate enamel on molars is seen in *Hypsiprymnodon moschatus* and some phalangeroids, and is thus probably a primitive retained condition in macropodids. This feature and the well-developed paraconid may indicate that this form is more primitive than either of the named species of *Balbaroo*. Although tentative evidence, this may be an indication that the Kangaroo Well local fauna is older than the Riversleigh or Bullock Creek local faunas.

Subfamily indeterminate

Galanarla n. gen.

Type species. *Galanarla tessellata* n. gen. and sp.

Generic diagnosis. *Galanarla tessellata* differs from potoroines and hypsiprymnodontines by having lophodont molars. It differs from bulungamayines by lacking a convex ventral margin of the dentary, an I_1 that is oval in cross section without a dorsal enamel flange, and by having a smaller opening for the masseteric canal. It differs from sthenurines and macropodines by having P_3 flexed buccally out of alignment with the molar row (the state of this character is not known for balbarines), and from balbarines by having a bowed molar row.

Etymology. The name refers to the presumed fluviatile nature of the deposit and to the fossils representing a wallaby now turned to rock, *Gala*, meaning river, and *Narlee*, meaning rock wallaby, in the Waanyi language, as spoken by MrsIvyStinken of Riversleigh station.

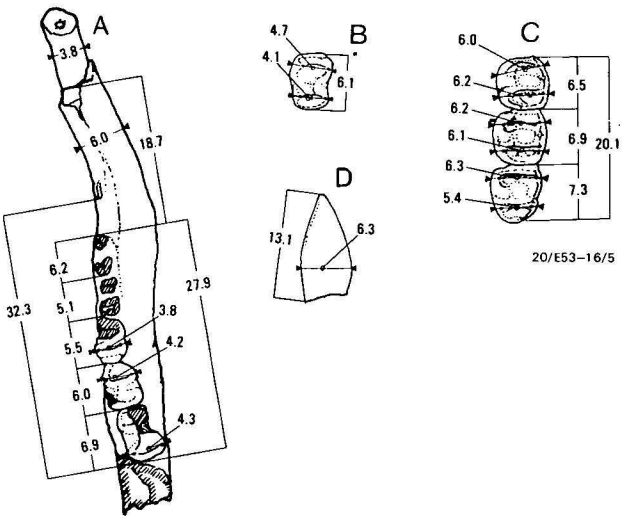

Figure 7. Drawings showing measurements (in mm) of A, occlusal view of holotype of *Galanarla tessellata* (QM F10644). B, occlusal view of M^5 (QM F10645) of *G. tessellata*. C, occlusal view of CPC22^{-4}(CPC22181) of a macropodid. D, buccal view of I_1 (CPC22184) of *G. tessellata* × 2.

Figure 8. A, buccal view, and B, stereopair of occlusal view of QM F10644, right dentary fragment containing I_1, fragmentary M_{2-5}, holotype of *Galanarla tessellata*. C, lingual view, and D, buccal view of CPC22184, crown of I_1. tentatively assigned to *Galanarla tessellata*. E, buccal view and F, stereopair of occlusal view of CPC22181, left maxilla fragment containing M^{2-4} of a macropodoid. G, buccal view, and H, stereopair of occlusal view of CPC22182, right M^1 of a macropodoid. I, buccal view, and J, stereopair of occlusal view of QM F10646, left premaxilla fragment containing I^{1-3} tentatively referred to *Galanarla tessellata*. K, stereopair of occlusal view and L, buccal view of QM F10645, M^5 referred to *Galanarla tessellata*.

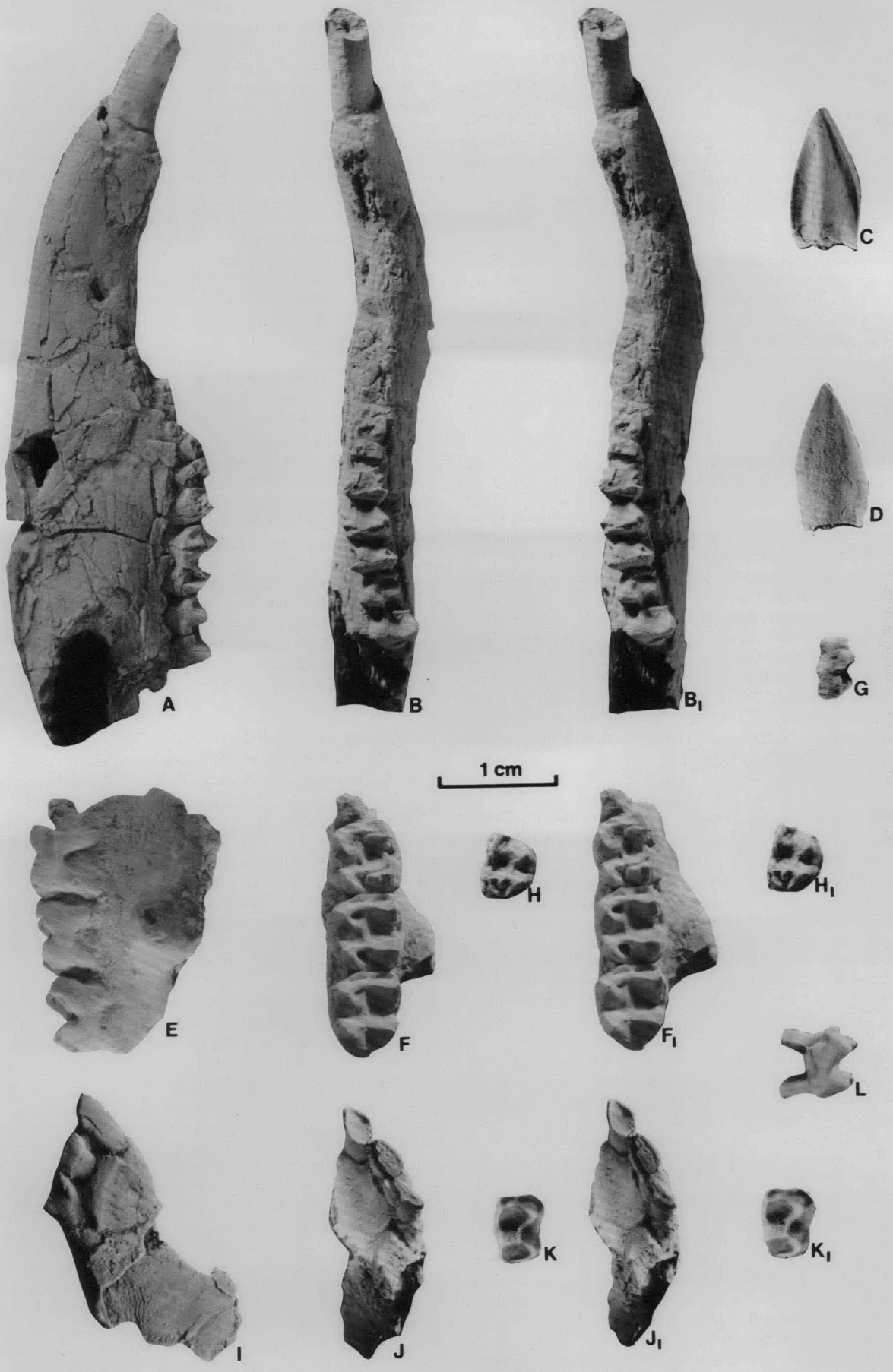
A
B
B1
C
D
G
1 cm
E
F
H
F1
H1
L
I
J
K
J1
K1

***Galanarla tessellata* n. sp.** (Figs 7–8, Table 1)

Holotype. QM F10644. A fragmentary left dentary containing the root and base of the crown of I_1, roots of P_3 and M_2 and the partial or complete crowns of M_{3-5}. A portion of the ascending ramus is preserved.

Referred specimens. QM F10645, an unworn right M^5. The following specimens are tentatively referred to *Galanarla tessellata:* CPC22184, the crown of a left I_1, a left premaxilla fragment, QM F10649 containing I^{1-3}, a further left premaxilla fragment, QM F10648 containing I^1 and an isolated I^1, CPC22180.

Type locality and age. All specimens of *Galanarla tessellata* were recovered from the upper unit of the Carl Creek Limestone at site D, except for CPC22180, which comes from the upper unit at site G (Fig. 1) on Riversleigh station, northwestern Queensland. The Carl Creek Limestone is believed to be middle Miocene in age (e.g. Archer & Bartholomai, 1978).

Diagnosis. The generic diagnosis will serve as that for the species until further species are discovered.

Etymology. *Tessellata* is Latin for 'mosaic', in reference to the mosaic nature of subfamilial traits exhibited by this enigmatic kangaroo.

Description. The partial left dentary (QM F10644) is in two fragments that cannot be fitted together, but were associated in situ. The anterior fragment contains the teeth, the posterior fragment part of the coronoid process and the angle of the dentary. The dentary lacks any flexion below the molar row. The diastema is approximately 12mm long. The mental foramen is situated ventral to a point approximately 4 mm anterior to the anterior root of P_3. The molar row is buccally convex, and the P_3 was flexed buccally out of alignment with the molar row. The symphysis is short dorsoventrally and elongate anteroposteriorly. It terminates posteriorly below the posterior root of P^3.

The I_1 is missing most of the crown. The root is robust and cylindrical in shape. The base of the crown preserves a portion of the dorsal enamel flange and part of the lingual enamel cap. Enamel appears to have been restricted to the lingual surface. The position of I_1 in the jaw appears to be slightly distorted, and it needs to be turned through approximately 20 degrees anticlockwise to resume its original position.

Only the roots of P_3 survive. They indicate that this tooth was at least 5 mm long, and obliquely oriented with respect to the long axis of the molar row, in much the same fashion as in *Bettongia penicillata* or *Hypsiprymnodon moschatus*.

The lower molar row forms a buccally convex arc. Only the roots and the base of the hypolophid remain of M_2. M_2 was smaller than M_3. Only the enamel of the hypoconid, a fragment of the anterior cingulum, and the posterior surface of the hypolophid survive on M_3. A posterior cingulum appears to have been present. The posterior portion of a very weak and low cristid obliqua, originating from near the hypoconid (the exact relationship being obscured by wear) is present. The M_4 is larger than M_3, and has most of the crown preserved, only missing the buccal portions of the protoconid and hypoconid. The tooth is moderately worn and low-crowned. The protolophid and hypolophid are subequal in width. The anterior cingulum is low. The paracristid is poorly developed. It originates from near the protoconid and joins the anterior cingulum at a point approximately one-third of the distance in from its buccal edge. A well-developed premetacristid defines the anterolingual margin of the tooth and fuses with the anterior cingulum. The interlophid valley is broad and crossed by a very weak cristid obliqua. The base of the rear face of the hypolophid is obscured by the anterior cingulum of M_5. The M_5 is larger than M_4. It is little worn and the hypolophid and protolophid are subequal in size. The metaconid is missing. M_5 is similar in morphology to M_4, except that a well-developed posterior cingulum can be seen at the base of the rear face of the hypolophid. A slight, rounded pre-entocristid is present.

A right M^5 (QM F10645) from the upper unit at site D in the Carl Creek Limestone is probably conspecific with this dentary. It is unworn and the crown undamaged. The hypoloph is slightly narrower than the protoloph. A preparacrista joins the anterior cingulum, which is narrow and low, and extends almost to the lingual margin of the tooth. A slight postprotocrista and postparacrista are present. The midlink is very weak and the interloph valley broad. The posthypocrista is prominent and the postmetacrista more weakly developed.

Two left premaxillae (QM F10649 & QM F10648) from the upper unit at site D of the Carl Creek Limestone are of the appropriate size to belong to *Galanarla tessellata*. The border of the premaxilla delineating the nasal opening ascends towards the nasals at a steep angle (about 80°) relative to the incisor row. The anterior part of the premaxillary palatal foramen appears to have been located laterally to the posterior part of the I^3. Much of the nasal–premaxillary suture and part of the maxillary–premaxillary suture are preserved in QMF10648. The premaxillary–maxillary suture appears to have been convex anteriorly, more resembling the condition seen in species of *Dorcopsis* than that seen in potoroids. In the latter, this suture tends to be straighter (an exception being *Hypsiprymnodon moschatus*, where the suture is convex anteriorly). These trends in suture shape, however, are difficult to quantify and may not be significant.

I^1 is represented in both specimens, but is heavily worn. The root of I^1 is not enamelled. Although worn, the occlusal edge appears to have been broad and blade-like, as in macropodines.

I^{2-3} are only represented in QM F10649, and are worn (Table 1). The crown of I^2 is oval-shaped in occlusal view, with the long axis oriented anteroposteriorly. It lacks a buccal groove. The crown of I^3 is longer than broad and has a deep buccal groove. The small portion of the tooth anterior to this groove is more prominent than the much larger narrow posterior section. An alveolus for a large canine is present immediately behind the alveolus for I^3 in QM F10648.

An isolated right I^1 (CPC22180), from the upper unit of the Carl Creek Limestone at site G, may represent an unworn I^1 of *Galanarla tessellata*. Both anterior and posterior margins are rounded, with the enamel more extensive buccally than lingually. It has a moderately long occlusal crest.

The crown of a left I_1 (QM F22184) from the upper unit at site G of the Carl Creek Limestone is of the appropriate size and morphology (judging from the morphology of the I_1 fragment remaining on the holotype) to represent *Galanarla tessellata*. The crown is laterally very compressed. It is enamelled buccally, with distinct ventral and dorsal enamel flanges. It is unenamelled lingually, and a bulge of dentine follows the long axis of the tooth on the lingual side. The crown is relatively short for its height. It differs from I_1 of hypsiprymnodontines in being less elongate, and from potoroines and bulungamayines by possessing a dorsal enamel flange and being less oval-shaped in cross section. It differs from I_1 of advanced sthenurines in lacking a lingual enamel covering (Flannery, in press).

Discussion. The degree of buccal flexion of P^3 seen in *Galanarla tessellata* occurs otherwise only in primitive potoroines (e.g. *Bettongia penicillata*) and hypsiprymnodontines. It is probably a retained plesiomorphic feature. The I_1 morphology, lack of a strongly convex ventral dentary margin, and the small opening of the masseteric canal, supports its classification as a macropodid rather than as a bulungamayine potoroid. The molar size gradient (increasing in size backwards) and lophodont molars are derived conditions seen in macropodids, but few potoroids.

The relation of *G.tessellata* to *Hadronomas puckridgi* is unclear. Both species have low-crowned simple molars with relatively large premolars. However, the buccal flexion of the P_3 and bowed molar row of *G. tessellata* are not seen in *H. puckridgi*, and the posterior cingulum of the lower molars is more weakly developed in *H. puckridgi* than in *G. tessellata*. The dentaries of these species also differ in details (e.g. the position of the mental foramen) and the species differ greatly in size.

The placement of *G. tessellata* in a particular macropodid subfamily is not yet possible. It has bowed molar rows, (a feature unknown in balbarines), yet P_3 is obliquely set with respect to the long axis of the molar row, (a condition not known in sthenurines or macropodines). It could represent a primitive macropodine, a balbarine or a new subfamily.

The premaxilla specimens here tentatively referred to *Galanarla tessellata* exhibit some synapomorphic states for macropodids. These include the presence of a strong buccal groove on I^3, and a broad cutting edge on I^1 (possibly even a macropodine synapomorphic state, as it is unknown in sthenurines and potoroids). Whilst these specimens support the placement of Galanarla tessellata within the macropodidae, the evidence is too weak to allow placement within the Macropodinae, particularly as the upper incisors of balbarines are not known.

Family indeterminate

Maxilla fragment containing M^{2-4}, and isolated M^1 and M^5.

A maxilla fragment (CPC22181) from the upper unit at site H in the Carl Creek Limestone (Fig. 1), and an M^5 (CPC22182) and M^1 (CPC22183) from the upper unit at site G, also in the Carl Creek Limestone, may be conspecific. They cannot at present be assigned to any named taxon.

Description. M^1 (CPC22183) is much smaller than M^2 (CPC22181). This, however, does not negate the possibility that they represent the same taxon. In most potoroids (i.e. *Hypsiprymnodon moschatus* and *Potorous platyops* and several macropodids M^1 is much smaller than M^2. A very prominent preparacrista, postparacrista and premetacrista and postmetacrista are present on M^1. The protoloph is weakly formed and no anterior cingulum is present. A very weak midlink runs directly back from a position one-third of the way from the buccal edge of the posterior face of the protoloph to a similar position on the anterior face of the hypoloph. The posthypocrista is well-developed. A very strong postlink, higher than the hypocone or metacone, is present on the posterior face of the hypoloph.

Maxilla fragment. The maxilla of CPC22181 is worn. The masseteric process forms a rounded hump, but it may have been reduced in size by erosion. P^3 is represented by a posterior root fragment. This fragment suggests that P^3 was a robust tooth.

M^2 exhibits considerable wear, the enamel of both the protoloph and hypoloph having being breached. A strong preparacrista joins the buccal end of the protoloph to the anterior cingulum. The heavily worn anterior cingulum extends from the buccal edge of the tooth to near its lingual margin. The midlink runs from a point just lingual to the centre of the anterior face of the hypoloph to a point near the protoloph (the exact position of its termination is obscured by wear). The interloph valley is broad and shallow. Buccally it is blocked by two longitudinal ridges with a deep pocket between them. There is a prominent posthypocrista and postmetacrista. A prominent postlink is situated on the rear face of the hypoloph, slightly nearer the postmetacrista than the posthypocrista.

The less extensively worn M^3 is slightly larger than M^2 and differs from it as follows. A forelink is present in the centre of the anterior cingulum (this area is obscured by wear on M^2). The buccal side of the interloph valley is blocked by a single crest, the serial homologue of the more lingually placed of the two crests that block the interloph valley on M_2. The more buccally positioned crest that also blocks the interloph valley on M^2 is reduced to form a slight crest on the buccal side of the paracone. The postlink is relatively reduced.

M^4 is approximately the same size as M^3, less worn, and differs from M^3 and M^2 as follows. The buccal crest that blocks the interloph valley in M^2, but not M^3, is reduced in strength. The midlink is less developed, and the postlink is absent. The hypoloph is narrower than the protoloph. There is a small interdental wear facet on the posterior edge of M^4, suggesting that M^5 had erupted.

An isolated unworn M^5 (QM F22183) is represented by a partial enamel cap that lacks the anterior cingulum and paracone. The midlink is very weak and the tooth low-crowned. On the buccal edge of the broad, interloph valley there is a well-developed crest that blocks the interloph valley. The posthypocrista and postmetacrista are well-developed. There is no postlink.

Discussion. These specimens are of the appropriate size and morphology to represent the upper dentition of *Wabularoo naughtoni* or *Balbaroo gregoriensis*, although they may also represent a macropodid as yet unknown from lower dentitions. The most striking structure on these teeth is the postlink. Only sthenurines and some species of *Protemnodon* amongst macropodids have strongly-developed postlinks on upper molars. Its presence in these Riversleigh fossils may indicate a relation between them and either of these groups. At present there is too little information available to refute any of these possibilities.

Postcranial elements

Several postcranial elements from the Riversleigh and Bullock Creek local faunas clearly belong to macropodoids, but because of lack of association cannot be confidently assigned to any particular species. These elements include a calcaneum, three unguals of the fourth toe and a metacarpal from the upper unit of the Carl Creek Limestone at site D (Fig. 1), and an astragalus and distal humerus fragment from the 'Horseshoe West' locality of the Camfield beds, Bullock Creek.

A macropodid left calcaneum (QM F10651) exhibits a very plesiomorphic morphology (Fig. 8). There is no distinct rugose area on the plantar surface. The tuber calcis is short and twisted medially. The astragalar articulation is broadly continuous, and is of a similar morphology to that of other primitive macropodoids (i.e. species of *Potorous*). The trochlear process is barely developed. The sustentaculum is thin dorsoventrally and extends considerably beyond the median portion of the astragalar articulation. The lateral (more distal) portion of the cuboid facet is much shorter than the medial (more proximal) one. A small rimmed depression is present on the dorsal side of the distolateral portion of the bone.

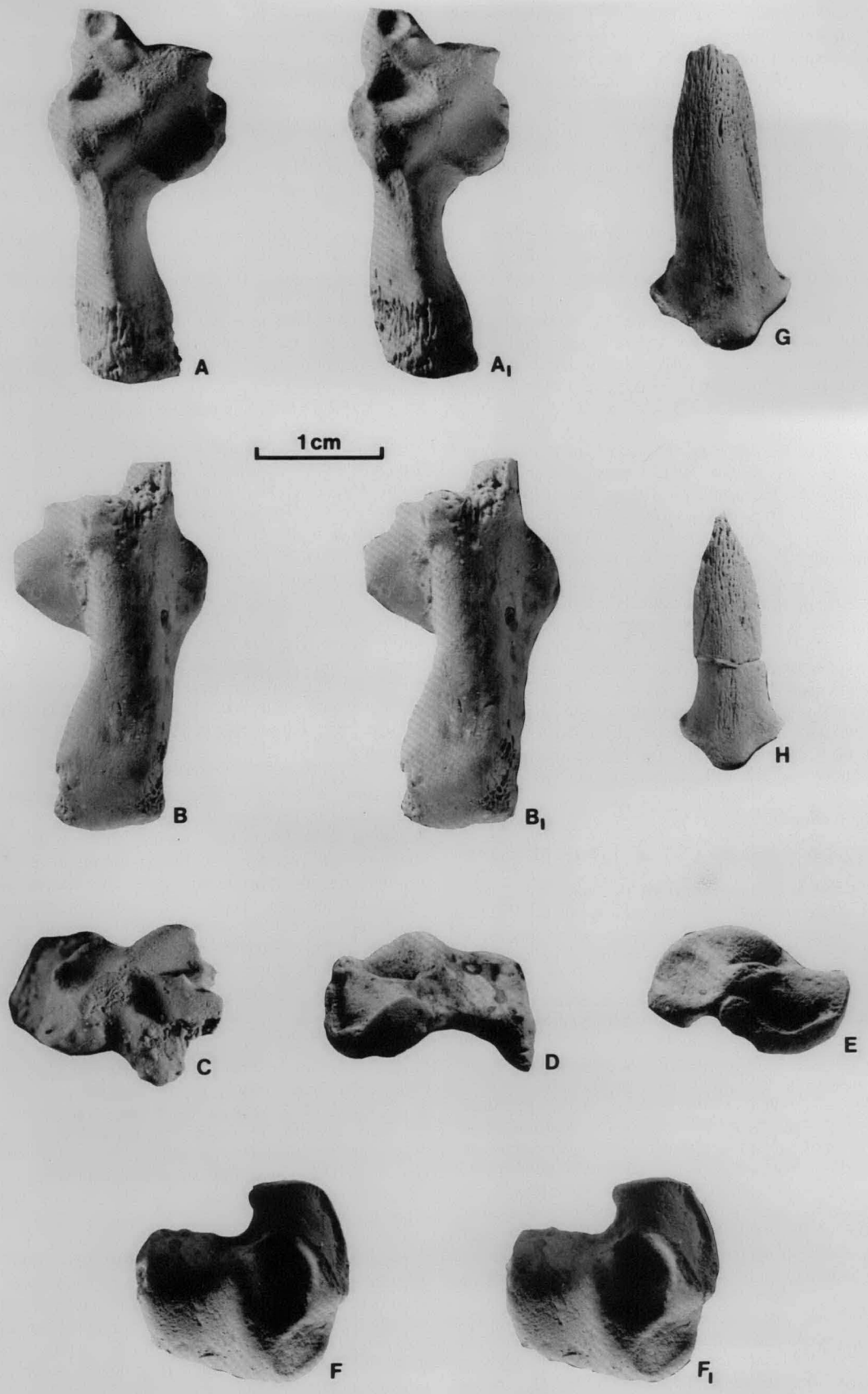

Figure 9. A, stereopair of dorsal view, B, stereopair of plantar view, and C, distal view of QM F10651, macropodoid left calcaneum. D, distal view, E, median view, and F, stereopair of dorsal view of MNV P165001, left astragalus of a macropodoid. G, dorsal view of QM F10653, ungual of the fourth toe of a macropodoid. H, dorsal view of QM F10654, ungual of the fourth toe of a macropodoid.

This specimen appears to represent a macropodoid, because it possesses the distinctly stepped calcaneal-cuboid articulation that is a synapomorphic feature in all macropodoids. However, it must represent an extremely plesiomorphic form, because the short, twisted tuber calcis, lack of a rugose area on the plantar surface, and minute trochlear process are reminiscent of the condition seen in phalangeroids (i.e. the species of *Trichosurus*) and *Hypsiprymnodon moschatus*. The very short lateral section of the calcaneal-cuboid articulation also probably represents an ancestral condition (although this appears to have been secondarily derived in monodactyl forms such as most sthenurines). The calcaneal-cuboid facet of phalangeroids is essentially 'L' shaped, and the stepped calcaneal-cuboid facet of macropodoids appears to have been derived from this morphology by a thickening of the anteroposteriorly oriented wall to form a rectangle of bone that forms the lateral (distal) section of the facet. Thus, in having the lateral section of the cuboid facet thinner than in other macropodoids, the Riversleigh calcaneum appears to be more primitive than that of other macropodoid calcanea.

A macropodoid third left metacarpal (QM F10652) from the upper unit at site D in the Carl Creek Limestone is present in the collection. It is gracile compared to that in species of *Dorcopsis*. Three unguals of the fourth toe from the upper unit at site D in the Carl Creek Limestone are probably also referable to macropodoids. The largest ungual (QM F10653) is curved and similar in morphology to that of *Macropus mundjabus* Flannery 1980. The Riversleigh ungual differs from it, however, in having a more distinct dorsal crest, thus being more triangular in cross-section. The distal tip is missing. The middle-sized claw (QM F10654) is similar in morphology to the large one, but is straight (Fig. 9, Table 1). The smallest claw (QM F10655) is markedly different from the others, being more oval in cross section, and probably represents a different species from the above unguals.

A left astragalus (NMV P165001) and distal humerus fragment (NMV P165002) were found close together at the Horseshoe West site of the Camfield beds, Bullock Creek. Some skeletons at this locality appear to be present as partially articulated or associated elements, and it is possible that these specimens belong to one individual. The astragalus is highly unusual in morphology. The crests of the tibial articulation are low. A large circular pit extends the tibial articulations onto the astragalar head. The astragalar head is large and the navicular articulation is semicircular, extending through nearly 180 degrees. This kind of navicular articulation is seen otherwise only in *Hypsiprymnodon moschatus*, and may indicate the presence of a fifth toe. The proximomedial process is broken off, but would have been of modest size. The calcaneal articulation is shallow and broadly continuous.

The humeral fragment does not preserve the distal articulation, but retains the entepicondylar foramen. It is broken off where the median blade-like process begins to diminish in strength.

Discussion

The macropodoid assemblages from the middle Miocene Riversleigh, Bullock Creek, and Kangaroo Well local faunas described here give us our first glimpse of the early phylogenetic history of the kangaroos. The relationships of these middle Miocene kangaroos to those of late Miocene and more recent deposits are suprisingly remote. Only a single subfamily, the Potoroinae (out of six subfamilies), and no genera are common to mid-Miocene and later kangaroo assemblages. Unfortunately, kangaroo remains from the later part of the Miocene are scarce, only one species being known from the Bullock Creek local fauna (thought to be about 10 million years old) and two species from the Alcoota local fauna (thought to be about 6–8 million years old). Whilst the remains are scarce, the kangaroo from Bullock Creek (*Balbaroo camfieldensis*) is clearly most closely related to other mid-Miocene forms, and the two species from Alcoota (*Hadronomas puckridgi* and *Dorcopsoides fossilis*) to early Pliocene and later kangaroos (Flannery, in prep.). The relatively short time span between these two faunas, then, would appear to be the crucial one in terms of macropodoid evolution. During this time, macropodines and sthenurines presumably made their first appearance, and balbarines and bulungamayines became extinct. This was clearly a time of rapid evolution for kangaroos.

The mid-Miocene faunal assemblages studied here are not dominated by macropodoids as are most Pliocene–Recent faunas. In addition, mid–Miocene macropodoids are all small compared even to late Miocene forms such as *Hadronomas puckridgi*. In Pliocene and more recent faunas, kangaroos dominate the 'small–medium sized terrestrial herbivore' niche. In the mid-Miocene they were only exploiting the 'small terrestrial herbivore' niche. The medium to large sized terrestrial herbivores at localities such as Riversleigh and Bullock Creek are mainly the large flightless birds, the dromornithids, and the marsupial diprotodontids.

Because of our limited understanding of the mid-Miocene kangaroos, they are not particularly useful at present in helping to provide relative dates for the Miocene Australian faunas. Species of only one genus, *Balbaroo*, are known from two or more deposits, and the stages of evolution of *B. camfieldensis* and *B. gregoriensis* are not sufficiently well understood to help provide a relative dating of the sites where they are found. However, the primitive morphology of *Balbaroo* sp. from the Kangaroo Well local fauna indicates that this fauna may possibly predate the Riversleigh and Bullock Creek local faunas.

Conclusions

1. Four new species of macropodoids, included in one new subfamily of potoroid (the Bulungamayinae), the Potoroinae, and a new macropodid subfamily (the Balbarinae) are found in the Riversleigh local fauna. One additional form remains unplaced in a subfamily, and at least one other (a potoroine) remains unnamed. One new species of balbarine, *Balbaroo camfieldensis*, is the only macropodoid thus far known in the Bullock Creek local fauna, and an unnamed species of *Balbaroo*, the only one thus far found at Kangaroo Well.

2. The mid-Miocene kangaroos are markedly dissimilar to later kangaroo assemblages, suggesting that macropodoids underwent rapid evolution in late Miocene times.

3. The species of *Balbaroo* from the Kangaroo Well locality is more primitive in morphology than the species of *Balbaroo* from Bullock Creek or Riversleigh, suggesting that the Kangaroo Well site may be older than the Riversleigh or Bullock Creek localities.

References

Archer, M., 1976 — Phascolarctid origins and the potential of the selenodont molar in the evolution of diprotodont marsupials. *Memoirs of the Queensland Museum*, 17, 367–71.

Archer, M., 1978 — The nature of the molar–premolar boundary in marsupials and a reinterpretation of the homology of marsupial cheekteeth. *Memoirs of the Queensland Museum*, 18, 157–64.

ARCHER, M. 1979 — *Wabularoo naughtoni* gen. et sp. nov., an enigmatic kangaroo (Marsupialia) from the middle Tertiary Carl Creek Limestone of northwestern Queensland. Results of the Ray E. Lemley Expeditions, part 4. *Memoirs of the Queensland Museum*, 19, 299–307.

ARCHER, M., 1981 — A review of the origins and radiations of Australian mammals. *In* KEAST, A. (editor), Ecological biogeography of Australia. *W. Junk, The Hague*, 1435–88.

ARCHER, M., 1982a — Review of the dasyurid (Marsupialia) fossil record, integration of data bearing on phylogenetic interpretation and suprageneric classification. *In* ARCHER, M. (editor), Carnivorous marsupials. *Royal Zoological Society of New South Wales, Sydney*, 397–443.

ARCHER, M., 1982b — A review of Miocene thylacinids (Thylacinidae, Marsupialia), the phylogenetic position of the Thylacinidae and the problem of apriorisms in character analysis. *In* ARCHER, M. (editor), Carnivorous marsupials. *Royal Zoological Society of New South Wales, Sydney*, 445–75.

ARCHER, M. & BARTHOLOMAI, A., 1978 — Tertiary mammals of Australia, a synoptic review. *Alcheringa*, 2, 1–19.

ARCHER, M., BARTHOLOMAI, A. & MARSHALL, L.G., 1978 — *Propleopus chillagoensis*, a new north Queensland species of extinct giant rat-kangaroo (Macropodidae: Potoroidae). *Memoirs of the National Museum of Victoria*, 39, 55–60.

CLEMENS, W.A. & PLANE, M., 1974 — Mid-Tertiary Thylacoleonidae (Marsupialia, Mammalia). *Journal of Paleontology*, 48, 652–60.

FLANNERY, T.F. 1980 — *Macropus mundjabus*, a new kangaroo (Marsupialia: Macropodidae) of uncertain age from Victoria, Australia. *Australian Mammalogy*, 3, 35–51.

FLANNERY, T.F. in press — A review of the macropodid subfamily Sthenurinae to include species of *Lagostrophus* and *Troposodon*. Submitted to *Australian Mammalogy*.

HAND, S., 1982 — A biogeographically unique Miocene mammal deposit from northern Australia. *Abstract from Australian Mammalogy Society general meeting for 1982*.

KEMPE, H., 1890 — A grammar and vocabulary of the language spoken by the aboriginies of the MacDonell Ranges, South Australia. *Transactions and Proceedings of the Royal Society of South Australia*, 14, 1–34.

KIRSCH, J.A.W., 1977 — The comparative serology of marsupials. *Australian Journal of Zoology, Supplementary Series*, 52, 1–152.

PLANE, M. & GATEHOUSE, C.G., 1968 — A new vertebrate fauna from the Tertiary of northern Australia. *Australian Journal of Science*, 30, 272–3.

RICH, P.V., 1979 — The Dromornithidae. *Bureau of Mineral Resources, Australia, Bulletin* 184.

STIRTON, R.A. TEDFORD, R.H., & WOODBURNE, M.O. 1968 — Australian Tertiary deposits containing terrestrial mammals. *University of California Publications in Geological Science*, 77, 1–30.

TEDFORD, R.H., 1967 — Fossil mammals from the Tertiary Carl Creek Limestone, northwestern Queensland. *Bureau of Mineral Resources, Australia, Bulletin* 92, 217–36.

WOODBURNE, M.O., 1967 — The Alcoota fauna, central Australia. An integrated palaeontological and geological study. *Bureau of Mineral Resources, Australia, Bulletin* 87, 1–187.

BMR Journal of Australian Geology & Geophysics, 7, 303-314

COMBINED SEISMIC–GRAVITY INTERPRETATION OVER THE DONNYBROOK ANTICLINE, CENTRAL QUEENSLAND

V. Anfiloff

Accurate modelling, using seismic and gravity data, has shown that the Donnybrook Gravity High, in central Queensland, is the result of a complex situation involving three discordant basins. The most significant is an old basin buried deep beneath the Drummond Basin, and apparently deposited in a valley carved out of a thick sequence of Silver Hills Volcanics and related acid volcanics. The Drummond Basin wedges out westwards under the Galilee Basin, and is bounded to the east by the same acid volcanics that subcrop near the Anakie Metamorphics. The illusion that the Donnybrook Gravity High is associated with the Donnybrook Anticline is the result of an intrabasement granite, which introduces a large negative component, cancelling the western flank of a much broader gravity high. After the cancellation, the granite is represented by a low of only 30 $\mu m.s^{-2}$. The already complex situation is further complicated by a topographic feature that introduces ambiguity in the most crucial area of the interpretation. This factor demonstrates the need to combine density profiling with forward modelling.

Introduction

The Donnybrook Anticline (Fig. 1.) is situated in a narrow zone of Permo-Carboniferous outcrops of the Drummond Basin in western Queensland (Olgers, 1972). This zone is bounded to the west by the Carboniferous to Triassic Galilee Basin, and to the east by Devonian to Carboniferous Silver Hills Volcanics and Lower Palaeozoic Anakie Metamorphics. The Bureau of Mineral Resources (BMR) carried out two combined seismic and gravity surveys in 1971 and 1976, over the 350 $\mu m.s^{-2}$ gravity high associated with the Donnybrook Anticline (Fig. 2). The gravity high is centred about the Donnybrook Anticline (Fig. 3), but the low to the east of it at H is offset from the Mistake Creek Syncline. Another gravity low at B is adjacent to a broad topographic feature, and the shape of the Bouguer profile there depends on the density chosen for the Bouguer correction.

The seismic survey carried out in 1971 crossed the western margin of the Galilee Basin and stopped just short of the Donnybrook Anticline. The reflection data revealed unconformities, wedges, and deep dipping events (Fig.4), but the deep events were not used in the interpretation and the gravity high was initially attributed to uplifted basement under the anticline (Harrison & others,1975). The model did not give a good fit for the gravity low at B, and a new model involving a reverse density contrast across a deep reflector was postulated (Flavelle & Anfiloff, 1976). In 1976, the seismic traverse was extended eastward as far as the Anakie Metamorphics, and revealed a discontinuous set of reflectors at various depths (Fig.4). The new reflection data were interpreted (Pinchin, 1978) in terms of a thrust bringing basement up slightly under the gravity high, but this structure does not account for the amplitude of the high, nor the shape of the low at B (Fig. 5). Pinchin & others (1979) presented alternative gravity models as part of an overall study of the Galilee Basin's eastern margin, but did not consider the Donnybrook High in detail.

Realisation of the importance of topography in the Donnybrook case was largely responsible for the coining of the term 'formal interpretation' (Anfiloff & Flavelle, 1979). A formal gravity interpretation accounts for the topographic effect by combining data reduction with modelling, and does not involve any steps unaccounted for in the final presentation. These rules are

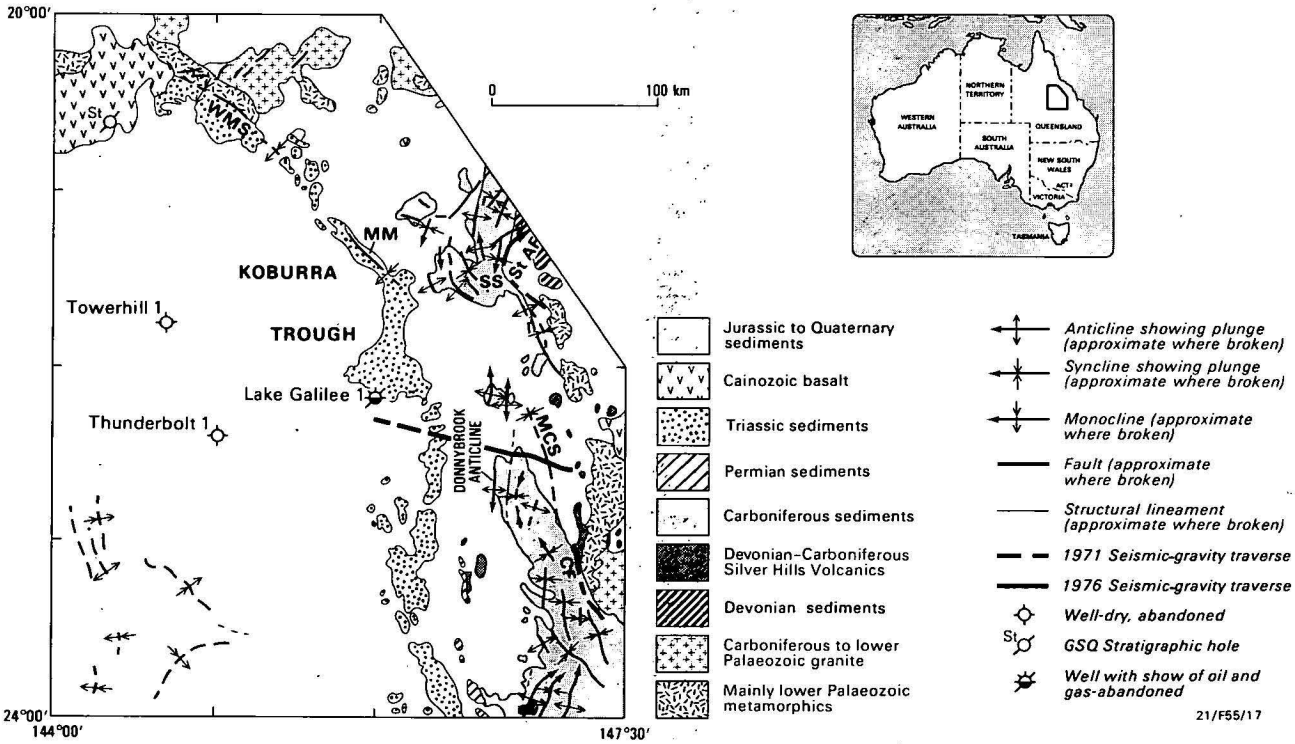

Figure 1. Geology, and location of the Donnybrook Anticline and seismic–gravity traverses.
From Pinchin (1978). MCS — Mistake Creek Syncline.

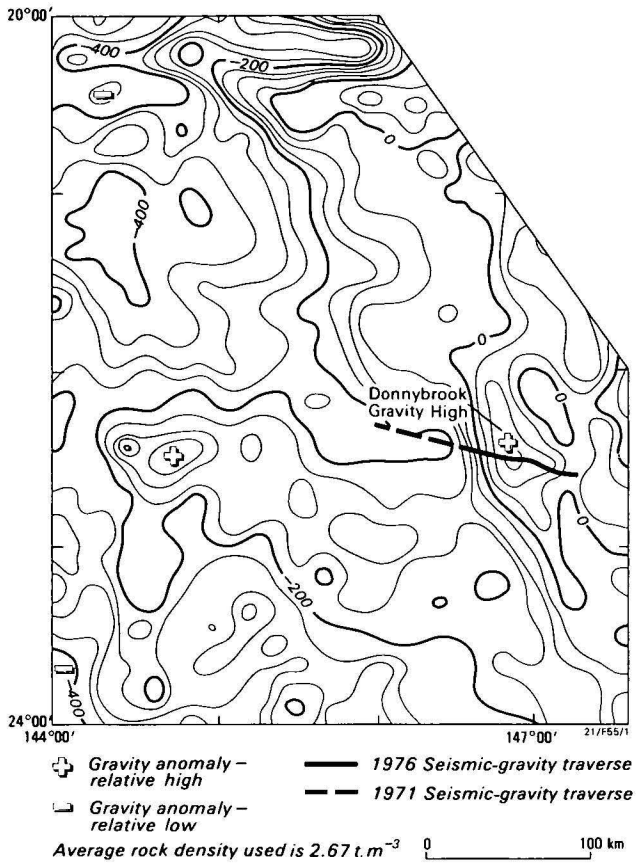

Figure 2. Reconnaissance gravity contours and location of seismic–gravity traverse.
Contour interval 50 μm.s^{-2}.

necessary to preserve integrity in gravity analysis, and in practice require that Nettleton's (1939) density profiling method be combined with forward modelling. The need for the formal interpretation concept is amply demonstrated by Fisher & Howard's (1980) attempt to interpret the Donnybrook gravity anomaly using an inversion method. As discussed by Anfiloff (1981), that attempt was unsuccessful because of a failure to use accurate data, to recognise the topographic problem, and because of the coarseness of the inversion method.

This paper extends the interpretation of Flavelle & Anfiloff (1976) eastwards, using the additional seismic and gravity data obtained in the 1976 survey. The extra data have a direct bearing on the Donnybrook anomaly, as they provide information on the Silver Hills Volcanics, which play a key role in the analysis. The analysis has been carried out by testing the following three possible explanations for the Donnybrook Gravity High: 1 — basement uplift; 2 — dense block in the basement; 3 — reverse density contrast between sediments and underlying Silver Hills Volcanics.

Seismic information

Seismic sections for the 1971 and 1976 surveys overlap, and SP1130 on the 1971 traverse coincides with SP2000 on the 1976 traverse (Fig. 4). The 1976 survey was designed to improve on the 1971 survey, and consolidate the exploration program, but instead revealed a complex picture involving numerous short segments of reflectors.

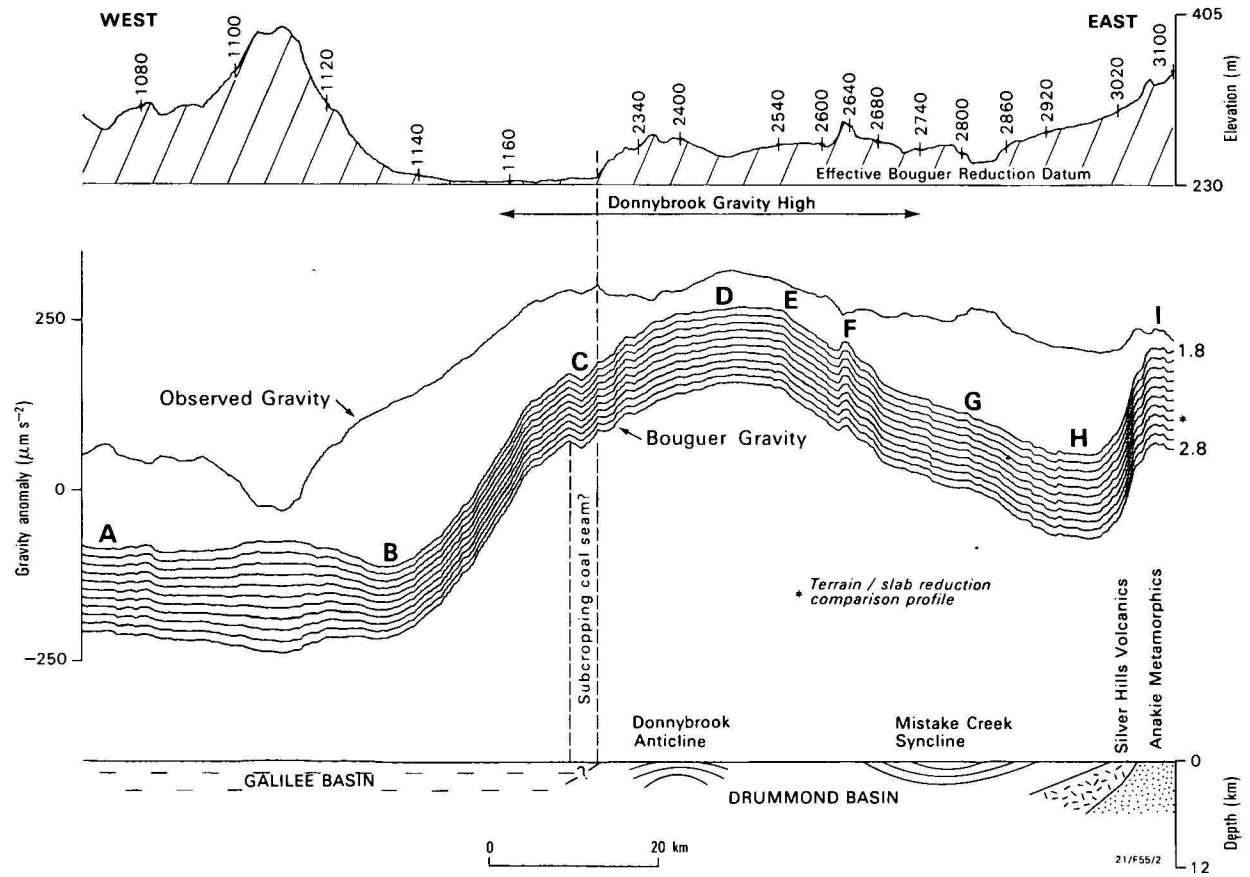

Figure 3. Gravity profiles and surface geology along the combined 1971–76 traverse.

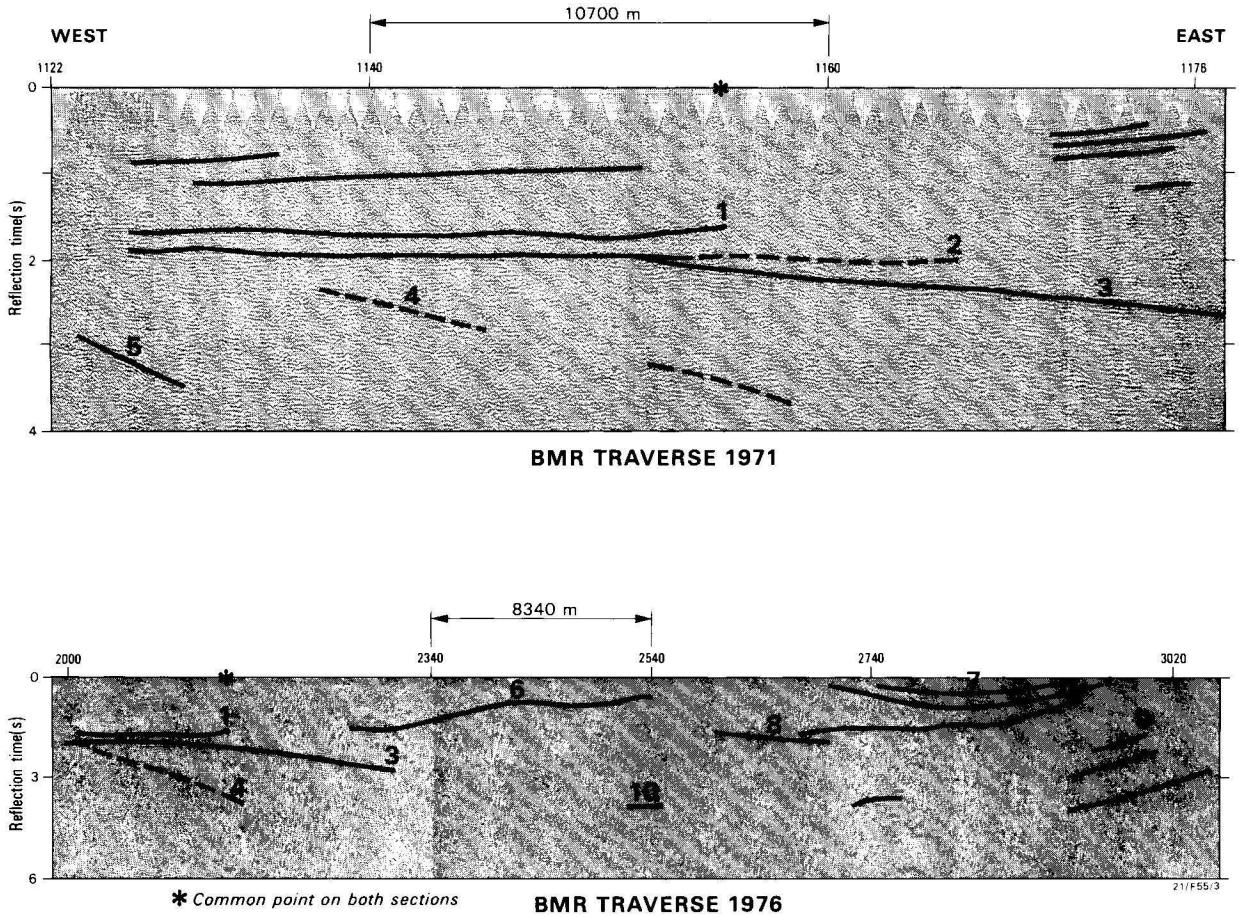

Figure 4. Reflection sections for the 1971 and 1976 seismic traverses, showing the main reflectors.
The sections overlap and have different horizontal and vertical scales. The discontinuous nature of reflectors results in considerable ambiguity.

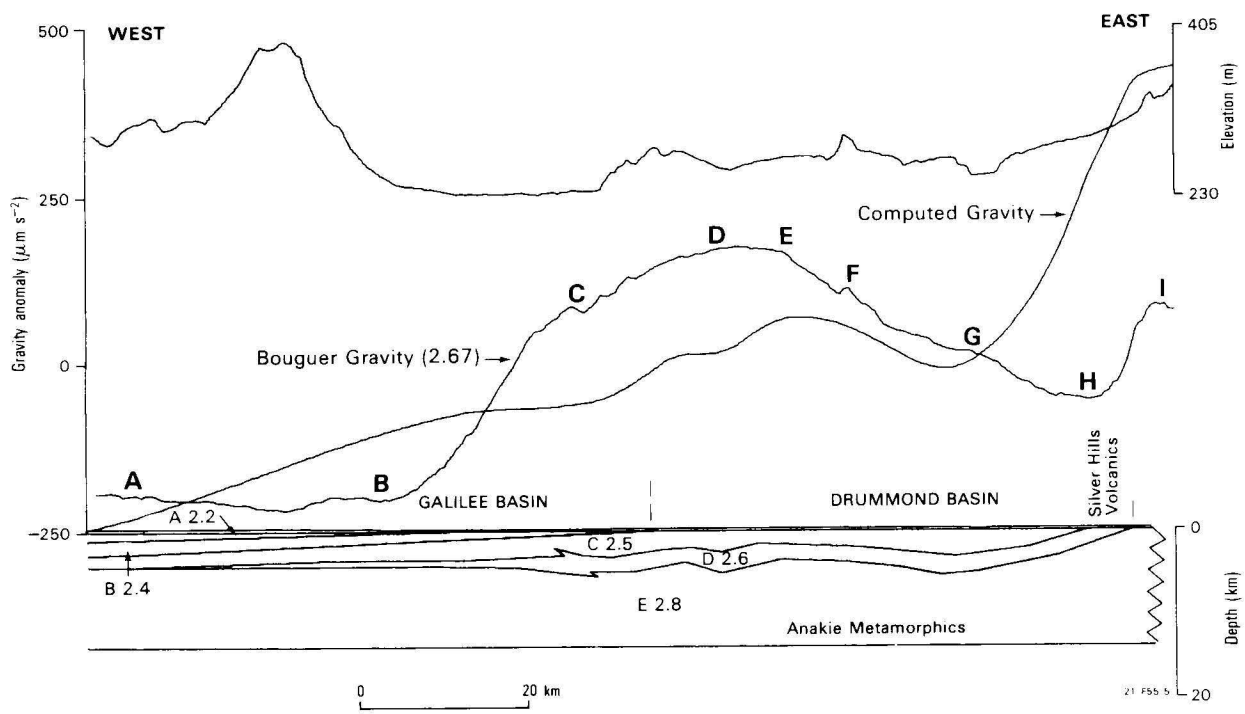

Figure 5. Gravity model of Pinchin's (1978) seismic interpretation.
This model shows that the seismic interpretation is inadequate and additional structures need to be invoked.

The 1971 section shows Galilee Basin sediments above 0.5 sec shallowing eastwards, but extrapolation to the surface is difficult, because there is a break in reflection continuity associated with the abrupt ending of reflector 1 at SP1154. Reflectors 2 and 3 and events 4 and 5 deeper in the section represent complex structures involving unknown rock types. Reflector 3 could represent Adavale Basin equivalents underlying the Drummond Basin, and indicates a considerable thickening of the total sedimentary section to the east. Event 4 was interpreted by Pinchin & others (1979) as a reflected refraction, but a change in reflection character across it suggests it could represent a series of diffractions arising from a dipping surface. Event 5 has both straight and curved components, suggesting reflections and diffractions from another dipping surface.

The 1976 section confirms reflectors 1 and 3 and event 4, but it is not obvious how these relate to reflectors 6,7,8 and 10, and a series of diffracting surfaces in the region of 9, where a fault indicated by these events corresponds to a strong gradient in the gravity anomaly. Reflector 6 shows the folds of the Donnybrook Anticline, but the connection with reflectors 7 and 8 of the Mistake Creek Syncline is not clear. An unconformity between reflectors 7 and 8 implies a degree of complexity in the Drummond Basin, and one of the surfaces at 9 may represent the base of the Silver Hills Volcanics. Reflector 10 is an isolated event deep in the section, and may correlate with reflector 3.

The overall picture is far from clear, because information is missing in crucial areas. The lack of clarity particularly affects the important area under the Donnybrook Anticline, where interpreted depth to basement can vary by a factor of three. The section can be interpreted in several ways, the main options being: 1 — connect reflectors 3,6 and 8 together; this implies uplift along a low-angle thrust, and a shallow basement under the Donnybrook Anticline (Pinchin, 1978); 2 — connect reflectors 1,6 and 8; connect reflectors 3 and 10; and connect events 4 and 9 to produce a deep basin under the Donnybrook Anticline.

Gravity information

The combined gravity data for the 1971 surveys are displayed in Figure 3. Symbols A-I are used to designate individual bumps and gravity levels discussed in the text. Each bump is important to the interpretation as it decreases ambiguity by providing an additional constraint on density contrasts and structure.

For the 2.5 t/m^3 Bouguer reduction, normal slab corrections and automatic 2-D terrain corrections (Anfiloff, 1976) have been applied separately, resulting in two profiles superimposed on one another for comparison. The profiles are almost identical, except for a slight thickening of the line in the region of the main topographic feature between A and B. This feature, which has a relief of 150 m, does not, therefore, require a terrain correction, and is hardly discernible in the elevation profile drawn at natural scale. Nevertheless the feature still causes a substantial change in the shape of the Bouguer profiles drawn for various densities, and in particular affects the shape of the gravity low at B. At the same time, the gravity low at B makes it impossible to determine the density of the topographic feature using Nettleton's (1939) minimum correlation principle, and the uncertainty in the topographic density in turn introduces uncertainty into the interpretation. The uncertainty cannot necessarily be removed, but the density profiling process at least enables the problem to be recognised.

The small gravity low at B (Fig. 3) has an amplitude of only 30 $\mu m.s^{-2}$, and does not correspond to any structures evident in the seismic section. This suggests that a major gravity low originating from within basement has cut into the western flank of the Donnybrook High, displacing it eastwards, and making it steeper. If this is the case, the cause of the Donnybrook High extends well west of the Donnybrook Anticline, and is unrelated to it. The gravity low at B is presumably caused by a granite, which cannot be shallower than the reflector at about 6 km.

The gravity low at H is east of the Mistake Creek Syncline, and must represent a large body of low-density material adjacent to the Anakie Metamorphics. The metamorphics consist of schist, slate, and sandstone, and would have a density in the range 2.6–2.7 t/m^3. To produce the anomaly between H and I, the body at H would have to have a density of 2.4–2.5 t/m^3, which is a relatively low value. The surface outcrops at H were identified as the Devono-Carboniferous Silver Hills Volcanics (Olgers, 1969), but the Telemon Formation, Mount Rankin beds, and Theresa Creek Volcanics could be included, as these contain low-density tuffs and acid volcanics. These formations have a widespread distribution, and, given that acid volcanics with a density of 2.42 t/m^3 were found to the west (Fig. 1) at the bottom of the Thunderbolt 1 well (Amerada, 1967a), it is possible that a thick low-density layer underlies the Galilee and Drummond Basins over the entire region. This layer appears to have been faulted against the Anakie Metamorphics at H and largely eroded from the upthrown block, leaving only scattered remnants.

The folds of the Donnybrook Anticline visible in the seismic section between SP-2340 and SP2540 (Fig. 4) have no gravity expression, implying that the anticline is underlain by rocks of similar density. This helps rule out the shallow basement option, and at the same time constrains the density in the lower part of the section. The bumps in the gravity at E and F are caused by density changes across formation boundaries at the surface. The bump at G is present only in the higher-density Bouguer profiles, and, being related to a dip in the elevation profile, suggests a low-density weathered layer at that location. The low at C has a short wavelength, and could be caused by subcropping Permian coal beds within the Galilee Basin sequence.

Interpretation

The basement uplift model

The abrupt termination eastwards of reflector 1 can be attributed to a thrust across which basement has been elevated. From the seismic data the total amount of uplift is limited (Fig. 4), and a large density contrast of 0.4 t/m^3 is needed to produce a sufficiently large gravity high (Fig. 6). However, the western flank of the computed anomaly is well offset from the true flank, and this cannot be altered, as reflectors 1 and 2 control the thrust position. This model, therefore, does not fit.

The dense basement block model

In Figure 7, an arbitrary horizontal datum is used to separate the Anakie Metamorphics from underlying basement, the metamorphics are extended, with a constant density, westwards under the section, and a dense block (body G) has been added to produce a gravity high. The gravity high extends the required distance to the west, while the granite (body F) cancels part of this high. The granite–dense block combination gives a reasonable anomaly in the first approximation, but there is a problem with matching the shape at B. A small granite produces a small low, but does not cancel enough of the

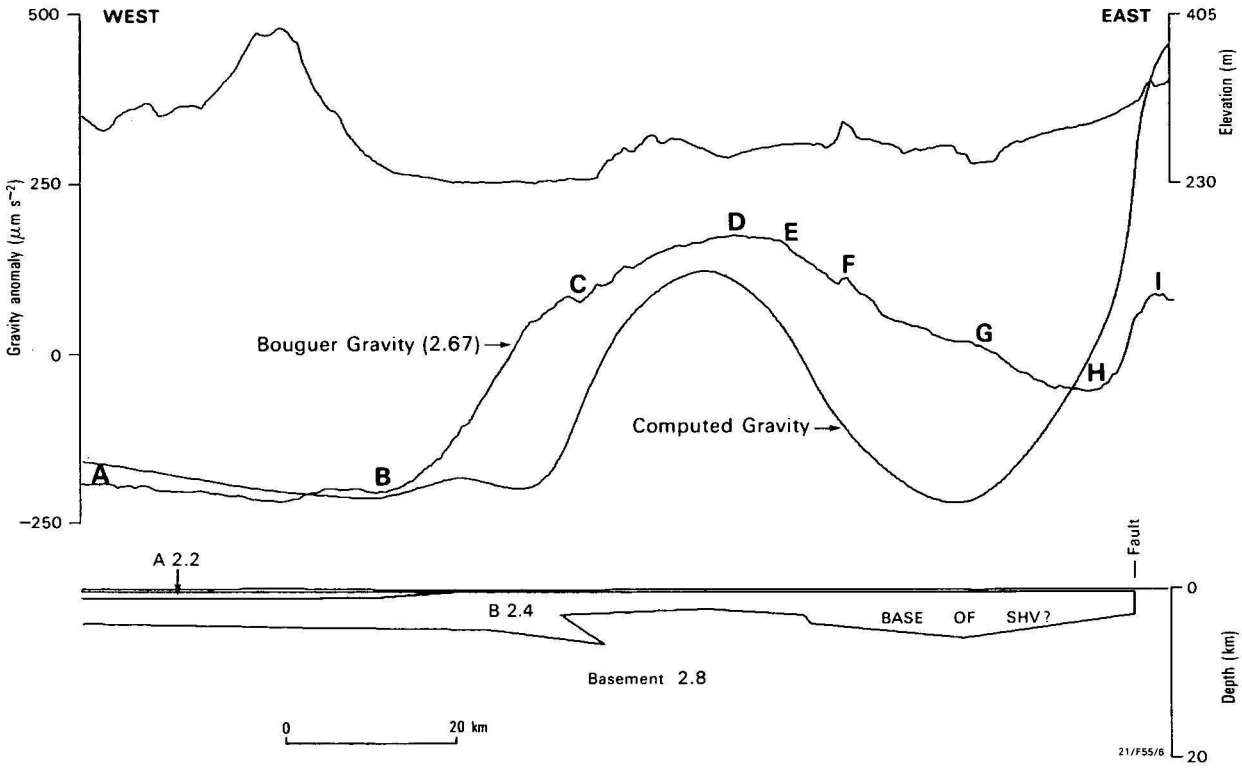

Figure 6. Gravity model, using basement uplift concept.
The interpreted thrust position is incompatible with the position of the western flank of the anomaly.

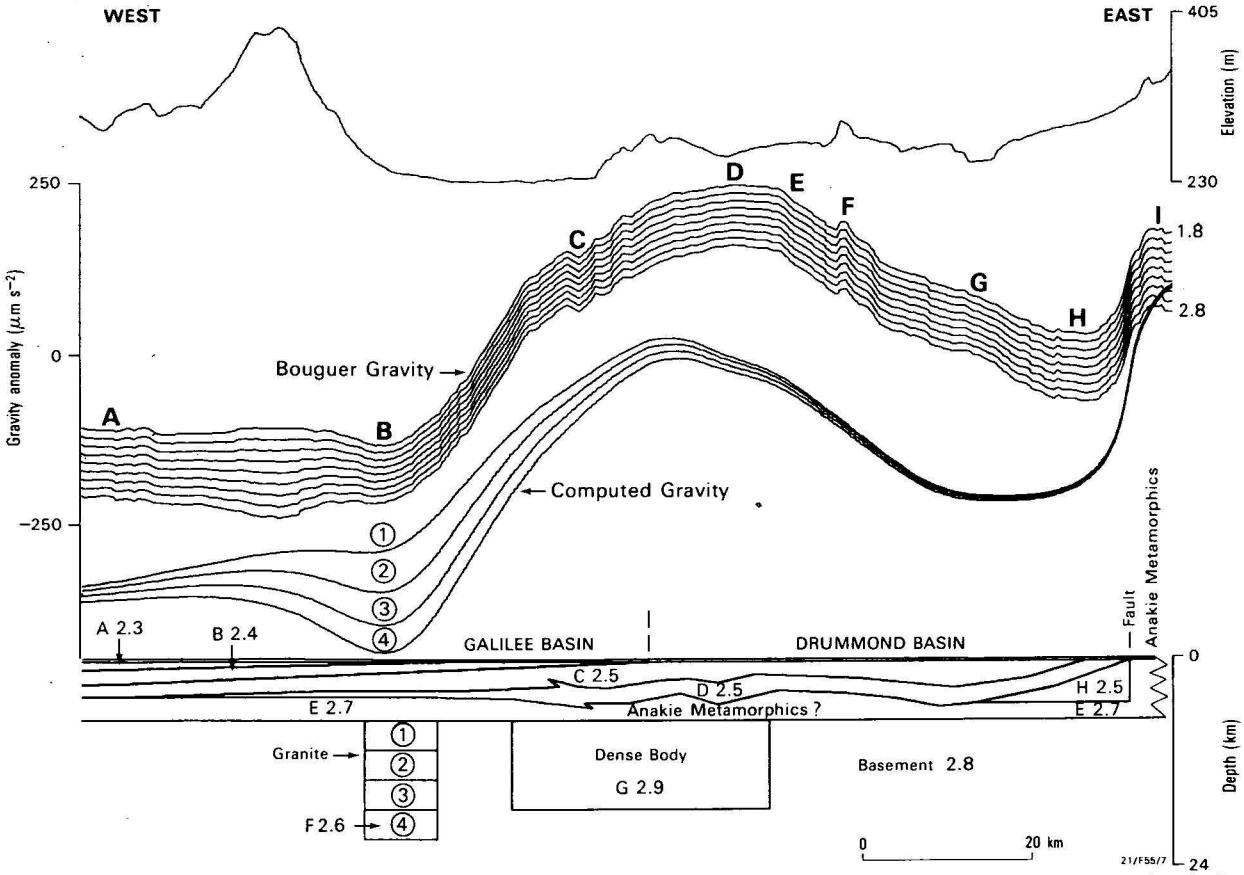

Figure 7. Combination of a granite pluton and a dense body in the basement gives a reasonable fit in the first approximation, but the low at B is not matched accurately.
The figure demonstrates multiple-pass modelling; the bottom of the granite is made progressively larger in four stages to produce four computed anomalies.

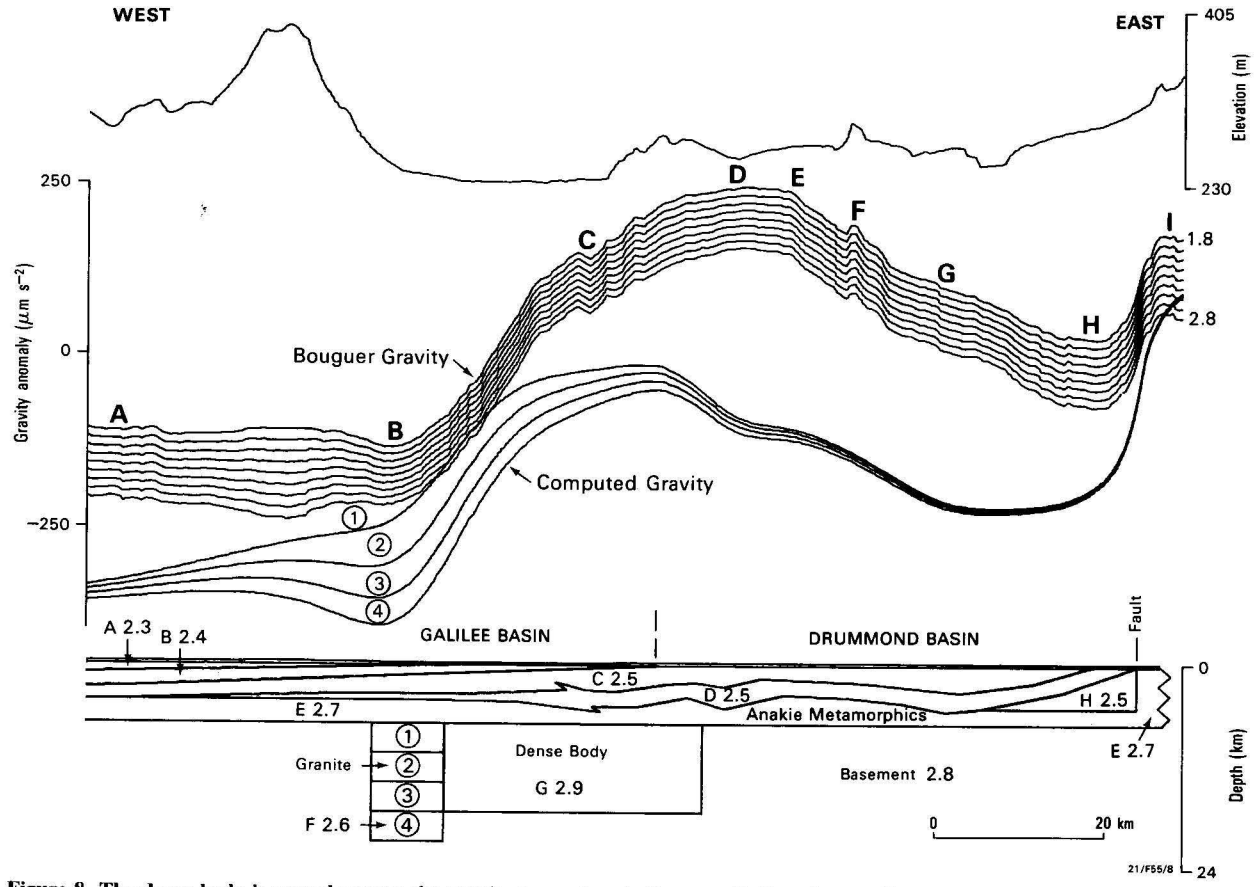

Figure 8. The dense body is moved next to the granite to produce better cancellation of anomalies.
The computed low at B is now smaller, but is still too large, and the interval A–B cannot be matched correctly.

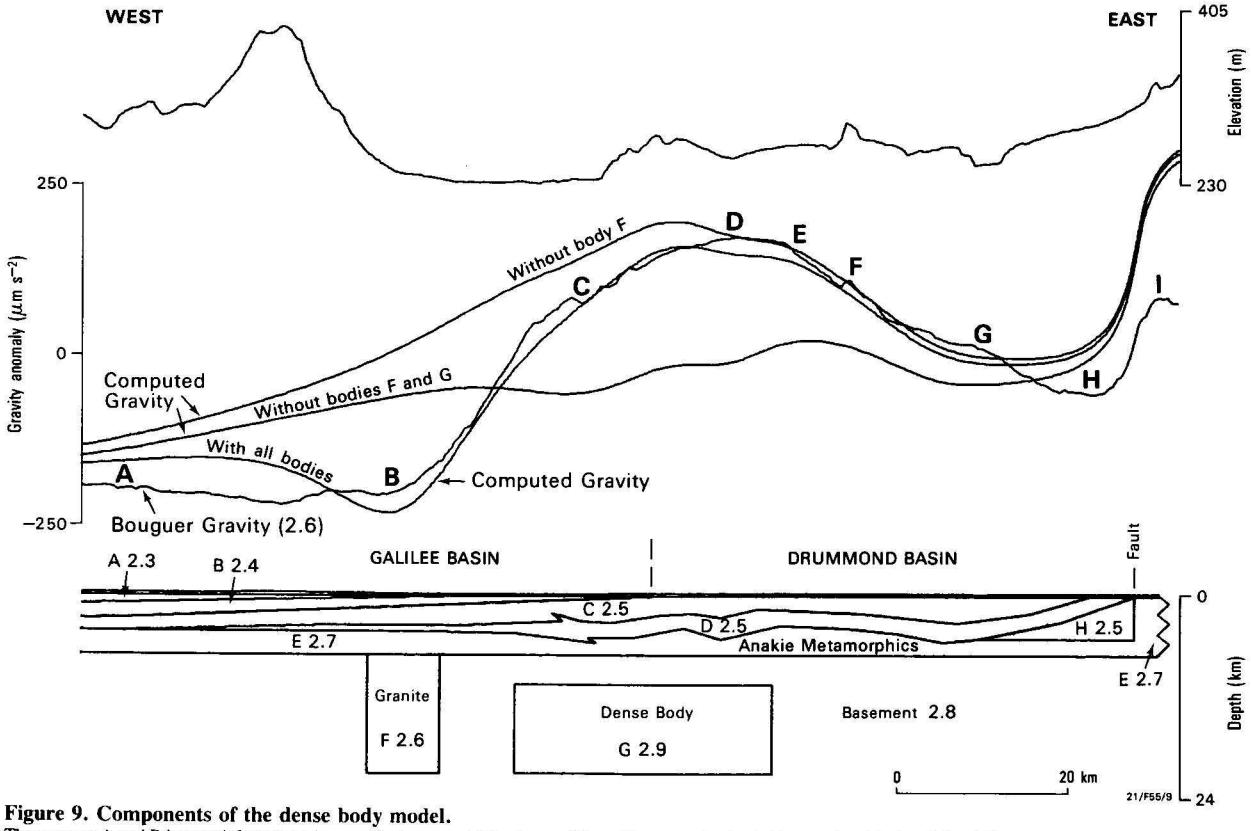

Figure 9. Components of the dense body model.
The curve at A and B is unsatisfactory and cannot be improved. The shape of the without-granite (body F) curve is critical and should be compared to that in Figure 10.

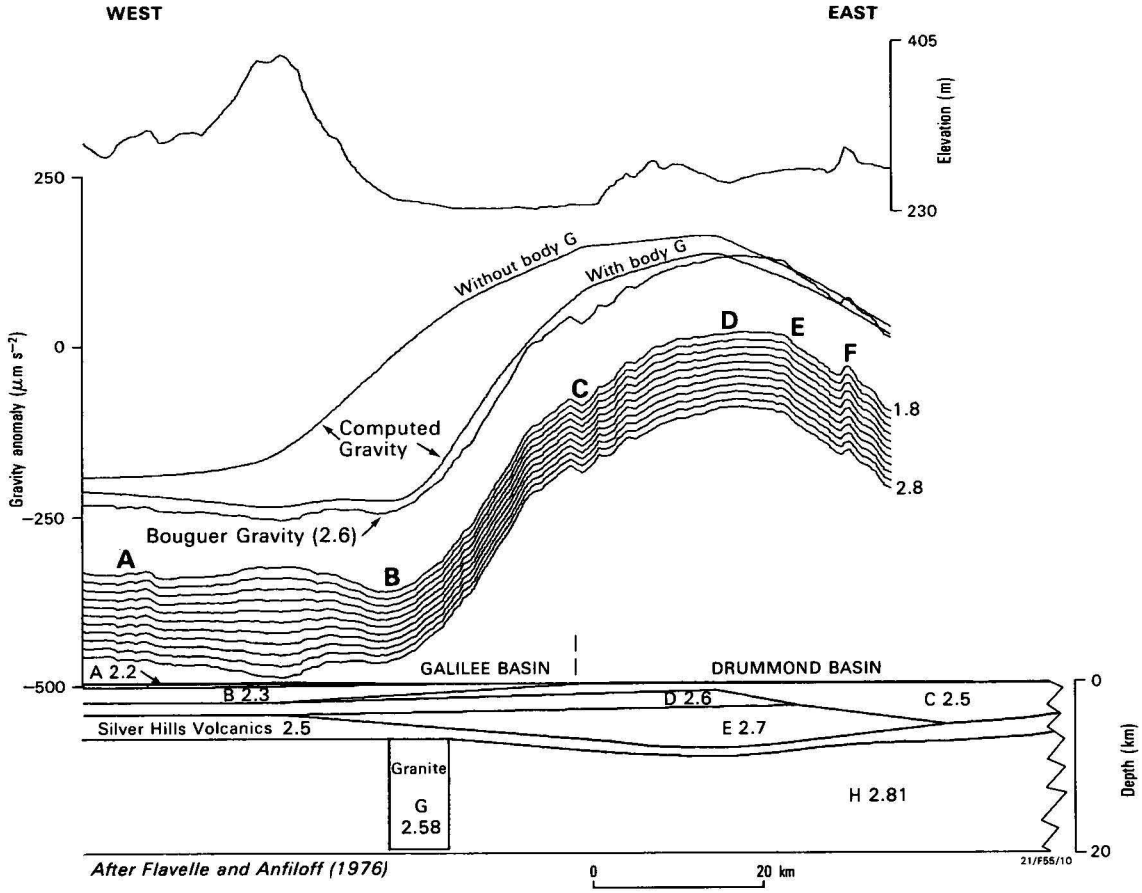

Figure 10. A reverse density contrast model based on the 1971 survey.
In this model a dense basin replaces less dense sub-basement (Silver Hills Volcanics) laterally, producing a good fit over the topographic feature with the 2.6–2.7t/m^3 Bouguer profiles. The reverse contrast wedge is close to the top of the granite, and produces part of the required cancellation of anomalies.

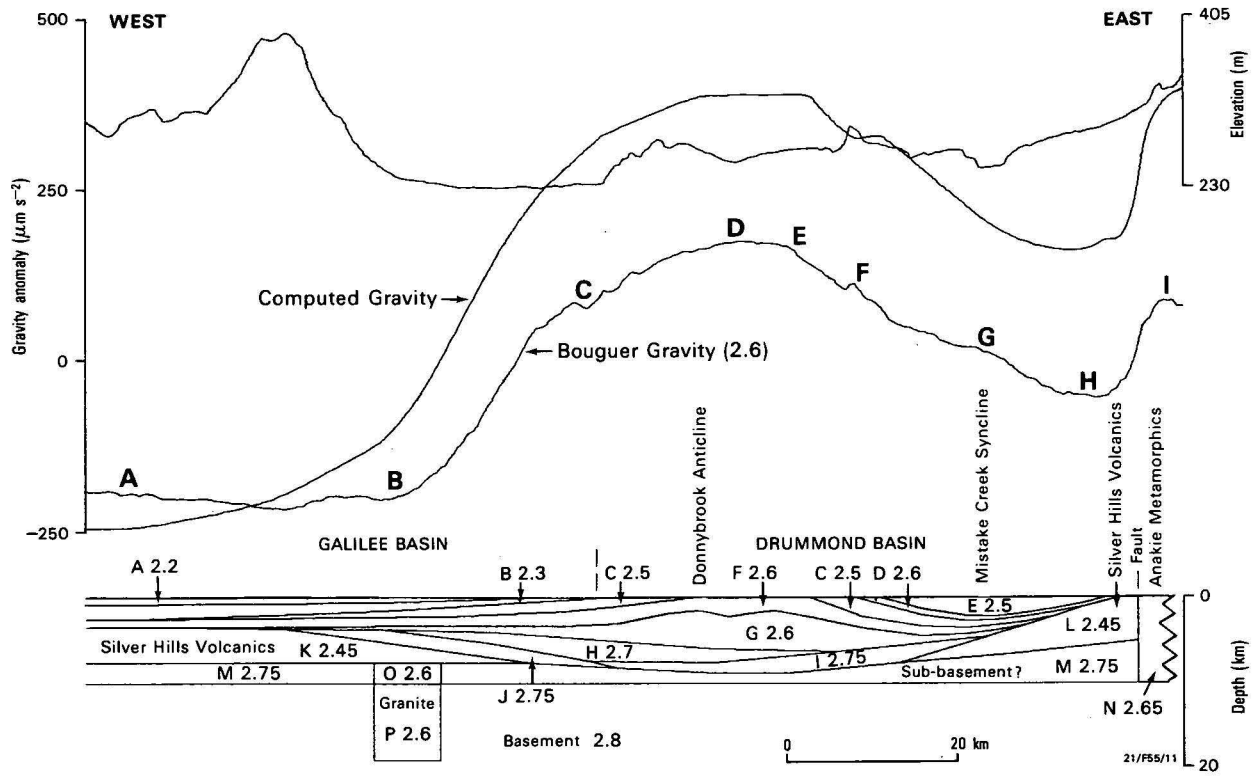

Figure 11. Extrapolation eastwards of the reverse contrast model, based on the 1976 seismic section.
The presence of a thick layer of Silver Hills Volcanics is established by the fault anomaly between H and I. The model suggests a complex depositional history and a deep basin under the Donnybrook Anticline. The fit at B is poor because the granite contribution is insufficient.

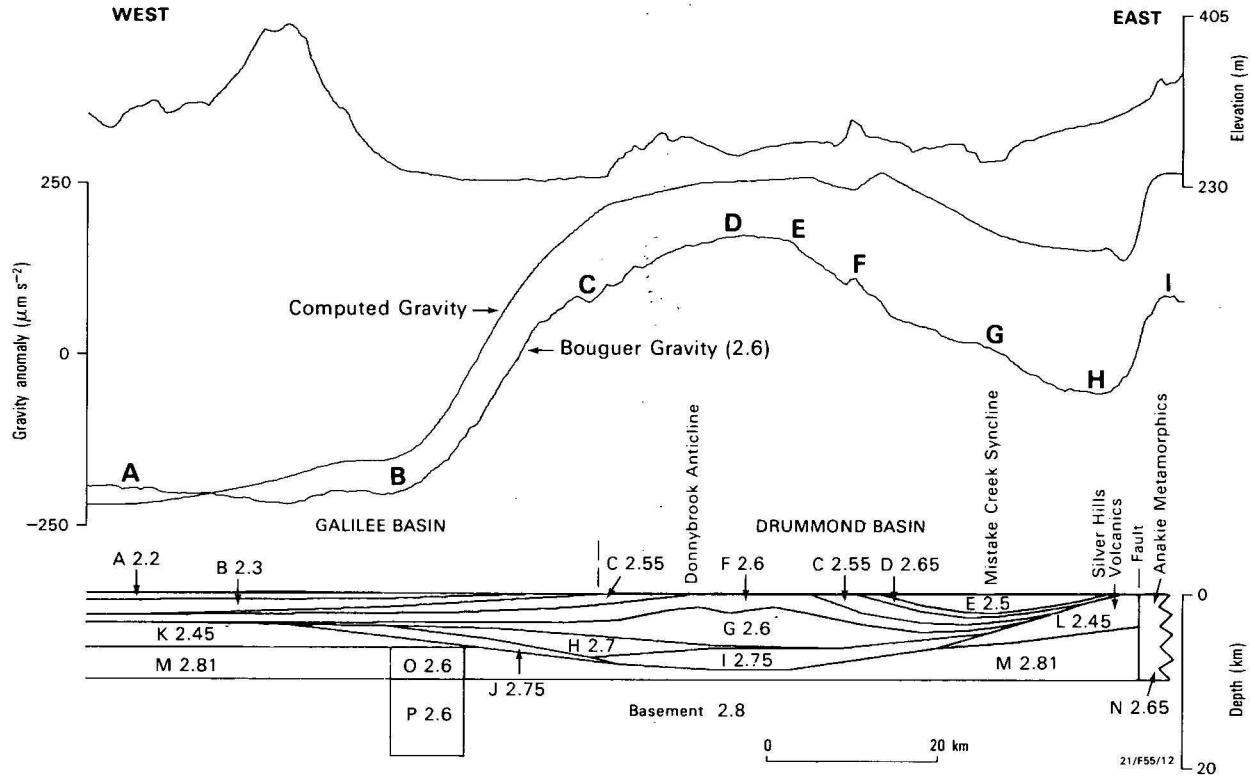

Figure 12. To give an improved fit at B, the model has to be modified to make the basement and granite shallower.
The basin now protrudes too far into the basement, adversely affecting the level at D.

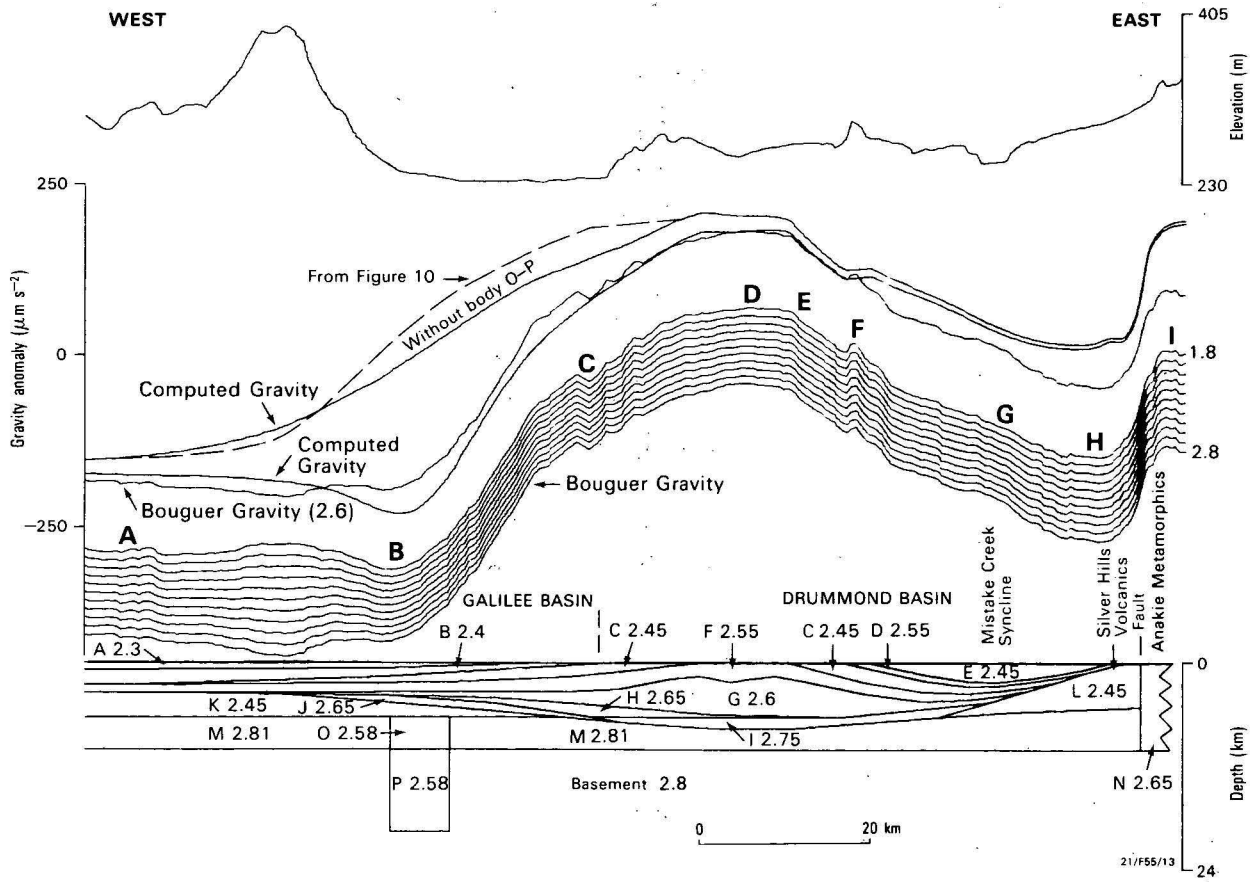

Figure 13. The western part of the section is now identical to that in Figure11, except for the shallow boundary between bodies B and C.
Comparing the without-granite curves shows the important effect this boundary has for the fit at B.

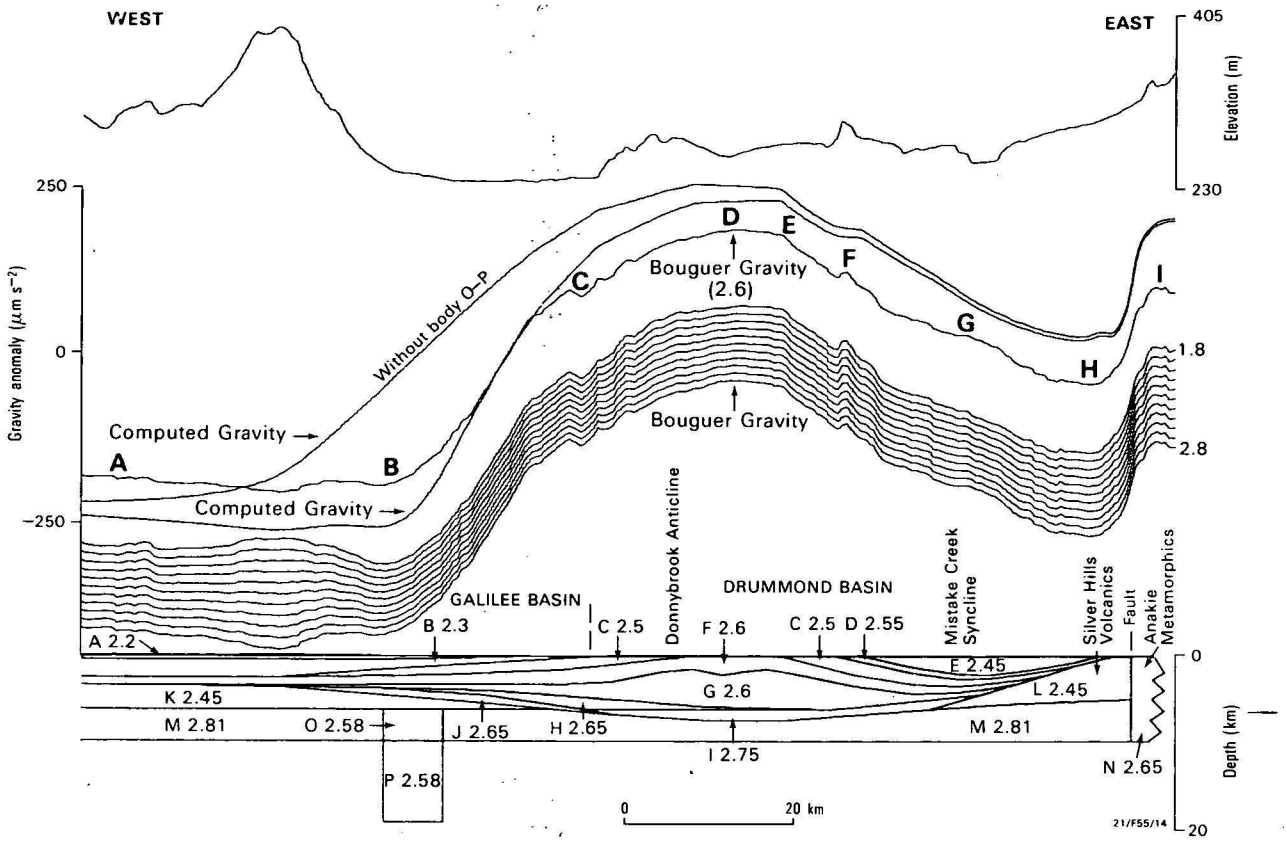

Figure 14. Making body C wedge out more rapidly westwards, as in the seismic interpretation of Harrison & others (1975), produces the correct fit at B, demonstrating the extreme sensitivity of the match to structural changes.

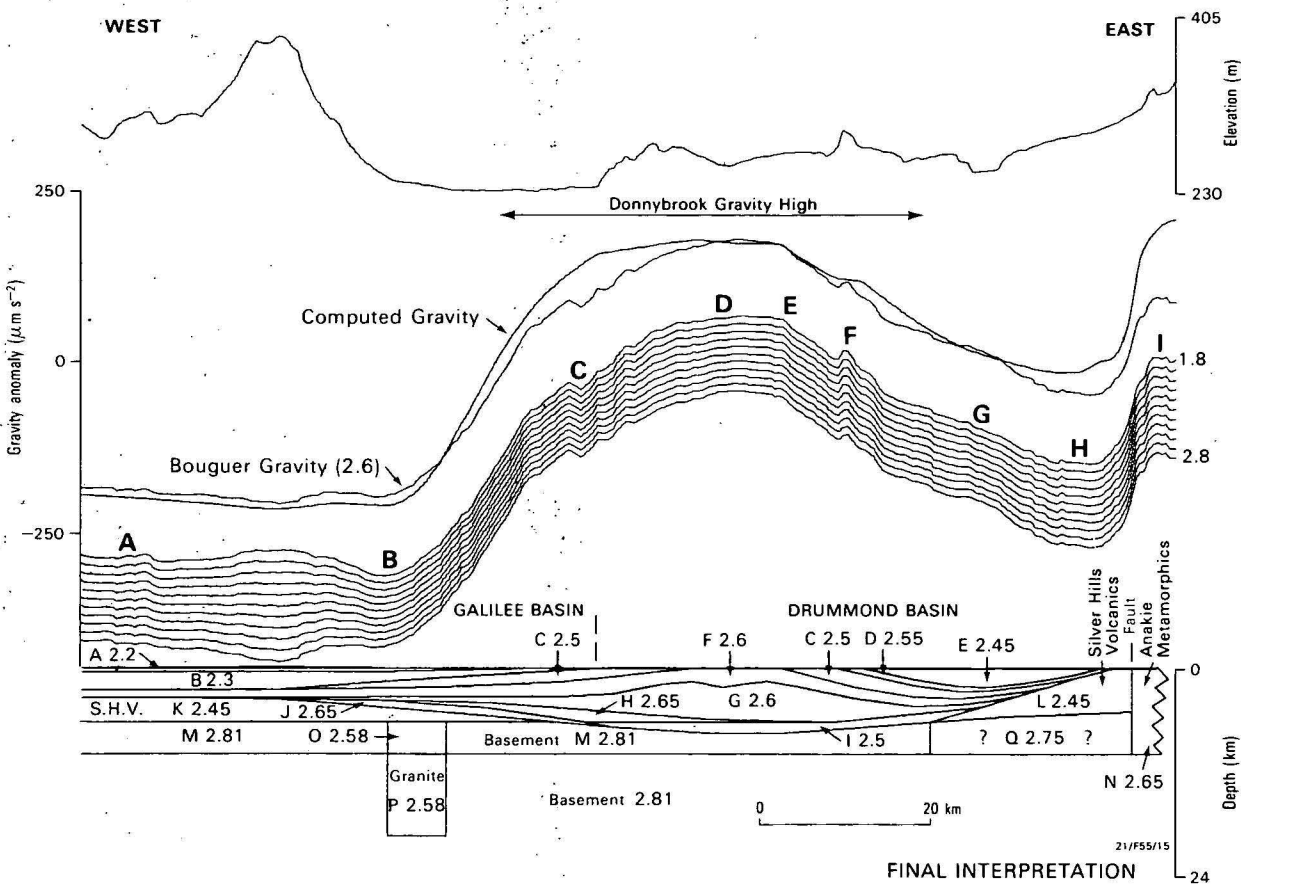

Figure 15: An arbitrary change to the density of body I and introducing body Q gives the necessary change in gravity levels to produce a satisfactory match over most of the section.

western flank of the Donnybrook Gravity High between A and B, while a large granite cancels the flank as required, but produces an excessively large low at B.

Figure 8 shows the improved effect of placing the dense basement block next to the granite; the cancellation is now more effective, but the low at B is still too large.

Figure 9 summarises the type of fit obtainable with the dense basement block model. Three computed anomalies are shown. One is the effect when neither the granite (body F) nor the dense block (body G) are present, a second shows the effect of introducing the dense block; the gravity high then extends considerably west of the actual anomaly. The third shows how the introduction of a granite body shifts the flank of the anomaly eastwards, modifies it, and produces a low at B. The fit could be considered to be reasonable, and this type of interpretation could be produced by an inversion program, which would adjust the two bodies in the basement until the R.M.S. error was minimised. In qualitative terms however, the fit is poor, because the correct anomaly shape has not been produced between A and B. Furthermore, as the true shape of the anomaly is not known, any automatic method would be guaranteed to fail. The solution requires a careful trial-and-error approach in which each computed curve is tested against each of the Bouguer density profiles.

The reverse density contrast model (1971 data)

Part of the Donnybrook Gravity High can be explained in terms of an older basin underlying the Drummond Basin. Events 3,4, and 5 in Figure 4, in combination with a thick low-density layer of Silver Hills Volcanics and related acid volcanics, form the basis of a reverse density contrast model, in which gravity increases as basement deepens. This relation also exists on Traverse R-56 of the Tower Hill seismic survey (Amerada, 1967b).

As about half the anomaly can be attributed to the transition from Galilee Basin sediments to denser Drummond Basin sediments, only about 200 $\mu m.s^{-2}$. needs to be accounted for. Given that tuffs and dacites can have a density of about 2.45 t/m^3, and that the material filling the older basin could include dense basalts, a reverse density contrast of about 0.2 t/m^3 could exist, operating over a section several kilometres thick. Using the 1971 seismic and gravity data, Flavelle & Anfiloff (1976) demonstrated how a reverse contrast model can produce a good match for the low at B. Their model, reproduced in Figure10, applies a reverse contrast across the easterly dipping event 5. This surface cuts across the top of the granite (body G) and produces the positive contribution needed to reduce the size of the low at B.

The low at B can be produced by a number of alternative granite bodies. The top of the granite cannot be deeper than about 7 km, while the seismic information restricts it to below about 6 km. The bottom of the granite can extend to 20 km, but not 25 km, and with a variety of cross-sectional shapes, can lie in the zone 15–20 km (Flavelle & Anfiloff, 1976).

In the zone A–B, the model produces a match with only the 2.6–2.7 t/m^3 Bouguer profiles, which is a reasonable density for the main topographic feature there, given that its existence as an erosional feature implies that its composition is not the same as Galilee Basin sediments generally.

The reverse density contrast model (1971 & 1976 data).

Figures 11-15 deal with the interpretation of the combined 1971 and 1976 data, using the reverse contrast concept. Figure 11 shows a comprehensive model based on 1971–76 seismic time-sections. It suggests a complex geological history: almost every boundary in the sedimentary section is an unconformity, and numerous episodes of movement are implied.

The boundary between bodies B and C is taken from the seismic interpretation of Pinchin (1978) (Fig. 5), and extends further west than the one mapped by Harrison & others (1975). The shallow formations (Fig. 11) are arranged to accord with the local bumps in the gravity. Body D produces the gravity high at F and must be at least 0.1 t/m^3 denser than adjacent bodies. The bump at E also indicates a 0.1 t/m^3 contrast between bodies C and F. The Donnybrook Anticline does not produce an anomaly, and the densities of bodies F and G must therefore be similar. The various bumps, when used in combination, mean that if a density is assigned to one formation, densities of the other formations are implied.

The deeper parts of the model are based on extrapolation of the seismic and geological data. Bodies G, H, I, and J represent formations deposited in a depression within the Silver Hills Volcanics (bodies K & L). Of these, bodies G, H, and J correspond to the three easterly-dipping events 3, 4 and 5.

The thickness of the Silver Hills Volcanics, and its density are constrained by the gravity low between H and I. At least 4km of the volcanics therefore appears to be faulted against the Anakie Metamorphics with a 0.2 t/m^3 contrast. It seems that the isolated pockets of Silver Hills Volcanics that occur over the Anakie Metamorphics are the remnants of a layer considerably thicker than previously thought.

Extending the interpretation eastwards causes major complications. The granite (bodies O & P) may penetrate two types of basement, the Anakie Metamorphics and an underlying denser Proterozoic basement. An arbitrary horizontal datum is used to separate the two, cutting the granite into bodies O and P. The model (Fig. 11) shows that if the Anakie Metamorphics have a density of 2.65 t/m^3 in the east, their density at B must be greater than 2.75 t/m^3 for the granite to cause a negative effect at a sufficiently shallow depth to produce the required low at B. The thickness of body K must also be decreased to raise the top of the granite as high as possible.

In Figure 12, the top of the granite is at 6 km. As the granite cannot be much less dense than 2.6 t/m^3, the basement density has to be increased to 2.81 t/m^3, which is presumably too dense for the Anakie Metamorphics. This arrangement is now beginning to produce the desired anomaly at B, but bodies H and I are now protruding too far into the basement, where they produce undesirable negative components.

In Figure 13, the section under the Donnybrook Anticline has been compressed to reduce the protrusion, and a new set of densities has been assigned to most of the bodies. There is now a good fit over most of the section, and the shape at B is improved. However, it is still larger than any of the lows in the Bouguer profiles for densities between 2.2 and 2.8 t/m^3, and is not the same as the low successfully matched in Figure 10. In fact the curves computed without the granite body are different. The curve from Figure 10, superimposed on the one in Figure 13, shows a steeper rise, reflecting the effect of a shallow structure. Although the models in Figures 10 and 13 have identical granites and reverse contrast wedges, they differ in the slope of the interface and the density contrast between the Galilee Basin (body B) and the Drummond Basin (body C). The interface represents a shallow wedge that generates a positive effect and cancels still more of the low at B, such that the 250 $\mu m.s^{-2}$ low generated by the granite registers as a low of only 20—30 $\mu m.s^{-2}$. Consequently, it appears that the

steeper interface in the seismic interpretation of Harrison & others (1975) is more appropriate than the shallower one in the seismic interpretation of Pinchin (1978).

In Figure 14, the boundary between bodies B and C has been made identical to the one in Figure 10. This gives the same without-granite curve as in Figure10, and when the granite is added, the required anomaly shape is produced at B. It is remarkable that a small change in structure can so drastically alter the shape of the final anomaly, and that only a shallow structure can produce this change.

Also in Figure 14, the contrast between bodies B and C has been increased to 0.2 t/m^3 by making body C denser, and, because the relative densities between bodies C, F, and D have to be maintained to satisfy the constraints imposed by the bumps in the gravity at E and F, this has resulted in a regionally higher level of gravity over the eastern part of the section. This problem is rectified in the next model (Fig. 15) by making an arbitrary reduction in the density of body I and arbitrarily introducing body Q.

The final interpretation is not altogether satisfactory at the eastern end of the section, but further modelling is not justified until the gravity profile is extended further east to determine the complete fault signature and the representative gravity level over the Anakie Metamorphics.

Conclusions

The analysis of 247 gravity observations has necessitated major revisions to previously published interpretations of the seismic data. Moreover, the gravity has clarified even the better parts of the seismic section, and enabled analysis of the geological section at depths beyond the range of seismic penetration. The combination of density profiling, forward modelling, and multiple-pass display has allowed a large number of complex geological and geophysical constraints to be welded together, and the accuracy of the final result is borne out by the reasonable value of 2.6–2.7t/m^3 diagnosed for the density of the main topographic feature.

The exercise has demonstrated that if stratigraphic relations of formations are known, and if lateral continuity of their density can be assumed, then each bump in a gravity profile enables the deduction of an additional constraint on the overall interpretation. Consequently, in general, the ambiguity of gravity data along a traverse will decrease as the traverse is made longer.

The low on the western flank of the Donnybrook Gravity High is the sum of positive and negative components. A 250 μm.s^{-2} low, originating from a presumed granite in the basement, has been largely cancelled by the positive contributions from two sedimentary wedges, resulting in a low of only 20—30 μm.s^{-2}. The shallower wedge indicates that the upper part of the Drummond Basin does not extend far under the Galilee Basin, and the deeper wedge indicates an old basin underlying the Drummond Basin.

The Silver Hills Volcanics provide the low-density basement essential for the reverse density contrast model, and the gravity itself verifies the presence of a thick low-density layer faulted against the Anakie Metamorphics. To cause a positive gravity effect, the volcanics cannot be merely depressed: a basin has to be formed within the layer by erosion. At the present time, the same volcanic layer is being eroded in exposed anticlines in several areas, and the same could have happened after the tuffs were deposited subaerially in the Devonian—Carboniferous. Figure 16 shows a cycle in which the tuff is eroded from an anticline, and the anticline then subsides, forming a basin, which fills with denser sediments.

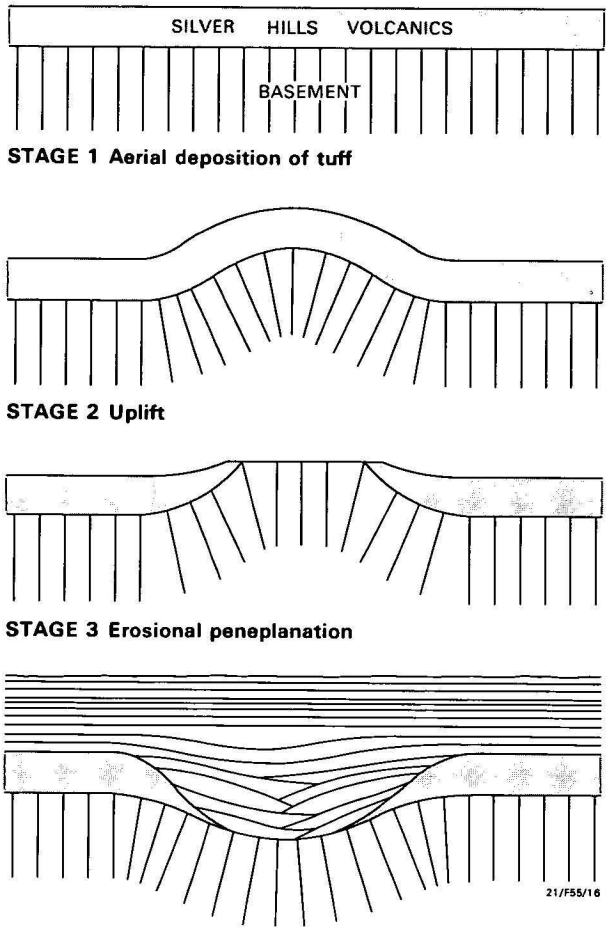

Figure 16. A generalised model that could produce a deep basin under the Donnybrook Anticline.

Acknowledgements

I wish to thank Mr J. Pinchin for examining the text and making valuable suggestions.

References

AMERADA, 1967a — Thunderbolt No. 1 Well Completion Report. *Amerada Petroleum Corporation of Australia Ltd* (unpublished).

AMERADA, 1967b — Tower Hill Geograph Seismic Survey, ATP 76P, Queensland. *Amerada Petroleum Corporation of Australia Ltd* (unpublished).

ANFILOFF, W., 1976 — Automated density profiling over elongate topographic features. *BMR Journal of Australian Geology & Geophysics*, 1, 57–61.

ANFILOFF, W., 1981 — Discussion on 'Gravity interpretation with the aid of quadratic programming'. *Geophysics*, 46, 340–2.

ANFILOFF, W., & FLAVELLE, A.J., 1979 — Gravity interpretation over escarpments and in two-dimensions generally. The formal interpretation method. *Geophysics*, 44(3), 371 (abstract).

FISHER, N.J., & HOWARD, L.E., 1980 — Gravity interpretation with the aid of quadratic programming. *Geophysics*, 45(3), 403–19.

FLAVELLE, A.J., & ANFILOFF, W., 1976 — Non-standard gravity anomalies over sedimentary structures. *The APEA Journal*, 16(1), 117–21.

HARRISON, P.L., ANFILOFF, W., & MOSS, F.J., 1975 — Galilee Basin seismic and gravity survey, Queensland, 1971. *Bureau of Mineral Resources, Australia, Report* 175.

NETTLETON, L.L., 1939 — Determination of density for the reduction of gravimeter observations. *Geophysics*, 4, 176–83.

OLGERS, F., 1969 — Clermont, Queensland, 1:250 000 Geological Series. *Bureau of Mineral Resources, Australia, Explanatory Notes* SF/55–11.

OLGERS, F., 1972 — Geology of the Drummond Basin. *Bureau of Mineral Resources Australia, Bulletin* 132.

PINCHIN, J., 1978 — A seismic investigation of the eastern margin of the Galilee Basin, Queensland. *BMR Journal of Australian Geology & Geophysics*, 3(3), 193–202.

PINCHIN, J., SCHMIDT, D.L., & ANFILOFF, W., 1979 — Eastern Galilee Basin seismic survey, Queensland, 1976. *Bureau of Mineral Resources, Australia, Record* 1979/78 (unpublished).

BMR Journal of Australian Geology & Geophysics, 7, 315-320

REDESCRIPTION OF *MIOGYPSINA NEODISPANSA* (JONES & CHAPMAN), FORAMINIFERIDA, CHRISTMAS ISLAND, INDIAN OCEAN

D.J. Belford

Miogypsina neodispansa (Jones & Chapman) is redescribed from oriented sections prepared from samples collected at the type locality on Christmas Island, Indian Ocean, and is referred to the subgenus *Lepidosemicyclina*. *M.neodispansa* is considered to be a senior synonym of *M. droogeri* Mohan & Tewari.

Introduction

Miogypsina neodispansa was described by Jones & Chapman in Andrews (1900); the original description was very brief, and gave no information on the embryonic/nepionic chambers. Nuttall (1926) emended the description, but was unable to obtain a section showing the nepionic chambers; he noted the development of hexagonal median chambers towards the periphery of the test.

M. neodispansa was one of the first miogypsinids described from the Indo-Pacific region, and for this reason is an important species. It has not been known how *M. neodispansa* differs from, or is related to, other described species of the genus from this region. Data on the periembryonic and median chambers of *M. neodispansa* have now been obtained, and have enabled a more detailed description of the species to be given.

The redescription of *M. neodispansa* given here is based on sections prepared from samples collected by Mr P.J. Barrett and Mr D.A. Powell in the area from which Andrews collected the original material, samples 924 and 220. The locality was given by Andrews (op. cit.) as 'in contact with the basalt bed..... to the south of Flying Fish Cove at Smith Point'. This locality was not found during a visit to Christmas Island by the writer in 1967, but subsequent work by Messrs Barrett and Powell located a limestone with abundant *M. neodispansa* in a position answering the description given by Andrews. Several samples of the limestone (G.840; G.852–G.862) were collected over a thickness of about 5 metres, with sample G.840 being at the base of the sequence; the position of G.840 is shown in Figure 1, at the northwestern end of Figure 2A of Andrews (1900). Detail of the cliff section at this point is given in Figure 2. The relationship between the *Miogypsina*-bearing limestone and the two samples at the top of the sequence, G.861 and G.862, which contain a lower Te fauna, is obscure. As noted in Adams & Belford (1974), the *M. neodispansa* limestone is thought by Mr Barrett to result from a fracture-filling (Figure 3); this would explain the *neodispansa* limestone against the basalt with an older limestone at a higher level.

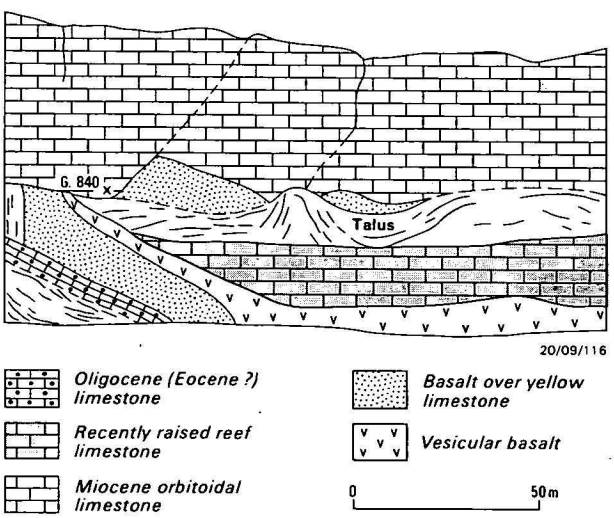

Figure 1. Enlargement of part of Figure 2A of Andrews (1900), showing position of sample G.840 at the base of the collected sequence.

Systematic description

Genus *Miogypsina* Sacco, 1893

Type species: *Nummulites globulina* Michelotti, 1841

***Miogypsina (Lepidosemicyclina) neodispansa* (Jones & Chapman, 1900)**

Figure 4, A–F; Figure 5, A–I

1900 Orbitoides (Lepidocyclina) neodispansa Jones & Chapman; pp. 235, 240 pl. 20, figs. 3,4.

1926 *Miogypsina neodispansa* (Jones & Chapman): Nuttall, p. 37, pl.5, fig.4.

1965 *Miogypsina neodispansa* (Jones & Chapman): Ludbrook, p.290, pl.2, fig.12 (part).

1974 *Miogypsina (Miogypsina) neodispansa* (Jones & Chapman): Adams & Belford, p.497, pl.71, figs.16-18; text–fig. 11a–c.

Test broad, flattened, fan-shaped, maximum length from apex to distal margin ranging from 2.50 mm to 4.25 mm, and maximum width from 2.50 mm to 4.00 mm. Some specimens are wider than long, forming a very broad test. Apex of test broadly rounded, side profile ranging from those specimens tapering gradually from apex to distal margin to those with an almost elliptical outline. Maximum height of test usually situated distally from the embryonic chambers, ranging from 0.83 mm to 1.50 mm; 5 to 11 layers of lateral chambers developed (Table 1). The surface of the test is ornamented by numerous pustules, the maximum diameter ranging from 50 μm to 200 μm. The pustules form the top of pillars that extend through the lateral chambers; the pillars often show distinct horizontal lamination.

The protoconch is spherical, ranging in diameter from 158 μm to 266 μm. The deuteroconch is slightly larger, ranging from 166 μm to 365 μm in diameter. The distance from the centre of the proloculus to the apex of the test ranges from 332 μm to 531 μm. Two principal auxiliary chambers are developed, unequal in size, followed by two main spirals of auxiliary chambers; no accessory auxiliary chambers have been observed. The auxiliary chamber count is very variable, the most frequent being 2½–1½ or 2½–2½, but also giving 3½–1½ (two specimens) and 1½–1½ (one specimen). Smaller incomplete third and fourth spirals also occur along the margin of the deuteroconch, towards the apex of the test. The variation observed in the embryonic/nepionic chambers is shown in Figure 6.

The median chambers are not always developed in the same plane as the embryonic chambers, which makes preparation of

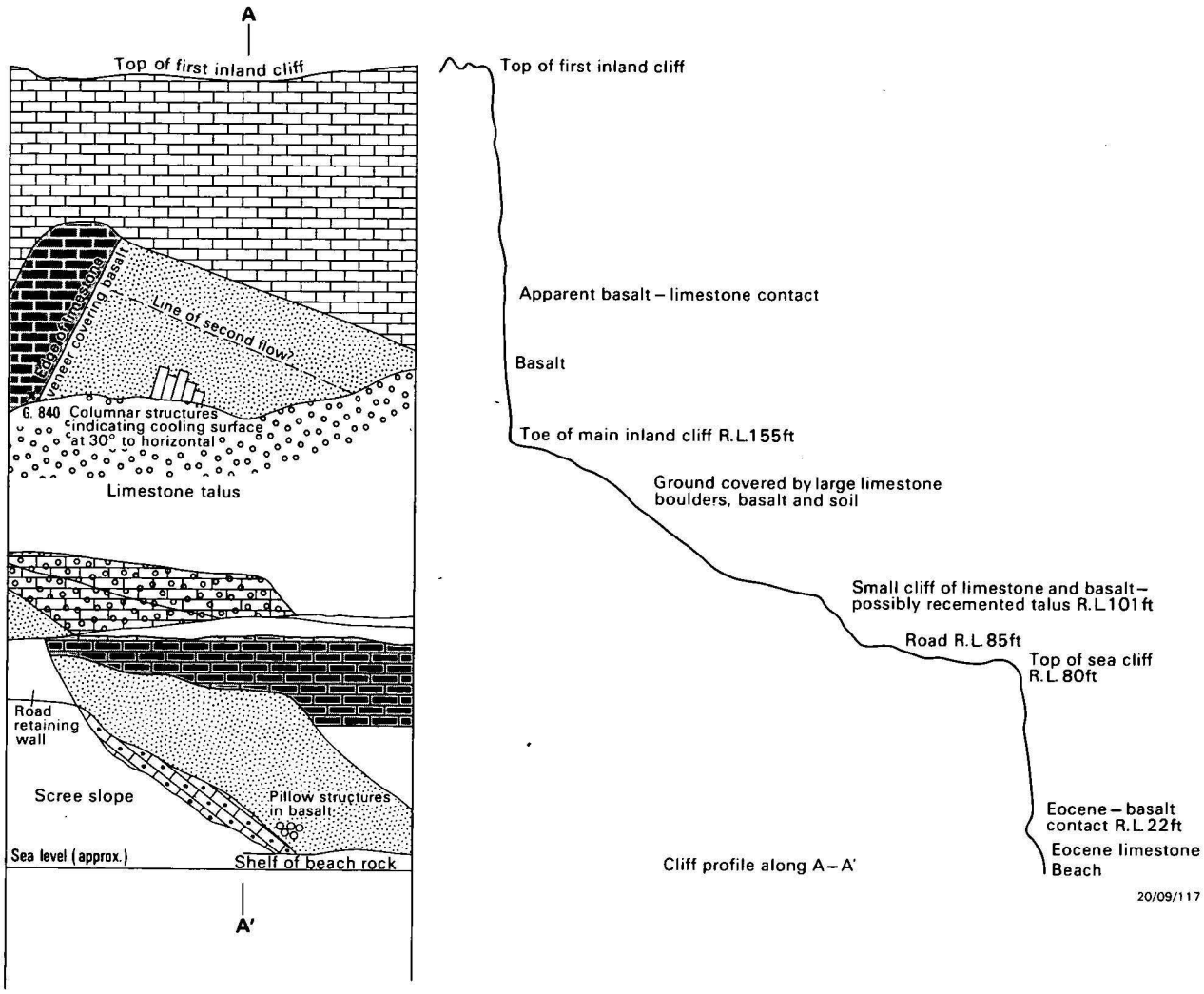

Figure 2. Detail of cliff and cliff profile at type locality of *M.neodispansa*.

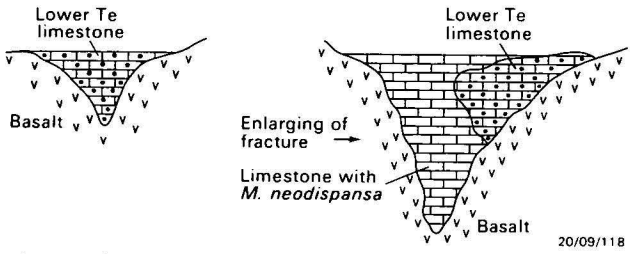

Figure 3. Suggested development of the *M. neodispansa* limestone as a fracture filling. From a sketch by Mr P.J. Barrett.

Table 1. Statistical measurements on specimens of *M. neodispansa*.

Maximum width of test (μm)	Number of lateral chamber layers
879.8	7
830.0	5
996.0	7
1494.0	10
1245.0	9
913.0	7
1195.2	8
1278.2	11
1411.0	9
1361.2	9
813.4	6
846.6	8

oriented median sections difficult. The median chambers range from 50 μm to 66 μm in height. Following the embryonic chambers, rhombic median chambers are developed, which become hexagonal, sometimes elongate hexagonal, in the outer part of the test.

The parameters V, γ, D1, D2, and ε, which have been used by, amongst others, Drooger (1952, 1963), Amato & Drooger (1969), Souaya (1961) and Raju (1974), have been measured in as many oriented sections as possible.

The parameter V(200 α/β), which is a measure of the relative lengths of the protoconchal nepionic spirals, ranges from 63.15 to 107.96, with a mean of 84.62 and a standard deviation of $\pm$11.61. The angle γ, discussed in detail by Amato & Drooger (1969), ranges from 4° to 33°, with a mean of 17.85° and a standard deviation of $\pm$9.71°. Details of these and other measured parameters are given in Table 2, and the relationship between V/D1, V/γ, and γ /D1 is shown graphically in Figures 7–9.

The development of hexagonal median chambers places *M. neodispansa* in the small group of species that have been included in the subgenus *Lepidosemicyclina*. Raju (1974) referred also to the high rate of embryonic-nepionic development in this group. Amongst the features mentioned by Raju (1974) is a change in the position of development of hexagonal median chambers from about 10–12 rows away from the embryonic/nepionic stage to the first row following this stage.

Figure 4. ***Miogypsina (Lepidosemicyclina) neodispansa*** **(Jones & Chapman)**
A, C, CPC.22418, sample G.853, median section showing hexagonal chambers and embryoconch. A, ×30; C, ×60. **B,D,** CPC.22419, sample G.856, median section showing hexagonal chambers and embryoconch. B, ×30; D, ×60. **E, F,** CPC.22420 and 22421, samples G.856 and G.840, respectively, median sections through the embryoconch. Both ×60.

Figure 5. ***Miogypsina (Lepidosemicyclina) neodispansa*** **(Jones & Chapman)**
A, B, CPC.22422 and 22423, samples G.856 and G.840, respectively, median sections through the embryoconch. Both ×60. **C-I,** CPC.22424 to 22430. C, E, F, G, sample G.840; D, sample G.852; H, I, sample G.856. Vertical sections showing variation in outline and development of pillars. All ×30.

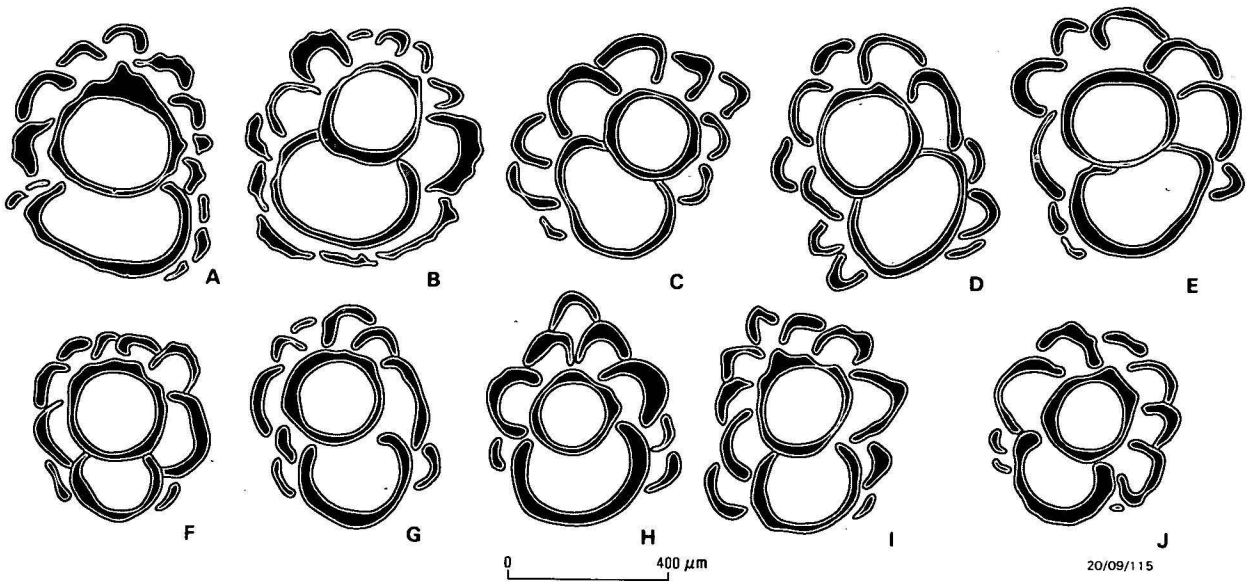

Figure 6. Variation in the embryonic/nepionic chambers.
In all cases the apical-frontal line is vertical. **A, G–J,** sample G.840; **B–C,** sample G.853; **D,** sample G.855; E–F, sample G.856.
A, CPC.22431; B, CPC.22432; C, CPC.22418; D, CPC.22433; E, CPC.22419; F,CPC.22420; G, CPC.22434; H, CPC.22423; I, CPC.22435; J, CPC.22436.

Table 2. Relation between width of test and number of lateral chamber layers.

Section No.	V(200 /β)	γ(degrees)	D1(μm)	D2(μm)	Σ(μm)
1	85.81	21	182.6	207.5	390.1
2	91.18	7	265.6	365.2	481.4
3	63.15	25	174.3	290.5	—
4	71.48	33	174.3	265.6	439.9
5	98.55	29	224.1	273.9	498.0
6	84.13	16	215.8	265.6	489.7
7	93.14	5	207.5	199.2	365.2
8	84.32	16	182.6	224.1	406.7
9	82.01	31	166.0	199.2	348.6
10	84.51	13	199.2	207.5	431.6
11	77.99	20	199.2	282.2	431.6
12	107.96	12	166.0	273.9	464.8
13	75.86	4	199.2	215.8	522.9
14	—	—	207.5	290.5	531.2
15	—	—	182.6	249.0	381.8
16	—	—	174.3	273.9	381.8
17	—	—	166.0	166.9	332.0
18	—	—	157.7	265.6	373.5
M	84.62	17.85	191.36	250.84	427.69
σ	±11.61	±9.71	±26.63	±47.09	±61.91
Coefficent of variability	13.72	54.40	13.92	18.77	14.47

As far as can be judged from the sections of *M. neodispansa* available, hexagonal chambers first appear no later than 6 to 7 rows away from the embryonic/nepionic chambers. *M. neodispansa* and *M. droogeri* Mohan & Tewari are very similar, each having a high value for parameter V, similar values for the angle γ, and a similar development of hexagonal median chambers. *M. droogeri* was described by Mohan & Tewari (*in* Mohan, 1958) as lacking accessory auxiliary chambers. However, Raju (1974) used the name *droogeri* for populations in which less than 50 per cent of the specimens have these chambers; it is only in *droogeri* sensu Raju that accessory auxiliary chambers occur. *M droogeri*, s.s. is here regarded as a junior synonym of *M. neodispansa*. *M. droogeri* sensu Raju may be intermediate between M. neodispansa and *M. excentrica*.

There is no direct biostratigraphical evidence for the age of the limestone on Christmas Island that contains *M. neodispansa*. No planktonic foraminifera have been observed; rare small

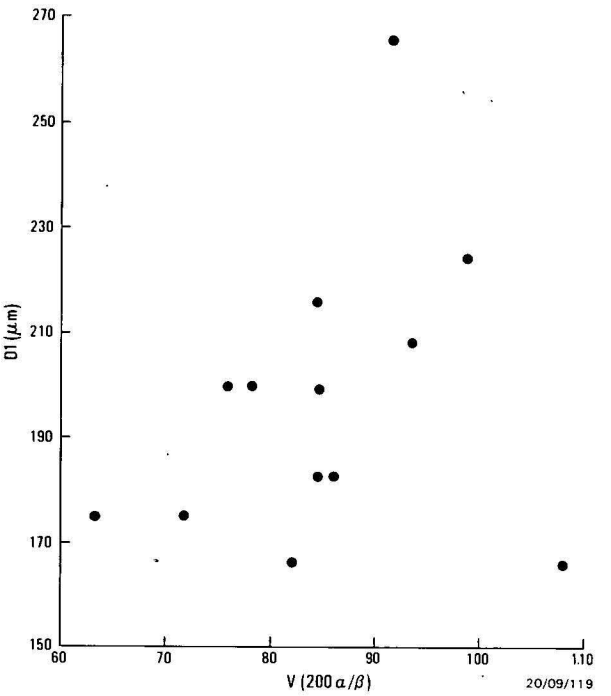

Figure 7. Relation between V and D1.

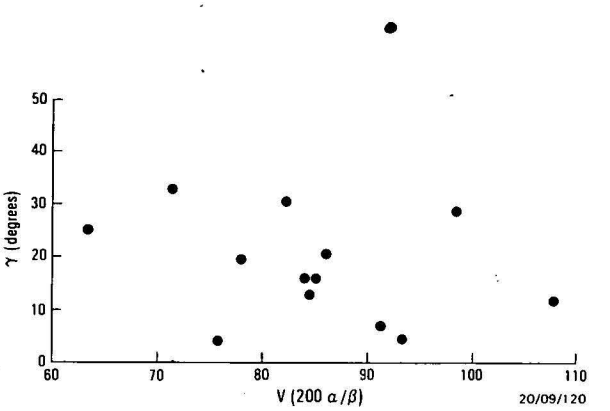

Figure 8. Relation between V and γ.

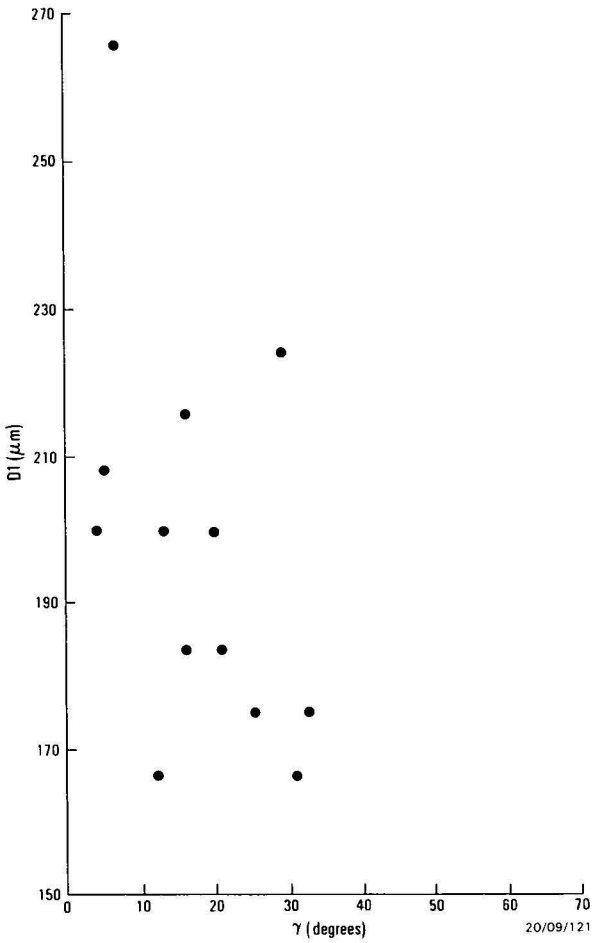

Figure 9. Relation between γ and D1.

lepidocyclinids in the limestone are rayed forms with an F number (see Chaproniere, 1980; 1981) of not less than 4. This would place the level of the limestone in the Tf_1 stage of the East Indies Letter Classification, at about the N.8–N.9 planktonic zonal boundary. Nuttall (1926) also noted the presence of indeterminate small lepidocyclinids in sample 220 of Andrews. Raju (1974), on the basis of associated planktonic foraminiferal species, referred the level of *M. excentrica* in the Madanam No. 1 Well, Cauvery Basin to Zone N.6 or lower N.7 of Blow (1969). This apparent discrepancy in the relative levels of occurrence of *M. excentrica* and *M. neodispansa* would be explained if the occurrence of *M. neodispansa* at its type locality represented the upper limit of its range. The species may have appeared in late upper Te, about planktonic Zone N.5, *M. excentrica* appearing soon after as a result of the rapid evolutionary development noted by Raju (1974). Rare specimens of *Miogypsina* from upper Te (probably late upper Te) samples from Christmas Island were referred by Adams & Belford (1974) to *M.* cf. *neodispansa*. Ludbrook (1965) figured a specimen identified as *M. neodispansa* occurring with *M. (Miogypsinoides) dehaarti* (van der Vlerk), which would also indicate an upper Te age. No information on the nature of the embryonic/nepionic chambers, or on the median chambers, is available on specimens occurring at this level, and it is not possible at this time to verify that the specimens are indisputably *M. neodispansa*. Alternatively, it is possible that the beds in the Madanam No. 1 Well containing *M. excentrica* are younger than stated by Raju (1974). The planktonic foraminifera in core 3 from this well include *Globorotalia (Clavatorella) bermudezi* which ranges, according to Blow (1969), from Zone N.8 to Zone N.10. Raju (1974) considered *G. (C.) bermudezi* to have a longer range, based on associated planktonic species.

M. neodispansa was also recorded in great abundance by Adams & Belford (1974) from sample K.129 in the South Point area. These specimens have been re-examined, but no well-oriented median sections are available. No indication of hexagonal median chambers has been seen; these chambers, when observed, are ogival/rhombic. Other differences are that the embryonic chambers are closer to the apex, the profile of the test is usually broadly oval, and the specimens are less strongly pillared. A detailed examination of these specimens is required to establish the relationship with *M. neodispansa*, but they are here regarded as a separate taxon, based on the features stated.

In conclusion, *M. neodispansa* is considered to be a member of the group of species that has been referred to the subgenus *Lepidosemicyclina*, and a senior synonym of *M. droogeri*, s.s. The stratigraphic level of the type locality is placed in the Tf_1 stage of the East Indies Letter Classification, now mainly in the early Miocene (Adams, in press); this may be the upper limit of its range. *M. neodispansa* has not definitely been identified in older limestones on Christmas Island, and its appearance in this area may be due to migration; its total stratigraphic range is not known.

Acknowledgements

I wish to thank Dr C.G. Adams, British Museum (Natural History) for reading and commenting on the manuscript.

References

Adams, C.G., in press — Neogene larger foraminifera, evolutionary and geological events in the context of Indo-Pacific datum planes. *In* Biostratigraphic datum planes of the Pacific Neogene. *Final Report, IGCP Project* 114.

Adams, C.G., & Belford, D.J., 1974 — Foraminiferal biostratigraphy of the Oligocene-Miocene limestones of Christmas Island (Indian Ocean). *Palaeontology*, 17(3), 475–506.

Amato, V., & Drooger, C.W., 1969 — How to measure the angle in the Miogypsinidae. *Revista Espanola de Micropaleontologia*, 1(1), 19–24.

Andrews, C.W., 1900 — A monograph of Christmas Island (Indian Ocean): physical features and geology. *British Museum (Natural History), London*, 1-13, 1–337.

Blow, W.H., 1969 — Late middle Eocene to Recent planktonic foraminiferal biostratigrapy. *Proceedings of the lst International Conference on Planktonic Microfossils, Geneva*, 1967, 1, 199–422.

Chaproniere, G.C.G., 1980 — Biometrical studies of Early Neogene larger Foraminiferida from Australia and New Zealand. *Alcheringa*, 4, 153–81.

Chaproniere, G.C.H., 1981 — Australasian mid-Tertiary larger foraminiferal associations and their bearing on the East Indian Letter Classification. *BMR Journal of Australian Geology & Geophysics*, 6, 145–51.

Drooger, C.W., 1952 — Study of American Miogypsinidae. *Thesis, University of Utrecht*, 1–80.

Drooger, C.W., 1963 — Evolutionary trends in the Miogypsinidae. *In* Von Koenigswald, G.H.R., Emeis, J.D., Buning, W.L., & Wagner, C.W. (editors), Evolutionary trends in Foraminifera. *Elsevier, Amsterdam*, 315–49.

Ludbrook, N.H., 1965 — Tertiary fossils from Christmas Island (Indian Ocean). *Journal of the Geological Society of Australia*, 12(2), 285–94.

Mohan, K., 1958 — Miogypsinidae from western India. *Micropaleontology*, 4(4), 373–90.

Nuttall, W.L.F., 1926 — A revision of the Orbitoides of Christmas Island (Indian Ocean). *Quarterly Journal of the Geological Society, London*, 82, 22–43.

Raju, D.S.N., 1974 — Study of Indian Miogypsinidae. *Utrecht Micropaleontological Bulletins*, 9, 1–148.

Souaya, F.J., 1961 — Contribution to the study of Miogypsina s.l. from Egypt.1. *Proceedings Koninklijke Nederlandse Akademie van Wetenschappen*, B,84, 665–705.

BMR Journal of Australian Geology & Geophysics, 7, 321-325

PLANORBULINELLA SOLIDA SP.NOV. (FORAMINIFERIDA) FROM THE MIOCENE OF PAPUA NEW GUINEA

D.J. Belford

Specimens from the Miocene of Papua New Guinea previously identified as *Linderina* sp.indet. are described as *Planorbulinella solida* sp. nov., which is widespread in beds of early Miocene age. Other records of *Linderina* in the Miocene of Papua New Guinea cannot be confirmed.

Introduction

Linderina sp.indet. was recorded by Paterson & Kicinski (1956) from the Cape Vogel area, Papua New Guinea, and mention was made of other occurrences in Papua New Guinea. The accompanying fauna in the Cape Vogel area indicates an early Miocene, upper Te-Tf_1, age. Reference was also made to the occurrence of this form in Te stage beds of western Papua.

Because *Linderina* has been regarded as an Eocene genus (Cushman, 1940; Glaessner, 1945; Freudenthal, 1969; Adams, 1970), although it has also been stated to range into the Miocene (Loeblich & Tappan, 1964), this form has been examined and is considered to be referable to the genus *Planorbulinella*. Adams (1970) noted that records of *Linderina* from lower Te limestones of Borneo are due to errors in determination of *Miogypsinoides* and/or *Planorbulinella*, or to reworked specimens. *Planorbulinella* and *Linderina* are closely related genera. Hofker (1927) placed *Linderina brugesi* Schlumberger in the synonymy of *Planorbulina larvata* Parker & Jones, and therefore regarded *Linderina* as a synonym of *Planorbulinella;* this synonymy has not been accepted by subsequent workers.

Figured specimens are deposited in the Commonwealth Palaeontological Collection, Bureau of Mineral Resources, Canberra, under numbers CPC.22437 to 22452; unfigured paratypes are also in this collection under numbers CPC.22453 to 22455. Other unfigured paratypes are in the ESCAP Fossil Reference Collection held at the Bureau of Mineral Resources under numbers E.923 to E.928.

Systematic description

Genus *Planorbulinella* Cushman, 1927

Type species. *Planorbulina larvata* Parker & Jones, 1865; original designation *Planorbulinella solida* sp.nov. (Figure 1, A–J; Figure 2, A–K)

Material examined. Numerous free specimens and random thin sections.

Derivation of name. From the Latin *solidus*, dense, thick, referring to the central thickened area of the test.

Diagnosis. An asymmetric species of *Planorbulinella* characterised by lamellar thickening of the test, and, generally, with two single-apertured chambers in megalospheric specimens.

Description. Test discoidal, trochoid, asymmetric; ventral surface flat or slightly convex; dorsal surface strongly convex; ranging from 0.5 mm to 2.0 mm in diameter and 0.2 mm to 0.6 mm in thickness. Test strongly thickened by subsequent shell lamellae formed over test surface; lamellae distinct in vertical section, forming a flat ventral and a convex dorsal surface. Periphery of test rounded, lobate. Test wall perforate, with elongate pores continuous through test lamellae. Surface of test, on rare well-preserved specimens, with numerous small irregularly distributed imperforate deposits of shell material; some specimens show development of pillars. Apertures central basal slits, two to each chamber, each with an imperforate lip.

Specimens are generally macrospheric, but four microspheric specimens have been observed. In the four microspheric specimens the number of single-apertured chambers ranges from 14 to 19. In macrospheric specimens this number (the statistic Y of Freudenthal, 1969) is two in all except two specimens, where it is three; one of these specimens is an oblique section, and this may affect the appearance of the embryoconch. The mean of the distance d1.2 (see Freudenthal, 1969) measured on 15 specimens is 204.73 μm, and for h1.3 is 210.27 μm; details of these measurements are given in Table 1. The pillars observed on some specimens are of the inflational type of Smout (1954). The symmetry of the spirals originating from the first chamber with two apertures, discussed by Freudenthal (1969, p. 65), varies in the present population. In all specimens observed the spiral is symmetrical around the third chamber; the spiral towards the protoconch and deuteroconch may be symmetrical, but is often irregular (Fig. 3).

Insufficient information is available on the external features of *P.solida* sp.nov. to permit comparison with other described species of *Planorbulinella*. On internal features the described species most similar to *P.solida* is *P.zelandica* Finlay, 1947. In each species Y=2, but on other features the two species may be differentiated. *P.zelandica* shows thickening of the test in topotype specimens that have been sectioned, but this thickening is restricted more to the central part of the test, and is also less distinctly lamellar, with stronger pillars developed. The embryonic chambers of *P.zelandica* are smaller than those of *P.solida* sp. nov., as is shown by the measurements given by Freudenthal (1969). *P. zelandica*, at least in the topotype specimens sectioned during this study, is also more symmetrical than is *P. solida*, being almost equally biconvex.

Table 1. Statistical measurements on *P.solida* sp. nov.

d1.2	h1.3	Y
207.5	232.4	2
224.1	215.8	2
157.7	157.7	2
190.9	249.0	2
224.1	215.8	2
240.7	224.1	2
224.1	240.7	?3
190.9	215.8	2
182.6	182.6	2
157.7	166.0	3
182.6	199.2	2
240.7	240.7	2
207.5	190.9	2
232.4	224.1	2
207.5	199.2	2
$M_{d1.2}$ = 204.73 ±27.10 Coefficient of variability = 13.24	$M_{h1.3}$ = 210.27 ±27.28 Coefficient of variability = 12.97	

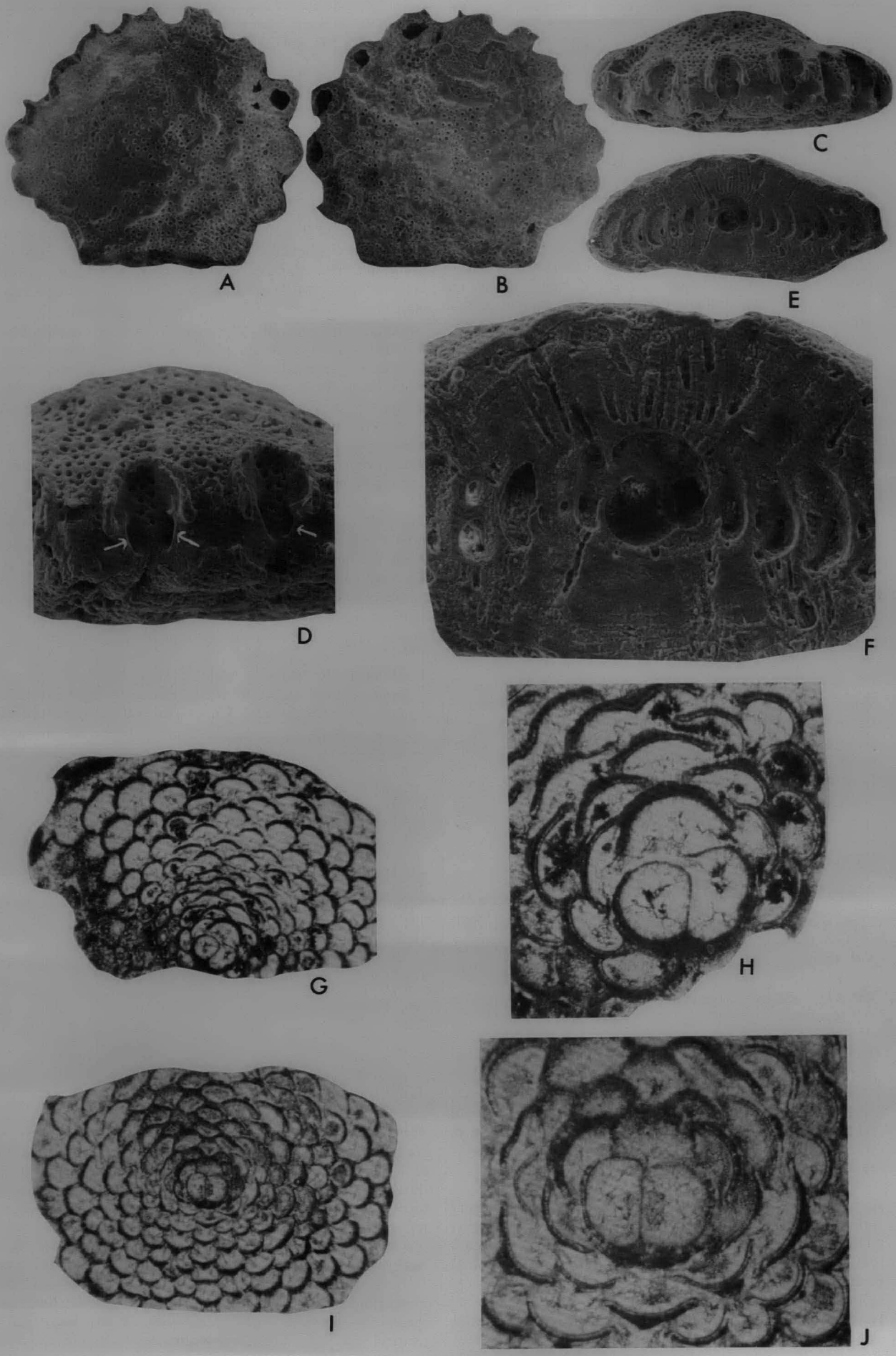
A
B
C
E
D
F
G
H
I
J

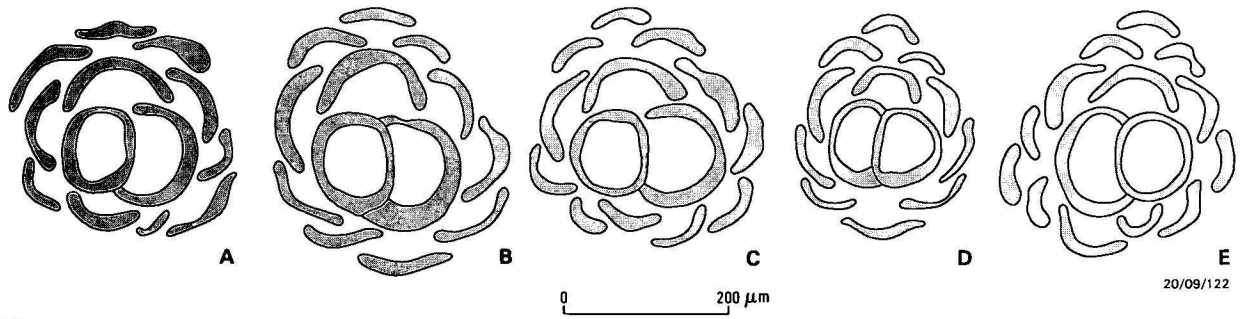

Figure 3. Embryonic and periembryonic chamber of *P. solida* sp. nov.
A–C, E, Omati No. 1 Well, Papua New Guinea, core 23, 1455 feet; **D,** sample LA.50, Cape Vogel area. A, CPC.22449; B, CPC.22450; C, CPC.22451; D, CPC.22440; E, CPC.22452.

This new species is referred to the genus *Planorbulinella* rather than *Linderina* because of the form of the test and the apertures. In species of *Linderina* the chambers, apart from the earliest chambers, are planispiral and the test is symmetrical. *P.solida* has the chambers arranged in a low trochoid coil, the test being asymmetrical in outline. Freudenthal (1969) noted that the aperture of *Linderina*, at least in the peripheral chambers, consists of two rows of 4–7 rounded openings at the chamber base. Specimens of *Linderina* in the collection of the Bureau of Mineral Resources, labelled as *Linderina buranensis (?brugesi)* from the Bahi No. 1 Well, Libya, at 230–240 feet have been sectioned, and show numerous small rounded apertures (see Fig. 2, O). The present specimens have two basal and median apertures to each chamber, as for *Planorbulinella*.

Occurrence of *Planorbulinella solida* sp.nov. in Papua New Guinea

Planorbulinella solida is widespread in Papua New Guinea and has been recorded in most cases as *Planorbulinella* sp. In addition to the occurrences already given, it is known from the general southeast region covered by the Abau, Samarai and Tufi 1:250 000 Sheet areas (Belford, *in* Smith & Davies, 1976). To the west it has been recorded from the Puri No. 1 Well, core 2; from the Omati No. 1 Well, between the depths of 1449 feet and 5633 feet (Kicinski, 1953; 1959), and from samples in the upper Sirebi area (Glaessner, 1950). It has also been recorded from several samples in the Ok Tedi and Wabag 1:250 000 Sheet areas (Belford, in press). The stratigraphic interval over which *P.solida* is known to occur is early Miocene (upper Te to Tf_1), and it may prove to be a characteristic form for this interval.

Records of the genus *Linderina* in the Miocene

Newton & Holland (1899) recorded *Linderina* sp. indet. from Borneo. Their illustration (pl. 10, fig. 6) shows an asymmetric specimen with distinct lamellar test thickening. Dr C.G. Adams, British Museum (Natural History), has examined this specimen and states (personal communication 22/7/82) that it is a *Miogypsinoides*, probably *M. dehaarti*. Davies (1927) recorded *Linderina* sp. from Pemba Island, but noted that the generic reference was not quite certain. The illustration shows a symmetrical test with lateral thickening, but lacking a lamellar structure and with 'beaded' median chambers. This specimen is regarded as *Miogypsina (Miogypsinoides)* sp., possibly *M.(M.) dehaarti*. Silvestri (1948), in describing the species *Linderina nuttalli*, placed the specimens figured by Newton & Holland and by Davies in synonymy, and therefore recorded the species in the lower Miocene. This synonymy is not accepted here.

Other records of *Linderina* from Papua New Guinea are those of Chapman (*in* Nason-Jones, 1930; *in* Stanley, 1932), who recorded it from several samples of younger Tertiary rocks in the Finsch coast and Matapau areas. It has not been possible to confirm these determinations. *Linderina brugesi*, recorded by Chapman (*in* Stanley, 1932) from sample 181, Wakip Creek, is a tangential section through a strongly pillared *Lepidocyclina* sp. (of *ferreroi* type). *Linderina* could not be located in available sections of sample 302 from Ninab Creek. Chapman (*in* Nason-Jones, 1930) also recorded *Linderina* from a sample in Oi Creek, north of Oimo village; sample JNJ288 is from this locality, but no specimens of *Linderina* occur in the sections. A sample from Nofula Creek was also given as containing *Linderina;* sample JNJ420 from this locality has been examined and contains a specimen of *Miogypsina (Miogypsinoides)*, which may have been misidentified as *Linderina*. Other records of Linderina in these reports cannot be checked as neither thin sections nor samples have been located. Specimen 1, from gravels at the mouth of Mahelem Creek, examined by Chapman (*in* Stanley, 1932) contains a microspheric specimen that is very similar to those of *Planorbulinella solida* sp.nov.

Acknowledgements

I wish to thank Dr C.G. Adams, British Museum (Natural History) for reading and commenting on the manuscript, and for information on the specimen recorded by Newton & Holland (1899) as *Linderina* sp.indet.

References

Adams, C.G., 1970 — A reconsideration of the East Indian letter classification of the Tertiary. *Bulletin of the British Museum (Natural History)*, 19(3), 87–137.

Belford, D.J., 1976 — Foraminifera and age of samples from south-eastern Papua. Appendix *in* Smith, I.E. & Davies, H.L., Geology of the southeast Papuan mainland. *Bureau of Mineral Resources, Australia, Bulletin* 165 (PNG 11), 73–86.

Belford, D.J., In press — Tertiary foraminifera and age of sediments, west central cordillera, Papua New Guinea. *Bureau of Mineral Resources, Australia, Bulletin* 216.

Cushman, J.A., 1940 — Foraminifera: their classification and economic use. 3rd edition. *Harvard University Press, Massachusetts.*

Figure 1 A–J, *Planorbulinella solida* sp. nov.
A–D, holotype, CPC.22437, Omati No. 1 Well, Papua New Guinea, core 23, 1455 feet. A,B, opposite sides; C, edge view; D, enlargement of edge view, showing apertures (arrowed). A–C, ×50; D, ×95. **E–F,** paratype A, CPC.22438, naturally broken specimen, same locality and level as holotype, showing lamination and perforation of test. E, ×50; F, ×130. **G–H,** paratype B, CPC.22439, sample LA50, section at Iwaia, Cape Vogel area, Papua New Guinea; horizontal section. G, ×40; H, ×120. **I–J,** paratype C, CPC.22440, same sample as CPC.22439; horizontal section. I, ×40; J, ×120.

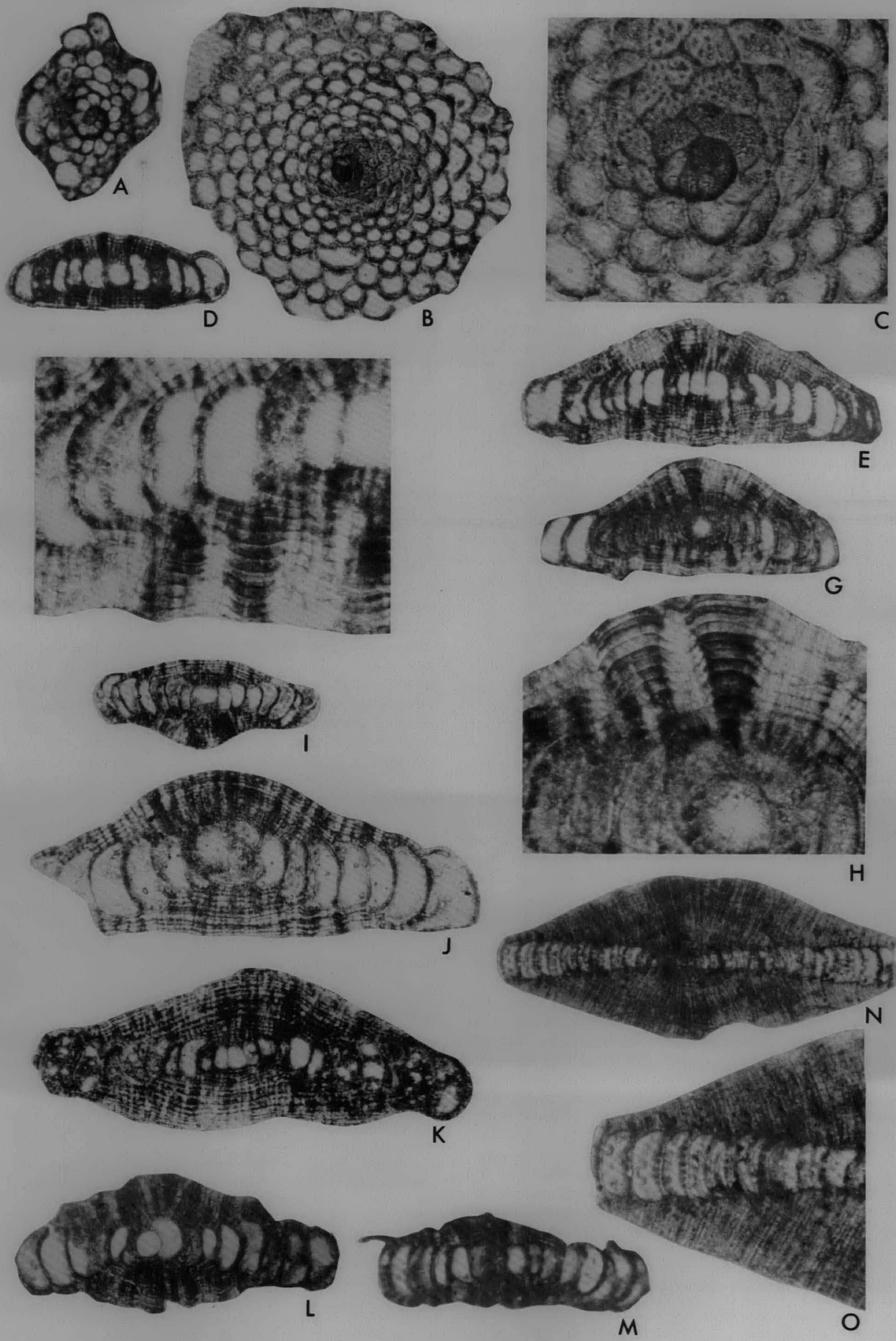
A
B
C
D
E
G
H
I
J
K
L
M
N
O

DAVIES, A.M., 1927 — Lower Miocene foraminifera from Pemba Island. *In* STOCKLEY, G.M., Stratigraphy of the Zanzibar Protectorate, 5–6 *Rep. Palaeont. Zanzibar Protectorate*, 7–12.

FREUDENTHAL, T., 1969 — Stratigraphy of Neogene deposits in the Khania Province, Crete, with special reference to foraminifera of the family Planorbulinidae and the genus *Heterostegina*. *Utrecht Micropaleontological Bulletins*, 1, 1–208.

FINLAY, H.J., 1947 — New Zealand Foraminifera: key species in stratigraphy — No. 5. *New Zealand Journal Science and Technology*, sec.B, 28(5), 259–292.

GLAESSNER, M.F., 1945 — Principles of micropalaeontology, *Melbourne University Press*.

GLAESSNER, M.F., 1950 — Preliminary palaeontological results, upper Sirebi survey. *In Australasian Petroleum Company Pty Ltd and Island Exploration Company Pty Ltd Report* KH (unpublished).

HOFKER, J., 1927 — The Foraminifera of the Siboga Expedition. Part 1: Families Tinoporidae, Rotaliidae, Nummulitidae, Amphisteginidae. *E.J. Brill, Leiden*.

KICINSKI, F.M., 1953 — Report on palaeontological examination of the rock samples from the Omati No. 1 Test Well (0'–11,540'). *In Australasian Petroleum Company Report* KOA (unpublished).

KICINSKI, F.M., 1959 — Report on palaeontological examination of samples from the Puri 1B (S. deviation) hole. *In Australasian Petroleum Company Report* KADB (unpublished).

LOEBLICH, A.R., Jr., & TAPPAN, H., 1964 — Part C, Protista 2, chiefly "Thecamoebians" and Foraminiferida. *In* MOORE, R.C. (editor), Treatise on Invertebrate Paleontology, *Geological Society of America and The University of Kansas Press*.

NASON-JONES, J., 1930 — Geology of the Finsch Coast Area, north-west New Guinea. The oil exploration work in Papua and New Guinea conducted by the Anglo-Persian Oil Company on behalf of the Commonwealth of Australia 1920–29, Volume 3. *Harrison & Sons Ltd, London*.

NEWTON, R.B. & HOLLAND, R., 1899 — On some Tertiary foraminifera from Borneo collected by Professor Molengraaff and the late Mr A.H. Everett, and their comparison with similar forms from Sumatra. *Annals and Magazine of Natural History*, ser. 7, 3, 245–64.

PARKER, W.J. & JONES, T.R., 1965 — On some foraminifera from the North Atlantic and Arctic Oceans, including Davis Straits and Baffin's Bay. *Philosophical Transactions of the Royal Society of London*, 155, 325–441.

PATTERSON, S.J. & KICINSKI, F.M., 156 — An account of the geology and petroleum prospects of the Cape Vogel Basin, Papua. *Bureau of Mineral Resources, Australia, Report* 25, 47–70.

SILVESTRI, A., 1948 — Foraminiferi dell'Eocene della Somalia; parte III. *In* Paleontologia della Somalie; iv. Fossili dell'Eocene. *Palaeontografia Italica*, 32, supplement 6, 1–56.

STANLEY, G.A.V., 1932 — The geology of the Matapau Concession Area, in the district of Aitape, Mandated Territory of New Guinea. *Oil Search Limited Report* N.G. 4B. 18(3) (unpublished).

Figure 2 A–K, *Planorbulinella solida* sp. nov.

A, paratype D, CPC.22441, Puri No. 1 Well, Papua New Guinea, core 2,610 feet; horizontal section, microspheric specimen. ×40. **B–C**, paratype E, CPC.22442, Omati No. 1 Well, Papua New Guinea, core 23,1455 feet; horizontal section, microspheric specimen. B, ×40; C, ×110. **D**, paratype F, CPC.22443, Puri No. 1 Well, Papua New Guinea, core 2,610 feet; vertical section, small specimen, showing test lamination. ×40. **E–F**, paratype F, CPC.22444, Omati No. 1 Well, Papua New Guinea, core 23,1455 feet; vertical section showing test lamination and pillars. E, ×40; F, ×120. **G–H**, paratype H, CPC.22445, same sample as paratype G; vertical section showing test lamination and pillars. G, ×40; H, ×120. **I**, paratype I, CPC.22446, sample LA50, section at Iwaia, Cape Vogel area, Papua New Guinea; vertical section, small specimen, showing test lamination, ×40. **J**, paratype J, CPC.22447, same sample as paratype I; vertical section showing test lamination, ×40. **K**, paratype K, CPC.22448, sample KH17, small tributary of Sireru River, just north of Sireru Fault, 6°56'S., 144°23'E., upper Sirebi River area, Papua New Guinea; vertical section showing test lamination, ×40.

L–M, *Planorbulinella zelandica* Finlay

Topotypes, CPC.22456 and 22457, F.5983, (BMR No. 79640006) Pourere, South Hawkes Bay, North Island, New Zealand; vertical sections showing thickening and lamination of the test, both ×40.

N–O, *Linderina buranensis* Nuttal & Brighton

Figured specimen, CPC.22458, Bahi No. 1, Well, Libya, 230–240 feet; vertical section, multiple apertures visible in O. N, ×40; O, ×75.

BMR JOURNAL
OF AUSTRALIAN GEOLOGY & GEOPHYSICS

VOLUME 7

1982

CONTENTS

VOLUME 7 NUMBER 1 MARCH 1982

VOLUME 7 NUMBER 2 JUNE 1982

VOLUME 7 NUMBER 3 SEPTEMBER 1982

VOLUME 7 NUMBER 4 DECEMBER 1982

CONTENTS

NOTES

Front cover: Scientific illustrator and artist Peter Shouten's reconstruction of *Wabularoo*, an extinct Middle Tertiary Bulungamayid from Riversleigh in northwestern Queensland, described in a paper in this issue. The name Wabularoo is a combination of 'Wa'bula', a Waanyi Aboriginal word meaning 'long time ago', and the Australian slang for kangaroo.

R81/103 (4) Cat. No. 82 0640 0